Coupled Abiotic and Biotic Cycling of Nitrous Oxide

by

Steffen Buessecker

A Dissertation Presented in Partial Fulfillment
of the Requirements for the Degree
Doctor of Philosophy

Approved March 2020 by the
Graduate Supervisory Committee:

Hinsby Cadillo-Quiroz, Chair
Hilairy E. Hartnett
Jennifer B. Glass
Sharon J. Hall

ARIZONA STATE UNIVERSITY

May 2020

ABSTRACT

Nitrous oxide (N_2O) is an important greenhouse gas and an oxidant respired by a diverse range of anaerobic microbes, but its sources and sinks are poorly understood. The overarching goal of my dissertation is to explore abiotic N_2O formation and microbial N_2O consumption across reducing environments of the early and modern Earth. By combining experiments as well as diffusion and atmospheric modeling, I present evidence that N_2O production can be catalyzed on iron mineral surfaces that may have been present in shallow waters of the Archean ocean. Using photochemical models, I showed that tropospheric N_2O concentrations close to modern ones (ppb range) were possible before O_2 accumulated. In peatlands of the Amazon basin (modern Earth), unexpected abiotic activity became apparent under anoxic conditions. However, care has to be taken to adequately disentangle abiotic from biotic reactions. I identified significant sterilant-induced changes in Fe^{2+} and dissolved organic matter pools (determined by fluorescence spectroscopy). Among all chemical and physical sterilants tested, γ-irradiation showed the least effect on reactant pools. Targeting geochemically diverse peatlands across Central and South America, I present evidence that coupled abiotic and biotic cycling of N_2O could be a widespread phenomenon. Using isotopic tracers in the field, I showed that abiotic N_2O fluxes rival biotic ones under *in-situ* conditions. Moreover, once N_2O is produced, it is rapidly consumed by N_2O-reducing microbes. Using amplicon sequencing and metagenomics, I demonstrated that this surprising N_2O sink potential is associated with diverse bacteria, including the recently discovered clade II that is present in high proportions at Amazonian sites based on *nosZ* quantities. Finally, to evaluate the impact of nitrogen oxides on methane production in peatlands, I

i

characterized soil nitrite (NO_2^-) and N_2O abundances along soil profiles. I complemented field analyses with molecular work by deploying amplicon-based 16S rRNA and *mcrA* sequencing. The diversity and activity of soil methanogens was affected by the presence of NO_2^- and N_2O, suggesting that methane emissions could be influenced by N_2O cycling dynamics. Overall, my work proposes a key role for N_2O in Earth systems across time and a central position in tropical microbial ecosystems.

DEDICATION

Diese Arbeit ist meinem Großvater Rolf Fehr gewidmet.

ACKNOWLEDGMENTS

First and foremost, I would like to thank my PhD advisor Hinsby Cadillo-Quiroz. My studies at ASU started as a journey in the scope of an internship and ended as an adventure. In a total of seven years under Hinsby's supervision, I have learned the fundamental tools that I believe are required to make my way through science. I extend my gratitude to the members of my PhD committee Hilairy Hartnett, Jennifer Glass, and Sharon Hall for their time commitment, enduring support and individual advice whenever needed. Thanks also goes to Thomas Day who agreed to represent Sharon Hall at the defense. I am very grateful to all co-authors of my dissertation chapters who contributed in a great way to each story. I point out some of them, who have become important mentors to me in their unofficial role: Hiroshi Imanaka, Steve Romaniello, Nathaniel Ostrom, and Björn Gücker. During the writing phases of the manuscripts, I also found more support from Ariel Anbar, Everett Shock, Andreas Kappler, Michael Russell and Tucker Dunn.

In the Cadillo Lab, I encountered friendship and collegiality from Analissa Sarno, Mark Reynolds, Patrick Browne, Michal Ziv-El, Jaime Lopez, Julian Yu, Damien Finn, Mike Pavia, Marc Fontanez Ortiz, Jackie Winston, Yan Rou Yap, and Jillian Ayers. Over the years, my work would not have been possible without my team of undergrads including Zac Zamora, Tiffany Maksimuk, Logan Kurgan, Amit Anilkumar, Kaitlyn Tylor, Carlos Courtney, Jack Liu, Martin Gonzalez, Nabil Fidai, Jordan Canning, and Francisco Campa. I owe tremendous gratitude to the friends and helpers on my field journeys, in particular to Joost van Haren, Outi Lähteenoja, Brian Crnobrna, Anna G. Pérez, Juan Rodrigo Trucios, Cely Mariela Cadillo-Quiroz, Jose and David Reyna.

TABLE OF CONTENTS

LIST OF FIGURES

CHAPTER 1

INTRODUCTION

Entanglement of Abiotic and Biotic Processes

To understand the planetary environment, it is of importance to discern biotic and abiotic processes and to determine their interactions. Life is a not state; it is a chemical process. A reaction is a chemical process in which one substance transforms into another. I define biotic reactions as those carried out by living organisms. Distinguishing between abiotic and biotic reactions is important because of the fundamentally different driving mechanisms. Deciphering mixed abiotic-biotic signatures has astrobiological relevance because in order to identify life in extraterrestrial environments, we have to be able to recognize the boundaries between life activity and the geochemical "noise" caused by spontaneous chemical reactions.

Mechanistic differences between abiotic and biotic reactions also determine the activation energy, with vast implications for ecosystem functioning. For instance, based on differences in apparent activation energies, the metabolic balance of ecosystems is more or less sensitive to temperature changes over long time scales, such as in the wake of global climate change (Yvon-Durocher *et al*., 2010; Yvon-Durocher *et al*., 2012). Activation energies are useful to deduce how quickly a reaction progresses in nature. Whereas the Gibbs energy change of two reactants contains information about the general favorability of a chemical reaction under defined conditions, the activation energy is related to the "energy barrier" between reactants and products in chemical reactions and

dictates the degree of kinetic hindrance (Anderson, 2005). The Gibbs energy change (ΔG)

can be defined as

$$\Delta G = \left(log \frac{\{ox\}}{\{red\}} - p\epsilon \right) 2.303 \ RT$$

where R is the ideal gas constant (8.3145 kJ mol^{-1} K^{-1}), T is the absolute temperature (K),

and $\{ox\}/\{red\}$ is the activity ratio of the oxidants and the reductants in the reaction. A

measure of the electron activity is introduced with $p\varepsilon$. The rate constant k of a reaction

can be derived from the Arrhenius equation:

$$k = A \ e^{\frac{-E_a}{RT}}$$

and rearranged to solve for the activation energy (E_a) as:

$$E_a = (log \ A - log \ k) \ 2.303 \ RT$$

where A is the Arrhenius factor, describing the collision of the reactants. Arrhenius'

definition of the activation energy is grounded in collision theory, in which the frequency

of oriented reactant collisions governs the overall reaction rate (Arrhenius, 1889a;

Arrhenius, 1889b). The differences of the two energy quantities become apparent because

ΔG is a function of "static" parameters ($\{ox\}/\{red\}$ and $p\varepsilon$), whereas E_a comprises

"dynamic" parameters (A and k). Abiotic and biotic reactions differ in these latter

parameters because enzymes create a fluctuating thermal bath around reactants (Marcus

and Sutin, 1985), which optimizes their oriented collision and accelerates electron

transfer. In natural systems, activation energies of abiotic reactions can be very similar to

biotic reactions. This occurs once abiotic catalysts (organics-metal complexes, minerals)

lower the reaction energetic barrier, when energy sources become available (light), or

when the chemical species are generally unstable. For example, oxidative mineralization

2

of phenolic substances to CO_2 can occur spontaneously in organic-rich soils and is driven by Fe^{3+} in the mineral phase ferrihydrite (Pracht *et al.*, 2001). Chemical oxidation of sulfide by dissolved oxygen is a commonly observed phenomenon in euxinic marine settings (Luther *et al.*, 2011), and photo-oxidation of Mn^{2+} is thought to be an important abiotic mechanism producing Mn oxide deposits in the early oceans (Anbar and Holland, 1992). Abiotic reactions that are competitive with life processes under ambient conditions are widely distributed across multiple geochemical cycles. The anoxic branch of the nitrogen cycle comprises denitrification, the step-wise reduction of nitrogen oxides to nitrogen gas (N_2), followed by nitrogen fixation. The pathways are marked by multiple abiotic reduction steps (Fig. 1.1), and include the intermediate nitrous oxide (N_2O).
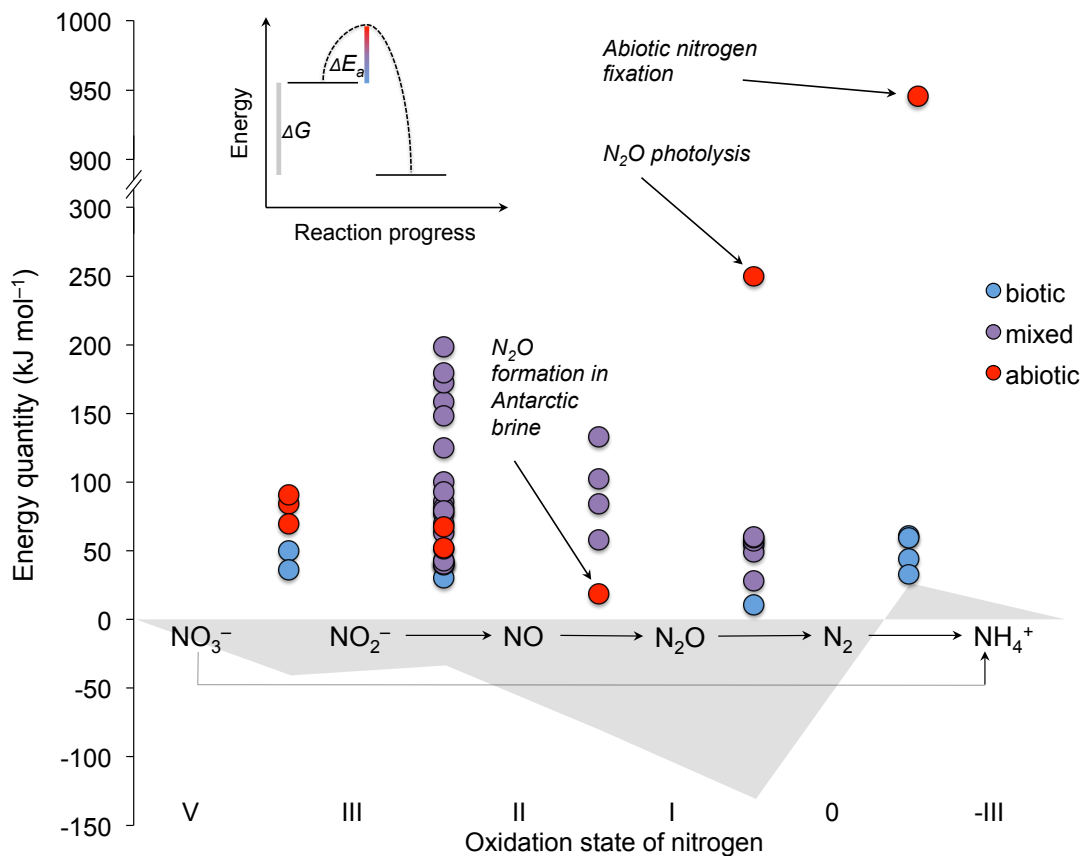
Fig. 1.1. Activation energies (E_a) and changes in Gibbs energies ($\varDelta G$) from reactants to products along the reducing branch of the nitrogen cycle. The gray area indicates $\varDelta G$ and is derived from half reactions given by Luther, 2010. Activation energy is shown as data points obtained from measurements (see Table A.1) and is of abiotic, biotic, or mixed abiotic-biotic nature (when experiments did not distinguish by sterilization).

Figure 1.1 illustrates why abiotic reactions of the nitrogen cycle may be very prevalent in natural systems, such as soils or sediments. Nitrate (NO_3^-) reduction is associated with activation energies that are only slightly higher when not carried out enzymatically. For example, NO_3^- reduction to N_2O is possible but typically very slow (Zhu-Barker *et al.*, 2015). The abiotic and biotic reduction of NO_2^- and NO have essentially indistuingishable activation energies, which could explain why these reactions are commonly observed in sterilized soil. Abiotic NO reduction to N_2O has been shown to have a very low energetic barrier (Samarkin *et al.*, 2010), suggesting this process may be much more widespread than previously thought. In contrast, N_2O reduction to N_2 has a very high (~ 250 kJ mol^{-1}) activation energy due to electronic delocalization that stabilizes the N_2O molecule. Thus, N_2O consumption in soils or sediments can almost conclusively be declared due to microbial activity. The same is true for N_2 reduction to ammonium, which requires an extremely large amount of energy input to overcome the activation barrier. Even though N_2O reduction is highly exergonic ($\varDelta G$ is strongly negative), the energetic barrier is significant. Nitrous oxide is a superb metabolic oxidant and is easily accessible for microbial cells because of its high solubility in water (Henry's law constant $K_h^{cc} = 0.611$, $T = 298$ K, Sander *et al.*, 2009). One can postulate that abiotic production followed by biotic consumption, or an abiotic-biotic N_2O cycle, could be a common phenomenon. Nitrous oxide is a potent greenhouse gas due to its positive radiative forcing and long atmospheric residence time (114 years; Stocker *et al.*, 2013). It

4

also has high ozone-depleting potential because it is an efficient source of NO, which reacts directly with ozone to form nitrogen dioxide and molecular oxygen (Ravishankara *et al.*, 2009). Given this environmental relevance, it is important to understand the entire spectrum of N_2O sources and sinks, including the abiotic ones (Zhu-Barker *et al.*, 2015).

The nitrogen cycle through time

Nitrogen is abundant on Earth, with its main reservoir residing in the N_2 of the atmosphere. No other celestial body in our solar system contains as much nitrogen in the form of N_2 as our planet (Titan, the saturnian moon, has the second most). Nitrogen is a bio-essential element contained in proteins and nucleic acids and respired by anaerobic microbes. The caveat for life has been to access nitrogen in a usable form, namely as ammonium for assimilation and nitrogen oxides for dissimilatory processes. Even though the extent is still debated in the scientific community, abiotic nitrogen fixation represents a pathway on the early Earth combining oxygen derived from atmospheric CO_2 and N_2 into nitrogen oxides (Chameides, 1986). The energy for this transformation was delivered by heat shock reactions from events such as galactic cosmic ray bursts, meteorite impacts, volcanic and thunderstorm lightning (Mancinelli and McKay, 1988; Kasting, 1990; Navarro-Gonzalez *et al.*, 1998). Fixed nitrogen could also have been produced by the interaction of high-energy particles from coronal mass ejections with atmospheric gases, enabled by a greater opening angle of the magnetic field very early in Earth's evolution (Airapetian *et al.*, 2016). While estimates of average NO_3^- and NO_2^- concentrations in Hadean and Archean seawater range from < 1 (R. Hu and Diaz, 2019)

to several hundred µM (M. L. Wong *et al*., 2017), these pools were highly dependent on the magnitude of sinks. The potential of NO_3^- and NO_2^- as precursors for N_2O remains underexplored, especially in light of reactivity with abundant reduced iron minerals in the ferruginous ocean. Significant N_2O abundances would have been consequential for the planetary climate and the early biosphere. As strong greenhouse gas, N_2O may have contributed to a warmer climate as inferred from the faint young Sun paradox (Gough, 1981). Exposure of the early biosphere to N_2O would also explain multiple lines of biochemical evidence suggesting its metabolically important role as terminal electron acceptor (Saraste and Castresana, 1994; Chen and Strous, 2013). Consistent with Fig. 1.1, the conversion of N_2 to ammonium (NH_4^+) in the anoxic early oceans occured at rates a factor of 50 to 5000 slower (Summers and Khare, 2007; Laneuville *et al*., 2018) than modern nitrogen fixation rates (Gruber and Galloway, 2008). Similarly, NO_3^- and NO_2^- were reduced to NH_4^+ at higher temperatures and via interactions with metallic iron, iron sulfide minerals, or magnetite (Brandes *et al*., 1998; Smirnov *et al*., 2008). Abiotic NH_4^+ production became limiting after the evolution of anoxygenic photosynthesis, forcing microbial life to abate the high activation energy of N_2 conversion to NH_4^+ by enzymatic catalysis. Nitrogenases relieved the early biosphere of nitrogen starvation (Raymond *et al*., 2004; Glass *et al*., 2009) and allowed higher productivity. A fundamental shift occurred in the nitrogen cycle when Earth's surface became gradually oxygenated at ~2.6-2.7 Ga (Ostrander *et al*., 2019). The emergence of nitrification enabled more effective formation of NO_2^- and NO_3^-. Subsequently, N_2O formation was also independent of microbial denitrification in the Proterozoic, as NO (now derived from microbial nitrification) was converted to N_2O by dissolved Fe^{2+} (Stanton *et al*., 2018),

underlining the role abiotic N_2O formation could have played to deliver significant amounts of N_2O for over half of Earth's history.

On modern Earth, anthropogenic sources of N_2O (~6.9 Tg N_2O-N yr^{-1}) are exceeded by natural sources of N_2O (~11 Tg N_2O-N yr^{-1}). These natural sources can be attributed to vegetated soils (~6.6 Tg N_2O-N yr^{-1}), the oceans (~3.8 Tg N_2O-N yr^{-1}), and atmosphere (~0.6 Tg N_2O-N yr^{-1}) (Ciais *et al.*, 2013). The dominant atmospheric sink for N_2O is destruction by UV photolysis and reaction with excited O_2 atoms $O(^1D)$ in the stratosphere. From all terrestrial sources, N_2O emissions revealed the highest contribution to total N_2O flux on the South American continent and were associated with high uncertainties predominantly in tropical regions (Pérez *et al.*, 2006; Huang *et al.*, 2008; S. Park *et al.*, 2011).

Tropical peatlands

Tropical peatlands are hotspots of N_2O production (Hatano *et al.*, 2016). Recent models suggest South America harbours unprecedented volumes of peat (Gumbricht *et al.*, 2017). Nitrous oxide emissions from wetlands of the Pantanal (West Brazil; 88-1496 ng cm^{-2} h^{-1}, Liengaard *et al.*, 2014) exceeded those from oxisol and ultisol at Amazonian tropical forest sites (0.1-13 ng cm^{-2} h^{-1}, Pérez *et al.*, 2006; S. Park *et al.*, 2011). Nitrous oxide fluxes have also been observed to fluctuate tremendously (Teh *et al.*, 2017), as reported from the Pastaza-Marañón foreland basin in East Peru (Fig. 1.2).
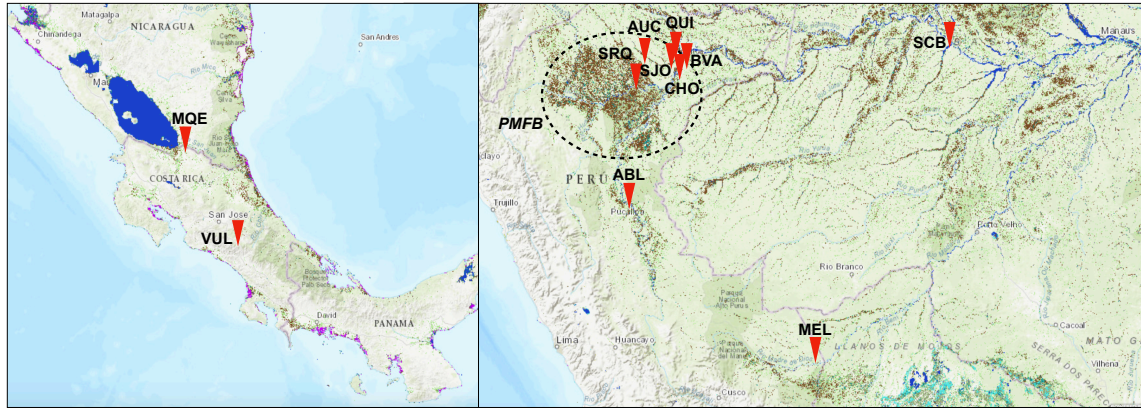
Fig. 1.2. Distribution of peatlands and study sites in Costa Rica (left) and the Amazon basin (right). Canonical types of wetlands are colored as follows: mangroves (pink), swamps and bogs (brown), fens (gray), floodplains (turquoise), marshes (light green), wet meadows (dark green). Peatlands are the most common type of wetlands and "characterized by the unique ability to accumulate and store dead organic matter from *Sphagnum* and many other non-moss species, as peat, under conditions of almost permanent water saturation" (Joosten and Clark, 2002). Tropical peatlands tend to deviate from this classification (Junk et al., 2011) which is based on northern and temperate peatlands (Brinson and Malvárez, 2002). Study site locations are not always consistent with mapped wetlands. AUC=Aucayacu (pole forest), ABL=Aqua blanca (mixed forest swamp), BVA=Buena Vista (mixed forest/palm swamp), CHO=Charo (mixed forest/palm swamp), VUL=Las Vueltas (mountain bog, *bofedales*), MEL=Melendez (mixed forest swamp, terrace peatland), MQE=Medio Queso (open peatland), QUI=Quistococha (palm swamp), SCB=Sitio Cacao (pole forest), SJO=San Jorge (pole forest), SRQ=San Roque (palm swamp), PMFB=Pastaza-Marañón foreland basin. FCA=Fazenda (fen) is located in the south-eastern Brazilian state of Minas Gerais and not shown on the map. Map obtained from *cifor.org*.

In the wake of a wide-ranging evolution of foreland basins along the eastern side of the Andes, riverine sediments accumulated and peatlands formed. The foreland basins, such as the Pastaza-Marañón, emanated from an active sub-Andean fault system from the late Permian to the Quaternary and are characterized by distinct areas of subsidence (Räsänen *et al*., 1987). Accumulated fluvial sediments are delineated by riverine geomorphic structures with implications for the modern ecosystems of the western Amazon. The discovery of novel tropical peatlands revealed that the local geomorphology induced the formation of peat that is several meters thick. The vegetation above the peat soil is highly influenced by the soil chemistry (Page *et al*., 1999) and,

8

together with riverine input, represents the main source of biomass. The distinct

hydrological conditions of wetlands create not only the geochemical framework needed

to sustain abiotic N_2O formation, but also habitats for diverse microbial communities.

The majority of my study sites are concentrated within the Pastaza-Marañón foreland

basin (Fig. 1.2; AU, BV, CH, QU, SJ, SR), and are complemented by peatlands inside

(SC, AB, ME) and outside (LV, MQ, FA) the Amazon basin. The diversity in

geochemical conditions across these sites is immense, spanning from oligotrophic (SJ,

AU) to relatively eutrophic (MQ, FA), from acidic (SJ, SC) to pH-neutral (LV, ME), and

from Ca-rich (BV) to Ca-poor (SJ). They all are rich in organic carbon (>20% by weight)

and, with the exceptions of MQ and FA, have not experienced significant anthropogenic

impact. A more detailed edaphic description is provided in the individual chapters.

In order to be spontaneously reduced, nitrogen oxides require a source of

electrons. In peat soil, electrons can be derived either from reduced metals (Fe^{2+}, Mn^{2+})

or from organic functional groups. Tropical soils are typically iron-rich. In peatlands of

the Amazon, iron may originate from the bedrock underlying the organic soil layers, or

from riverine inputs as a result of rock weathering in the Andes. Soil Fe^{2+} has been

shown to be an effective reductant driving abiotic N_2O production in several studies,

predominantly under anoxic conditions (Zhu-Barker *et al*., 2015). The lack of oxygen

causes organic matter decomposition to remain incomplete (Page *et al*., 1999; Jauhiainen

et al., 2005; T. Hirano *et al*., 2009), resulting in recalcitrant organics, such as humic and

fulvic acids, with a great variety of reducing functional groups. These also comprise

hydroxy-substituted aromatic structures. Humic and fulvic acids promote N_2O production

because hydroxy-groups undergo nitrosation with soil NO_2^-, and tautomerize into

9

nitrosophenols and quinone monoximes prior to the release of N_2O (Thorn and Mikita, 2000; Thorn *et al.*, 2010).

To overcome the activation energy barrier that N_2O reduction to N_2 poses (Fig. 1.1), microbes have evolved N_2O reductase. This enzyme is made up of tightly linked head-to-tail homodimers of 130 kDa (Pomowski *et al.*, 2011) and the active sites contain two multi-copper centers, CuA and CuZ. The CuA site relays electrons received by cytochrome-type electron carriers (Rasmussen *et al.*, 2005) to the CuZ site, where the reduction of the bound substrate N_2O occurs. The gene sequence encoding the catalytic subunit of N_2O reductase, *nosZ*, has been used to investigate the taxonomic and phylogenetic representation of N_2O-reducing microbes in soils and sediments. The *nosZ* phylogeny is divided into two clades based on enzyme structural aberrations. Clade I comprises classical denitrifiers with the enzymatic repertoire to carry out complete denitrification; the novel clade II comprises N_2O reducers that have N_2O reductase but lack at least some of the other nitrogen oxide-reducing enzymes (Hallin *et al.*, 2018). The emerging phylogenetic group of N_2O-reducing microbes is highly diverse. The *nosZ* genes are distributed across 16 phyla (Sanford *et al.*, 2012), including *Bacteria* and *Archaea*. By comparison, the broadly distributed sulfate-reducing bacteria, which carry out an alternative anaerobic respiratory pathway and are marked by the functional gene *dsrAB*, are found in a total of 13 phyla (Anantharaman *et al.*, 2018).

The extended diversity of N_2O reducers is the basis for a N_2O sink potential in soils that has been overlooked for a long period of time, but which has become evident from discrepancies between classical denitrification gene distributions in metagenomes and measured consumption activity in soils (C. M. Jones *et al.*, 2014). Biological N_2O

10

consumption and the fate of N_2O in tropical soils, predominantly under acidic and anoxic conditions in water-logged soils, is widely unknown despite the large range of fluxes that has been reported (see at the beginning of this section). The N_2O sink potential in tropical soils could be regulated by the available organic substrates owing to the individual plant debris and the associated organic matter mineralization cascade (Ishii *et al*., 2011), the soil pH (B. Liu *et al*., 2014), or differences in N_2O reduction kinetics between clades (S. Yoon *et al*., 2016). These parameters all affect the community composition of N_2O reducers and the intrinsic capacity for soils to produce N_2O abiotically. Enhanced substrate availability induces N_2O reductase expression to harvest the energy released by N_2O reduction. It is, thus, an ecological advantage for anaerobic soil microbes to be capable of N_2O respiration, especially if abiotic pulses of N_2O are frequent.

Geochemical N_2O formation may represent an influential abiotic ecosystem component in peatlands. If reaction rates are sufficiently high, abiotic N_2O production may compete with biotic N_2O production and could fill a catalytic gap resulting from missing denitrification enzymes (Graf *et al*., 2014). Microbial N_2O consumption is complementary to abiotic N_2O production, as it completes a production-consumption cyle for N_2O as microbial cells adapt to the fundamental conditions of their environment. The two sides of this cycle may therefore be "coupled", assuming the above mentioned stimulation of biotic activity by abiotic fluxes. The dynamics of this cycling could be essential to understanding the high temporal and spatial variability observed in tropical ecosystems and it is, thus, of high importance to explore these processes in tropical peatlands to better constrain the global N_2O budget.

Focus and scope

Life co-evolved with its planetary evironment (Dietrich *et al*., 2006). The coupled

abiotic-biotic cycling of N_2O is a process in which organismic response follows abiotic

stimuli in an intricately connected manner. Given its behavior as greenhouse gas, N_2O

can influence climatic conditions and provide life with a lever to regulate its habitat. This

example of a "Gaian" control system (Lovelock, 1988) was likely prevalent over

different stages of our planet's history. Therefore, I formulated the following three main

questions:

1.   How significant was abiotic N_2O formation on the early (> 2.7 Ga) anoxic
      Earth?

2.   How significant is abiotic N_2O formation, in modern tropical
      peatlands of Central and South America?

3.   To what extent is biotic N_2O consumption "coupled" to its abiotic
      production, and thus, how do peat soil microbial communities adapt in
      activity and diversity to abiotic N_2O fluxes?

In this dissertation, I approached these questions in four chapters. First, I assessed

mineral-catalyzed reduction of NO_3^- and NO_2^- to N_2O as a significant source of N_2O in

an Archean ocean-atmosphere system. Given the role of N_2O as a greenhouse gas and as

a strong oxidant for anaerobic metabolisms, an abiotic, or even prebiotic, source of N_2O

would have had wide-reaching consequences for the early climate and potentially for the

evolution of microbial respiration. *An abiotic N_2O cycle on the anoxic early Earth*

emphasizes the cycling nature of abiotically driven processes without the intervention of

life. I considered photolysis in the atmopshere as the abiotic consumption pathway. I

combined lab simulation experiments to determine reaction rates with diffusive and

photochemical models to estimate atmospheric abundances on the basis of distinct

mineral reactions involving the mixed-valent iron minerals green rust and magnetite. A

key finding was that Archean atmosphere N_2O concentrations in the ppb range were

possible but higher levels were confined by reactant supply from abiotic nitrogen

fixation.

Second, I assessed abiotic N_2O formation in soils. I laid this groundwork by the

evaluation of seven sterilization techniques, including physical and chemical treatments,

on organic-rich peat soil from a Peruvian wetland (Fig. 1.2; QUI). I focused on changes

in the reactant pools, i.e., soil iron as well as organic matter by deploying inductively

coupled plasma-optical emission spectroscopy (ICP-OES) and fluorescence spectroscopy.

I found clear differences in the effects of sterilization techniques on chemodenitrification

and abiotic N_2O production. Gamma-irradiation was identified as the method that caused

the fewest artifacts in the reactant pools and in measured rates. In principle, my results

are applicable to any soil or sediment and I hope to aid future assays on the determination

of abiotic N_2O production in their methodological strategy.

Third, I report research on Central and South American peatland systems that bear

on questions 2 and 3. The true extent to which abiotic N_2O formation contributes to

modern N_2O fluxes and the global N_2O budget is unknown. Abiotic N_2O production has

been described in artificial systems under controlled conditions in many other studies

(Zhu-Barker *et al*., 2015), or very sparsely in marine sediments (Otte *et al*., 2019) and

brines of Antarctica (Samarkin *et al*., 2010; Ostrom *et al*., 2016). A thorough

investigation of the distribution of this enigmatic process has been missing. *Coupled*

abiotic-biotic cycling of nitrous oxide in tropical peatlands remedies this lack of

knowledge by focusing on hotspots of N_2O emissions and systems for which high variability in N_2O emissions has been observed: tropical peatlands (Liengaard *et al.*, 2014; Teh *et al.*, 2017). I used isotopic (^{15}N) tracers to measure N_2O cycling rates *in-situ* and complemented these efforts with molecular analysis of the *nosZ* gene phylogeny and distribution in 10 geochemically diverse soils from Costa Rica, Peru, and Brazil (Fig. 1.2). In addition, I measured soil Fe^{2+} contents after extraction to explain the driving force of the abiotic N_2O production observed. Six soils revealed a nearly complete abiotic denitrification potential and two soils showed a complete abiotic denitrification potential. I observed discrete groups of clade I- and II-dominated N_2O reducing communities. The clade I organisms were seemingly more dominant, based on *nosZ* gene quantities, at sites with higher abiotic N_2O fluxes. I present evidence that a mixed abiotic-biotic form of denitrification may be more distributed across wetlands than previously thought.

Fourth, I addressed the effects of nitrogen oxides on peat microbial communities, with an emphasis on carbon mineralization to methane. Three peatlands of the Pastaza-Marañón foreland basin (Fig. 1.2; QUI, SJO, BVA) were geochemically characterized and the distribution of the whole microbial community as well as methanogenic groups was explored. The molecular work comprised phylogenetic analysis of the 16S ribosomal RNA (rRNA) and the functional gene encoding for the enzyme at the heart of microbial methane production, methyl-coenzyme M reductase (*mcrA*). I also probed methane and dissolved inorganic carbon (DIC) pools and their stable isotopic composition. I found highly heterogeneous soil geochemistries across the study sites, emerging from distinct ^{13}C enrichments in soil methane and DIC, different soil pH, and contrasting pore water concentration profiles of DOC, NO_3^-, and C/N ratios. Different nitrifiers and denitrifiers

14

inhabited equivalent niches in the soils, with an intriguing partitioning of ammonia-oxidizing archaea in acidic sites and ammonia-oxidizing bacteria in more pH-neutral sites. Lastly, I compiled evidence that methane production is affected by soil NO_2^- and that effects could be due to N_2O emanating from NO_2^-.

In summary, this dissertation is focused on abiotic N_2O production and biotic N_2O consumption. Over four research chapters, these processes are placed into two different systems; the Fe-rich anoxic ocean of the early Earth (Chapter 2) and organic soils in the modern tropics (Chapter 3-5). At the heart of these efforts, I investigated to what extent abiotic N_2O production is coupled to biotic consumption. The magnitude of abiotic N_2O production and the degree of the coupling may influence N_2O cycling rates and, thus, emissions. Both, N_2O retention within ocean or soil systems as well as emissions to the atmosphere, can have strong implications for microbial life and the planetary climate. Findings from my research are presented in the following Chapters 2-5 and conclusions are made in the final Chapter 6.

CHAPTER 2

AN ABIOTIC N$_2$O CYCLE ON THE ANOXIC EARLY EARTH[1]

Abstract

Nitrous oxide (N$_2$O) is a powerful greenhouse gas and deemed an indicator for life processes. It has been considered insignificant on the anoxic early Earth, due to its dependence on microbial denitrification and to the absence of a protective ozone layer because UV photolysis poses the major sink for atmospheric N$_2$O. However, iron mineral phases in Fe^{2+}-rich (ferruginous) oceans could have catalyzed reactions with abiotically fixed nitrogen oxides leading to the formation of N$_2$O. We experimentally simulated surface-catalyzed reduction of nitrite and nitrate via green rust and magnetite, and used these measured rates to model N$_2$O diffusion in ferruginous seawater. While N$_2$O escaped to the atmosphere (63% of nitrite-nitrogen), the byproduct nitric oxide remained associated with precipitates in the form of nitrosyl (7% of nitrite-nitrogen, with green rust as catalyst). Surface emissions lead to significant N$_2$O tropospheric abundances (>10 ppb) as shown by photochemical modeling. Our findings imply a complete abiotic N$_2$O cycle operative on the early Earth, independent of enzymatic catalysis.

Introduction

The Archean atmosphere prior to the Great Oxidation Event (GOE) was likely dominated by N_2 and CO_2, with ppm-levels of CO, CH_4, and H_2 (Kasting, 2014). The introduction of even trace amounts of more oxidized gases, such as nitrous oxide (N_2O), or laughing gas, could have created a significant source of thermodynamic disequilibrium to drive early Archean ecosystems.

Despite the proposed key role of N_2O in the early stages of the Earth's biosphere (Chen and Strous, 2013; Stanton *et al*., 2018) and climate under a faint young Sun (Gough, 1981), it is unknown whether the ocean acted as a net N_2O source to the atmosphere prior to ~2.7 Ga. While earlier estimates of atmospheric N_2O abundances were based on biological production rates (Godfrey and Falkowski, 2009; Roberson *et al*., 2011), more recently, abiotic sources of N_2O have been considered for the early Earth (Airapetian *et al*., 2016; Stanton *et al*., 2018). Stanton *et al*. first showed through experiments and modeling that iron could have acted as driver for chemodenitrification to form abiotic N_2O in ferruginous Precambrian oceans (Stanton *et al*., 2018). Multiple lines of evidence suggest that the oceans were rich in Fe^{2+} (ferruginous) from >3.8 to ~2.7 Ga and had a tendency to export reduced species to the atmosphere (Poulton and Canfield, 2011). The ferrous-ferric hydroxy salt carbonate green rust (GR; $[Fe^{2+}_{(1-x)} Fe^{3+}_x (OH)_2]^{x+} \cdot [(x/2)CO_3^{2-} \cdot (m/2)H_2O]^{x-}$) has been shown to precipitate from Archean seawater-analog solutions, consistent with thermodynamic modeling predicting a predominance of GR in the Fe sink fraction along the water column (Halevy *et al*., 2017). It has been argued that

settling GR particles could have provided a transport mechanism for trace compounds to the seafloor (Halevy *et al.*, 2017), where reducing conditions converted GR to magnetite (Fe_3O_4), which is an important constituent of banded iron formations. Nitrogen oxides are prone to spontaneously react in presence of iron mineral phases (Sorensen and Thorling, 1991; Hansen *et al.*, 1994). As a consequence of abiotic nitrogen fixation, nitrite (NO_2^-) and nitrate (NO_3^-) reached seawater concentrations in the lower μM range (Mancinelli and McKay, 1988; Summers and Khare, 2007; M. L. Wong *et al.*, 2017; Ranjan *et al.*, 2019). Thus far, possible geochemical consumption mechanisms for dissolved NO_x^- species on early Earth included reduction to ammonia (Summers and Chang, 1993) and reduction to N_2 in the crust (Brandes *et al.*, 1998; Laneuville *et al.*, 2018). However, the NO_x^- conversion to ammonia was not significant at pH $\leq$ 7.3 (Summers and Chang, 1993), a regime that persisted in the bulk of the early ocean (Halevy and Bachan, 2017), and therefore restricted this NO_x^- sink to more alkaline environments such as ultramafic-hosted hydrothermal vents. In light of the NO_x^- reduction catalyzing potential of GR and magnetite, the question arises as to whether their precipitation in ferruginous seawater could have driven abiotic reactions that form N_2O at relevant rates sufficient to maintain atmospheric N_2O pools. As the major sink for N_2O is atmospheric photolysis back to N_2, such reactions could complete a fully abiotic denitrification from NO_x^- to N_2, hundreds of millions of years prior to the biological and more efficient production of N_2O (Buick, 2007).

Here, we evaluated the role of Archean abiotic N_2O production, including intermediary NO cycling, from NO_x^- compounds based on microcosm experiments with seawater mimicking ferruginous conditions. We used the mixed-valent iron minerals GR

18

and magnetite as catalysts for the reduction of low (1-5 μM), moderate (20-35 μM), and high (200-350 μM) NO_2^- and NO_3^- abundances and a simple end-member artificial seawater recipe with a 20% CO_2-HCO_3^- buffer devoid of sulfur. These experiments, together with diffusive and photochemical models, allowed for the estimation of NO and N_2O abundances within the ocean-atmosphere system of the Archean.

Methods

Mineral synthesis. Synthesis of carbonate green rust followed a slightly modified protocol (Bocher *et al*., 2004). In brief, 18.2 MΩ·cm water was made anoxic by boiling and sparging with CO_2/N_2 (20:80). Anoxic 0.4 M Fe^{2+}/Fe^{3+} solution (0.1 L) was prepared by mixing 7.42 g of $FeSO_4$*7 H_2O (>99%, Sigma Aldrich) and 2.66 g of anhydrous $Fe_2(SO_4)_3$ (97%, Sigma Aldrich). An alkaline, anoxic solution of 0.466 M Na_2CO_3 (Fisher Scientific) in 0.8 M NaOH (Fisher Scientific) (0.1 L) was prepared by dissolving NaOH first under constant stream of CO_2/N_2 gas, after which Na_2CO_3 was added. Both solutions were stirred continuously at 500 rpm. The alkaline solution was injected into the Fe^{2+}/Fe^{3+} solution using CO_2/N_2 flushed syringes. Precipitation occurred immediately and the suspension was stirred in the dark for 24 hours. Magnetite was synthesized as nanoparticles following previously described protocols (Pearce *et al*., 2012; Byrne *et al*., 2015).

Mineral harvest. Green rust and magnetite precipitates were washed in an anaerobic chamber (0.5% H_2 in N_2, Coy Laboratory Products) using a vacuum filter unit

(Nalgene, Mfr # 130-4020) and 0.45 μm cellulose-acetate filter membranes (Sartorius).

Anoxic 18.2 MΩ·cm water was poured onto the precipitates for a minimum of 8 cycles

(pouring followed by extracting water). When filtrate flow ceased to a minimum, the wet

mineral paste was removed from the filter. Wet carbonate green rust (73.8% water

content) and wet magnetite (47.2% water content) were added to microcosms. Wet

minerals were also used for product characterization (XRD and microscopy). For BET

analysis, a defined amount of precipitate was dried in small boxes filled with drierite and

placed into the anaerobic chamber. Dry weight was constant after 3-5 days.

X-ray diffractometry (XRD). Powder X-ray diffractometry was conducted on a

subset of samples after synthesis and washing of the mineral products. A glycerol smear

was prepared with 10 mg sample in the anaerobic chamber and sealed in a glass vial to

prevent oxidation prior to analysis. To collect the XRD data, the sample was removed

from the vial and stroke out onto a quartz zero background plate that was placed onto a

horizontal stage in a Bruker D-5000 diffractometer (Bruker, Germany) equipped with a

Co Kα X-ray tube (30 kV, λ = 1.791Å). Signal peaks were compared to reference

diffractograms in the RRUFF database (Downs, 2006). Instrument broadening was

determined by a standard polycrystalline alumina sample. X-ray diffractometry data was

analyzed with the CrystalDiffract software version 6.8.2 for Mac.

Scanning- and transmission-electron microscopy (SEM, TEM). Samples for SEM

imaging were mounted on aluminum pin stubs with double-sided carbon tabs in the glove

box and transported in a sealed jar with anoxic atmosphere to the microscope. Samples

were not sputter-coated. Images were taken on an XL30 ESEM-FEG (Philips) operated at a 30 kV accelerating voltage and a 21 pA beam current. TEM samples were dispersed on a Lacey Carbon film using 200 mesh copper grids. The instrument used was a CM200 Field Emission Microscope at 200KV (Philips) with C_s = 1.2 mm and a PTP resolution of 0.25 nm. Imaging was done on a Gatan Orius CCD system.

BET surface area measurements. For analysis of the Brunauer-Emmett-Teller (BET) surface area, dried mineral precipitate was weighed inside the anaerobic chamber and added to a Florence flask that was subsequently closed with a stopper for transport to the instrument. The BET surface in replicate samples (n = 3 for GR, n = 2 for magnetite) was quantified using N_2 gas on a Tristar II 3020 analyzer (Micromeritics Inc.). The instrument has a limit of detection of 1 m^2. Our results (Table B.1) are roughly consistent with previously determined BET values of 47 m^2 g^{-1} for GR (Williams and Scherer, 2001) and 95 m^2 g^{-1} for magnetite (Sun *et al*., 1998).

We performed calculations of the mineral surface area for both minerals to supplement our measurements. To derive the mineral density, we calculated the average crystallite size by inserting the full width at half maximum, as determined from the diffractograms and the Bragg angle of the GR 0 0 3 reflection and of the magnetite 3 1 1 reflection, into the Scherrer equation. Mineral density was then calculated using the formula ϱ = (M*Z)/(V_c*0.60225) where M is molar mass, Z is the number of molecules per crystallite and V_c is crystallite size. The density and the grain volume as measured by TEM/SEM were used to calculate the grain mass. The final value in m^2 g^{-1} was derived

from the grain mass and the grain surface (TEM/SEM). For magnetite, we calculated a surface area of 88.8 $m^2\ g^{-1}$. For green rust, we calculated a minimum approximation (surface of green rust sheets only) of 27.6 $m^2\ g^{-1}$ and a maximum approximation (including surface between sheets) of 538.5 $m^2\ g^{-1}$. Thus, our measured value for magnetite is somewhat lower than the calculated and literature value. The measured value for green rust is in good agreement with the literature value and at the lower end of the calculated range.

Incubation conditions. Interactions of nitrogen oxides with Fe minerals were tested in anoxic microcosms designed to mimic Archean ocean conditions as closely as possible. Borosilicate glass bottles (30-120 mL) were closed with thick butyl rubber stoppers and a headspace consisting of 20% CO_2 in N_2 was used throughout the experiment. All glassware was washed with 2 M HCl prior to use. The liquid phase constituted one third of the microcosm total volume. We used a previously applied recipe for artificial Archean seawater (Anbar and Holland, 1992) and omitted any sulfur species. The pH was initially set to 7.3 using a CO_2–HCO_3^- buffer. We boiled 18.2 MΩ·cm water and sparged it with CO_2/N_2 (20:80) while it was cooling on ice. Salts were added during sparging. The anoxic solution was then dispensed with a pipetor into microcosms in an anaerobic chamber (0.5% H_2 in N_2, Coy Laboratory Products). Nitrate and nitrite stock solutions were prepared with their respective sodium salts $NaNO_3$ (≥99%, Fisher Scientific) and $NaNO_2$ (≥97%, Acros Organics) and dissolved in artificial seawater. The solutions were then sparged with N_2 and filter-sterilized (0.8/0.2 μm pore seize, VWR) in the anaerobic chamber. Controls with aqueous Fe^{2+} were prepared with anoxic artificial

seawater and $FeCl_2$ (≥99%, Fisher Scientific). Wet minerals were weighed in the anaerobic chamber and distributed into microcosms using ethanol-washed plastic spatulas. Prior to start of the incubations with the injection of the NO_x^- solution, mineral agglomerates were dissipated in an ultrasonic bath (Ultrasonic cleaner 2510, Branson Ultrasonics). Microcosms were shaken at 250 rpm in the dark and at room temperature over the whole duration of the experiment. Controls were incubated in the anaerobic chamber to test for potential leaking through stoppers, which did not occur. To dissolve mineral particles during incubations, 1.6 mL of concentrated 12N HCl or 37N H_2SO_4 was slowly injected through bottle septa to 10 mL mineral seawater-suspension. Dissolution of solid particles occurred instantly and the liquid first turned turbid orange-green and then clear green-yellow (HCl) or light yellow (H_2SO_4) within 15-20 hours. The last measurement of NO in the headspace was taken when the liquid was clear (Fig. B.5).

Dissolved nitrite, nitrate, ammonium, ferrous and ferric iron measurements. All dissolved analytes were quantified spectrometrically with plate assays. Nitrite in solution was quantified with the Griess reagent (Promega, Kit G2930). Nitrate was first reduced to nitrite by vanadium(III) chloride and then quantified as nitrite (Miranda *et al.*, 2001). Ammonium production was verified with the salicylic acid assay (Kandeler and Gerber, 1988). To determine the Fe^{2+}/Fe^{3+} solid phase ratio, mineral particles were settled, after which supernatant artificial seawater was removed from the microcosms. Anoxic acidic extraction of green rust and magnetite was conducted as described previously (Byrne *et al.*, 2015). Ferrous and ferric ions in the extracts were measured by reaction with ferrozine (Stookey, 1970).

23

N$_2$O gas measurements. To quantify N$_2$O production, 200 μL of headspace gas was sampled with a gas-tight syringe (VICI Precision Sampling) and injected onto a gas chromatograph (GC, SRI Instruments) equipped with an electron-capture detector (ECD). Two continuous HayeSep-D columns were kept at 90°C (oven temperature) and N$_2$ (UHP grade 99.999%, Praxair Inc.) was used as carrier gas. The ECD current was 250 mV and the ECD cell was kept at 350°C. The N$_2$O measurements were calibrated using customized standard mixtures (Scott Specialty Gases, accuracy ±5%) over a range of 0.25–100 ppmv. Gas accumulation in the microcosms was monitored over time. Gas concentrations were corrected using Henry's law and the dimensionless concentration constant K_H^{cc}(N$_2$O) = 0.6112 (Stumm and Morgan, 2012) to account for gas partitioning into the aqueous phase at 25°C.

NO gas measurements. Nitric oxide (NO) was quantified in the microcosm headspace with a chemiluminescence-based analyzer (LMA-3D NO$_2$ analyzer, Unisearch Associates Inc.). Headspace gas was withdrawn with a CO$_2$-N$_2$-flushed gas-tight syringe and injected into the analyzer. The injection port was customized to fit the injection volume and consisted of a T-junction with an air filter at one and a septum at the other end. An internal pump generated consistent airflow. In short, sample NO was oxidized to NO$_2$ by a CrO$_3$ catalyst. The NO$_2$ flew across a fabric wick saturated with a Luminol solution. Luminol was obtained from Drummond Technology Incorporated. Readings were corrected for background NO$_2$ every 15 minutes ("zeroing"). Shell airflow rate was kept at 500 mL min^{-1} and the span potentiometer was set to 8. Measurements were

calibrated with a 0.1 ppm NO (in N_2) standard (<0.0005 ppm NO_2, Scott-Marin,

Riverside, CA, USA) over a range of 5–1,000 ppbv. Gas concentrations were corrected

using Henry's law and the dimensionless concentration constant $K_H^{cc}(NO) = 0.0465$

(Stumm and Morgan, 2012) to account for gas partitioning into the aqueous phase at

25°C.

Diffusion modeling. The partial fluxes of the overall flux balance $\Phi_{sed} + \Phi_{par} = \Phi_{atm}$ were normalized to a 100 m vertical slab with 1 m^2 basis. The upper 100 m ocean

water are typically considered as well-mixed, hence, reactant and catalyst are

homogeneously distributed in that space. Depending on the water depth, a portion of the

NO_x could reach the ocean floor, which is why we added a generic sediment flux (Φ_{sed}) to

the balance equation. The dominant flux would emerge from floating GR mineral

particles (Φ_{par}) that are distributed along the water column. For simplicity, we assume

that all GR had aged into magnetite in the sediment and all suspended particles were GR

phases. The sediment N_2O flux was derived as follows.

$$\Phi_{sed} = - \Phi_{NO2-} = -D_e \frac{dC}{dR} (x = 0)$$

where D_e is the effective diffusion coefficient (4.1*10^{-6} m^2 hr^{-1}), and dC/dR (x = 0) is the

concentration gradient at the sediment-water interface (–55.7 μM m^{-1}). In this simple

pore water diffusion model, Φ_{sed} equals the flux of NO_2^- into the sediment (Φ_{NO2-}). The

model parameters were obtained from Li and Gregory, 1974. We used the NO_2^- diffusion

coefficient determined for seawater. Since we assumed a dominance of magnetite over

GR in sediments, the reaction rate constant based on magnetite-catalyzed reactions was

used ($3.2*10^{-3}$ hr^{-1}). We also assumed a steady-state NO_2^- concentration of 2 μM in the bottom water just above the sediment (M. L. Wong *et al.*, 2017; R. Hu and Diaz, 2019).

We tested if diffusion limitation would occur in the GR particle phase. Based on our kinetic results from the GR experiment, we assumed a reaction rate constant of $3.2*10^{-2}$ hr^{-1}. Using a particle size of 1 μm (particle diameter, SEM) up to 0.5 mm (agglomerates), the spherical particle model applied (Magyari, 2010) did not indicate a concentration gradient of NO_2^- from the particle surface to the center. Thus, the Fe mineral phase was completely disseminated in the seawater. We formulated the N_2O particle flux as follows.

$$\Phi_{par} = r(\text{GR})\,SA_{GR}\,[GR]\,100m$$

where mineral surface area is $SA_{GR} = 57.1$ m^2 g^{-1} and a molecular N_2O production rate $r(\text{GR})$ is depending on the initial reactant concentration:

low NO_2^- 0.004 ± 0.001 nmol m^{-2}_{GR} hr^{-1}

moderate NO_2^- 0.07 ± 0.01 nmol m^{-2}_{GR} hr^{-1}

high NO_2^- 2.6 ± 0.5 nmol m^{-2}_{GR} hr^{-1}

Including the components of the partial fluxes, we can rewrite the overall flux balance as function of the green rust particle concentration [GR].

$$\Phi_{atm}([GR]) = \Phi_{sed} + r(\text{GR})\,SA_{GR}\,[GR]\,100m$$

Informed by seven modern marine and freshwater anoxic basins (Bacon *et al.*, 1980; B. L. Lewis and Landing, 1991; Viollier *et al.*, 1997; Rodrigo *et al.*, 2001; C. Jones *et al.*, 2011; Staubwasser *et al.*, 2013; Llirós *et al.*, 2015), we used [GR] values

equivalent to half and 5 times the particle Fe^{2+} concentration reported for Kabuno Bay

(KB) in East Africa (Llirós *et al.*, 2015).

We also calculated the N_2O steady-state concentration based on equilibration with

the atmosphere (Table B.4). Actual dissolved N_2O concentrations, especially in proximity

to GR particles, may have been higher (out of equilibrium). We used a frequently applied

and updated method (Wanninkhof, 2014) to describe gas exchange at the sea-air

interface. The equation was solved for the difference in partial pressures of N_2O in the

water and the air above.

$$pN_2O_{water} - pN_2O_{air} = \frac{\Phi_{atm}}{0.251 < U^2 > \left(\frac{S_c}{668}\right)^{-0.5} K_0}$$

where $<U^2>$ is the average squared wind speed (U=7.4 m s^{-1}) and S_c is the Schmidt

number for N_2O (697 at 20°C, (Weiss and B. A. Price, 1980)). The volumetric solubility

coefficient K_0 was $2.729*10^{-2}$ mol L^{-1} atm^{-1} at 20°C and 10 ‰ salinity (Weiss and B. A.

Price, 1980).

Error propagation. We used a developed matlab script (Robens, 2017) to

propagate the error caused by co-variation of basic parameters. These comprised the

measured molecular N_2O production rates from green rust r(GR) (n = 9-10). First, a

Monte Carlo parameter simulation with 1 million iterations by bootstrapping generated a

distribution around the mean. Second, the error was propagated based on the 95%

confidence interval and using the flux equation for Φ_{atm}. The four fluxes that were used as

input for the photochemical model have a statistical distribution as shown in Figure B.7.

Thermodynamic calculations. The affinity per electron of each redox reaction depicted in Figure B.8 was calculated via

$$A_r = \left(\frac{1}{e_r}\right) RT \ln \left(\frac{K_r}{Q_r}\right)$$

where R is the gas constant, T is the temperature in kelvin, K_r is the reaction constant, Q_r the reaction quotient, and e_r is the number of electrons transferred, all for the reaction r. K_r is

$$K_r = \prod_i a_i^{v_{i,r}}$$

where a_i is the thermodynamic activity of species i and $v_{i,r}$ its stoichiometry in r. K_r becomes a ratio when the standard convention of negative stoichiometry for reactants and positive stoichiometry for products is applied. Thus K_r is defined at equilibrium by the ratio of products to reactants for a system experiencing no net movement of r in either direction. Q_r is defined similarly, but populated with the activities of species in an actual system (equilibrium or otherwise). In this way, the affinity calculation is a measure of the amount of energy, which might be realized if Q_r is brought to K_r (i.e., if a system is brought to equilibrium). In the reactions explored here, K_r has been calculated from thermodynamic data in the same manner as references Shock and Canovas, 2010; Shock *et al*., 2010 and sources therein, utilizing the SUPCRT family of codes (Johnson *et al*., 1992), and Q_r has been set experimentally to explore the potential for these reactions in Archean conditions.

Archean ocean conditions in our experiments and model represent approximations based on literature and our own data. H_2 abundance was informed by reference (Canfield *et al.*, 2006) and includes typical values for marine systems undergoing active methanogenesis. NO_3^- was set to 20 μM to be consistent with our tested conditions and the NO_3^-/ NO_2^- ratio was 4:1 as derived experimentally (Summers and Khare, 2007). We used the calculated steady-state concentration for N_2O (~5 nM) and 635 μM dissolved N_2, which is in equilibrium with modern atmospheric N_2 levels. CO_2 concentration was set to the experimental value and methane was chosen on a tentative range with a maximum value as measured at marine methane seeps (Joye *et al.*, 2004).

Photochemical modeling. We have used an atmospheric photochemistry model to simulate the effects of N_2O emission into an anoxic atmosphere akin to the Archean Earth's condition. The photochemistry model used (R. Hu *et al.*, 2012; R. Hu *et al.*, 2013) has been validated by computing the atmospheric compositions of present-day Earth and Mars, as the outputs agreed with the observations of major trace gases in Earth's and Mars' atmospheres (R. Hu, 2013). For this work, we simulate a 1-bar atmosphere of 95% N_2 and 5% CO_2 to approximate the anoxic and CO_2-rich environment of the Archean Earth. We assume a surface temperature of 288 K and a stratospheric temperature of 200 K, and adopt the eddy diffusion coefficient derived from the number density profiles of trace gases on Earth (Massie and Hunten, 1981). The photochemistry model includes a comprehensive reaction network for O, H, C, N, and S species including sulfur and sulfuric acid aerosols, and includes volcanic outgassing of CO, H_2, SO_2, and H_2S. The outgassing rate is not high enough to produce a H_2SO_4 aerosol layer in the atmosphere.

Results & Discussion

We first compared the reactivity of NO_2^- and NO_3^- with GR, magnetite and

aqueous Fe^{2+} separately. For all reductants, consumption of NO_3^- and N_2O production

was negligible (< 0.03 nmol h^{-1}, Fig. 2.1A) even over a prolonged period of 100 days

(data not shown). In contrast, NO_2^- showed reactivity in the presence of both mineral

catalysts, and was stable in controls with 500 μM aqueous Fe^{2+}. The contrasting reactivity

of the nitrogen oxides was also reflected in the solid phase Fe^{2+}/Fe^{3+} ratio determined at

the end of the experiment (Fig. 2.2), revealing a trend of higher mineral oxidation with

increasing NO_2^- concentration. Magnetite and GR showed contrasting potential to

produce N_2O. Concomitant with a more rapid NO_2^- consumption, N_2O production rates

were more than 10 times higher when GR was the catalyst (Fig. 2.1B). At specific GR

surface areas as observed for the Archean ocean analogue Lake Matano, Indonesia

(Zegeye *et al*., 2012, Fig. 2.1C), abiotic N_2O production rates were more than twice the

biotic production rates measured in modern oxygen minimum zones ($\sim$1 nM day^{-1}, Ji *et*

al., 2015).
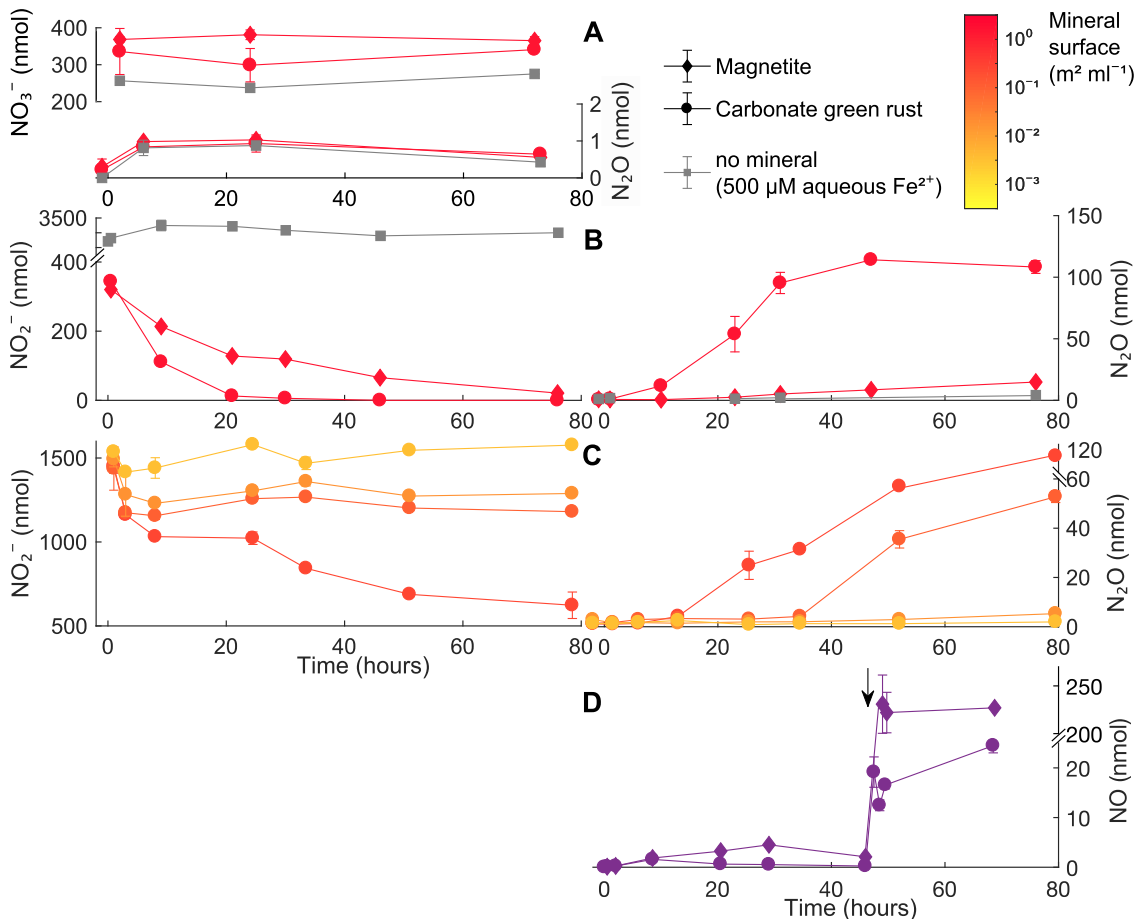
Fig. 2.1. Molecular NO_x^- consumption followed by NO and N_2O production with Fe minerals or aqueous Fe^{2+}. Dissolved NO_3^- and NO_2^- in anoxic artificial seawater solution was quantified concomitantly to NO and N_2O in the headspace. The y-axes depict total quantities (gas + liquid phase) and are sometimes interrupted by breaks to better illustrate changes. (**A**) NO_3^- amended microcosms with GR and magnetite. (**B**) NO_2^- amended microcosms with GR and magnetite. (**C**) NO_2^- reduction and N_2O production under varying GR mineral surface area as controlled by the GR mass added. After an initial phase of rapid NO_2^- consumption, mineral surface may become space-limited hindering the reduction of more NO_2^-. (**D**) NO formation during mineral incubations with moderate (33 μM) initial NO_2^-. The arrow indicates addition of concentrated hydrochloric acid resulting in subsequent mineral particle dissolution and outgassing of NO. Error bars denote one SD (n = 3).
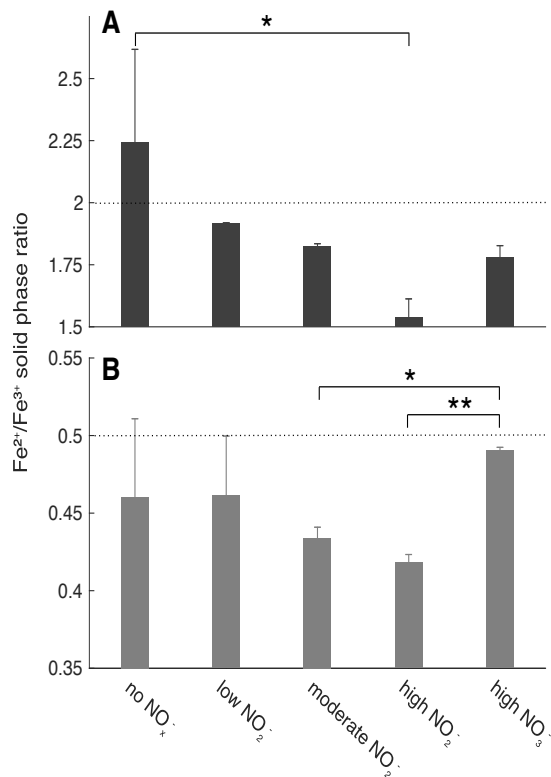
Fig. 2.2. Solid phase ratio of reduced and oxidized Fe in GR (A) and magnetite (B). Data was collected after acid digestion at the end of incubations. The spotted lines indicate stoichiometric GR and magnetite, respectively. For initial $[NO_x^-]$, see Fig. 2.1 and table B.3. $*P < 0.05$, $**P < 0.01$, Student's t test. Error bars denote one SD (n = 2-3).

The conversion of NO_2^- to N_2O was not equimolarily balanced and we therefore considered accumulation of NO as intermediary species (Grabb *et al*., 2017). After observing an initial mild NO accumulation, we injected concentrated hydrochloric acid in order to dissolve mineral particles and release any fraction bound to mineral surfaces (Fig. 2.1D). Indeed, the dissolution of mineral particles was followed by a spike in headspace NO concentration. At least 92% of the total amount of NO produced was bound to GR surfaces (97% was bound to magnetite surfaces). To rule out reaction of the acid itself with residual NO_2^-, we conducted controls with sulfuric acid and NO_2^- (Table

B.2). Other controls to evaluate the stability of NO in the mineral suspension included acid injection at later time points in time-extended experiments observing NO yields at 220 hours ($< 2.5 \, \mu$M NO$_2^-$) similar to those at 50 hours after NO$_2^-$ addition (Table B.2). We calculated the yield of NO in respect to the total added NO$_2^-$ and, accordingly, 7% reacted to NO (over 63% that reacted to N$_2$O) with GR as catalyst and 69% reacted to NO (over 8% that reacted to N$_2$O) with magnetite as catalyst. The remaining product pool could be N$_2$ (Grabb *et al*., 2017) and would only constitute a minor fraction of the total added nitrogen. Our data show that mineral-associated NO, presumably in the form of nitrosyl species (Gordon *et al*., 2013), is a significant byproduct and geochemically stable in presence of Fe mineral phases.

To elucidate the impact of the experimentally derived production rates for the dispersion of N$_2$O in the seawater and emission to the Archean atmosphere, we combined diffusion models into a simple flux balance model (Methods). We considered a 100 m deep slab of ocean beneath the photic zone as the part of the water column with a maximum overlap of NO$_x^-$ ions from the surface and GR formation fueled by upwelling water rich in Fe^{2+} from the depth. An estimate of the GR particle concentration in the Archean ocean was informed by observed Fe particle numbers from seven modern marine and freshwater anoxic basins, including the anoxic lake basin Kabuno Bay (KB) in East Africa (Llirós *et al*., 2015). The peak Fe^{2+} concentration in the particulate fraction of KB anoxic waters (11 μM) closely reflects concentrations used for the thermodynamic modeling of GR precipitation in Archean seawater (Halevy *et al*., 2017), which is why we used KB levels as a reference and enveloped that value with a putative lower and upper boundary of 50% and 500%. Archean seawater Fe^{2+} could have reached

concentrations of 55 μM, as constrained by Fe^{2+} toxicities on cyanobacteria (Swanner *et al.*, 2015). At that upper boundary, net N_2O emissions conceivably reached 3627.0 [2103.7 - 5411.5] nmol m^{-2} h^{-1} (95% CI, Fig. B.7, Table B.4), implicating 64 times the modern marine average flux (Battaglia and Joos, 2018). Overall, N_2O emissions from the ferruginous ocean gradually increased with the GR particle concentration in the water column.

To simulate the effect of N_2O fluxes triggered by mineral catalysis into an anoxic Archean atmosphere, we applied a photochemical model (R. Hu *et al.*, 2012). We probed four different N_2O fluxes corresponding to low and moderate NO_2^- levels and Fe^{2+} concentrations in GR phases around the KB reference (Table B.4). Intriguingly, the upper boundary of our estimates implicated near-modern N_2O concentrations in the troposphere (0-13 km altitude, Fig. 2.3). Even particulate Fe^{2+} concentrations equivalent to those found in KB resulted in atmospheric N_2O abundances that resided within one order of magnitude of modern levels and our lowest estimates predicted N_2O abundances of 1-7 ppb. This range is consistent with mixing ratios from Proterozoic atmosphere models assuming 1% of present oxygen levels (Roberson *et al.*, 2011; Stanton *et al.*, 2018). A striking difference is, however, the source of NO_x^- compounds, which was assumed to be microbial nitrification in the Proterozoic and abiotic nitrogen fixation prior to the GOE. Thus, abiotically derived NO_x^- can potentially produce tropospheric N_2O levels equal to those from biological origins.
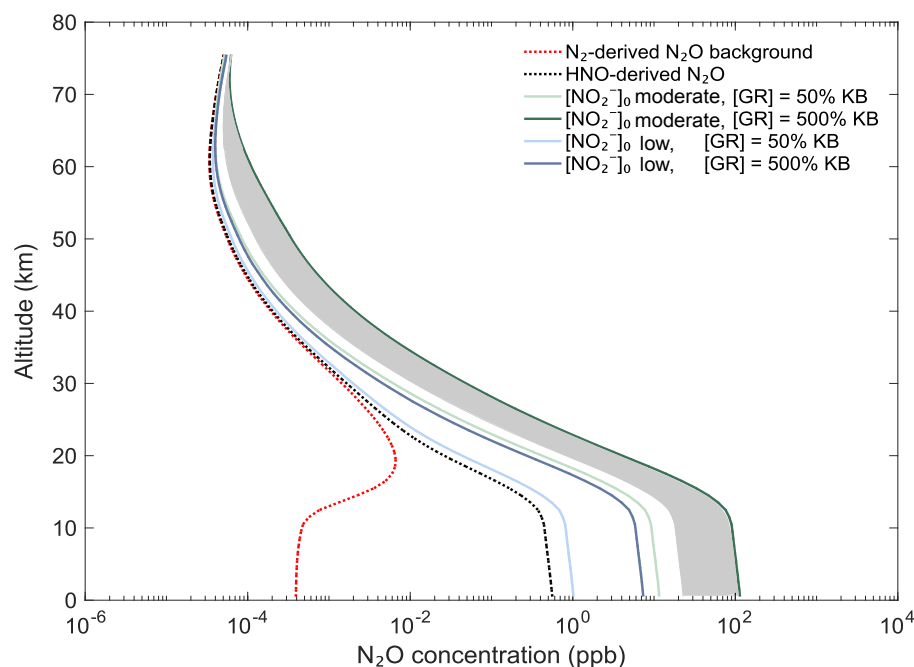
Fig. 2.3. Atmospheric N_2O abundances under influence of mineral-catalyzed N_2O production in the Archean ocean. Abundances are based on fluxes assuming GR phases in KB equivalents and low (blue) and moderate (green) seawater NO_2^- levels. The gray area marks the flux range potentially limited by NO_2^- supply (see text). Background N_2O formation occurred via the reaction $N_2 + O(^1D) + M \rightarrow N_2O + M$ and $O(^1D)$ was produced by photodissociation of CO_2 with photons more energetic than 167 nm. N_2O can also be derived directly through dehydrative dimerization of HNO that did not polymerize into NO_3^- or NO_2^- (R. Hu and Diaz, 2019), but that contribution appeared to be minor. N_2O profiles based on mineral-catalyzed production do not account for N_2O from the HNO pathway.

On basis of the model outputs we evaluated how abiotic nitrogen fixation rates or availability of mineral surfaces could have potentially limited N_2O source fluxes. Given GR phases at 50% KB equivalence (lower boundary), moderate seawater NO_2^- levels, and a 70% ocean cover of Earth's surface, N_2O emissions exported 32.9 Tg N yr^{-1} into the Archean atmosphere. Significant amounts of mineral surface-bound NO could have been transported down to the seafloor by settling of GR and magnetite precipitates. Assuming a particle sinking velocity of 50 m day^{-1} (McDonnell and Buesseler, 2010), 5.8 Tg N yr^{-1}

in the form of NO could have reached ocean sediments. Considering that heat shock reactions maintained a constant N_2 to NO_x^- flux of up to ~40 Tg N yr^{-1} (Laneuville *et al.*, 2018), it becomes clear that NO_x^- fluxes sufficed to maintain N_2O ocean-atmosphere fluxes at 50% KB, but that doubling of the Fe particle concentration would exceed total NO_x^- supply. We indicated this critical point with a gray area in Figure 2.3 to highlight fluxes that were feasible based on mineral catalysis, but likely restricted by reactant supply. Therefore, the formation of N_2O and NO in the ferruginous ocean was limited by the rate of abiotic nitrogen fixation and not by mineral abundance.

The main sink of N_2O is photolysis by radiation < 230 nm (Kaiser *et al.*, 2003) in the stratosphere which governs the shape of the concentration profiles (Fig. 2.3). In the Archean atmosphere, N_2O abundances could have been higher due to i) additional sources and ii) protective agents against UV light. For instance, high-energy particles from solar flares led to N_2O formation most active at higher altitudes and could complement surface sources (Airapetian *et al.*, 2016). These pathways played perhaps a more significant role in the Hadean or early Archean when the Sun was more active (Airapetian and Usmanov, 2016) and the magnetic field openings were greater at the poles (Tarduno *et al.*, 2014). Furthermore, in the presence of methane hazes as proposed for the Archean, N_2O could have been shielded through strong UV absorption by fractal haze particles (E. T. Wolf and Toon, 2010), which prolonged its lifetime. Both processes could have helped to stabilize atmospheric N_2O abundances that resulted from mineral-catalyzed N_2O production in the oceans.

Despite the tropospheric abundances predicted by our model, effects on the planetary climate were probably modest because N_2O would not be sufficiently concentrated to compensate overlay of absorption bands with those from CO_2. Especially in high CO_2 atmospheres, the N_2O radiative forcing is diminished since it may not occupy otherwise transparent infrared windows. The infrared window between 6 and 8 μm could potentially be filled by N_2O absorption, but this is dependent on atmospheric methane which absorbs at similar wavelengths (Roberson *et al.*, 2011). Since methane concentrations were likely > 100 ppmv (Catling *et al.*, 2001), greenhouse warming by N_2O under our simulated conditions therefore contributed only weakly to a warmer climate under the faint young Sun of the Archean (Gough, 1981).

It is plausible that as life co-evolved with the Earth system (Dietrich *et al.*, 2006), it could have done so on a molecular level as an adaptation to abiotic NO and N_2O fluxes, too. Under generally accepted Archean ocean conditions, N_2O reduction to N_2 is thermodynamically favorable. For example, coupled to H_2 oxidation (H_2 as a simple and available reductant), an affinity of up to 300 kcal per electron accepted by N_2O is significantly higher than that of any other redox reaction tested (Fig. B.8). Settling of GR precipitates may have been an effective way of shuttling NO molecules to benthic microbial life, where it then acted as a biological electron sink (Ducluzeau *et al.*, 2009), Fig. 2.4). Indeed, based on enzymatic structural resemblance of NO and N_2O reductases (Nor and Nos) with cytochrome c oxidase (Viebrock and Zumft, 1988; Saraste and Castresana, 1994; Stanton *et al.*, 2018) a primitive form of N_2O reduction likely preceded aerobic respiration. This concept is supported by a simple make-up of the respiratory chains involving quinone-dependent Nor and membrane-bound Nos, as present in some

gram(+) bacteria (Suharti and de Vries, 2005; Chen and Strous, 2013). Along these lines, the existence of NO and N_2O in the water column could have been feasibly exploited for the conversion of free energy and can at least explain biochemical patterns in modern respiratory enzyme complexes.
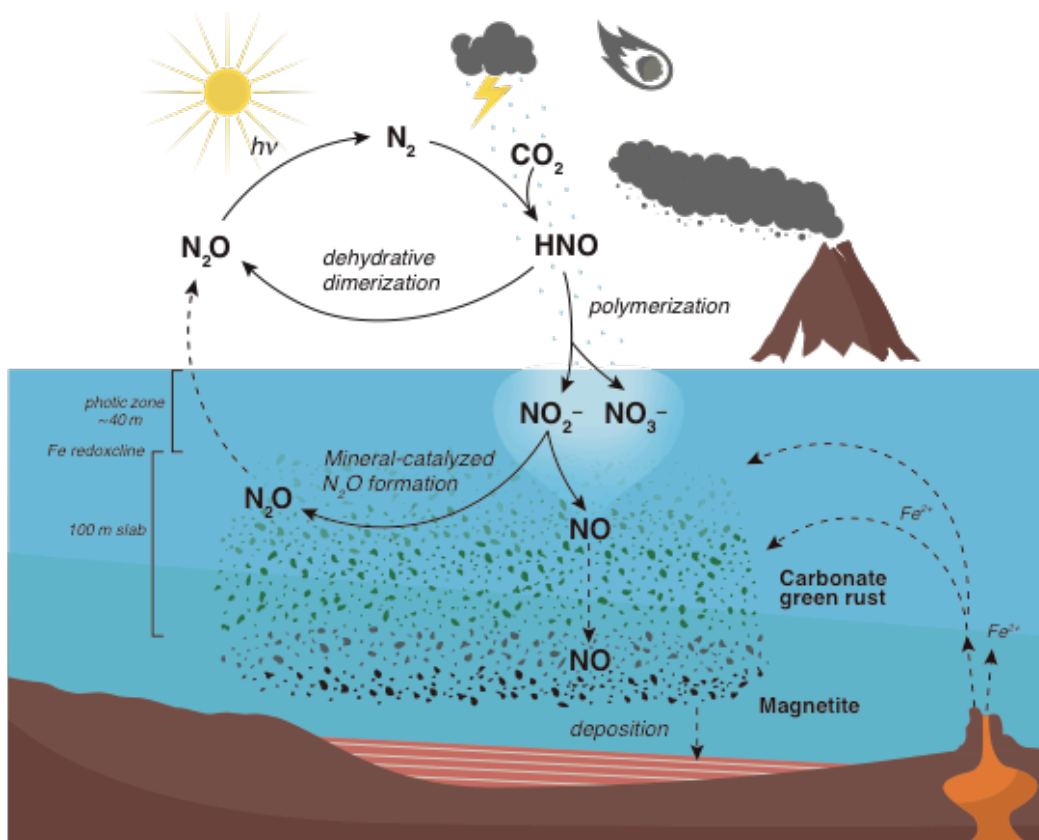
Fig. 2.4. Schematic depiction of mineral-catalyzed NO and N_2O formation at the junction of the early nitrogen and iron cycle. Heat shock reactions, such as stimulated by galactic cosmic rays, meteoritic impact plumes, volcanic and thunderstorm lightening, produced the central precursor HNO, which dimerized directly to N_2O or polymerized into NO_2^- and NO_3^- (R. Hu and Diaz, 2019). These nitrogen oxides became interspersed into the surface ocean as plumes in the wake of distinct rain events and could have maintained average concentrations in surface seawater corresponding to low and moderate levels used in our experiments. Any NO_3^- accumulated due to inefficient sinks. Upwelling Fe^{2+} precipitated into Fe oxyhydroxides and GR in the Fe redoxcline. Driven by Fe mineral phases, NO_2^- was reduced to N_2O. The abiotic nitrogen cycle was closed by photolytic destruction of emitted N_2O to N_2. As a byproduct, NO molecules remained bound at the mineral surface as nitrosyl. This way, GR may have served as an NO shuttle enabling transport of nitrogen oxides into the deep ocean. Sinking GR particles

transformed into magnetite, which then was deposited. Dashed lines mark diffusive or gravitational transport, whereas solid lines indicate chemical reactions.

Conclusion

Our findings show that a significant portion of NO_x^- in the ferruginous Archean ocean was likely diverted to N_2O and NO leading to more oxidized products when compared to other sink channels (ending in N_2 or ammonia). If this was the case, then the degree of thermodynamic disequilibria in the redox balance of the Archean nitrogen cycle may have been underestimated (Krissansen-Totton *et al*., 2018). Correspondingly, we caution to use N_2O as unique biosignature in exoplanet exploration. It is possible that conditions for the mineral-catalyzed N_2O production on early Earth-like exoplanets are even more favorable, resulting in N_2O atmospheric concentrations that could exceed modern ones (higher abiotic nitrogen fixation rates, higher Fe mineral load). Signals could be interpreted as false positives without any biological basis.

We present evidence that higher ozone levels may not be required to reach near-modern (ppb) N_2O concentrations prior to the GOE and lay out a concept of a complete abiotic N_2O cycle driven by mineral-catalyzed reactions (Fig. 2.4). Rather than being a mainly biological invention, the abiotic nitrogen cycle was seemingly co-opted by early organisms. Even though the effects of abiotic N_2O production were probably modest on the early climate, it could have markedly influenced the evolution of microbial respiration.

CHAPTER 3

EFFECTS OF STERILIZATION TECHNIQUES ON CHEMODENITRIFICATION

AND N$_2$O PRODUCTION IN TROPICAL PEAT SOIL MICROCOSMS[2]

Abstract

Chemodenitrification – the non-enzymatic process of nitrite reduction – may be

an important sink for fixed nitrogen in tropical peatlands. Rates and products of

chemodenitrification are dependent on O$_2$, pH, Fe^{2+} concentration, and organic matter

composition, which are variable across peat soils. Assessing abiotic reaction pathways is

difficult because sterilization and inhibition agents can alter the availability of reactants

by changing iron speciation and organic matter composition. We compared six

commonly used soil sterilization techniques – γ irradiation, chloroform, autoclaving, and

the use of three different chemical inhibitors (mercury, zinc, and azide) – for their

compatibility with chemodenitrification assays for tropical peatland soils (organic-rich,

low-pH soil from the eastern Amazon). Out of the six techniques, γ irradiation resulted in

soil treatments with the lowest cell viability and denitrification activity and the least

effect on pH, iron speciation, and organic matter composition. Nitrite depletion rates in γ-

irradiated soils were highly similar to untreated (live) soils, whereas other sterilization

techniques showed deviations. Chemodenitrification was a dominant process of nitrite

consumption in tropical peatland soils assayed in this study. Nitrous oxide (N$_2$O) is one

possible product of chemodenitrification reactions. Abiotic N$_2$O production was low to

moderate (3 %–16 % of converted nitrite), and different sterilization techniques lead to

significant variations on production rates due to inherent processes or potential artifacts.

---

[2] This chapter was published in *Biogeosciences* (Buessecker *et al.*, 2019).

Our work represents the first methodological basis for testing the abiotic denitrification and N_2O production potential in tropical peatland soil.

Introduction

Across ecosystems, physical and chemical factors, such as solar radiation or redox gradients, can drive abiotic chemical transformations. The nitrogen (N) cycle, in particular, includes abiotic reactions that can affect the retention of nutrients or substrates (Clark, 1962; McCalley and Sparks, 2009; Parton *et al.*, 2007). Abiotic formation of N-containing gases has long been known (Wullstein and Gilmour, 1966; Jun *et al.*, 1970). A major abiotic process in the N cycle is chemodenitrification, the stepwise reduction of nitrite (NO_2^-) to gaseous products, namely nitric oxide (NO), nitrous oxide (N_2O), or dinitrogen (N_2), often coupled to iron (Fe^{2+}) oxidation, as described in Eqs. (1) and (2) (Davidson *et al.*, 2003; Kampschreur *et al.*, 2011; X. Zhu *et al.*, 2013; Zhu-Barker *et al.*, 2015).

$$NO_2^- + Fe^{2+} + 2H^+ \rightarrow NO + Fe^{3+} + H_2O \qquad \text{(Eq. 1)}$$

$$2NO + 2Fe^{2+} + 2H^+ \rightarrow N_2O + 2Fe^{3+} + H_2O \qquad \text{(Eq. 2)}$$
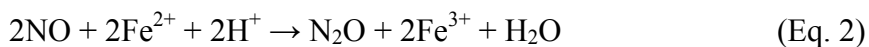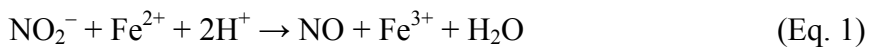
Equations (1) and (2) are plausible in soils and sediments (L. C. Jones *et al.*, 2015). The abiotic reduction of N_2O to N_2 is not well known. It has been associated with the presence of copper (Moraghan and Buresh, 1977), but this species is unlikely to be present at sufficient levels in peat soils to promote this reaction. Anoxic tropical peat soils are expected to have the ideal conditions for chemodenitrification: low O_2, low pH, high organic matter (OM), and high Fe^{2+} (Porter, 1969; Nelson and Bremner, 1969; Van Cleemput *et al.*, 1976; Kappelmeyer *et al.*, 2003). In these ecosystems, NO_x^- is supplied

by nitrification fueled by organic N mineralization or from external sources (fertilization, wet or dry deposition). Besides metals, reduction of NO_x^- compounds can also be mediated by organic functional groups found in soils. Abiotic phenol oxidation occurs at oxic–anoxic interfaces in tropical soils and may be linked to the N cycle (Steven J Hall and Silver, 2013). In such reactions, NO_2^- can be reduced by phenolic groups to form the nitrosonium cation NO^+, which can either (1) remain fixed within the organic compound as nitrosophenol (Thorn and Mikita, 2000; Thorn et al., 2010) or (2) be emitted in gaseous form. After tautomerization to an oxime (Raczyńska et al., 2005) and reaction with NO^+ derived from a second NO_2^- ion, hyponitrous acid ($H_2N_2O_2$) can be produced, which further decomposes to N_2O (Porter, 1969):
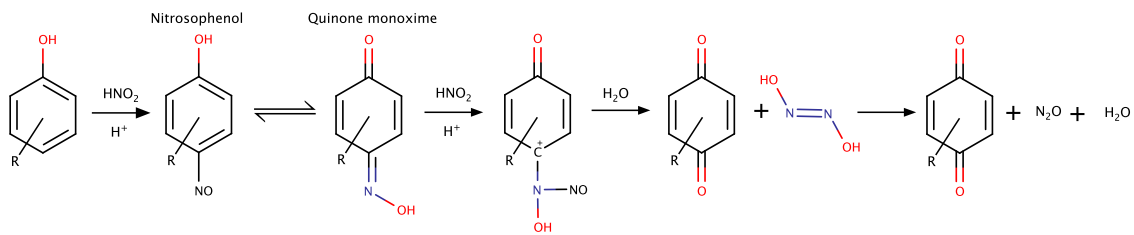
Other OM-dependent NO_2^- reduction pathways can produce NO and N_2 (McKenney et al., 1990; Thorn et al., 2010) instead of N_2O. The importance of abiotic N transformations in environmental samples has been notoriously difficult to quantify due to the artifacts emerging from physical or chemical "killing" methods intended to eliminate biological activity but affecting metals, organic matter, or other pools. In order to distinguish denitrification from chemodenitrification, enzymes contributing to gaseous N production must be inactivated, most commonly by addition of sterilants or inhibitors. An efficient sterilization treatment ideally (1) contains a negligible number of live cells, (2) eliminates biological activity, and (3) has little or no effect,

directly or indirectly, on abiotic reactions (e.g., it should neither alter mineral structure nor lyse cells because release of cellular contents could influence abiotic reactions). Because rates and products of chemodenitrification are dependent on O_2, pH, Fe^{2+} concentration, and OM composition, it is important to assess whether a sterilant or inhibitor elicits a physicochemical change that can affect the availability or interaction of these reactants.

Soil sterilization techniques include γ irradiation, chloroform ($CHCl_3$) fumigation, autoclaving, and addition of chemical inhibitors such as mercury (Hg), zinc (Zn), or azide (N_3). Highly energetic γ irradiation damages enzymes and cell components, rendering cells nonviable and inactive, generally with minimal effect on soil chemistry (Trevors, 1996). Autoclaving with high-pressure steam disrupts cell membranes, denatures proteins, and decreases aromaticity and polycondensation of soil OM (Jenkinson and Powlson, 1976; Trevors, 1996; Berns *et al*., 2008). Fumigation with $CHCl_3$ induces cell lysis and has minimal effect on enzymes (Blankinship *et al*., 2014). Chemicals like Hg, Zn, and N_3 do the opposite: they inhibit enzymes (Bowler *et al*., 2006; McDevitt *et al*., 2011) but do not lyse cells (D. C. Wolf *et al*., 1989).

We evaluated the appropriateness of six sterilants (γ irradiation, autoclaving, $CHCl_3$, Hg, Zn, and N_3) for chemodenitrification measurements in low-O_2, low-pH, high-OM soils from a tropical peatland. First, we tested the effects of sterilants on cell membrane viability and biological denitrification activity. Next, we evaluated the effects of sterilants on soil chemistry (pH, OM composition, and extractable Fe). Finally, we assessed the effects of the six sterilants on chemodenitrification measured by NO_2^- depletion and N_2O production.

43

Methods

Sample characteristics. Soil samples were collected in October 2015 from a
tropical peatland, locally known as Quistococha (03°50.024′ S 73°19.235′ W), near Iquitos
(Loreto, Peru). The soil geochemistry of this site has been described previously
(Lähteenoja *et al.*, 2009; Lawson *et al.*, 2014). The samples were obtained from depths of
15–30 cm below the water table and kept strictly anoxic during transport and storage at
4°C in the dark. Water saturation and organic carbon content were determined by oven
drying and loss on ignition, respectively. Dissolved organic carbon (DOC) was
determined by high-temperature combustion using a Shimadzu TOC-V Total Organic
Carbon Analyzer (Shimadzu Scientific Instruments). Inorganic N species were quantified
photometrically using an AQ2 Discrete Analyzer (Seal Analytical) and method EPA-103-
A Rev.10 for ammonium (NH_4^+; LoD 0.004 mg N L^{-1}, range 0.02–2.0 mg N L^{-1}) and
method EPA-127-A for NO_3^-/NO_2^-; LoD 0.003 mg N L^{-1}, range 0.012–2 mg N L^{-1}).
Hydroxylamine was measured photometrically using the iodate method (Afkhami *et al.*,
2006).

Soil sterilization and slurry incubations. Experiments were started within 6 weeks
of soil collection. For each sterilization procedure, anoxic wet soil was exposed to the
chemical sterilant 48 h prior to start of the NO_2^- incubation or sterilized by physical
treatment and allowed to equilibrate for at least 12 h. The untreated (live) control was
incubated as a slurry without any additions or treatments for 48 h prior to start of
the NO_2^- incubation. Anoxic vials filled with wet soil were irradiated with a ^{60}Co source
for 7 d, yielding a final radiation dose of 4 Mrad (40 kGy). The irradiated soil was then

prepared for incubation in an anoxic glove box (0.5 % H_2 in N_2) with disinfected surfaces

and sterilized materials to prevent contamination. For autoclaved samples, soil was

prepared for incubation in closed vials and autoclaved at 121°C and 1.1 atm for 90 min.

The $CHCl_3$-treated samples were fumigated for 48 h under a 100 % N_2 atmosphere.

Because volatilized $CHCl_3$ corrodes electron capture detectors used for N_2O detection

(see below), $CHCl_3$ was removed by flushing the vials with N_2 for 5–7 min immediately

before the start of incubations.

In contrast to the physical sterilization treatments, soil samples were continuously

exposed to the chemical inhibitors throughout their incubation. Sodium azide (NaN_3,

Eastman Organic Chemicals), zinc chloride ($ZnCl_2$, Fisher Scientific), and mercuric

chloride ($HgCl_2$, 99.5 %, Acros Organics) were added from anoxic stock solutions to final

concentrations of 150, 87.5, and 3.7 mM, respectively. The Hg concentration was the

minimum needed to eliminate microbial heterotrophic growth based on visual inspection

of soil extract on agar plates exposed to 0.5 to 92.1 mg L^{-1}, which includes concentrations

demonstrated to be effective previously (Tuominen *et al*., 1994).

After the initial physical or chemical treatment, triplicate incubations were

diluted 1:10 in 20 mL of autoclaved 18.2 MΩ·cm water in 60 mL glass serum vials. All

microcosms were prepared in an anaerobic glove box (0.5 % H_2 in N_2) prior to

incubation. Triplicate soil slurries were amended from an anoxic, sterile stock solution to

a final concentration of 300 μM NO_2^- (6 μmol in 20 mL) and sealed with thick butyl

rubber stoppers. A parallel set of samples was amended with 300 μM NO_3^- to evaluate

denitrification potential with CO_2 measurements. Control incubations received an

equivalent volume of autoclaved 18.2 MΩ·cm water without NO_x^-. Soil microcosms were

incubated in the dark at a constant temperature of 25°C. NO_2^- was quantified in all soil treatments using the Griess assay (Promega, Kit G2930). pH measurements were taken with an Orion 3 Star meter (Thermo Scientific) before and after sterilization, and at the end of the experiment after 70–76 h of incubation.

Gas chromatography. To quantify N_2O and CO_2 production, 200 µL of headspace gas was sampled with a gas-tight syringe (VICI Precision Sampling) and injected onto a gas chromatograph (GC, SRI Instruments) equipped with both an electron-capture detector (ECD) and a flame-ionization detector (FID). Two continuous HayeSep-D columns were kept at 90 °C (oven temperature); N_2 (UHP grade 99.999 %, Praxair Inc.) was used as carrier gas, and for FID combustion H_2 was supplied by a H_2 generator (GCGS-7890, Parker Balston). For CO_2 measurements, a methanizer (which reduces CO_2 to the detectable CH_4 via a Ni catalyst at 355°C) was run in line before the FID. The ECD current was 250 mV and the ECD cell was kept at 350°C. The N_2O and CO_2 measurements were calibrated using customized standard mixtures (Scott Specialty Gases, accuracy ±5 %) over a range of 1–400 and 5–5000 ppmv, respectively. Gas accumulation in the incubation vials was monitored over time. Gas concentrations were corrected using Henry's law and the dimensionless concentration constants $K_H^{cc}(N_2O)=0.6112$ and $K_H^{cc}(CO_2)=0.8313$ (Stumm and Morgan, 2012) to account for gas partitioning into the aqueous phase at 25°C.

Live or dead cell staining. To assess the efficacy of sterilants or inhibitors visually, the bacterial viability kit LIVE/DEAD BacLight L7012 (Molecular Probes,

Invitrogen) containing SYTO9 and propidium iodide dyes was used to stain and distinguish dead and living cells on the basis of intact cell walls. The green (live) and red (dead) signals were counted at 60× magnification from 10 squares of 0.01 mm^2 randomly distributed in the center of a 5 µLNeubauer chamber, using an Olympus BX-61 microscope with the FITC/Cy5 filter set. Photographs were taken with an Olympus DP-70 camera attached to the microscope. Particles were counted with ImageJ software version 1.50i (Abràmoff *et al.*, 2004).

Fe extraction and quantification. Dissolved Fe species were extracted from peat soil incubations following the protocol of Veverica *et al.* (Veverica *et al.*, 2016). The method is based on an ionic liquid extraction using *bis*-2-ethylhexyl phosphoric acid (Pepper *et al.*, 2010), which was shown to be more suitable for extraction of Fe from humic-rich matrices than the traditional ferrozine or phenanthroline methods. Briefly, 2.5 mL of soil slurry was filtered (0.2 µm nylon filter; Celltreat Scientific Products) and mixed with 7.5 mL of HCl (0.67 N) in an extraction vial in a 0.5 % H_2 in N_2 glove box. The O_2 concentration in the glove box was continuously monitored and remained <10 ppm. To separate Fe^{3+} from Fe^{2+}, 10 mL of 0.1 M *bis*-2-ethylhexyl phosphate (95 %, Alfa Aesar) in *n*-heptane (99.5 %, Acros Organics) was added to the acidified sample. Next, the organo-aqueous emulsion was shaken at 250 rpm in closed extraction vials for 2 h. The *bis*-2-ethylhexyl phosphate chelates Fe^{3+} more effectively than it chelates Fe^{2+}. The Fe^{2+}-containing aqueous phase was sampled into a 3-fold HCl-washed HDPE vial (Nalgene) in the glove box. The Fe^{3+} fraction chelated in the organic phase was then back-extracted into an aqueous phase by the addition of 10 mL 4 N HCl

and shaking at 250 rpm in closed extraction vials for 20 min. Fe^{3+} and Fe^{2+} fractions were quantified separately in acidified aqueous solution by inductively coupled plasma–optical emission spectrometry (ICP-OES; Thermo iCAP6300 at the Goldwater Environmental Laboratory at Arizona State University). The ICP-OES pump rate for the Ar carrier was set to 50 rpm, and Fe2395 and Fe2599 lines were used for Fe quantification. Iron concentrations were determined from a calibration curve ($0.01–10$ mg L^{-1}) by diluting a standard solution (100 mg L^{-1}, VHG Labs, product no. SM75B-500) in 0.02 N HNO_3.

Dissolved organic matter fluorescence analysis. Three-dimensional fluorescence analysis was performed on a Horiba Jobin-Yvon Fluoromax 4 spectrofluorometer. Excitation–emission matrices (EEMs) were generated by obtaining emission spectra (λ_{Em}=300–550 nm, at a step size of 2 nm) at excitation wavelengths from 240 to 450 nm at a 10 nm step size. All EEMs were blank-corrected and normalized daily to the Raman peak of ultrapure water (deionized, carbon-free,18.2 MΩ·cm; Barnstead™ NanoPure). The samples were taken at the same time as those for Fe analysis. Prior to analysis, soil slurries were filtered using a solvent-rinsed Whatman Glass Microfiber Grade F GF/F filters (nominal pore size 0.7 μm) to obtain ~10 mL filtrate. Samples were diluted with ultrapure water if their UV absorbance exceeded 0.3 so that inner-filter corrections could be made (Stedmon *et al*., 2003). We calculated total fluorescence as the matrix sum of all signals in the EEM. Fluorescence indices were used to characterize various classes of fluorophores in the dissolved organic matter (DOM) pool. Fluorescence index (FI) was calculated as the sum of the intensity signal in the emission spectra from 470 to 520 nm collected at an excitation wavelength of

48

370 nm (Cory and McKnight, 2005). Humification index (HIX) was determined from the peak area under the emission spectrum from 435 to 480 nm, divided by the area from 300 to 445 nm, both collected at an excitation wavelength of 254 nm (Ohno, 2002). The "freshness" was determined to be β/α, the ratio of emission intensity at 380 nm to the emission intensity maximum between 420 and 435 nm, both collected at an excitation wavelength of 310 nm (Wilson and Xenopoulos, 2009).

Statistical analyses. All basic statistical tests were performed with JMP Pro software (Version 13.1.0, SAS Institute Inc.).

Results

Composition of high-OM tropical soils. The tropical peat soil used for the incubation experiments had 5.5–5.8 pH, 92.2 % water content, 307±5 mg TOC g^{-1} dry weight, and 3.8±0.9 g total Fe kg^{-1} soil. The extractable iron fraction partitioned as 54±3 μM extractable Fe^{3+} and 213±16 μM extractable Fe^{2+}. The native soil pore water had 13.2±1.2 mg L^{-1} DOC, 436±79 μg N L^{-1} NH_4^+, 9.7±1.3 μg N L^{-1} NO_3^-, and 3.9±0.2 μg N L^{-1} NO_2^-. Hydroxylamine was below detection in all cases (< 3 μM). Soil pH dropped from 5.5 to 5.8 in untreated soil to 3.6, 4.8, 5.0, 5.2, and 5.4 after treatment with Hg, Zn, γ irradiation, autoclaving, and $CHCl_3$, respectively. Only N_3 treatment increased soil pH (to 6.4).

Effects of sterilants on cell integrity and potential of denitrifying activity. Live and dead dyes were used to assess microbial viability by means of membrane integrity,

where a "dead" signal indicates disrupted or broken cell membranes (Stiefel *et al.*, 2015).

The majority (74 %) of cells in the live incubation displayed the "live" signal (Fig. 3.1).

The $CHCl_3$ and γ-irradiated treatments were most effective at reducing the number of

viable cells (~15 % intact membranes after sterilization). Chemical inhibitors (Hg, Zn,

and N_3) were less effective at killing cells (~30 % intact membranes after sterilization).

Autoclaved samples did not fluoresce, likely due to cell lysis during steam pressurization.

Biological denitrification activity was measured over 3 d in live and sterilized

soils based on the difference in CO_2 production with and without added NO_3^-. An

efficient sterilization treatment would show no changes in CO_2 beyond those due to

equilibration between the gas phase and aqueous phase. Nitrate

stimulated CO_2 production in live soil (ANOVA, $p < 0.05$) and not in the γ-irradiated, Zn,

Hg, N_3, or autoclaved incubations (Fig. 3.2), indicating that residual cells in the sterilized

treatments were not capable of denitrification.
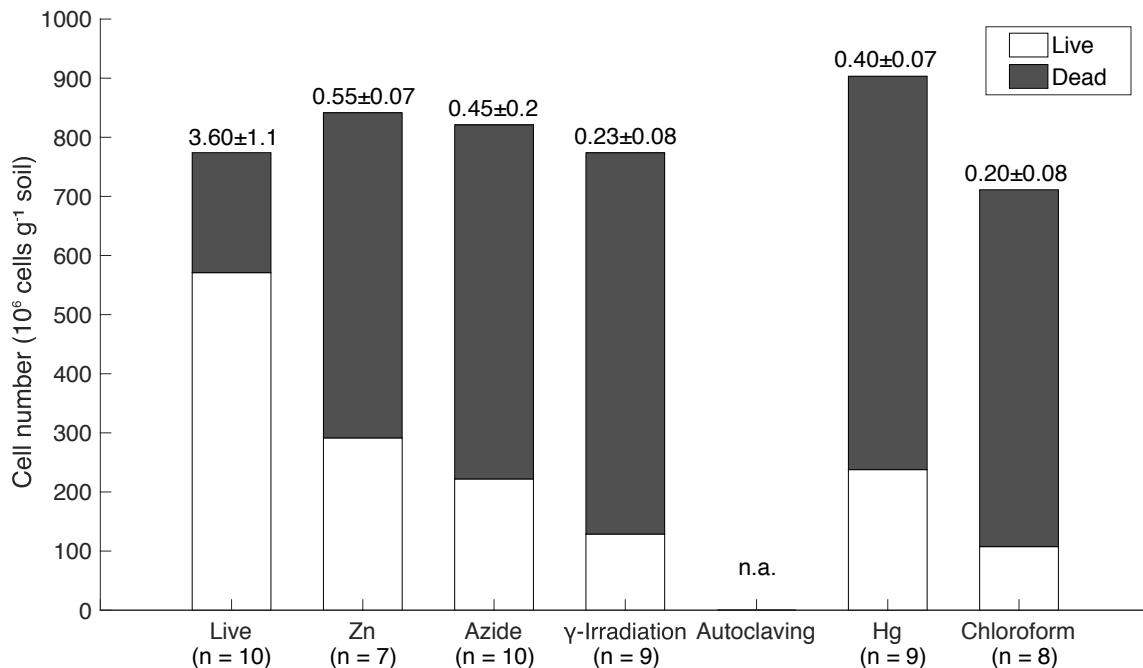
Figure 3.1. Live/dead microbial cell counts of tropical peatland soils. The numbers above the bars indicate the live to dead signal ratio ± *SD*. No detectable signal was observed in autoclaved samples. The x-axis represents treatments, including Live = no treatment, Zn = $ZnCl_2$, Hg = $HgCl_2$, Azide = NaN_3.
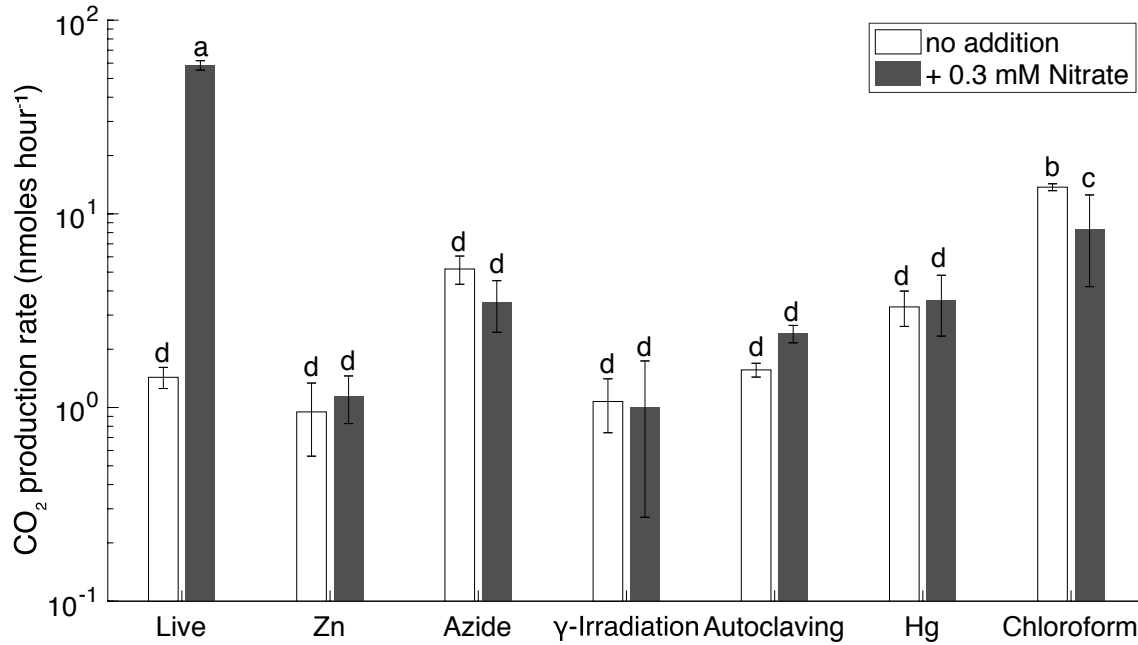
Figure 3.2. CO_2 production rates in 3-day soil slurry incubations of Quistococha peat soil amended with and without 0.3 mM NO_3^-. Error bars are one *SD* (n=3). Columns marked with the same letter are not statistically different from each other (Student's *t*, *p* > 0.05, n=3). The x-axis represents treatments as in the legend of Fig. 3.1.

Effects of sterilants on soil chemistry. In general, sterilization increased extractable Fe^{2+} and Fe^{3+} relative to live controls (Fig. 3.3). This trend was particularly pronounced in Zn treatments, which had 9× higher extractable Fe^{2+} (1915±26 µM) and 1.6× higher extractable Fe^{3+} (87±3 µM) than live controls. The Hg treatment showed the second-largest increases. In the presence of NO_2^-, extractable Fe^{2+} decreased and extractable Fe^{3+} increased in live, Zn, and $CHCl_3$-fumigated treatments, as expected if Fe^{2+} was oxidized by NO_2^- during chemodenitrification. However, autoclaving, *γ* irradiation, and N_3 lowered Fe^{3+} concentrations, suggesting the influence

of unknown concomitant reactions. For instance, autoclaving (largest drop in Fe^{3+}) already showed lower Fe^{3+} concentrations after sterilization. Production of Fe^{3+}-reduction artifacts in treatments could lead to Fe^{3+} depletion and, hence, mask increase in Fe^{3+} due to chemodenitrification. NO_2^- addition resulted in near-complete depletion of extractable Fe^{2+} in live, $CHCl_3$-fumigated, and γ-irradiated soils. Changes in Fe speciation with other sterilants were more moderate. Minimal changes were observed for other metals in soil samples (e.g., Mn, Al, Cu, and Zn; data not shown).
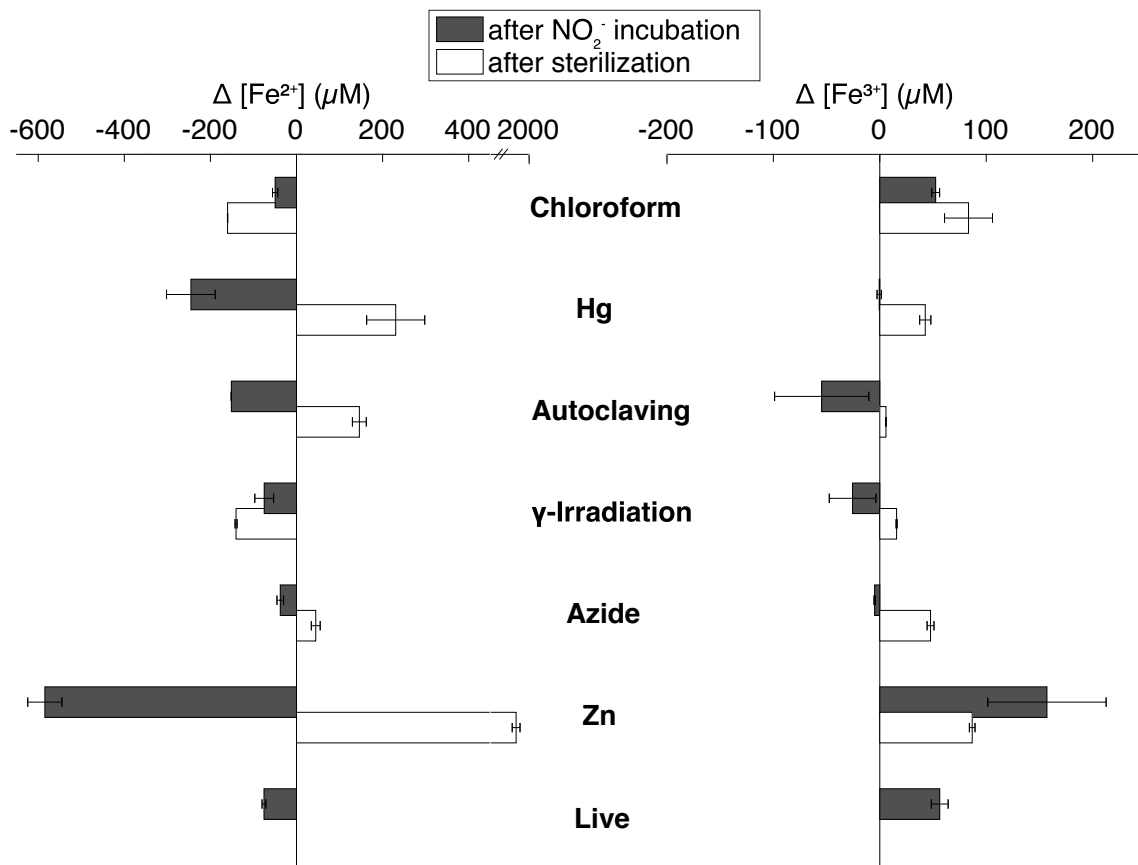
Figure 3.3. Changes in extractable Fe^{2+} (left) and Fe^{3+} (right) concentration in Quistococha peat soil incubations after sterilization (difference between sterilization baseline and live baseline value) and after NO_2^- amendment and incubation (difference between NO_2^- and control incubations). Note the difference in scales. Values represent the extractable fraction of both species. Error bars are one *SD* (n=2). The y-axis represents treatments as in the legend of Fig. 3.1.

Fluorescence analysis of soil extracts using excitation–emission matrices (EEMs) was used to evaluate changes in DOM-containing aromatic moieties or conjugated double bonds (Stedmon *et al.*, 2003; Fig. 3.4). The N_3 treatment was excluded from this analysis due to an interference with N_3 absorbance that prevented inner-filter corrections from being made. The EEM signals showed the greatest change in the "humic" region (λ_{Ex}<240–270 nm, and λ_{Em}=460–500 nm; Fellman *et al.*, 2010), especially in Zn and Hg treatments, which significantly increased the FI from 1.20 (in live soil baseline, prior to NO_2^- incubation) to 1.49 (Table 3.1). Zn and Hg may elicit direct fluorescence quenching through the formation of Zn and Hg metal complexes (McKnight *et al.*, 2001) or possibly due to indirect quenching by more highly dissolved Fe^{2+}. Signal strength in the humic region was enhanced by NO_2^- addition in the live, $CHCl_3$-fumigated, and γ-irradiated treatments. All five sterilization treatments had lower aromaticity (HIX) than live controls (Table 3.1). Autoclaved samples had 10-fold higher total fluorescence compared to live soils, suggesting that autoclaving degraded insoluble humics into more soluble and less condensed OM.
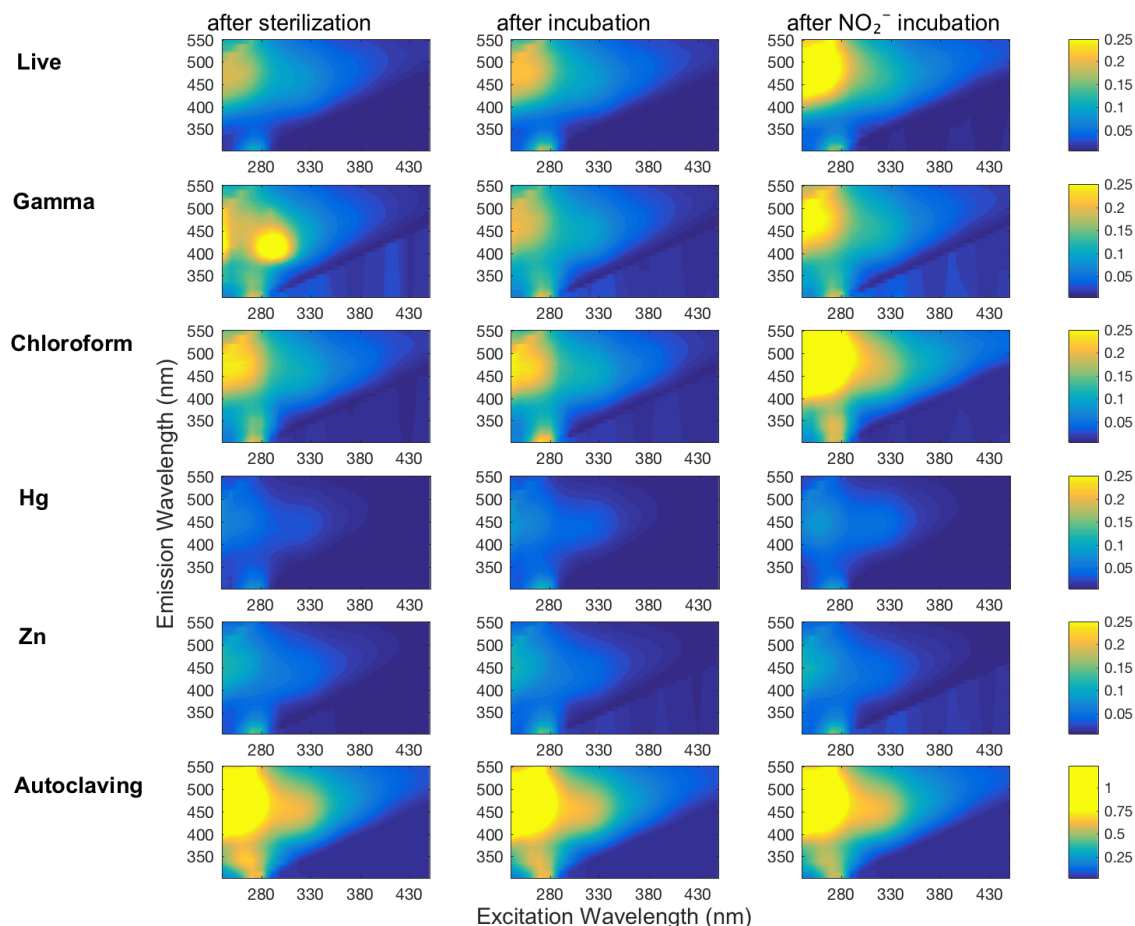
Figure 3.4. Representative plots of DOM fluorescence in soil slurry incubations of Quistococha peat soils. DOM fluorescence is presented as excitation-emission matrices (EEMs) collected for each treatment (rows) after the sterilization procedure or live control (left column), after incubation with no amendment ("after incubation" control, middle column), and after incubation with 300 µM NO_2^- (same time point as control, right column). The colored bar shows the individual signal intensity. All but "autoclaving" treatment has same scale of signal intensity, autoclaving effects increased about 5 times the signal intensity scale. Treatments as in the legend of Fig. 3.1.

Effects of sterilants on chemodenitrification and abiotic N_2O production. In the first 48 h, NO_2^- consumption rates were the highest in live soil (5.2 µM h^{-1}), closely followed by irradiated samples (4.5 µM h^{-1}, Fig. 3.5). The major chemodenitrification pathway for N_2O formation was likely NO_2^- reduction by Fe^{2+}, resulting in consumption of ~1.5 µmol Fe^{2+} and accumulation of ~1.1 µmol Fe^{3+} in the live control (Fig. 3.3). After

54

48 h, NO_2^- depletion continued to completion in the live control but slowed in all treatments other than the metal additions. After 72 h of incubation, 3 %–16 % of NO_2^--N was converted to N_2O-N across treatments. N_2O production rates were assessed by linear regression of data points over the whole duration of the experiment. Higher rates were observed in live, Zn^{2+}, and N_3 treatments (0.5–0.7 nmol N_2O g^{-1} h^{-1}, $r^2 > 0.95$) than in γ-irradiated, $CHCl_3$-fumigated, autoclaved, and Hg treatments (0.1–0.2 nmol N_2O g^{-1} h^{-1}, $r^2 > 0.9$). Production rates within treatments showing high or low rates were not significantly different (Student's t, $p > 0.05$), although comparisons across treatments with high or low rates were statistically different (Student's t, $p < 0.05$). Thus, we identified a higher and lower group of sterilant-dependent N_2O production rates from the same soil samples. The live control showed logarithmic N_2O accumulation, while the sterilized treatments had linear accumulation over time; the latter is expected in abiotic accumulation (Fig. 3.5).
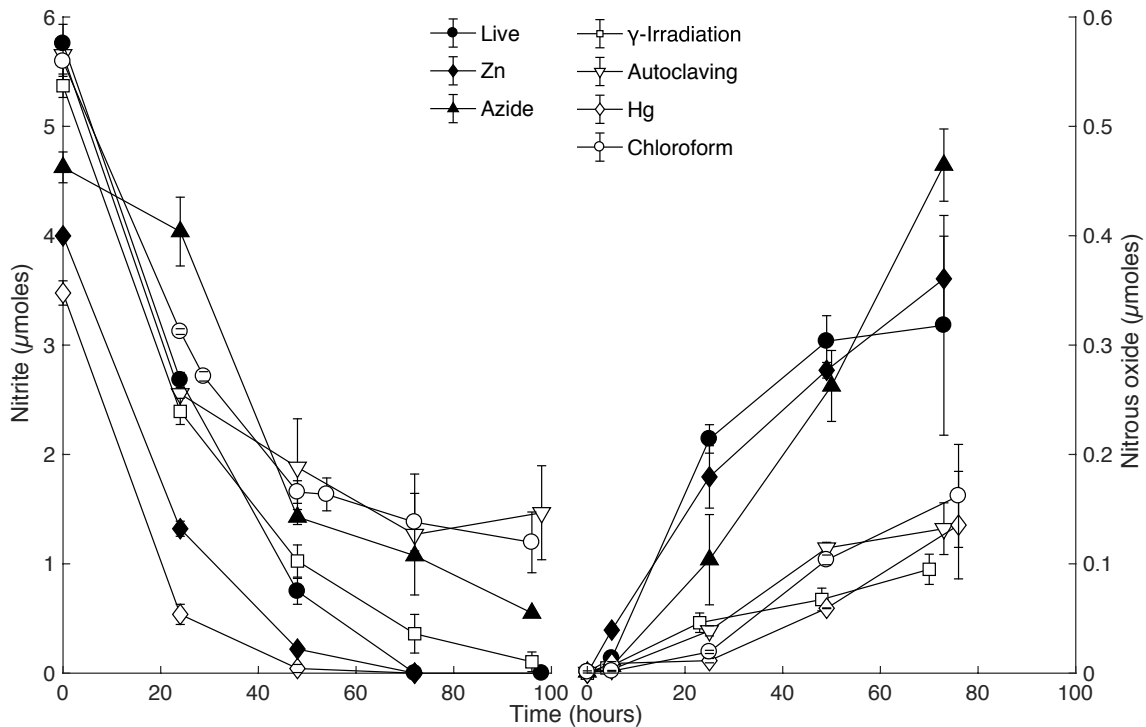
Figure 3.5. NO$_2^-$ consumption (left) and N$_2$O production (right) for different sterilant treatments in soil slurry incubations of Quistococha peat soil. Both N species were simultaneously measured in all treatments. The product yield represents N$_2$O-N as molar fraction of NO$_2^-$-N. Note the difference in left and right y-axis scales. Error bars are one *SD* (n=3). Treatments as in the legend of Fig. 3.1.

Discussion

Chemodenitrification is a dominant NO$_2^-$ consumption process in slurry incubations of tropical peat soils. Similar NO$_2^-$ consumption rates between live and irradiated treatments imply that NO$_2^-$ depletion was dominated by abiotic processes over the first 48 h. In general, abiotic reactions tend to be linear processes, whereas microbially mediated reactions can be affected by enhanced expression of genes or cell reproduction in a nonlinear fashion (Duggleby, 1995). Linearity is more reflected in the N$_2$O curve than in the NO$_2^-$ curve. The difference in linearity of N$_2$O production in sterilized vs. live treatments (Fig. 3.5) suggests that biological denitrification did not occur in sterilized soils.

Compared to our study, incubations of artificial media with 200 µM NO$_2^-$, 0.5–8.1 mM Fe^{2+}, and pH 7–8 had similar rates of Fe^{2+} depletion but 10× higher rates of NO$_2^-$ reduction, and higher (~10 %–50 %) N$_2$O yields (Buchwald *et al.*, 2016; Jones *et al.*, 2015). In our peat incubations, reactive OM likely trapped NO$_2^-$ in the soil matrix via OM-bound nitrosation reactions (Thorn and Mikita, 2000; Thorn *et al.*, 2010) and the lower pH likely promoted conversion of NO$_2^-$ to NO (Porter, 1969; Kappelmeyer *et al.*, 2003) or N$_2$. Studies in low-pH northern temperate peat soils have shown the primary product of abiotic NO$_2^-$ reduction was NO and not N$_2$O (McKenney *et al.*, 1990).

Artifacts due to sterilization methods for chemodenitrification assays. Azide and

Zn exhibited enhanced NO_2^- conversion to N_2O, at rates at least 2 to 5 times as high as

those measured for the other sterilants (Fig. 3.5), likely due to higher pH and Fe

availability, respectively. In the N_3 treatments, elevated N_2O production could be

explained by the reaction of protonated NO_2^- with N_3 in a pH-dependent manner

(Stedman, 1959) and other changes in soil solution that originated from the increase in

pH. Nitrite reaction with N_3 has been characterized in marine and freshwater solutions

reaching its maximum at pH 4.5 and proceeding slowly yet significantly (20 %

conversion in 1 h) at pH > 5 (McIlvin and Altabet, 2005), as in our slurries.

Moreover, N_3's self-fluorescence impeded OM measurements, making N_3 an

incompatible sterilizing agent for chemodenitrification studies. Zn increased Fe

availability and may have increased NO_2^- affinity for reactive OM groups; both effects

would lead to an abiotic increase in N_2O production (Parton *et al*., 2007; McCalley and

Sparks, 2009). Zinc treatment lowered the soil pH, which may have promoted cation

displacement and stability of dissolved Fe^{2+} (Hutchins *et al*., 2007), thus

enhancing N_2O production. Several studies have used Zn treatments as a valuable agent

for field applications (Babbin *et al*., 2015; Ostrom *et al*., 2016). Zn is less hazardous to

humans than some of the other sterilants. We propose that the use of Zn could provide

useful information about abiotic in situ rates as long as Zn-induced chemodenitrification

is accounted for. A correction could be applied if a complementary laboratory assessment

(using the more efficient γ irradiation) were used to develop an ecosystem-specific

correction factor.

Divalent Hg^{2+} can be abiotically methylated by fulvic acid-type substances

(Rogers, 1977). The reaction oxidizes OM and can diminish its reducing power, as

indicated by decreased reactivity of humic acid with NO_2^- (Gu *et al*., 2011; Zheng *et al*.,

2011), thus interfering with the abiotic assay. Given the pH effect of the Hg treatment, we

cannot rule out that decomposition of nitrous acid (HNO_2) contributed to NO_2^-

consumption (Fig. 3.5, J. Y. Park and Lee, 1988). Another potential factor associated

with the Hg treatments is metal sorption. At low pH (3.6), 98 % of Hg was sorbed to

humic acids, whereas only 29 % of Zn was sorbed at pH ~4.8 (Kerndorff and Schnitzer,

1980). Full sorption capacity of peat is presumably reached in seconds (Bunzl *et al*.,

1976), and the differing sorption behavior of Hg and Zn may play a role in the reaction

potential of NO_2^- with OM. It has been demonstrated that Hg introduced into peat soil

leads to sorption of Hg ions to various functional groups, including phenols (Xia *et al*.,

1998; Drexel *et al*., 2002). Hence, it is plausible that Hg sorbed to functional groups

subject to electrophilic attack by NO^+ (e.g., nitrosophenol) may hamper nitrosation, and

therefore protect OM from reacting with NO_2^-. This could lead to a selective suppression

of the OM-dependent N_2O production pathway.

Chloroform fumigation resulted in potential N_2O production rates within the

lower production range treatments with minor differences in Fe speciation and DOM

fluorescence. However, unlike the other sterilized samples, $CHCl_3$-fumigated samples

showed enhanced CO_2 production stimulated by NO_3^- addition. Removal of $CHCl_3$ from

our samples before substrate addition could have provided an opportunity for a few

surviving heterotrophs to regrow and use the easily degradable organic material derived

from dead cells. Indeed, chloroform can lyse cells, providing substrates for growth

to $CHCl_3$-resistant microorganisms (Zelles et al., 1997). Continued exoenzyme activity

has been also described as a CO_2 source; however, this would not include denitrification

enzymes, since no enzymes involved in the denitrification pathway are exoenzymes

(Jenkinson and Powlson, 1976; Blankinship et al., 2014). Chlorination of natural OM

may prompt formation of quinones (Criquet et al., 2015), which are intermediates in the

OM-based abiotic N_2O production (Thorn and Mikita, 2000); indeed, regions of the

EEMs corresponding to hydroquinones (Cory and McKnight, 2005) appear to be slightly

higher in $CHCl_3$ treatments. The benzene derivative produced during nitrosophenol

reaction with NO_2^- leads to reduced π electron delocalization. Because excitation

of π electrons produces fluorescence, reactions with NO_2^- might be expected to reduce

OM fluorescence. However, the experiment duration is important, and if microbial cells

indeed reproduce after the treatment, short experimental periods (e.g., hours or days) or

reapplication of $CHCl_3$ might keep down the numbers of any potential denitrifiers

improving the use of this method.

Autoclaved peat soil revealed abiotic N_2O production rates close to the average of

the lower production range group, along with ICP-OES and fluorescence spectroscopy

results that showed significant changes in Fe speciation and DOM composition. EEMs

demonstrate lower values for the HIX in autoclaved peats (Table 3.1), consistent with

fluorescence data from a study that demonstrated a decrease in the aromaticity and

polycondensation of soil extracts from autoclaved soil (Berns et al., 2008). Autoclaving

likely caused degradation and solubilization of insoluble humic components. The direct

effects of autoclaving are very much dependent on the heat and pressure stability of the

indigenous soil constituents, but the substantial soil structural changes likely introduce chemical artifacts that are absent in the native live soil.

Gamma irradiation is the preferred sterilization method for chemodenitrification assays. The fewest chemical artifacts were observed in γ-irradiated samples. Soil that had been exposed to γ rays showed the lowest N_2O production rates, approximately one-fifth of those observed in live samples. Irradiation also caused only very small changes in Fe speciation relative to live controls and yielded EEMs that were remarkably similar to those obtained from live soil extracts. Our measurements of sterility and respiratory activity indicated the lowest potential for biological activity and hence the least amount of interference for the time period tested. We therefore confirmed γ irradiation to be a preferred method for sterilizing soil (Trevors, 1996) and for assessing abiotic N_2O production potential. In practice, the long preparation time needed to reach a sufficient dose (dependent on radiation source; see Methods) was compensated for by the lack of chemical artifacts during the experiment and the reduced number of hazardous waste products. Limited accessibility to irradiation facilities and the absence of a field portable option remain the main challenges to wide distribution of this approach.

Conclusion

High N_2O emissions occur in tropical regions with water-saturated soils (Pérez *et al*., 2001; S. Park *et al*., 2011; Liengaard *et al*., 2014). Whether these tropical N emissions are solely biotic or have abiotic contributions is not well known because rates

60

of chemodenitrification are not commonly evaluated. Abiotic processes in the N cycle remain overlooked, partly due to the lack of reliable means of quantifying abiotic reactions. This study showed that chemodenitrification occurs in a tropical peat soil, leading to a low to moderate fraction of N_2O conversion from nitrite amendment. We also demonstrated that γ irradiation is the "gold standard" for chemodenitrification assays. The application of N_3 to quantify abiotic N_2O production is unsuitable because changes associated with the fraction of the sterilant itself may react to form N_2O and affect increased pH. $CHCl_3$ and γ rays have slightly reducing effects on the soil Fe pool and might lead to a weak discrimination against pathways involving Fe as a reactant. $CHCl_3$ fumigation was another approach with limited effects on Fe chemistry that lowered the number of viable cells greatly; however, the potential for microbial regrowth after $CHCl_3$ removal is its main drawback. Autoclaving seemed to have minor disadvantages for abiotic N_2O production, despite the substantial changes to soil OM. Unlike other lab-intensive treatments, the application of Zn and Hg are amenable for field experiments; however, we observed distinct chemical artifacts when using both of these options. Care is warranted if using Zn and Hg chemical inhibitors, which can increase Fe availability and may thus overestimate Fe-dependent abiotic N_2O production rate. A potential disadvantage of the application of toxic metals is a decrease in soil pH. We cannot exclude pH-driven effects on N intermediates; however, no major deviation in the final N_2O production rate related to acidification was observed. With the methodological evaluation presented here, we determined that a directed selection of approaches can allow for better constrained and more detailed studies of the role of abiotic pathways and soil components shaping denitrification and N_2O fluxes from soil ecosystems.

CHAPTER 4

COUPLED ABIOTIC-BIOTIC CYCLING OF NITROUS OXIDE IN TROPICAL

PEATLANDS[3]

Abstract

Tropical soils are considered hotspots for N_2O emissions, but are also associated

with high uncertainties and variation. Denitrification is one of the main sources of these

N_2O emissions and is thought to be almost exclusively mediated by microorganisms.

However, we accumulated evidence that abiotic reaction pathways, besides biotic ones,

drive N_2O production in peat soils across Central and South America. Using ^{15}N tracers,

we found abiotic N_2O production generally contributed more than biotic N_2O production

to the overall N_2O flux. The conversion of NO_2^- into gaseous forms was achieved based

on solely abiotic reactions in two peatlands. Microbial N_2O consumption was explored

across the two N_2O-reducer clades I and II based on the phylogenetic separation by

structurally divergent N_2O reductases encoded by the *nosZ* gene. Metagenomics and

amplicon sequencing show Rhodocyclales accounted for >50% of bacterial reads;

specifically *Thauera linaloolentis* (~20%) for clade II and *Hyphomicrobium* (19-40%)

and *Methylocystis* (28-32%) for clade I. The *nosZ* clade I : II gene ratios suggest spatial

patterns, with clade II N_2O reducers outnumbering clade I N_2O reducers in the majority

of Amazonian peats. We observed a correlation between microbial N_2O consumption and

abiotic N_2O formation rates. While the field incubation data suggested coupling of abiotic

N_2O production and microbial consumption in the majoriy of sites, the lab incubations at

---

[3] This work is in preparation and has not been shared with co-authors yet.

higher substrate levels did not. Accordingly, denitrification in tropical soils is not a purely biological pathway, but rather a "mosaic" of biotic and abiotic reduction reactions.

Introduction

Denitrification is the major loss pathway of fixed nitrogen across terrestrial ecosystems (Bouwman *et al.*, 2013). The five-electron stepwise transfer from the aqueous ions, nitrate (NO_3^-) and nitrite (NO_2^-), to the gaseous forms nitric oxide (NO), nitrous oxide (N_2O) and molecular nitrogen (N_2) occurs widely throughout terrestrial systems where oxygen is depleted to concentrations < 6 µM O_2 (Seitzinger *et al.*, 2006). In addition, nitrifier-denitrification converts ammonium (NH_4^+) directly to NO or N_2O, and can also proceed under aerobic conditions (Kim *et al.*, 2005). Recent work on denitrifying microbial communities suggests a modular structure of the denitrification pathway, with natural populations to mediate one or two reduction steps only (Graf *et al.*, 2014; Roco *et al.*, 2017). However, while biological interactions have been considered as the basis for the modularity, an abiotic-biotic interplay has not been explored so far. If abiotic reactions contribute to overall denitrification, nitrogen loss pathways may be differentially sensitive to environmental change, such as global warming, based on divergent activation energies of abiotic and enzymatically mediated reactions (Yvon-Durocher *et al.*, 2010; Yvon-Durocher *et al.*, 2012).

Gas fluxes from terrestrial denitrification have long been underestimated by up to 98% (Fang *et al.*, 2015). The balance between the production and consumption of N_2O is pivotal for net gas fluxes and, thus, climate feedback because of the positive radiative forcing of N_2O and long atmospheric residence times (114 years; Stocker *et al.*, 2013).

Across natural and anthropogenic sources, soils under pristine vegetation show highest

N_2O emissions of 6.6 Tg N_2O-N yr^{-1} (Ciais *et al*., 2013). Tropical soils are a major source

of atmospheric N_2O. The largest contribution to global N_2O flux and the highest

uncertainties were observed over the South American continent (Huang *et al*., 2008;

Zhuang *et al*., 2012). In waterlogged peat soils, anoxic conditions and the reactants for

the abiotic formation of N_2O are provided (Buessecker *et al*., 2019), which could

contribute to sustained emissions as reported from wetlands of the Pantanal in Western

Brazil (88-1496 ng cm^{-2} h^{-1}) (Liengaard *et al*., 2014). As abiotic N_2O sources are known

from polar ecosystems (Samarkin *et al*., 2010; Ostrom *et al*., 2016), coastal sediments

(Otte *et al*., 2019), and from several artificial systems (Zhu-Barker *et al*., 2015), the true

extent of this potentially significant process has remained enigmatic. While some

environments appeared to sustain abiotic rates with Fe mineral phases (Samarkin *et al*.,

2010; Ostrom *et al*., 2016; Otte *et al*., 2019), others showed regulation by organic matter

(OM; Buessecker *et al*., 2019). In spite of the potential of both reactants (Fe and OM) to

stimulate abiotic N_2O production (Thorn and Mikita, 2000; Thorn *et al*., 2010; L. C.

Jones *et al*., 2015), organic soils have been rarely targeted by studies on

chemodenitrification, which further contributed to an incomplete understanding of

chemical processes within the nitrogen cycle of soil systems. Taken together with high

estimates of the global extension of peatlands in the tropics (1.7 million km^2, Gumbricht

et al., 2017), this source pathway suggests a potentially significant role in shaping the

global atmospheric N_2O budget.

Denitrifying microbes are well adapted to the conditions found in peat soils

because they anaerobically respire organic substrates using nitrogen oxides as terminal

electron acceptors (Pihlatie *et al*., 2004; Palmer and Horn, 2012). The discovery of the clade II N_2O-reducing bacteria confirmed the microbiological basis for an extensive N_2O sink potential in diverse soils (Sanford *et al*., 2012; Orellana *et al*., 2014; C. M. Jones *et al*., 2014; Domeignoz-Horta *et al*., 2016; Espenberg *et al*., 2018). While clade I N_2O-reducers are affiliated to the *Proteobacteria*, clade II N_2O reducers are more diverse and are also affiliated to *Actinobacteria, Bacteroidetes,* and *Firmicutes*. Active N_2O-reducers from clade II could explain the fluctuating N_2O emissions and sink potential reported from peatlands. The clade II members tend to lack NO_2^- reductases (Hallin *et al*., 2018). From an ecological perspective, this trait might correspond with the intrinsic capability of the soil habitat to reduce NO_2^- chemically (chemodenitrification). Energetic resources could thus be saved and relocated to the expression of NO and N_2O reductases (Lycus *et al*., 2018). The compatibility of abiotic N_2O production with the concept of modular microbial denitrification led us to the hypothesis that a coupled abiotic-biotic N_2O cycle is operative in tropical peatlands.

To test our hypothesis, first, we assessed the soil potential to produce N_2O abiotically from NO_2^- and then determined production rates for 10 peatlands; 7 of which were spread over the Amazon basin and 3 were located outside (Table 4.1). We compared rates obtained from $^{15}NO_2^-$ incubations in the field that were sterilized by zinc treatment to laboratory incubations at higher substrate levels that were sterilized by γ irradiation. Second, we measured microbial N_2O reduction rates with doubly labeled $(^{15}N)_2O$. We complemented rate measurements with amplicon sequencing, metagenomics, and quantitative PCR (qPCR) assays targeting the *nosZ* gene phylogeny and abundances. In

order to assess the potential coupling of abiotic N_2O production and biotic consumption, we correlated rates of both processes from all peatlands.

Methods

Field sites and data sets. The peatlands were chosen to cover a broad geochemical spectrum, including acidic (pH 3.7-5) soils, low (10 µM) and high (>5 mM) Fe^{2+} concentrations (Table 4.3). All soils had high organic content (>20% w/w) and contained a peat layer of at least 30 cm in thickness. The study sites had little anthropogenic influence, with two exceptions: Fazenda Córrego da Areia (FCA) within a catchment experiencing agricultural run-off in Brazil and Medio Queso (MQE) in a Costa Rican river delta surrounded by plantations off the border to Nicaragua (A. D. Cohen *et al.*, 1986). The peatlands Quisticocha (QUI), San Jorge (SJO), Aucayacu (AUC), Charo (CHO), and San Roque (SRQ) were located within the Pastaza-Marañón foreland basin in East Peru (Fig. 1.2; Lähteenoja *et al.*, 2011). Melendez (MEL) can be found in the Madre de Dios river terraces (Householder *et al.*, 2012), and Sitio Cacau (SCB) was located in Central Amazonia (Amanã Reserve) in proximity to the city of Tefé. Las Vueltas (VUL), located in the cloud forests of the Cerro Las Vueltas Reserve (A. D. Cohen *et al.*, 1986), differed most drastically from the other sites because of its higher altitude (2,500 meters a.s.l.) and lower soil temperature (Table 4.3). The field trips were conducted in September 2017 (SJO, MEL) and during the months of April (MQE, VUL) to July (SCB, FCA) in 2018.

Due to analytical limitations, it was not possible to conduct field measurements in all peatlands. However, the subset of peatlands with associated *in-situ* measured rates

66

(Table 4.1) covers the diversity in N_2O cycling dynamics well (i.e. half of those field sites are a high N_2O- or high NO-site, respectively; see Table 4.3). The Brazilian sites SCB and FCA have associated abiotic data, but biotic data is missing because of logistic issues concerning the shipment of non-sterilized soil. We used publicly available metagenomes of the peatlands SJO and QUI to further our evaluation of the microbial community, which we based on amplicon sequencing throughout all sites (Table 4.1).

Table 4.1. Overview on field sites and data sets. Sites marked with * are located outside the Amazon basin.

Site	Code	Lati-tude (°)	Longi-tude (°)	_in-situ_ N₂O production data	N₂O consumption data	Meta-genome	Ampli con data
Medio Queso, Los Chiles, Costa Rica	MQE *	11.038	-84.687	yes	yes	no	yes
Charo, Iquitos, Peru	CHO	-4.270	-73.254	no	no	no	yes
Las Vueltas, Dota, Costa Rica	VUL *	9.624	-83.848	yes	yes	no	yes
Melendez, Puerto Maldonado, Peru	MEL	-12.467	-69.178	yes	no	no	yes
Aucayacu, Iquitos, Peru	AUC	-3.935	-74.384	no	no	no	yes
Fazenda Córrego da Areia, Prados, Brazil	FCA *	-21.024	-44.086	yes	yes	no	yes
Quistococha, Iquitos, Peru	QUI	-3.837	-73.318	no	yes	yes	yes
San Roque, Iquitos, Peru	SRQ	-4.540	-74.622	no	no	no	yes
San Jorge, Iquitos, Peru	SJO	-4.058	-73.189	yes	yes	yes	yes
Sitio Cacau, Tefé, Brazil	SCB	-2.374	-64.336	yes	yes	no	yes

[15]N tracer experiment in the field. To determine ambient soil NO_2^- and NO_3^- concentrations, we used a YSI 9500 portable spectrophotometer (YSI Inc.). All

67

spectrophotometric assays were conducted according to the manufacturer's manual. Soil temperature and pH were measured with a YSI A10 pH probe (Ecosense, YSI) calibrated prior to each measurement at each site.

We used inflatable anaerobic glove bags (Cole-Parmer) filled with Ar to create anaerobic conditions in the field while distributing soil into glass incubation vials (160 mL). Soil was sampled with customized corers, consisting of plastic 30 mL syringe barrels that were cut at the ends. These were inserted 10 cm into the top soil layer. In the glove bag, the center 5 cm (~15g) was diluted 1:5 (w/v) in each vial with anoxic water extracted directly from 10-20 cm deep peat soil with a water line connected to the glove bag. Separate sample sets received 100x the soil ambient concentration (Table 4.3) of $^{15}NO_2^-$ (label fraction = 0.1, Cambridge Isotopes) and 10x the soil ambient concentration (~2 ppm) of doubly labeled $(^{15}N)_2O$ (label fraction = 1.0, Cambridge Isotopes), respectively. The $^{15}NO_2^-$ incubations comprised untreated and 87.5 mM zinc chloride-poisoned (ZnCl$_2$, Fisher Scientific) soils in replicates of four (n = 4), with each replicate derived from single soil cores. The soil slurries were incubated on the site, within separate thermo-containers (Mira Brands) that were partially buried in the soil to maintain temperature and dark conditions. Gas samples were taken for $(^{15}N)_2O$ analysis at the beginning and once after 24 hours, and for $^{30}N_2$ analysis at 4 time points spread over 36 hours (n = 3). Gas sampling was done destructively (entire headspace used) for $(^{15}N)_2O$ analysis or by replacement with 5 mL Ar gas for $^{30}N_2$ analysis. The sample times for the $^{30}N_2$ analysis were adapted from a previous study (Babbin et al., 2015). We also prepared zinc-poisoned $(^{15}N)_2O$ incubations to test for abiotic N$_2$O consumption. The gas samples were stored underwater in glass vials closed with thick butyl rubber stoppers

(Hamilton and Ostrom, 2007) until analysis at Michigan State University. Isotopic

composition of N_2O and N_2 were measured using an Elementar Isoprime isotope ratio

mass spectrometer (IR-MS) interfaced with an Elementar TraceGas chromatographic

system. Rate calculations closely followed a previously developed and tested protocol

(Ostrom *et al.*, 2016). Given the constraints of sterilant applications in the field, we

repeated the zinc-amended incubations in the lab, parallel to incubations with γ-irradiated

soils. The rates from both experiments were used to calculate a correction factor

accounting for artifacts caused by the zinc addition in accordance to our previous study

(Buessecker *et al.*, 2019). The rates derived in the field were then multiplied by the

correction factor (Table 4.2).

Table 4.2. Correction of N_2O production rates measured *in-situ*.

Site	Rates in zinc-treated incubations (nmol N_2O g^{-1} h^{-1})	Rates in γ-irradiated incubations (nmol N_2O g^{-1} h^{-1})	Correction factor
MQE	14.1	15.5	1.1
VUL	12.5	8.1	0.65
MEL	6.9	6.8	0.98
FCA	n.a.	0.6	0.5*
SJO	3.4	1.4	0.4
SCB	n.a.	1.6	0.3*

*Estimated based on similarities of NO and N_2O yields within the high-NO group.

The final rates were combined according to the following equation for net *in-situ*

N_2O formation:

$$B = M + C - A$$

where B is the biotic N_2O production rate, M is the mixed rate (from untreated $^{15}NO_2^-$ incubations), C is the microbial N_2O consumption rate [from $(^{15}N)_2O$ incubations], and A is the abiotic N_2O production rate (from poisoned $^{15}NO_2^-$ incubations).

Laboratory incubations. In a glove box with a reducing, O_2-free atmosphere (0.5% H_2 in N_2), γ-sterilized soil was separately prepared from fresh, untreated soil. Gamma sterilization followed a previous method (Buessecker *et al.*, 2019). Treated and untreated soils were root-picked, coarse particles (> 5 mm in diameter) were removed, and slurried 1:10 (w/v) in anoxic, sterile 18.2 MΩ·cm water. The slurry was well homogenized before equal quantities were distributed into 60 mL serum bottles, and closed with autoclaved butyl rubber stoppers. All glassware used was washed with 2M HCl prior to use and tools for work in the glove box were repeatedly ethanol-sterilized. For the NO_2^- incubations, an anoxic and filter-sterilized NO_2^- stock solution was injected (final concentration 100 μM NO_2^-), and the headspace immediately purged with pure N_2. For the N_2O incubations, the headspace was reset with pure N_2 and N_2O was injected using a N_2-flushed, gas-tight syringe (VICI Precision Sampling; final concentration 2.5 μM dissolved N_2O). The microcosms were agitated briefly to disperse the added substrates and then kept under dark, static conditions at room temperature for ~100 hours.

Dissolved NO_2^- was quantified with the Griess reagent (Promega, Kit G2930) and NO and N_2O were analyzed as described below. At the end of the experiment, Fe^{2+} and Fe^{3+} were extracted and separated as previously described (Buessecker *et al.*, 2019), and quantified in acidified aqueous solution by inductively coupled plasma–optical emission spectrometry (ICP-OES; Thermo iCAP6300 at the Goldwater Environmental Laboratory

at Arizona State University). The ICP-OES pump rate for the Ar carrier was set to 50 rpm, and Fe2395 and Fe2599 lines were used for Fe quantification. Iron concentrations were determined from a calibration curve (0.01–10 mg L^{-1}) by diluting a standard solution (100 mg L^{-1}, VHG Labs, product no. SM75B-500) in 0.02 N HNO_3.

N_2O gas measurements. To quantify N_2O production, 200 µL of headspace gas was sampled with a gas-tight syringe (VICI Precision Sampling) and injected onto a gas chromatograph (GC, SRI Instruments) equipped with an electron-capture detector (ECD). Two continuous HayeSep-D columns were kept at 90°C (oven temperature) and N_2 (UHP grade 99.999%, Praxair Inc.) was used as carrier gas. The ECD current was 250 mV and the ECD cell was kept at 350°C. The N_2O measurements were calibrated over a range of 0.25–100 ppmv using customized standard mixtures (Scott Specialty Gases, accuracy ±5%). Gas concentrations were corrected for solubility effects using Henry's law and the dimensionless concentration constant $K_H^{cc}(N_2O) = 0.6112$ (Stumm and Morgan, 2012) to account for gas partitioning into the aqueous phase at 25°C and 1 atm.

NO gas measurements. Nitric oxide (NO) was quantified in the microcosm headspace with a chemiluminescence-based analyzer (LMA-3D NO_2 analyzer, Unisearch Associates Inc.). Headspace gas (50 µL) was withdrawn with a CO_2-N_2-flushed gas-tight syringe and injected into the analyzer. The injection port was customized to fit the injection volume and consisted of a T-junction with an air filter at one and a septum at the other end. An internal pump generated consistent airflow. Our method generally followed a previous protocol (Homyak *et al*., 2017), and included adjustments based on

71

our experimental setup. In short, NO was oxidized to NO_2 by a CrO_3 catalyst. The NO_2 flew across a fabric wick saturated with a Luminol solution. Luminol was obtained from Drummond Technology. Readings were corrected for background NO_2 every 15 minutes ("zeroing"). Shell airflow rate was kept at 500 mL min^{-1} and the span potentiometer was set to 8. Measurements were calibrated with a 0.1 ppm NO (in N_2) standard (<0.0005 ppm NO_2, Scott-Marin, Riverside, CA, USA) over a range of 5–1,000 ppbv. Gas concentrations were corrected using Henry's law and the dimensionless concentration constant $K_H^{cc}(NO) = 0.0465$ (Stumm and Morgan, 2012) to account for gas partitioning into the aqueous phase at 25°C.

Molecular analyses. Peat samples from four randomly distributed locations (coinciding with incubation locations) within a peatland were collected and frozen at -20°C for subsequent DNA extraction at ASU. Genomic DNA was extracted using a NucleoSpin Soil DNA extraction kit (Macherey-Nagel).

For quantitative polymerase chain reactions (qPCR), we used two previously identified primer pairs and a total reaction volume of 15 µL with 1.5 µL DNA template (35-50 ng genomic DNA). The clade I *nosZ* gene was amplified in a PowerUp SYBR Green master mix (Applied Biosystems), to which 3 mM $MgCl_2$ was added. Forward and reverse primer concentrations were 1 µM and previous cycler conditions were used (Henry *et al.*, 2006). The clade II *nosZ* gene was amplified using SYBR Fast, ROX low master mix (Kapa Biosystems) and 1.2 µM primer concentration (C. M. Jones *et al.*, 2013). Thermal cycling was initiated with 3 min denaturing at 95 °C, followed by 40 cycles of the following stages: 30 s at 95 °C, 60 s at 58 °C, 30 s at 72 °C, 30 s at 80 °C,

72

and a final melting-curve. Samples were run in technical duplicates on 96-well plates

using a Quantstudio 3 thermocycler (Applied Biosystems). Standards were prepared

using linearized plasmids. Standard curves indicated efficiencies of 94% (r^2 = 0.99, *nosZ*

clade I) and 85% (r^2 = 0.99, *nosZ* clade II) and melting-curves showed no detectable

primer dimers over the duration of 40 amplification cycles.

Metagenomes were assembled in the scope of CSP project #1141599 using the

default pipeline (version 4.15.1) of the Joint Genome Institute (JGI). On assembled

metagenomes in amino acid format, we performed a profile search based on hidden

Markov models (Eddy, 2011) implemented in the package GraftM

(https://github.com/geronimp/graftM). Using modular gene packages, GraftM searched

the provided sequences using hmmsearch (HMMER) and placed the identified sequences

into a pre-constructed phylogenetic tree. HMMs were based on manually curated *nosZ*

gene libraries comprising 2817 (clade I) and 2929 (clade II) sequences. Reference

sequences were retrieved from the FunGene repository (Fish *et al.*, 2013) using the

search parameters 80% HMM coverage and a minimum length of 550 amino acids.

GraftM output was loaded into Megan version 6.18.0 (Huson *et al.*, 2016) and from there

on, subsequent steps were identical to amplicon sequence analysis (see below).

For an extended analysis of the N_2O-reducer community composition, we

developed independent *nosZ* clade I and II libraries for Illumina amplicon sequencing.

PCR-amplification of both *nosZ* genes used the Promega GoTaq qPCR kit (Promega) for

and 1 µL of DNA template (25-50 ng genomic DNA) in a total reaction volume of 20 µL.

Targeting the clade I *nosZ* gene, we used a novel primer pair (Christopher Penton, unpublished) that showed coverage superior to other commonly used primers. The reaction mix included 0.2 mg mL^{-1} bovine serum albumin (BSA) and 0.8 µM primer concentration. For the clade II *nosZ* gene we used the same primer as used for qPCR in reactions of 1 mg mL^{-1} BSA and 0.8 µM primer concentration. Cycling conditions were used as described (C. M. Jones *et al*., 2013) for clade II *nosZ* amplification. Thermal cycling conditions for clade I *nosZ* amplification were an initial 2 min denaturing step at 95 °C, followed by 33 cycles of 95 °C for 45 s, annealing by 53 °C for 45 s, and a 72 °C extension for 30 s, and a final extension at 72 °C for 7 min. Amplification specificity was verified by gel electrophoresis using 1% agarose in 1 Tris-acetate-EDTA buffer. Samples were multiplexed (Herbold *et al*., 2015), normalized (SequalPrep kit #1051001, Invitrogen), and submitted for sequencing to the DNASU core facility at Arizona State University, with 2x 300-bp paired-end Illumina MiSeq.

Paired-end sequences were merged and demultiplexed with in-house scripts. We used the USEARCH pipeline (R. Edgar, 2010) to 1) correct strand orientations, 2) sort out singletons, and 3) denoise the dataset. We used *alpha* = 2 for a stringent denoising of sequences (R. C. Edgar, 2016) because reads were not clustered with any identity radius. The sequences were translated and frameshift-corrected by Framebot (Q. Wang *et al*., 2013) with low sequence loss (< 10%). The amino acid sequences obtained were classified using Diamond version 0.9.25 (Buchfink *et al*., 2015). Sequences were parsed through the NCBI database RefSeq (release 95) containg 146,381,777 non-redundant protein sequences. The search was conducted in Diamond's *sensitive* mode, with an e-

value cutoff of 10^{-5}, resulting in the top 5% hits. The output was imported into Megan version 6.18.0 (Huson *et al.*, 2016) where a weighted lowest common ancestor (LCA) algorithm (default parameters from Huson *et al.*, 2018) was run to assign a single taxonomic lineage to each read. Zero-radii OTU tables were pasted into Krona (Ondov *et al.*, 2011) for visualization of results.

Note on missing nosZ clade II amplicon data: At the time this thesis was completed, reads were still processing in the analysis pipeline. The data will be included in the projected paper publication.

Statistical Analyses. All basic statistical tests were performed with JMP Pro software (Version 13.1.0, SAS Institute Inc.). Analysis of variation (ANOVA) was used with $p > 0.05$ to test significantly different values for gene quantities across soils. K-means clustering (MacQueen, 1967) was used to evaluate data clusters based on a minimum cluster r^2. Plotting and regression analysis was done with the Matlab R2018a software package (Version 9.4.0.813654, Mathworks Inc.).

Results & Discussion

Chemodenitrification in tropical peat soils results in NO and N₂O production. Measured steady-state concentrations of NO_2^- in soil pore water were below detection (< 1 μM) in the majority of sites (Table 4.3), indicating rapid cycling rates. We spiked the peat soil at 6 of the 10 sites with $^{15}NO_2^-$ and measured $^{14}N^{15}NO + {}^{15}N^{14}NO + {}^{15}N^{15}NO$ production. Biotic activity was arrested by adding 87.5 mM zinc chloride. Even though the addition of zinc can liberate Fe^{2+} ions stimulating N₂O production (Buessecker *et al.*,

2019), we accounted for this bias for each individual soil. A larger sample set was sterilized using γ irradiation in the laboratory parallel to zinc treatments of soils from the same sites (Table 4.2). We corrected the rates from zinc-treated *in-situ* incubations to obtain estimates of N_2O production from less altered peat soil. All our reported *in-situ* rates are therefore corrected for zinc effects.

To assess the capacity of the tropical peatlands for chemodenitrification, we calculated nitrogen yield accounting for NO_2^- reduction to NO and N_2O. In two peatlands (SJO, SCB), complete denitrification was achieved based on solely abiotic transformation, and three other peatlands (QUI, SRQ, FCA) showed nearly complete denitrification (>75% yield, Table 4.3, Fig. C.1). The conversion of nitrogen from the reactant NO_2^- into the products NO and N_2O resulted in dominant yields in either one pool or the other (Fig. C.1), suggesting unequal diversion of nitrogen driven by the local peat chemistry. Thus, we grouped the various peat soils into high-N_2O (MQE, CHO, VUL, MEL) and high-NO (AUC, FCA, QUI, SRQ, SJO, SCB) sites. This categorization may help to identify common chemical drivers for the abiotic reactions. We also observed a pH dependence on the formation of both NO and N_2O species. Abiotic NO production yield was enhanced under acidic conditions (pH $\leq$ 5.4), whereas abiotic N_2O production revealed a yield optimum at pH ~6.

Our results are consistent with previous reports indicating larger amounts of NO as the final product in increasingly acidic milieu (Van Cleemput *et al*., 1976). The decomposition of nitrous acid explains faster NO_2^- consumption at lower pH (Van Cleemput and Baert, 1984). Based on our experimental design, we were unable to confirm N_2 as byproduct (Wullstein and Gilmour, 1966) that was presumably dominant at

76

circum-neutral pH, i.e., at MEL and VUL. However, at all other sites, NO and N_2O together were the dominant product pools (> 50% nitrogen yield). The substrate NO_2^- showed very low concentrations that are typical for soil (L. C. Burns *et al.*, 1995; L. C. Burns *et al.*, 1996). Nitrite is not the only possible precursor of N_2O. Hydroxylamine (NH_2OH) has very low steady-state soil concentrations as well, but has proven to be a viable source of soil N_2O (Heil *et al.*, 2015). As abiotic N_2O production can have multiple source pathways, we focused our investigations onto chemodenitrification under anoxic conditions.

Table 4.3. Relevant geochemical parameters and calculated nitrogen yield of abiotic reactions. According to the nitrogen yield, sites were classified as either high-N_2O (MQE, CHO, VUL, MEL) or high-NO (AUC, FCA, QUI, SRQ, SJO, SCB). High-N_2O sites also differed from high-NO sites in pH ($P < 0.001$, Student's t test) and Fe^{3+} ($P < 0.05$).

	MQE	CHO	VUL	MEL	AUC	FCA	QUI	SRQ	SJO	SCB
Soil temp. (°C)*	29.9	26.1	13.6	26.8	25.4	16.3	25.6	26.1	27.3	26
pH*	6	5.6	6.4	6.1	4.2	5.4	5	4.6	3.7	4.9
NO_3^- (µM)*	7.4	n.a.	5.9	< 1	n.a.	2.6	1.1	n.a.	< 1	5.6
NO_2^- (µM)*	< 1	n.a.	2.9	< 1	n.a.	< 1	< 1	n.a.	< 1	< 1
Fe^{2+} (µM)[†]	181.6	68.9	5,128	1,431	117.3	10	72.6	57.9	39.2	36.5
Fe^{3+} (µM)[†]	673.9	800.8	910	503.9	367.4	322.9	69.8	479.1	109	785
N yield in NO (%)	1.3	1.9	0.2	0.2	52.7	74.3	74.5	81.3	92.8	97.2
N yield in N_2O (%)	55.9	50.6	24.6	12.1	9.8	4.0	5.0	8.1	4.8	4.8
Total yield (%)	57.2	52.5	24.8	12.3	62.5	78.3	79.5	89.4	97.6	102

* measured at the study sites.
† measured in the laboratory.

Abiotic N_2O production is prevalent across all tested peatlands. Significant abiotic N_2O production was observed in all peatlands (incl. high-NO sites). *In-situ* rates ranged from low values (0.05-0.3 nmol N_2O g^{-1} day^{-1}) at FCA and SCB, to moderate

values (2.4-3.3 nmol N_2O g^{-1} day^{-1}) at MQE and SJO, to high values (9.2-39.0 nmol N_2O g^{-1} day^{-1}) at MEL and VUL. Abiotic N_2O production contributed to the overall N_2O flux to a greater extent than biotic N_2O production at half the field sites (Fig. 4.1). Laboratory incubations led to a consistent underestimation of the abiotic contribution by a difference as much as 56% (MEL).
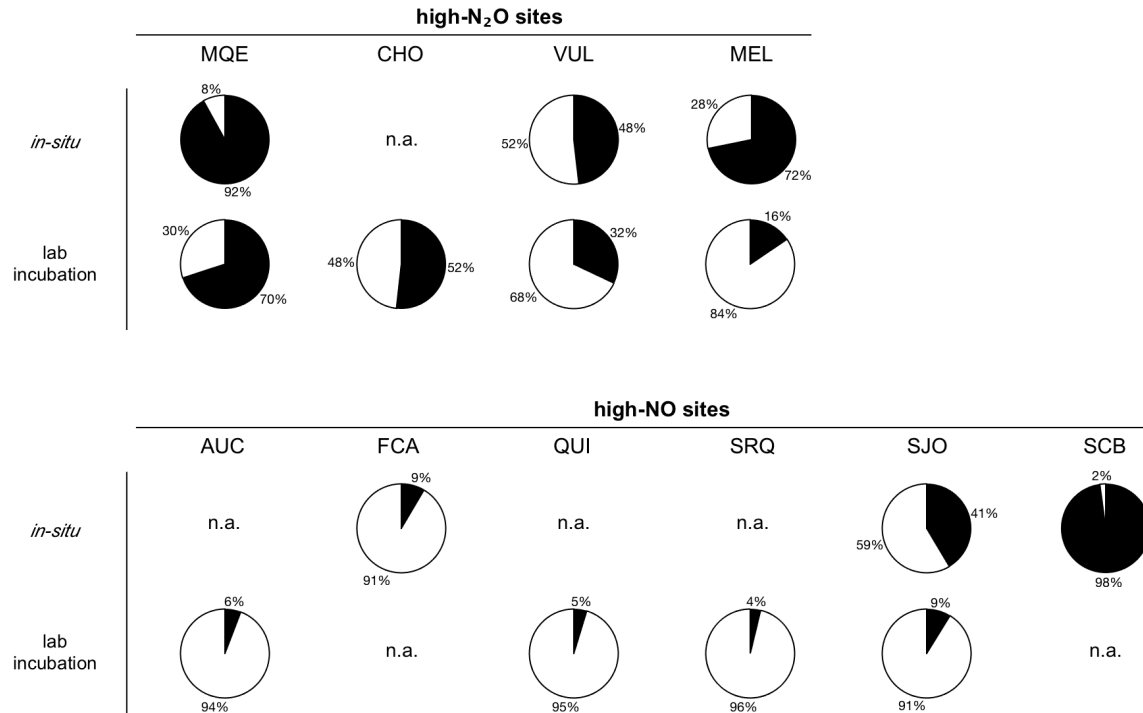
Fig. 4.1. Abiotic (black) and biotic (white) N_2O production rate fractions. Percentage relates to total N_2O production rate. Rates from lab incubations were derived from the linear slope of the N_2O production curve (n=4). *In-situ* rates were derived from the enrichment of ^{15}N in N_2O after addition of $^{15}NO_2^-$ to soil in the field (n=4).

The conditions in the anoxic peat soils were favorable for abiotic N_2O formation. The measured N_2O production rates were 1-2 orders of magnitude higher than rates measured in Antarctic brine (Samarkin *et al.*, 2010). While those brines were rich in Fe, they were low in organic matter, which may hint at the additional reducing power peat may hold, with triggering effects on N_2O production. Aqueous Fe^{2+} and Fe^{2+}-bearing

mineral phases have been shown to interact with the chemodenitrification reaction in soils (L. C. Jones *et al*., 2015). While extracted Fe^{2+} concentrations correlated with *in-situ* abiotic N_2O production rates ($r^2 = 0.99$, n = 6, Fig. C.2B), there was no significant ($r^2 <$ 0.75, n = 10) linear relationship with rates measured in batch incubations (Fig. C.2B). Peat soils also supply an overabundance of recalcitrant organic carbon with functional groups prone to interact with NO_2^- (Thorn and Mikita, 2000; Thorn *et al*., 2010). For instance, phenolic moieties can bind two NO_2^- ions inducing tautomerization to hyponitrous acid that degrades to N_2O. In this process, the carbon ring loses one pi-electron pair. The residual benzoquinone is more oxidized, which could be indicated by a decreased electron donating capacity or reduced fluorescence. Both of these properties could be characterized experimentally. Besides soil pH, the mixture of functional groups could also be a crucial factor in the NO to N_2O balance. With the exception of dimethyl glyoxime and quinone oximes, oxime groups preferentially produce N_2O and aromatics produce NO (Porter, 1969). The organic matter composition and, hence, the plant litter it originated from, may play an important role in supporting different abiotic reaction mechanisms. Nevertheless, it is likely a combination of complexed Fe^{2+} and reduced organic functional groups that contribute to the electron transfer onto NO_2^- and N_2O formation.

Active microbial N_2O reduction is based on divergent nosZ gene numbers across soils and diverse communities. We consistently observed N_2O sink potential in denitrification assays in which we added NO_2^- to peat soils and tracked NO and N_2O production (Fig. C.1). N_2O production was followed by rapid consumption in non-

sterilized samples (Fig. C.1). Abiotic N_2O consumption did not occur (data not shown).

Incubations with $(^{15}N)_2O$ in the field showed accumulation of ^{15}N label in N_2 (Fig. C.3) that we used to derive rates of N_2O reduction (Table 4.4). The trends observed for abiotic N_2O production were also reflected in N_2O consumption rates ranging from low (0.1-0.3 nmol N_2O g^{-1} day^{-1}) in SCB and FCA to moderate (0.7-1.5 nmol N_2O g^{-1} day^{-1}) in MQE and SJO, to high (3-9.5 nmol N_2O g^{-1} day^{-1}) in VUL and MEL. Rates determined in laboratory incubations were higher than *in-situ* rates by roughly a factor of 10 (Table 4.4), which is consistent with 10 times decreased substrate concentrations that were used in the field. N_2O-reductive activity at pH as low as 3.7 (SJO) was surprising because of post-transcriptional inhibition of the N_2O reductase assembly by acidic pH (B. Liu *et al.*, 2010). The measured N_2O reduction rates were higher than previously observed rates at similarly acidic pH (Palmer *et al.*, 2012) and extend the known physiological boundaries for this metabolism. These results suggest the presence and activity of N_2O-reducing communities adapted to a wide range of soil pH, including N_2O-reducers adapted to highly acidic soil pH.

Table 4.4. Microbial N_2O reduction rates in tropical peatlands.

Site	N_2O reduction rate, lab (nmoles g^{-1} hr^{-1})	N_2O reduction rate, *in-situ* (nmoles g^{-1} hr^{-1})
MQE	18.3	0.7
CHO	18	n.a
VUL	25.2	3
MEL	39.6	9.5
AUC	52.9	n.a
FCA	n.a.	0.3
QUI	37.2	n.a
SRQ	43.8	n.a
SJO	15	1.5

SJO

QUI

FCB 1%
Gemmatimonadaceae 0.8%
Aquificaceae 0.8%
Terrabacteria 0.7%
Chlorobi 0.1%

Aquificaceae 1%
FCB 0.9%
Acidobacteria 0.7%
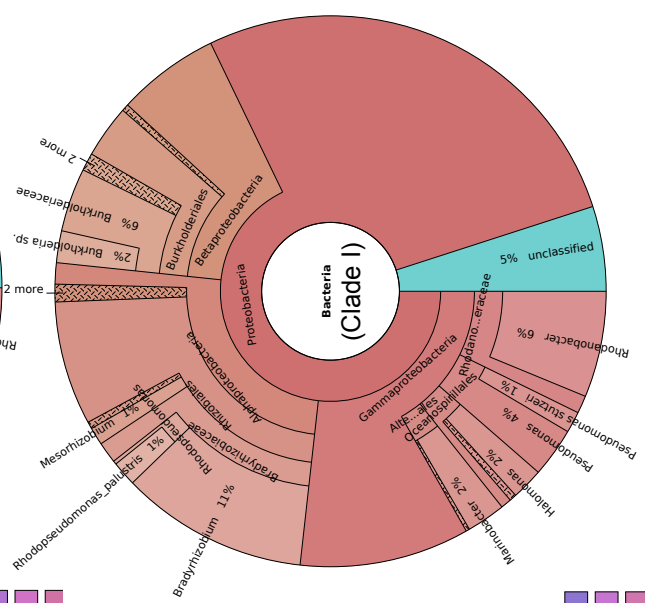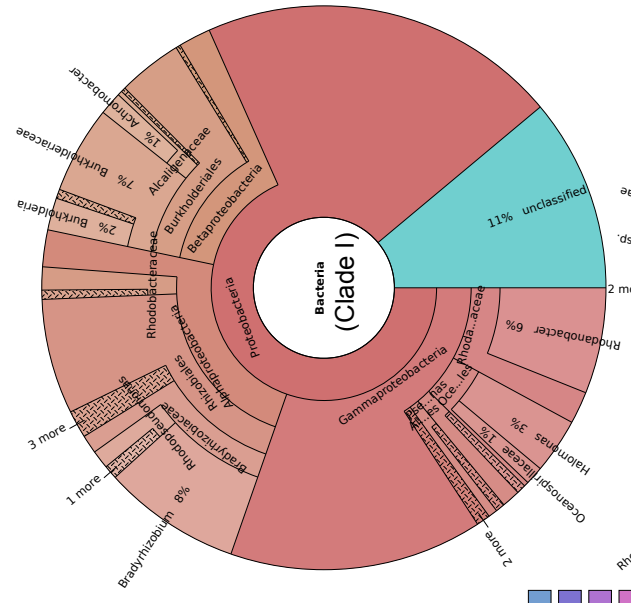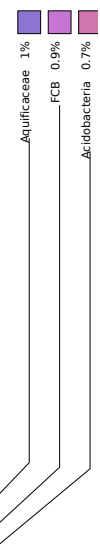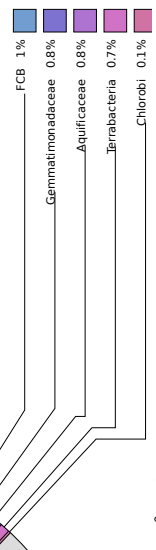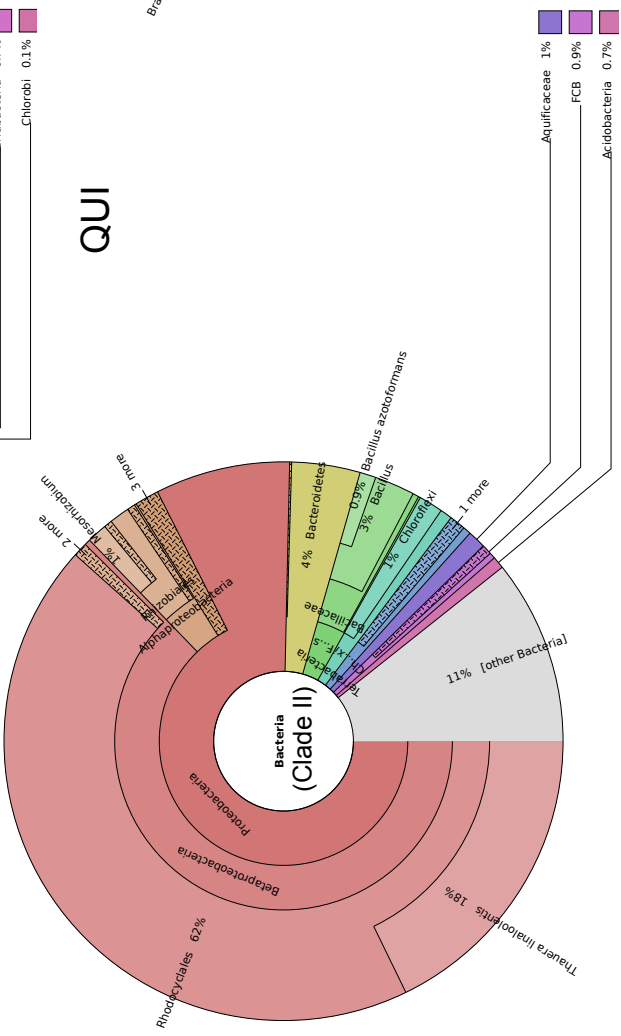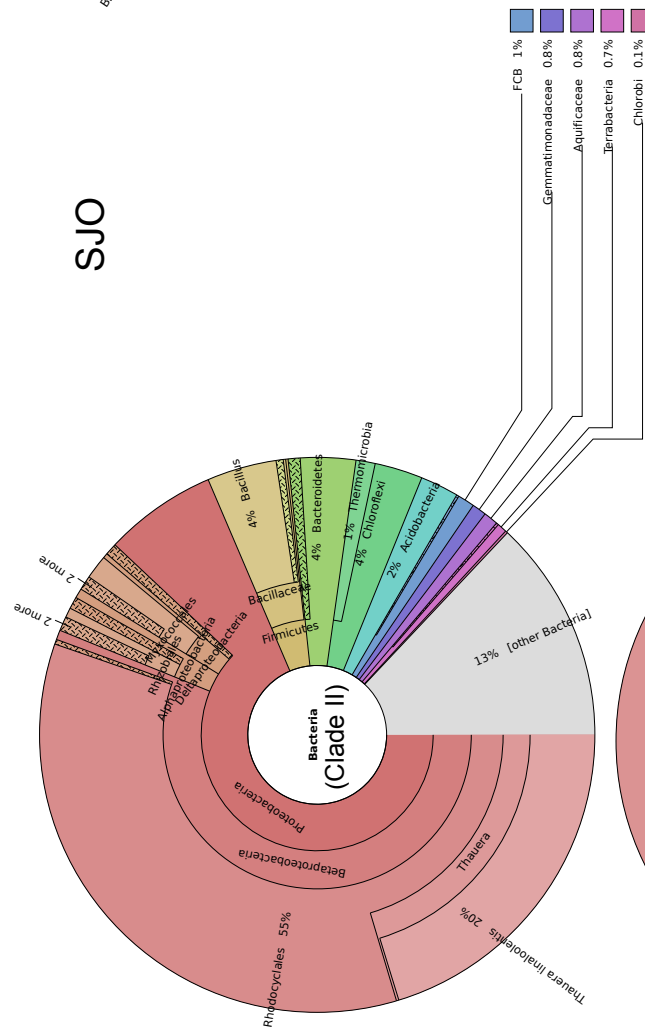
Fig. 4.2. N$_2$O-reducing microbial community composition. Metagenomes from representative peatlands SJO and QUI comprised both clade I (482 and 379 counts) and clade II (921 and 763 counts) members.

To assess the diversity and relative abundance of N$_2$O-reducing microorganisms, we used metagenomic analyses in two representative peatlands (SJO, QUI) and amplicon sequencing on all the studied peatlands. We performed an HMM profile search on the metagenomes. The reads taxonomically classified into Proteobacteria (clade I-associated reads). A higher diversity was shown by clade II sequences that were classified into 10 (SJO) and 14 (QUI) phyla, respectively. We observed a high abundance of Rhodocyclales with >50% of bacterial reads as well as dominant *Thauera linaloolentis* (~20% in both soils). Metagenomic and amplicon sequence data showed slight differences in the abundances of Gammaproteobacteria (these were more abundant in metagenomes), but were otherwise consistent on the class level. Based on amplicon-sequencing, *Hyphomicrobium* (19-40% in SRQ, CHO, MEL, FCA) and *Methylocystis* (28-32% in MEL and FCA) were abundant among clade I bacteria (Fig. C.4). *Rhodanobacter*, of which an N$_2$O-reducing isolate was recently obtained from acidic (pH 5.7) soil (Lycus *et al.*, 2017), was also present in our clade I metagenomes (6%). However, no sequences affiliated to *Rhodanobacter* were among our amplicon data (Fig. C.4).

We used BLAST to examine NO$_2^-$ and NO reductase gene sequences in the *Thauera linaloolentis* genome and did not find a match for NO reductase. Despite the missing reductase gene, the species may still be able to denitrify (i.e. convert NO$_2^-$ to N$_2$), if their soil micro-habitat has the capacity to abiotically reduce NO to N$_2$O. Admittedly, a much more extended genome evaluation of the taxa found would be

82

necessary to establish a robust link between missing denitrification enzymes and the soil capacity for chemodenitrification. Nevertheless, *Thauera linaloolentis* is an example of a dominant microbial community member that would physiologically benefit from abiotic reactions sustained by the peat chemistry in an abiotically-biotically modulated fashion.

In addition to the phylogenetic analysis, we quantified both *nosZ* genes via quantitative PCR (qPCR) in order to assign individual clade I : II abundance ratios to the peat soils. The *nosZ* gene accounted for approximately 1% of 16S ribosomal RNA (rRNA) from the soil microbial community (data not shown). Our results suggest spatial patterns. Relatively high numbers of clade I N_2O reducers were found in peatlands of the Pastaza-Marañón foreland basin (Fig. 4.3, QUI, SJO, CHO, SRQ, 10^7-10^8 gene copies g^{-1}). Clade II N_2O reducers had higher abundances ($>10^8$ gene copies g^{-1}) at AUC and SRQ. In contrast, we did not detect any *nosZ* sequences affiliated with clade II in the CHO peatland. With the exception of CHO, all peatlands of the Amazon basin showed higher proportions of clade II N_2O reducers (*nosZ* I:II ratio 0.1-0.9), whereas the peatlands outside of the Amazon basin consistently showed more N_2O reducers of the clade I guild (*nosZ* I:II ratio 1.5-6.9).

Alterations in relative clade I and II abundances have been reported previously from Puerto Rican peatlands (Espenberg *et al*., 2018) and between communities of the rhizosphere and bulk soil across biomes (Graf *et al*., 2016). Our data indicate that clade II bacteria generally outcompete clade I bacteria in the pristine Amazonian peats. This is supported by the *NosZ* enzyme kinetic properties described for clade II (S. Yoon *et al*., 2016; Suenaga *et al*., 2019) and predicted for conditions that meet those found in some of

the tropical peat soils tested (soil N_2O steady-state concentrations <5 ppm; Chapter 5).

Although evidence suggesting higher N_2O affinity for clade II N_2O reducers has been

contradictory (Conthe *et al*., 2018), the adaptation to lower steady-state N_2O

concentrations would explain our observed abundance patterns.
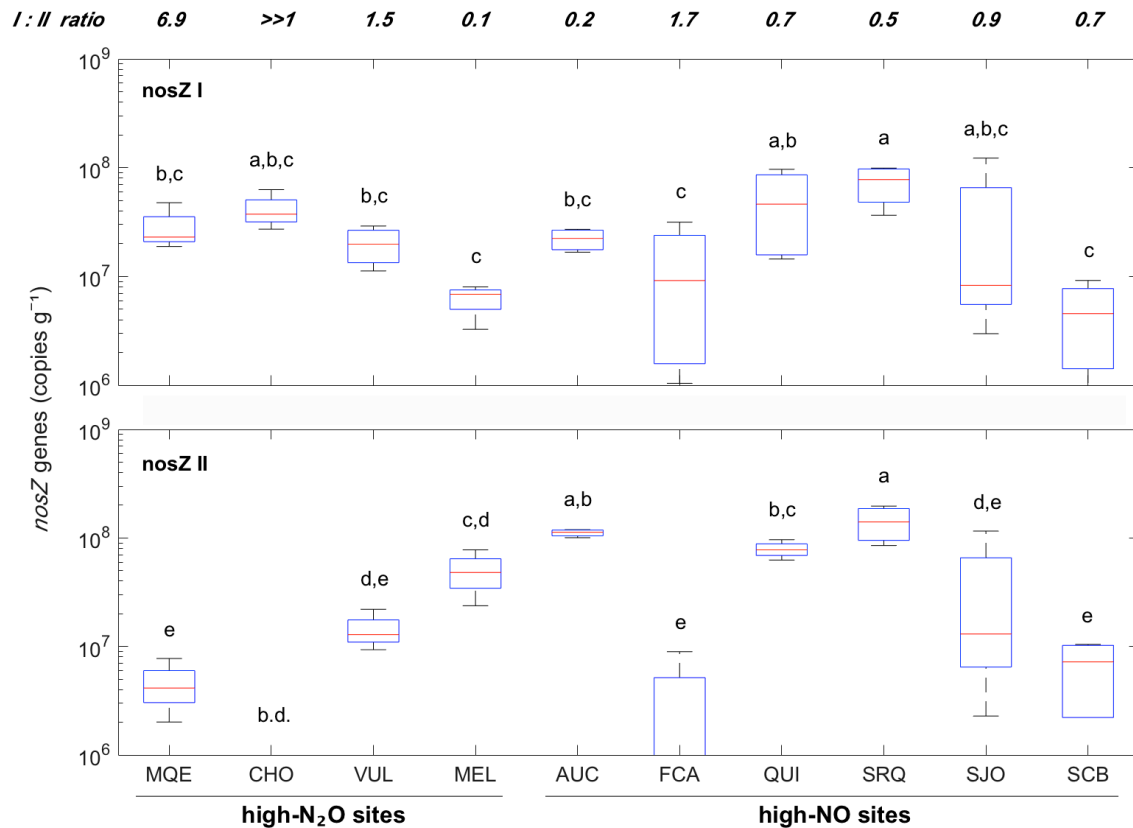
Fig. 4.3. *NosZ* gene quantities across peatlands. *NosZ* clade II sequences were not
detected in CHO peat soil within the limit of detection of our qPCR method. Units were
normalized to soil dry weight. Red central marks indicate the median, bottom and top
edges of boxes show 25th and 75th percentiles, respectively, and whiskers extend to the
most extreme data points. Data boxes marked with the same letter are not significantly
different from each other (ANOVA, $p > 0.05$, n=4).

Constraining a coupled abiotic-biotic N_2O cycle. To explore the observed trend of

concomitantly increasing N_2O production and consumption rates in our ^{15}N data, we

plotted the abiotic production potential against the consumption potential. We then

overlaid the kinetic data with *nosZ* I:II ratios of the individual peatlands (Fig. 4.4). K-

means clustering (MacQueen, 1967) indicated 3 distinct clusters. A cluster of lower-rate

values (FCA, SCB, SJO) and two clusters with increased N_2O production and

consumption rates, respectively (Fig. 4.4A). Sites QUI, SRQ, MEL and AUC consumed

N_2O at potential rates >30 nmol N_2O g^{-1} h^{-1} and had *nosZ* I:II ratios <0.7. Sites VUL,

CHO and MQE were characterized by high potential abiotic N_2O production rates ($\geq$8

nmol N_2O g^{-1} h^{-1}) and had *nosZ* I:II ratios >1.5. Similar patterns were also reflected in *in-

situ* measured rates (Fig. 4.4B). Microbial N_2O reduction correlated with abiotic N_2O

production at all sites (r^2 = 0.93, n = 5, Fig. 4.4B) after the exclusion of N_2O cycling rates

from VUL. In regards of the differences in substrate concentration between laboratory

and *in-situ* conditions (NO_2^- levels were 100 times and N_2O levels were 10x their

ambient concentrations), the biotic rates increased accordingly but the abiotic rates did

not.
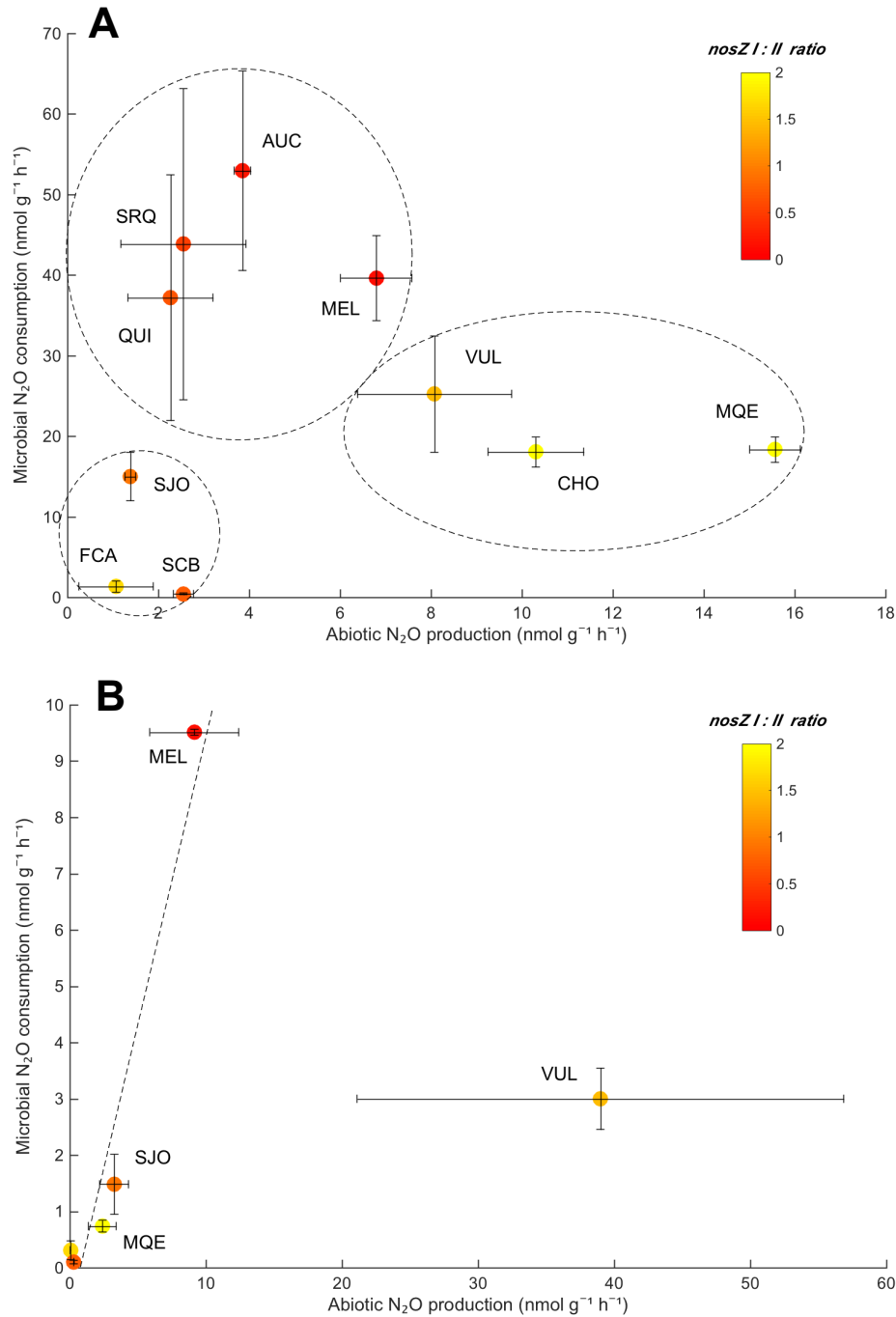
Fig. 4.4. Relation of abiotic N$_2$O production and microbial N$_2$O consumption in lab (A) and *in-situ* incubations (B). (**A**) K-means clustering was applied to identify significant data clusters (dashed ellipses). *NosZ* I:II ratios < 2 are marked with a color gradient (CHO and MQE are off the scale for better visibility). Units were normalized to soil dry weight. Error bars denote *SD*. (**B**) Linear regression was conducted with VUL treated as outlier. The regression line (dashed) has a slope = 1.05. *NosZ* I:II ratios < 2 are

marked with a color gradient (MQE is off the scale for better visibility). Data points at the lower left were from FCA and SCB soil.

Nitrous oxide cycling, where abiotically derived N_2O is followed by N_2O consumption mediated by chemodenitrifiers (Onley *et al.*, 2018), revealed distinct balances across peatlands at increased substrate levels in lab incubations. Higher sink potential was associated with a predominance of clade II N_2O-reducers over clade I reducers and *vice versa*. Microbial N_2O reduction exceeded abiotic N_2O production in all samples except of SCB under the controlled laboratory conditions (Fig. 4.4A). However, at substrate levels closer to environmental conditions, *in-situ* N_2O reduction rates resembled abiotic N_2O production rates more similarly (Fig. 4.4B). Both *in-situ* and laboratory abiotic N_2O production rates from the bulk of the sites remained in the same range, which may suggest limited availability of Fe^{2+}/organic reaction sites. This limitation is not present for the biotic N_2O consumption process because microbial cells possess the advantage of an adaptive response to increased substrate availaibity by a more pronounced expression of *NosZ* enzyme. The regression line slope of ~1 (Fig. 4.4B) suggests coupling of production and consumption under *in-situ* conditions. We note that rates obtained from VUL peatland had a higher standard deviation (Fig. 4.4) and we cannot exclude temperature effects retarding metabolic rates (Jauhiainen *et al.*, 2014). Moreover, VUL peatland is a highland peat bog with a very contrasting plant cover than encountered in the other sites. The plant debris organic substrates derive from can strongly affect heterotrophic activity levels and therefore N_2O reduction rates (Shirokova *et al.*, 2016). Assigning a specific clade to the adaptation to abiotic N_2O fluxes seemed complex because in incubations, clade I-dominated sites were closer to a slope = 1

trajectory while the sites under *in-situ* conditions (except VUL) had mixed abundances from both clades. We must also acknowledge that our insight into the temporal activity response is limited. Information on the actual *in-situ* transcription levels are needed to better assess how the clades are stimulated by abiotic pulses of N_2O (Drewer *et al*., 2020). Such stimulations may not necessarily serve the metabolic purpose of energy conservation. First, N_2O can have cytotoxic effects on microbial cells due to inactivation of vitamin B_{12} which is needed for DNA and methionine synthesis (Drummond and Matthews, 1994a; Drummond and Matthews, 1994b; Sullivan *et al*., 2013). Rapid N_2O consumption would therefore make sense as a detoxification strategy. Second, abiotically derived N_2O could aide to overcome O_2 starvation. Clade II bacteria have been shown to be positively impacted by either N_2O or O_2 exposure. For example, *Azospira* (Rhodocyclales) exhibited more resilience in reducing N_2O under aerobic conditions than clade I species (Suenaga *et al*., 2018). In contrast, N_2O reduction helped the obligate aerobe *Gemmatimonas aurantiaca* to overcome O_2 starvation (D. Park *et al*., 2017). Therefore, clade II N_2O reducers could have a physiological advantage in soils that experience hydrological fluctuations, such as our peat soils with water tables that can deviate by several meters between rain and dry seasons (S. Wang *et al*., 2018).

Conclusion

We presented evidence that abiotic N_2O formation succeeded by microbial N_2O consumption may be prevalent in tropical peatlands. The implications provide a fruitful avenue to a more accurate picture of the reductive branch of the nitrogen cycle. Our results suggest denitrification in tropical soils is not a purely biological pathway, but

rather a "mosaic" of biotic and abiotic reduction reactions. They also support the idea that functional modularity not only complements the mutuality of microbial groups, but also a synchronized interaction between microbes and spontaneous abiotic chemical reactions. The larger ramifications of this abiotic process remain to be evaluated; specifically, in the context of organic carbon sequestration in tropical peatlands. It would be interesting to test how oxidation of soil organic matter differs between microbial denitrification and chemodenitrification, how this would affect the identity of recalcitrant organics, and if CO_2 and methane emissions were possibly influenced. Lastly, the extension of abiotic N_2O formation beyond tropical peatlands, such as to northern peatlands, must be explored. The biotic or abiotic origin of N_2O could essentially determine net N_2O fluxes from systems affected by global climate change. Our study represents a first glance at the magnitude of a coupled abiotic-biotic process in the nitrogen cycle of tropical peatlands. With more abiotic activity data from other environments on hand, it will be possible to assess its global importance.

CHAPTER 5

MICROBIAL COMMUNITIES AND THE PUTATIVE INTERACTIONS OF

METHANOGENS WITH NITROGEN OXIDES IN DIVERSE PEATLANDS OF THE

AMAZON BASIN[4]

Abstract

High uncertainties and spatial variation in methane (CH_4) fluxes from the

Amazon basin pose a problem for predicting greenhouse gas sources. Tropical peatlands

have been identified as hotspots of CH_4 as they provide conditions (anoxia, high

abundance of organic matter) for microbial methanogenesis. Nitrogen oxides have been

known for their inhibitory effects on methanogenesis from culture experiments, but their

interactive role in CH_4 cycling in tropical peats has never been evaluated. We

investigated the effects of soil NO_x (nitrate, nitrite, nitric oxide) and nitrous oxide (N_2O)

on methanogenic abundance and activity in three geochemically diverse peatlands of the

Pastaza-Marañón foreland basin. To characterize the soil geochemistry, we probed 1-m-

soil profiles and measured concentrations of (in)organic nitrogen and carbon species,

redox, and ^{13}C enrichment in dissolved inorganic carbon and CH_4 pools. The overall soil

microbial community was characterized based on 16S rRNA and the functional gene

mcrA was used to assess methanogen diversity as well as abundance deploying

quantitative PCR (qPCR). Our molecular data revealed high potential of novel and

diverse methanogens affiliated to the Methanomicrobiales order. Geochemical conditions

---

[4] This chapter is in preparation as manuscript for publication in *Environmental Microbiology*. Co-authors are S. Buessecker, Z. Zamora, A.F. Sarno, D. R. Finn, A.M. Hoyt, J. van Haren, J.D. Urquiza Muñoz, H. Cadillo-Quiroz.

were distinct, based on pH, DOC, NO_3^- pore water concentrations and C/N ratios of shallow soils. We observed a strong stratification in abundances of microbial groups putatively involved in NO_x cycling. Thaumarchaeota and Nitrospira, both producers of NO_x, claimed similar ecological niches, with the archaea being more abundant in more acidic peat. We also conducted nitrite incubations with soil slurries and obtained N_2O-spiked enrichments from two of the peat soils to evaluate cross-effects of nitrogen oxides on CH_4 formation. Methanogenesis in contrasting soils showed differential sensitivity to nitrite and N_2O, which may have implications on net CH_4 outputs. Overall, we present evidence that potential interactions of nitrogen species with methanogens contribute to variable CH_4 fluxes.

Introduction

Though oxygen (O_2) depletion remains a main regulator of methanogenesis, influence from other high-redox species, such as nitrogen oxides (NO_x), have remained poorly understood in microbial soil habitats. In particular, peat soils are commonly anoxic due to slower O_2 diffusion in water-saturated soils and because heterotrophic respiration rapidly consumes free O_2 at the soil-atmosphere or soil-root interface (Elberling *et al*., 2011). Vertical soil stratification under anoxic conditions dictates microbial composition in peatlands (Noll *et al*., 2005; Jackson *et al*., 2008; Watanabe *et al*., 2010; Puglisi *et al*., 2014; R. Bai *et al*., 2017) and leads to the formation of NO_x gradients (Pett-Ridge *et al*., 2006; Stone *et al*., 2015; Senga *et al*., 2015; X. Wang *et al*., 2016).

NO$_x$ species are a set of N-O compounds, including nitrate (NO$_3^-$), nitrite (NO$_2^-$), and nitric oxide (NO). Importantly, the microbial metabolism for NO$_x$ production and consumption has been found to change with depth in sub-tropical forest soil (Y. Tang *et al*., 2018). Within diverse microbial communities, fermentative enzymes and NO$_x$ reductases have been found to correlate with chemical gradients (Chen *et al*., 2017). In tropical soils, heterotrophic denitrification and dissimilatory nitrate reduction to ammonium (DNRA) – a competitive reductive reaction to denitrification – have been identified as the main pathways of NO$_x$ cycling. Of these two pathways, denitrification (i.e. the reduction of NO$_x$ into N$_2$O and N$_2$) has been found to be the dominant nitrogen loss pathway in tropical biomes, accounting for 24-53% of total ecosystem nitrogen loss (Sharon J Hall and Matson, 1999; Houlton *et al*., 2006).

Depending on the geochemical conditions (pH, DOM, metals) and microbial activity, NO$_x$ are differently distributed in the soil, which can affect the microbial community. For instance, NO$_3^-$ concentrations are typically higher in shallow soil layers where microbial nitrification is most active, but it can also accumulate in deeper layers, where its consumption may be inhibited by humic substances (Senga *et al*., 2010). Meanwhile, NO$_2^-$ is unstable in acidic peat pore water, because it decomposes under acidic conditions (pH < 5.5) and rapidly reacts with organic soil moieties or metals (Cleemput and Samater, 1996). The relative degree to which soil microbiota are exposed to NO$_2^-$ is controlled by the inherent soil properties in addition to the activity of microbial NO$_2^-$ oxidoreductases or reductases. Also, NO$_2^-$ reducing reactions generate NO as reactive intermediate, which typically is a very transient species with negligible steady concentrations. Its various availability and interactions makes NO$_x$ generally

difficult to identify as stimulators or inhibitors of microbial processes. Effects of NO_x

have to be evaluated within the geochemical context of their soils or complementarily

tested under controlled conditions.

Methanogens have been shown to be inhibited by free NO_x in pure culture

experiments (Klüber and Conrad, 1998b) and paddy soil incubations (Klüber and Conrad,

1998a). However, inhibitory effects showed different sensitivity depending on the

methanogenic species tested. In addition, NO_x can also serve as oxidants in the anaerobic

oxidation of CH_4 (AOM). In contrast to marine taxa that rely on sulfate, members of both

the domains *Archaea* and *Bacteria* possess the potential to use NO_3^- (Haroon *et al.*, 2013)

and NO_2^- (Ettwig *et al.*, 2010) to oxidize CH_4. The metabolism of AOM-mediating

bacteria (known as NC-10, and affiliated with *Candidatus* Methylomirabilis oxyfera) has

been demonstrated, and members of this clade were detected in sub-tropical peat soil (B.

L. Hu *et al.*, 2014). Thus, the concentration and species make-up of NO_x has the potential

potential to influence the production and flux of CH_4 in anaerobic soils, such as those in

tropical peatlands.

Peatlands have been overlooked as strong CH_4 sources within tropical latitudes

(A. C. I. Tang *et al.*, 2018; G. X. Wong *et al.*, 2018; Sakabe *et al.*, 2018; G. X. Wong *et

al.*, 2020), including recently documented sites in the Peruvian Amazon (Teh *et al.*, 2017;

Winton *et al.*, 2017). However, CH_4 emissions in the tropics have been associated with

high uncertainties due to lacking spatial and temporal *in-situ* monitoring and a poor

mechanistic understanding of soil CH_4 fluxes (Kirschke *et al.*, 2013). The origin of this

CH_4 is accumulated organic matter. Tropical peatlands are a type of wetlands where the

accumulation of organic matter exceeds its rates of decomposition (Gore, 1983) and large

swaths of areas holding tropical peatlands have been reported in the Amazon basin (Gumbricht *et al.*, 2017). The Pastaza-Marañón foreland basin (PMFB) contains soil carbon (SC) stocks estimated to be at least 3.1×10^{12} kg, or ~32% that of South America in total (Draper *et al.*, 2014), which could be slightly underestimating true extents according to more recent models (Gumbricht *et al.*, 2017). Therefore, peatlands of the PMFB pose a major potential source pool for atmospheric CH_4 in the region. Given the role of CH_4 as a powerful greenhouse gas and the predicted shift in environmental conditions of the Amazon basin in the wake of global climate change (Davidson *et al.*, 2012), it is critical to address uncertainties in the CH_4 flux of these environments.

To assess the origin and flux of CH_4 vertically through peat soils of the PMFB, we conducted field measurements in soil profiles at three vegetation and hydrologically distinct peatland sites, characterized the geochemical conditions, and assessed the overall and methanogenic microbial community composition. We focused on the distribution of inorganic nitrogen species (incl. NO_x) and tested activity responses of soil methanogens under manipulated, NO_2^- and N_2O amended conditions.

Methods

Study sites and field sampling. The peatlands in this study are located in the Pastaza-Marañón basin, Loreto Region, in the Western Peruvian Amazon. We chose peatlands with contrasting geochemistry and formation history (Lähteenoja *et al.*, 2009). *San Jorge* (SJO, 4°03'41.6" S, 73°11'48.1" W), is a dome-type peatland that receives most of its water from precipitation (ombrotrophic), has oligotrophic and acidic conditions in its soils and is a "pole forest" dominated site. *Quistococha* (QUI) is

94

adjacent to a lagoon (3°50'5.6" S, 73°19'24.0" W) and is characterized as a forested

swamp dominated by *Mauritia flexuosa* palms, with intermediate to poor nutrient levels

and mildly acidic soils. In contrast, *Buena Vista* (BVA, 4°14'23.3" S, 73°12'08.2" W) is

a forested minerotrophic peatland with a groundwater-influenced hydrology undergoing

long riverine floods, high nutrient content and soils with pH ~6-6.5. Field work was

conducted in Summer 2014 (QUI, SJO) and 2015 (BVA) after onset of the rain season

when the water tables were at or close to the surface (QUI, BVA) or at ~10 cm below soil

surface (SJO). Samples for isotopic analysis were collected in 2017.

To extract soil pore water from a vertical profile of 1m deep, PTFE tubing ending

in a porous teflon macro-rhizon (4.5 mm OD, 0.15 μm pore seize, Sunvalley Solutions)

was pushed into the peat soil. Peat pore water was pulled with a plastic syringe and

filtered (0.8/0.2 μm pore seize, Acrodisc) into acid-washed Nalgene HDPE plastic bottles

(Nalge Nunc Int.). Samples for ion chromatography and spectrometric analysis received

the biocide Thymol (Fisher Scientific) to a 100 mg/L final concentration (Cape *et al*.,

2001). To sample soil gas for the quantification of CH_4 and CO_2, we used a modification

to a soil gas equilibration-by-diffusion through gas-permeable teflon membrane method

(B. L. Hu *et al*., 2014). Ten PTFE tubes of 10-100 cm length with a 10cm-long teflon

stub were inserted into the soil over an area of ~1 m^2, closed at the top, and left at place

for 24 hours. After the equilibration period, a gas-tight syringe (Monoject) was used to

draw sample gas and to inject it into pre-evacuated glass vials through a butyl rubber

stopper. All liquid and gas samples were stored under cold or frozen conditions upon

analysis. To sample soil for DNA extraction, a Russian soil corer was used to take 1 m

cores. Three samples of 500 mg soil were aseptically weighted into screw cap tubes at every 10 cm, for two soil cores at each site (60 samples per site). Soil samples were frozen and kept at $< 0°C$ throughout the field work and transport. pH measurements were done on a 1:5 soil sample dilution using the same soil intervals as for the molecular work with a pH meter 10A (Ecosense, YSI).

Geochemical analyses and determination of the C isotopic composition. Pore water cations were analyzed by ion chromatography using the Dionex ICS2000 series at a 1 mL/min eluent flow rate. A CG12A pre-column, followed by a CS12A analytical column was used with an eluent of 35 mM methanesulfonic acid. DOC was determined by a TOC-V Total Organic Carbon Analyzer (Shimadzu Scientific Instruments). Inorganic nitrogen species were quantified spectrometrically using an AQ2 Discrete Analyzer (Seal Analytical) and approved method EPA-103-A Rev.10 for ammonium (LoD 0.004 mg-N/L, range 0.02- 2.0 mg-N/L) and method EPA-127-A for NO_3^-/NO_2^- (LoD 0.003 mg-N/L, range 0.012- 2 mg-N/L). TC and TN in soil pore water was determined with a Shimadzu TOC-V/CSN connected to a TNM-1 unit (Shimadzu Scientific Instruments) and GEL method based on Standard Methods 5310B and ASTM D8083 was used. $\delta^{13}C$ in CH_4 was measured with a ThermoScientific Precon concentration unit interfaced to a ThermoScientific Delta V Plus isotope ratio mass spectrometer (ThermoScientific) at the Stable Isotope Facility at U.C. Davis. A more detailed method description can be obtained consulting the facility website (https://stableisotopefacility.ucdavis.edu, July 2018). DIC concentrations and $\delta^{13}C$ of DIC measurements were measured on the SHIVA platform in the EcoLab laboratory

(Toulouse, France). The $\delta^{13}C$ of DIC was analyzed using a mass spectrometer (Isoprime 100, Elementar) coupled with an equilibration system (MultiFlow-Geo, Elementar). Samples were acidified using phosphoric acid and flushed with helium. Standards included Na_2CO_3 and $NaHCO_3$ as well as internal water standards. All standards were analyzed every 8 samples to check for instrument stability. All samples were analyzed in replicates.

The fractionation factor α was derived with the formula

$$\alpha = \frac{\delta_{CO_2} + 10^3}{\delta_{CH_4} + 10^3}$$

Trace metal (Mo) soil content was determined by inductively coupled plasma mass-spectrometry (ICP-MS) after acid digestion. In brief, an acid mix ($HF+HNO_3+HCl$) was added to soil samples in acid-cleaned Teflon vials. Soil organic matter was oxidized overnight. After another HCl addition, the sample was microwaved and the top liquid was decanted and evaporated on a hotplate. Repeated acid addition and evaporation concentrated the residual soil metals. A diluted sample was then measured on an iCAP-Q (Thermo Scientific) with Mo calibrated for 0.018–126 ppb (3% error range).

E_h *calculations.* The partial pressure of CO_2 and CH_4 ($\frac{p_{CO2}}{p_{CH4}}$) in soil gas samples was used to derive the equilibrium redox potential (E_h) between the redox couple. For each depth interval, E_h was pH-corrected. All calculations were based on the equation $CO_2 + 4\,H_2 = CH_4 + 2\,H_2O$ for methanogenesis.

$$E^0_{pH} = E^0_{pH,0} - \left(\frac{0.059\, v_{H^+}}{n}\right) pH$$

The standard potential at pH = 0 ($E^0_{pH,0}$, Bratsch, 2009), the stoichiometric

coefficient v_{H^+} = 8, and the number of electrons transferred per 1 mole of CO_2 and CH_4

(n = 8) were used to derive the standard potential at distinct soil depths (E^0_{pH}). From there

we calculated E_h using the Nernst formula. The temperature (T) was set to 298 K and we

used 8.314 J mol^{-1} K^{-1} for the ideal gas constant (R) and 96,485 C mol^{-1} for the Faraday

constant (F) according to (Stumm and Morgan, 2012). We used partial pressure as proxy

for the activity of the redox species.

$$E_h = E^0_{pH} - 2.303 \left(\frac{R\,T}{n\,F}\right) log \left(\frac{p_{CH_4}}{p_{CO_2}}\right)$$

DNA extraction, amplification and amplicon sequencing of 16S rRNA and mcrA.
Frozen peat samples from the individual corer segments were used for subsequent DNA

extraction at the lab. Soil DNA was extracted using a NucleoSpin Soil DNA extraction

kit (Macherey-Nagel GmbH). PCR was performed with the archeal-bacterial primers

515F/909R (Tamaki *et al.*, 2011) and *mlas/mcrA*-rev (Steinberg and Regan, 2009) to

target methanogenic euryarchaeota. Both pairs were combined with unique barcodes

(Tamaki *et al.*, 2011). For 16S rRNA amplification reactions, we used 0.3 μM of forward

and reverse primers, 0.2 mg/L bovine serum albumin, and 1x GoTaq Green Master Mix

(Promega). The thermal cycling conditions were the following: initial denaturation at

95°C for 5 min, 25 cycles of denaturation at 94°C for 30 sec, annealing at 52°C for 1 min,

and extension at 72°C for 1 min, as well as a subsequent final elongation step at 72°C for

10 min. The reaction chemistry for *mcrA* amplification reactions was used as described

elsewhere (Steinberg and Regan, 2009). Thermal cycling included denaturation at 95°C for 3 min, 5 cycles of denaturation at 95°C for 30 sec, annealing at 48°C for 45 sec, and extension at 72°C for 30 sec, accompanied by another 30 cycles of 95°C for 30 sec, 55°C for 45 sec, 72°C for 30 sec, and one final elongation at 72°C for 10 min.

PCR products were verified by fragment size in a 1% (w/v) agarose gel with 0.5x TBE buffer. Samples were multiplexed (Herbold *et al.*, 2015), normalized (SequalPrep kit #1051001, Invitrogen), and submitted for sequencing to the DNASU core facility, with 2x 300-bp paired-end Illumina MiSeq (Tempe, AZ).

For archeal 16S rRNA and *mcrA* gene quantification, the Promega GoTaq qPCR kit (Promega) was used for standards and samples. The reaction mix consisted of 4 mM MgCl2, 1.5x CXR reference dye, 0.3 µM of forward and reverse primer, and 1x GoTaq qPCR master mix. The universal primer pair ARC787f /ARC1059r (Y. Yu *et al.*, 2005) was used to broadly target archaea, whereas *mlas/mcrA*-rev (Steinberg and Regan, 2008) served to target *mcrA*. Optimal qPCR cycling conditions in reactions with ARC787f /ARC1059r were found to be denaturation at 94°C for 10 min, 45 cycles of 94°C for 10 sec and 60°C for 30 sec. Cycling stages for *mlas/mcrA*-rev comprised primary denaturation at 95°C for 2 min, followed by 40 cycles of 95°C for 30 sec, 55°C for 45 sec, 72°C for 30 sec, and 83°C for 8 sec. A melting-curve was established to exclude chances of primer dimers. Standard curves were created with sufficient efficiency and linearity ($R^2 > 0.99$) in the measurement range of the samples.

16S rRNA and mcrA phylogenetic analyses. Sequencing data was merged and demultiplexed with an in-house script developed in R, all subsequent analysis was conducted on the Qiime 2 platform (https://qiime2.org, releases 2017.12 and 2018.8, (Caporaso *et al*., 2010). Each soil core was run through the pipeline as sample set of 10 samples with duplicate cores per site. Reads' dereplication was done via the VSEARCH module. The dereplicated sequences were then *de-novo* chimera-checked. After chimera-filtering, open-reference clustering was applied at a 97% identity level and using the SILVA database (release 128). Dereplication and clustering reduced the mean and median of sequences per sample from 87,379 and 70,016 to 54,155 and 44,371, respectively. As a next step, singletons were removed by utilizing the *feature-table filter-features* command. An alpha-rarefaction curve was created for every sample set to test for species richness (Figure D.2). The maximum sampling depth was chosen to be 75,000 across all sets. Taxonomic classification was done using VSEARCH consensus classifier with SILVA's 99 majority taxonomy as a reference. Percentage identity was set to 0.94, min-consensus was set to 0.6, and maximum hits accepted were 10. Next, a phylogenetic tree was constructed de-novo with the built-in module FastTree 2 (M. N. Price *et al*., 2009). First, multiple sequence alignment was perfomed using MAFFT Version 7 (Nakamura *et al*., 2017) before unconserved and highly gapped columns were masked from the alignment. FastTree command created an unrooted tree, on which midpoint rooting was applied.

The *mcrA* pipeline was made up of concatenated single steps that were part of the Qiime 2 or USEARCH (R. Edgar, 2010) pipeline, and other stand-alone programs. First, sequences were dereplicated using the *-fastx_uniques* command in USEARCH. Then,

samples were normalized to ~20,000 sequences per sample (Yang *et al.*, 2017). We tested

potential artifacts with repeated subsampling (n = 3) of the same input sequences and

found no major differences in OTU abundances. Next, USEARCH's *unoise3* command

was applied to denoise and to filter chimeras. Singleton sequences were retained (-

minsize 1) to include very low abundance OTUs. The sequences were then translated and

frameshift-corrected by Framebot (Q. Wang *et al.*, 2013) with a low loss (< 10%) of

sequences. Subsequent clustering was administered using 85% identity level in

accordance to a previous assessment of processing *mcrA* data as amino acids (Yang *et al.*,

2017). *-cluster_fast* (variant of the UCLUST algorithm) was fed with centroid sequences

which were derived from a custom-made database. The database was built with

sequences retrieved from the FunGene collection (http://fungene.cme.msu.edu) in

January 2018, and complemented with additional reads from tropical mangroves

(Taketani *et al.*, 2010) and a peat swamp forest (Kanokratana *et al.*, 2010). The output of

the *-cluster_fast* command was used to make an OTU table, to classify centroid

sequences, and to derive core diversity metrics. At this stage, OTUs with 5 or less

sequences over all soil layers were removed. To classify the ~150 amino acids long

centroid sequences, we tested two different search algorithms on their performance with a

subset of our sample data. The standalone version of BlastP (2.7.1+) and HMMer 3.0

(Eddy, 2011) did not show substantial differences in sensitivity and specifity as noted

previously (Orellana *et al.*, 2014). Hence, BlastP was run on the non-aligned centroid

queries and typically attained e-values of 10^{-80} or lower, as done in earlier studies of

relevance (Takeuchi *et al.*, 2011; Penton *et al.*, 2015). We determined the depth of the

lineage taxonomy with an optimized approach as developed previously (Steinberg and

Regan, 2008). We refined the evaluation of sequence similarity cutoffs for methanogen taxonomic levels by (i) including 102 methanogen species that were all represented by *mcrA* sequences from isolates in swissprot, (ii) extending the taxonomy to 14 methanogen families, (iii) using the Jone-Taylor-Thornton (JTT) algorithm, (iv) introducing archaea-adjusted gamma-distribution based on an elongation factor specifically determined for archaea (Gaucher *et al.*, 2001). Distance matrices and phylogenetic trees were derived in MEGA Version 7.0.26 (Kumar *et al.*, 2016). The phylogenetic tree was constructed by aligning sequences while ambiguous positions were removed for each sequence pair. Distances were calculated using the JTT method.

Microcosm incubations and activity measurements. In a glove box with a reducing, O_2-free atmopshere (0.5% H_2 in N_2), fresh soil (not older than 2 months) was root-picked, coarse particles (> 5 mm in diameter) were removed, and diluted 1:10 in anoxic, sterile 18.2 $M\Omega \cdot cm$ water. The slurry was well homogenized and mixed before equal quantities were distributed to culture vials, which were subsequently closed with butyl rubber stoppers. Next, an anoxic stock solution of NO_2^- was injected (final concentration 200 μM) to a subset before the vial headspace was flushed with pure N_2. The microcosms were agitated briefly to disperse the NO_2^- added and were then kept under dark and static conditions at room temperature for a total of 3 weeks. 200 μL of headspace was sampled in even time steps with a gas-tight, N_2-purged syringe (VICI Precision Sampling) and injected into a gas chromatograph (GC) equipped with a flame-ionization detector (FID). Two continuous HayeSep-D columns were kept at 90°C (oven temperature) with N_2 (UHP grade 99.999%, Praxair Inc.) as carrier gas and H_2 for FID

combustion (supplied by a H_2 generator GCGS-7890, Parker Balston). CH_4 concentration measurements were calibrated with customized standard mixtures (Scott Specialty Gases, accuracy ±5%) over a range of 5-5,000 ppmv. Gas phase concentrations were corrected using Henry's law and the dimensionless concentration constants $K_H^{cc}(CH_4) = 0.0342$ (Stumm and Morgan, 2012) to account for gas dispersed into the aqueous phase at 25°C. CH_4 production rates were calculated based on the linear part of the concentration curve for manipulated and control incubations.

Soil enrichments. Wet peat soil was initially inoculated into anaerobic peat media (Cadillo-Quiroz *et al.*, 2008) at a 1:10 (w/v) proportion and well blended. We adjusted pH to in-situ measured values for BVA and SJO using organic buffers as described previously (Cadillo-Quiroz *et al.*, 2008). Sterile glass beads (0.5 g) were added to 5 mL of inoculated media within closed Balch tubes to stimulate microbial interaction. Then, culture vials were overpressurized by 12 PSI of an H_2/CO_2 (80/20) mixture and N_2O was injected to 500 ppm final headspace concentration. Methane development and N_2O consumption was monitored by GC injections as described above. For N_2O detection, an electron-capture detector (ECD) was used in line with the FID. Once N_2O levels dropped below detectability, the cultures were spiked again with 500 ppm N_2O. Turbidity (OD_{600} measurements) and hence biomass growth was generally very low for enrichments from BVA and SJO. Therefore, microbial growth was confirmed by microscopy. Cultures were incubated at 30°C incubation temperature.

Statistical Analyses. All basic statistical tests were performed with

JMP Pro software (Version 13.1.0, SAS Institute Inc.). Raw sequence counts were

normalized by Johnson transformation. Principal components were explored using the

multivariate analysis toolbox on JMP. PERMDISP and PERMANOVA was conducted

on the Qiime 2 platform using the *diversity beta-group-significance* command including

pairwise testing on 9999 permutations. Alpha and beta diversity indices were calculated

using the *diversity core-metrics-phylogenetic* command configured with sampling depths

according to individual sample sets. Plotting and regression analysis was done with the

Matlab R2018a software package (Version 9.4.0.813654, Mathworks Inc.).

Results & Discussion

The peatlands *Quistococha* (QUI), *San Jorge* (SJO), and *Buena Vista* (BVA)

served as the study sites and represent the geochemical diversity of anoxic, tropical peat

soils found in the PMFB (Figs. D.1 and D.2). The dome-type, ombrotrophic peatland San

Jorge is characterized by low soil pH (~3.5), whereas the minerotrophic peatland Buena

Vista has Ca-buffered peats at circum-neutral pH (~6.5). The palm swamp Quistococha is

in the middle of this spectrum (pH ~4.3). We explored these soils by complementing

geochemical profile data collected in the field with molecular analyses and laboratory

incubations.

*PMFB peatlands show differing soil CH_4 profiles, DOC loads, and inorganic N

levels*. We measured maxima in CH_4 concentrations with up to 2.5% (v/v) in SJ, 4.7%

(v/v) in QUI and 6.9% (v/v) in BVA predominantly in deep peat (Fig. 5.1). N_2O

104

concentration showed that throughout the profiles (Fig. 5.1) all sites contained roughly 10 times higher N_2O levels than the mean ambient atmosphere (Stocker *et al.*, 2013). We observed that particularly soil cores of the less acidic site (BVA) showed increasing N_2O concentrations with soil depth (Fig. 5.1). Also, NO_2^- concentrations in SJO and QUI did not show statistically significant differences from the method's limit of detection (LoD), and only BVA samples yielded NO_2^- levels statistically above LoD ($p < 0.05$). Across evaluated peatlands, NO_3^- reached highest concentrations in shallow soil layers, with maxima at 0.4 mg L^{-1} (BVA), 0.05 mg L^{-1} (QUI), and 0.02 mg L^{-1} (SJO). NO_x were 10 times more concentrated in BVA than at other sites. Ammonium (NH_4^+) showed a vertical pattern opposite to the other nitrogen species. Concentrations increased by roughly a factor of 4 from top to bottom layers in SJO, and followed a similar, but less pronounced, trend at the other locations.

Since molybdenum (Mo) is an important trace metal in N_2 fixation, we determined soil Mo abundances to exclude the possibility of Mo limitation at the beginning. Acid-digested peat extracts yielded molybdenum concentrations of 0.53±0.01 ppm (QUI), 1.25±0.2 ppm (SJO), and 1.32±0.1 ppm (BVA, all n = 3). Soil pore water dissolved organic carbon (DOC) profiles differed significantly across sites (ANOVA, $p <$ 0.05, Fig. 5.1). QUI showed the lowest DOC pore water levels, with a mean minimum at 40 cm depth (12.8 mg L^{-1}) and a maximum at 70 cm (15.1 mg L^{-1}). Conversely, SJO profiles reached a mean minimum at 80 cm (16.8 mg L^{-1}) and a mean maximum at the top layer (20.3 mg L^{-1}). Highest DOC concentrations were found in BVA peat (up to 29.1 mg L^{-1}), where the entire 1 m-profile could not be obtained due to a dense network of roots that impeded the deployment of some but not all our sample tubing. Unlike DOC

profiles, C/N ratios resulted in significant variation along soil depth. A trend of increasing C/N values with increasing depth was observed in BVA where the mean ratio at the 60 cm-layer was ~3.6 times the mean ratio of the surface layers (Fig. 5.1). In contrast, the C/N profile at SJO was decreasing with increasing depth with values from uppermost and lowermost layer being ~2.4 fold apart.
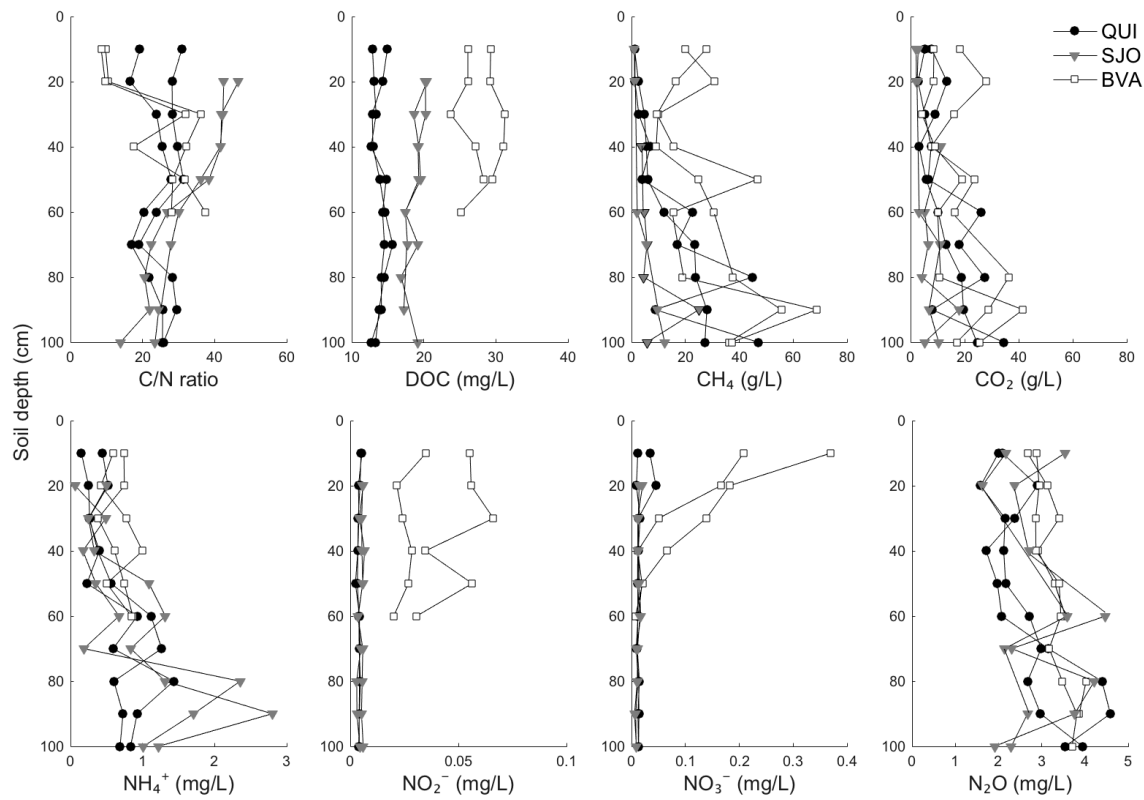
Figure 5.1. Levels of carbon and nitrogen along soil profiles of three tropical peatlands (QUI, SJO, BVA). Two separately sampled (duplicate) profiles from Quistococha (QUI), San Jorge (SJO), and Buena Vista (BVA) were each set up to sample pore water and soil gas. Ions, total carbon and nitrogen abundances, and DOC were determined from pore water, whereas gas concentrations were measured in equilibrated gas samples. Liquid samples in BVA were not collected below 60 cm due to blocked sampling paths.

DOC has emerged as an important predictor of CH_4 production in wetland soils (D. Liu *et al*., 2012; Morrissey *et al*., 2013). DOC concentrations obtained in this study are at the lower end of values compared to tropical peat soils of Borneo (Gandois *et al*., 2014). All concentration profiles appear stable along soil depth with no indication of sinks. These would conceivably occur in more shallow regions where the fraction of refractory SC is less prevalent (Artz *et al*., 2006). A DOC sink due to mineralization is not present based on our data. The DOC pool is comprised of diverse organic molecules characterized by a wide molecular size range, organic acids, humic substances of different aromaticities, and protein groups. These compounds may vary with depth even though the bulk concentration may be stagnant. Extracellular enzymes and humic substances may play a crucial role in diverting electron flow from methanogenesis, given the thermodynamic preference over CO_2 (Heitmann *et al*., 2007; Knorr and Blodau, 2009), that would ultimately suppress CH_4 production. Based on our results, we can exclude fluctuations of the total DOC pool to have major effects on carbon mineralization in distinct soil layers, but organic compounds could structurally differ along depth and impact specific microbial activities.

C/N ratios are important indicators of potential nitrogen limitation (Sharon J Hall and Matson, 2003). The moderate ratios observed in the QUI cores are consistent with previous measurements at that site (Lawson *et al*., 2014). SJO profiles show comparably high C/N values indicating relative nitrogen scarcity. High NO_3^- concentrations in BVA shallow peat and low concentrations throughout the SJO soil profile lower and raise the C/N ratio, respectively. The source for NH_4^+ includes release from OM through

107

ammonification, N_2 fixation, or DNRA. The latter would not serve as a net source of dissolved inorganic nitrogen. Plant debris with low C/N ratio tends to trigger net N mineralization (Manzoni *et al.*, 2010) which would result in increasing NH_4^+ concentrations as observed in SJO deep peat. Microbial fixation of N_2 mediated by the molybdenum-based nitrogenase enzyme represents another source of NH_4^+. The unusual temperature dependence of the enzyme grants a high N_2-fixing capacity to tropical peats (Houlton *et al.*, 2008), with implications for the retention of inorganic nitrogen. In fact, the measured molybdenum content among sites are above the limiting range for N_2 fixation by free-living heterotrophic bacteria in tropical forest soils (Barron *et al.*, 2008). We consider that active N_2 fixation in the anoxic regime of SJO soils could exist. In contrast to NH_4^+, NO_x species were more abundant in shallow soils, irrespective of the site-specific geochemistry, which is consistent with previous reports (B. L. Hu *et al.*, 2014; Palmer and Horn, 2015; Y. Tang *et al.*, 2018). Based on observed N_2O profiles, we propose that higher sink potential at the top and higher source potential in bottom layers (Palmer and Horn, 2015) is likely in the evaluated sites.

Overall microbial community composition in peat soil profiles. The geochemical diversity of the three peatlands was reflected in their contrasting microbial community composition. A total of 4,980,584 data reads were clustered to operational taxonomic units (OTUs) with 3% identity radius for taxa assignment on the family level or above. Alpha rarefaction analysis showed an appropriate sampling depth was achieved for most sites (Fig. D.3). SJO with 6,636 OTUs had the lowest richness while BVA yielded about 3 times as many OTUs (18,649).

To evaluate co-dependencies of the geochemistry and specific microbial taxa, we focused henceforth on microbial groups putatively relevant to the cycling and vertical distribution of soil NO_x (Table D.1) but also included very abundant groups or those known to undergo syntrophic relationships with methanogenic archaea (Fig. 5.2). We assumed ecological coherence within the family taxonomic rank as proposed elsewhere (Philippot *et al*., 2010). Accordingly, *Acidobacteriaceae* were abundant in QUI and SJO soil (up to 8.2% and 5.0% of total OTUs in average along soil depth). Shallow soils of SJO harbor a substantial fraction of *Acidothermaceae* with 4-9% of total OTUs. *Bacillaceae* and *Paenibacillaceae* seem to be a special occurrence in the palm swamp of QUI with abundances of up to 8%. *Nitrospiraceae* were most abundant in BVA in soil layers slightly below the top layer (15-25 cm in both duplicate cores), suggesting preference to suboxic niches. *Xanthobacteraceae* revealed interesting distribution patterns in all sites. Abundances peaked at mid profile depth in QUI (5.4% and 3.5% of total OTUs in each core). In SJO peat soil, the group reached even higher values of 17.9% and remained significant at ~1% of total OTUs in a depth of 75 cm before ceasing in the bottom layers. BVA showed maximum abundances for *Xanthobacteriaceae* (4.7% and 5.4%) exclusively in shallow layers. Interestingly, we detected sequences affiliated with *Desulfurellaceae*, which were represented by almost 2% of total OTUs in SJO and BVA predominantly in surface soils. We subsequently included this group as NO_x non-metabolizing taxon. Another taxon whose relative abundance seems homogenous and can be interpreted as a group not affected by the soil vertical gradients might be *Spirochaetaceae* (consistent abundances of 0.5-1.0% in average per core).

Bathyarchaeota was a very abundant phylum frequently making up 20% of total OTU counts. Their distribution suggests they may persist in deeper regions of the peat soils. In contrast, OTUs assigned to Euryarchaeota were less abundant and did not show a preference for deeper layers. The uppermost soil layer in BVA cores was among the richest in Euryarchaeota with ~3% of total OTUs. In QUI and SJO, maxima in Euryarchaeota OTUs (1.5% and 1%, respectively) were found in moderate depths. Thaumarchaeota showed a peculiar distribution across sites, with high abundances in QUI and SJO (up to 23.7% and 16.8%), and low abundances in BVA. Principal component (PC) analysis showed data point clusters well separated into the three peat soils (Fig. 5.3A). OTU abundances of Bathyarchaeota, Methanomicrobia and Methanobacteria were similarly associated to principal component 1 (PC 1), while CH_4 concentration was related to PC 2.

The high abundance of *Xanthobacteriaceae*, and Bathyarchaeota (Fig. 5.2) across sites is likely related to a putative role as degraders of peat organic matter. Particularly under O_2-limiting conditions, *Xanthobacteriaceae* have a broad suite of organic substrates, including alkanes, alkenes, (poly)aromatic compounds, thiopenes, organic acids, or xylose and xylan (Zaichikova *et al.*, 2010). Those substrates are common and accumulate in peat soils (Moers *et al.*, 1990). Bathyarchaeota is an abundant group likely to have been overlooked by the lack of recognition of the phyla in older databases (as in SILVA 115 or priors; Y. Bai *et al.*, 2018), or because several primers are incapable of amplification (like the *mcrA* set in this study that has 10-18 base pair mismatches; Evans *et al.*, 2015). The genetic potential of Bathyarchaeota includes enzymes to hydrolyze plant-derived carbohydrates and detrital proteins, and to produce acetate for energy

110

conservation (Lazar *et al*., 2016). PC analysis (Fig. 5.3B) indicates interactions where over 50% of data variation along PC-1 is concomitantly explained by Bathyarchaeota diversity, pH and NO_x. A putative relationship Bathyarchaeota-NO_x is supported by a report indicating that NO_2^-/NO_3^- transporter proteins, an enzymatic set to support DNRA, were detected in reconstructed Bathyarchaeota metagenomes (Lazar *et al*., 2016).

Figure 5.2. Relative 16S rRNA abundance heatmap of archaeal (left) and bacterial (right) taxa. Archaeal 16S abundances were summarized on the phylum level with Bathyarchaeota, Euryarchaeota, and Thaumarchaeota consistently making up >90% of all taxa. Only Bacterial 16S taxa at the family level that were either most dominant (at least

112

2% of total OTUs), had the potential of a syntrophic relationship to methanogens, or were affiliated to known metabolic reactions involving NOx are depicted here. The number of unassigned sequences (no match in the SILVA database) increased notably in deeper layers. Table D.1 contains the abundance values for individual cores.

Two other abundant groups, Thaumarchaeota and *Nitrospira* (Fig. 5.2) likely play an important role in regulating pulses of NO_x through peat soils. Thaumarchaeota are ammonia-oxidizing archaea (AOA), while *Nitrosomonadaceae* (genus *Nitrosomonas*) and *Nitrospiraceae* (genus *Nitrospira*) are members of the ammonia-oxidizing bacteria (AOB). AOA and AOB generally prefer inorganic N sources, even though AOA have been shown to metabolize organic N, too (Weber *et al*., 2015). Both AOA and AOB aerobically convert NH_4^+ into NO_2^-. Several studies have pointed out that AOA are more dominant in acidic soils than their AOB counterparts (Zhang *et al*., 2011), which could be due to indirect pH effects on the preferred substrates (Höfferle *et al*., 2010; Yao *et al*., 2011; Daebeler *et al*., 2014; Weber *et al*., 2015). The partitioning of AOA and AOB groups across the peatlands in this study reflects this pH and NOx patterns with the dominance of AOB over AOA in BVA, and the opposite pattern in mildly acidic QUI and highly acidic SJO. We propose nitrification to be mostly carried out by archaea in the oligotrophic and acidic sites and AOB-dependent nitrification to prevail in the minerotrophic closer to neutral pH site. This preferential niche selection would have further implications on the NO_3^- to NO_2^- ratio. Some species of the *Nitrospiraceae* (AOB) are also able to oxidize NO_2^- further to NO_3^-, therefore complete nitrification (Daims *et al*., 2015; van Kessel *et al*., 2015) can explain the higher levels of NO_3^- detected in the NOx profile of BVA (Fig. 5.2).
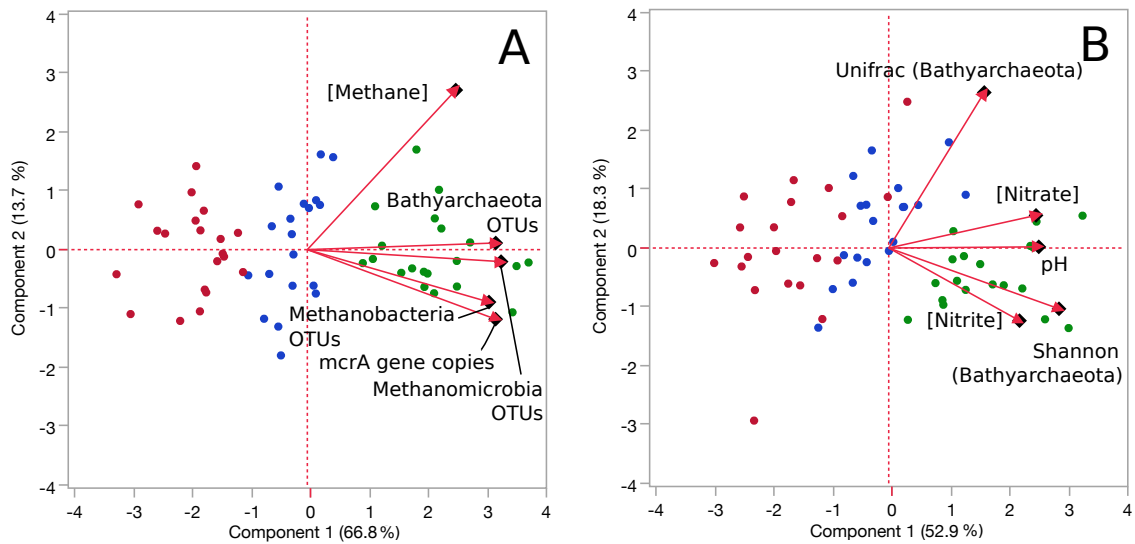
Figure 5.3. PCA ordination plots of microbial and environmental data from three soil profiles of contrasting Amazon peatlands. Samples were derived from QUI (blue), SJO (red) and BVA (green) with abbreviations as in Fig. 5.1. (**A**) CH_4 concentration, 16S rRNA OTU abundances, and *mcrA* gene copy number (A) and Bathyarchaeota alpha (Shannon) and beta (Unifrac) diversity indices, NO_x concentrations and pH (**B**) were evaluated against microbial distribution.

Methanogenic pathways, vertical distribution and redox conditions are reflected in the structure of methanogenic communities. To evaluate the potential pathways of methanogenesis across sites, we measured the isotopic composition ($\delta^{13}C$) of dissolved CH_4 and inorganic carbon (DIC) of several soil layers. $\delta^{13}C$ values in CH_4 and DIC from BVA and QUI were indistinguishable from each other but distinct from SJO, which had a more depleted $\delta^{13}C$ signature (Fig. 5.4). In SJO, $\delta^{13}C$ abundances in CH_4 also showed variation between duplicate cores with a core showing a sudden depletion at 20 cm depth by 6‰ (Fig 5.4). This "hook" shape of the ^{13}C-CH_4 profile likely indicates aerobic methane oxidation (AMO), which preferentially converts $^{12}CH_4$ to CO_2, resulting in an enrichment of $^{13}CH_4$ in the residual dissolved CH_4 pool. All sites showed evidence of active methanogenesis. The isotopic CH_4 and DIC proportions yield fractionation factors

114

(α) of 1.075±0.0015 in SJO, 1.071±0.0009 in QU, and 1.067±0.0015 in BVA (±SD/2, n = 10-12), and are within the range observed in a tropical peatland in Panama (Holmes *et al.*, 2015). According to the current consensus, $\alpha < 1.055$ and $\alpha > 1.065$ are characteristic for environments dominated by acetoclastic or hydrogenotrophic methanogenesis, respectively (Whiticar, 1999). Thus, the source of CH_4 is preferentially H_2/CO_2 in the studied peatlands, with a more noticeable contribution of acetoclastic methanogenesis in BVA.

We also estimated the redox potential (E_h) based on the CH_4/CO_2 pair and soil pH (Fig. 5.4). Along soil profiles, E_h in SJO decreased from –0.03 to –0.035 V, increased in QUI from –0.098 V to –0.067 V, while BVA showed negligible change at –0.21 V. The average E_h among sites decreased with more positive values in SJO, followed in order by QUI and BVA, consistent with observed levels of CH_4 emissions and abundance trends of the *mcrA*/16S rRNA fraction (see below).
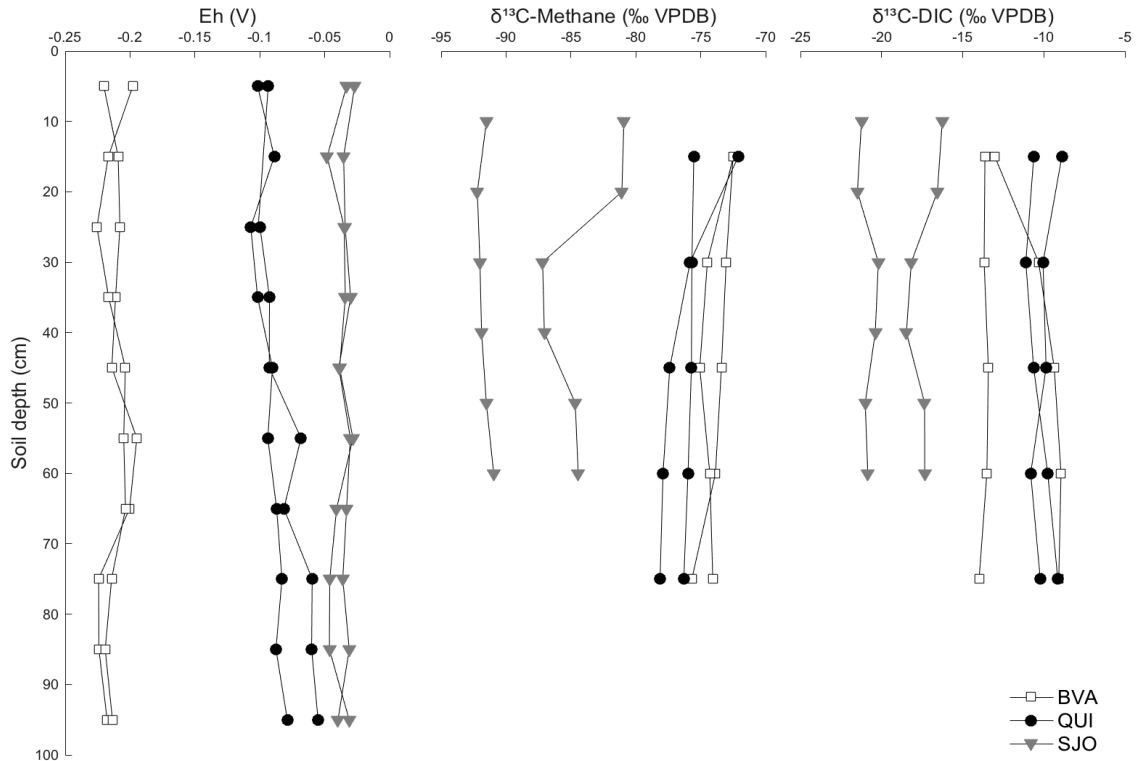
Figure 5.4. Redox gradient and carbon isotope composition of CH$_4$ and dissolved inorganic carbon along soil profiles of three tropical peatlands (BVA, QUI, SJO). Redox potential (E_h) is based on the ratio of the redox couple CH$_4$-CO$_2$ and soil pH-corrected. VPDB, Vienna Pee Dee Belemnite. Each data point corresponds to one replicate soil core.

The methanogen functional composition was evaluated by sequencing and quantitative PCR of the alpha subunit gene of the MCR enzyme (*mcrA*), which catalyzes the final step in methanogenesis (Ermler *et al.*, 1997). PERMANOVA tests on *mcrA* amplicons from all cores indicated significant differences among peatlands. Site replicates were not distinguishable (F = 1.11, *p* = 0.2494), but values across sites showed increasing dissimilarity with BVA closer but distinct to QUI (F = 7.5±1.6), p <0.0005), and further and more distinct to SJO (F = 11.4±0.7, p < 0.0001). *McrA* analysis identified 264, 509, and 1104 OTUs for all sequences from SJO, QUI, and BVA, respectively, and

a standardized OTU abundance analysis (Table D.1) confirmed BVA as the site with the

most diverse methanogen community followed by QUI, and SJO as the least diverse.

Also, a large fraction of unclassified Methanomicrobiales was detected in all soils (62-

33%), and further verification efforts (see Methods) found those sequences to cluster with

environmental clones outside the established phylogeny (Fig. 5.5). Those OTUs were less

than 67% similar to any known family and are likely novel groups in the order.
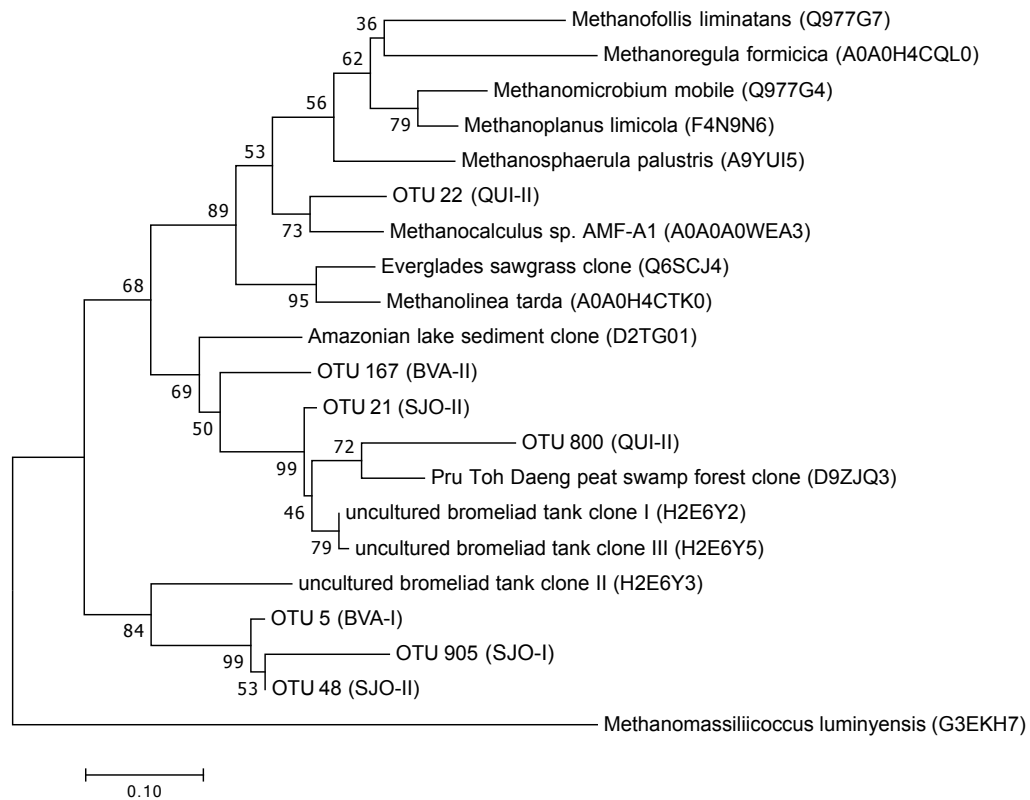
Figure 5.5. Neighbor-joining (1000 iterations) phylogenetic analysis of selected Methanomicrobiales *mcrA* sequences from three Amazon peatlands. Reference sequences were picked from environmental data derived from tropical peatlands, Amazon lakes (Conrad *et al.*, 2010), and tropical vegetation (Goffredi *et al.*, 2011), and from isolates for which the accession number is provided.

OTU abundances allow comparison of methanogens and their putative

methanogenic pathways contributions (Table 5.1). Jointly, Methanobacteriales and

Methanomicrobiales OTU's abundance (87%-71%) explain the dominance of hydrogenotrophic methanogenesis across the contrasting peatlands, consistent with the calculated $\delta^{13}C$ fractionation factors. Methanomicrobiales are most dominant across sites (~75-42%) especially in SJO, while Methanobacteriales reached its highest fraction (39%) in BVA and lowest (12.5%) in acidic oligotrophic SJO. OTU fractions also evidenced the putative acetoclastic contribution by *Methanosaetacea and Methanosarcinacea* particularly in BVA (~22%), a lesser degree in QUI (15%) and SJO (9%). In BVA, the site with highest pH (~6.5) and minerotrophic conditions, *Methanosaetaceae* (including *Methanothrix*) represented nearly a fifth (18.5%) of the community. Meanwhile, in QUI *Methanosarcinacea* (including *Methanosarcina*) made up a bigger fraction (9%) than *Methanosaetacea* (5.9%), suggesting differential acetoclastic contributions likely related to acetate availability and the much lower minimum threshold for acetate utilization of *Methanothrix* than *Methanosarcina* (Min and Zinder, 1989; Jetten, 1992).

Table 5.1. *mcrA*-based standardized taxa abundances with soil layers and cores combined for each peatland in study.

Class	Order	Family	Genus	Relative OTU abundance (%)		
				SJO	QUI	BVA
Methano-microbia	unclassified Methano-microbiales			62.5	45.4	33.4
		Methanoregulaceae		9.1	7.3	6.3
		Methanoregulaceae	*Methano-regula*	2.7	1.4	1.0
		Methanoregulaceae	*Methanolinea*	0.8	0.4	1.7
	Methano-sarcinales	*Methanosaetaceae*		7.2	5.7	18.1
		Methanosaetaceae	*Methanothrix*	0.4	0.2	0.5
		Methano-sarcinaceae		0.8	8.1	3.3
		Methano-sarcinaceae	*Methano-sarcina*	0.8	1.0	0.5
	Methano-cellales	*Methanocellaceae*		6.8	7.9	3.6
		Methanocellaceae	*Methanocella*	1.5	0.6	0.5
Methano-bacteria	Methano-bacteriales	*Methano-bacteriaceae*		6.8	15.9	24.7
		Methano-bacteriaceae	*Methano-bacterium*	5.7	11.4	14.3
Thermo-plasmata	Methano-massiliicocca-les	unclassified *Methano-massiliicoccaceae*		3.0	4.3	3.3
Shannon index	(*SI*)			2.7±0.5	3.6±0.4	4.3±0.4

Importantly, qPCR gene copy results exhibited distinct abundances and vertical distributions across sites. To relate the *mcrA* gene quantification to that of the total microbial community (16S rRNA), we expressed the ratios of gene copy numbers of *mcrA* versus 16S rRNA. In general, all three peatlands showed distinct ranges, orders of magnitude apart, of the putative fraction of *mcrA* (methanogenic) abundance (Fig. 5.6)

with the following order: QUI > SJO > BVA. This is consistent with measured CH$_4$

surface fluxes and dissolved CH$_4$ concentrations (Fig. 5.1) as well as Euryarchaeota 16S

rRNA abundances (Fig. 5.2). In soil profiles, *mcrA* relative frequency increased from the

surface to 20-30 cm deep in QUI and SJO, while in BVA a notable decrease (2 orders of

magnitude) from the surface to 35 cm deep was observed. Depths below 30-40 cm

showed a decrease (SJO, BVA) or had no variation (QUI) but maintained overall
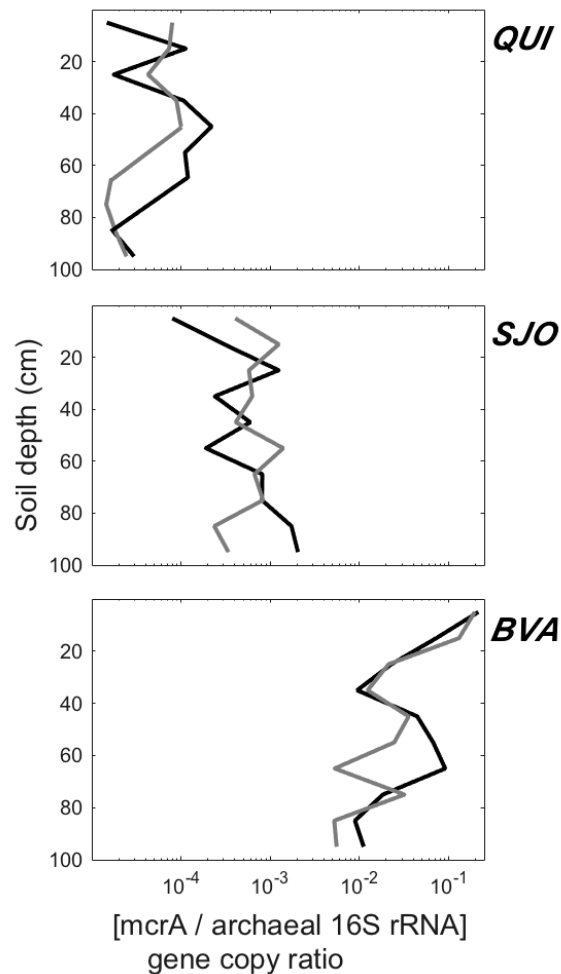
differences of abundance among sites.

Figure 5.6. *McrA*/archaeal 16S rRNA gene copy ratios along soil depth. Gene copy
ratios are based on qPCR analysis and data from both soil cores are shown (dark and light
gray lines).

Composition of methanogenic community along vertical profiles correlate with

NO_x values. We tested the differences in the methanogen communities along vertical

profiles within sites and found them statistically significant, although at lesser degree

than across peatlands. Specifically, PERMANOVA tests indicated a significant shift of

the overall *mcrA*-derived methanogenic community between the depth interval that was

relatively enriched in NO_x (0-50 cm) and the one relatively depleted in NO_x (50-100 cm)

for both cores in BVA (F = 5.39, *p* = 0.0170), QUI (F = 4.13, *p* = 0.0190), and SJO (F =

3.71, *p* = 0.0493). The differences in variation were unaffected by dispersion (*p* > 0.05).

Additional testing of Bathyarchaeota alpha and beta diversity indices did not

correlate with NO_x profiles, although there was a significant correlation of

Bathyarchaeota OTU abundance with pH (Spearman's rank, ρ = 0.78, *p* > 0.001).

Spearman's rank correlation pointed out significant relationships between counts of

sequences assigned to *Methanosaetaceae* and NO_3^- (ρ = 0.76, *p* < 0.005) in SJO,

Methanosarcinaceae and NO_3^- (ρ = 0.73, *p* < 0.005) in SJO, and *Methanoregulaceae* and

NO_2^- (ρ = -0.79, *p* < 0.005) in BVA. At the SJO site, other geochemical parameters tested

(pH, phosphate, sulfate) did not reveal significant relationships.

In summary, we obtained different trends in the correlations of NO_x with

abundances of distinct methanogenic groups along soil profiles. Together with the PC

analysis (Fig. 5.3), Spearman correlation pointed to an overall positive correlation of

NO_3^- with methanogen abundances. However, NO_2^- did not show clear trends across

approaches. We therefore subjected soil samples to NO_2^- incubation experiments at the

lab in order to assess effects on the potential activity of these methangenic groups.

CH$_4$ production potentials in SJO, QUI, BVA peat soils show different responses to NO$_2^-$ amendment and N$_2$O halts methanogenesis. To explore the interaction of NO$_x$ compounds with methanogenesis in peat soils, we tested effects of (i) NO$_2^-$ on methanogenesis rates in soil slurries and (ii) N$_2$O on methanogenesis rates in enrichment cultures. To address (i), we amended anoxic soil microcosms with 200 μM NO$_2^-$ and followed CH$_4$ evolution. As illustrated by the residual percentage of CH$_4$ production with reference to untreated controls (Fig. 5.7A), NO$_2^-$ exerted differential, although mostly negative, effects on the potential for net CH$_4$ production across contrasting tropical peatlands. Samples from deeper soils showed the highest reduction (~10% or below detection residual activity) across all sites. However, shallow, presumably most active, soil samples showed the most variation. The oligotrophic site with the least CH$_4$ accumulation (SJO) was not affected or instead stimulated (90% or over 100% residual activity). The intermediate site (QUI) had a mild or moderate reduction (~60-80% residual activity), and the minerotrophic and most CH$_4$-producing site (BVA) had the harshest reduction (~15-30% residual activity). This differential response is likely born from the geochemical conditions and microbial groups affecting NO$_x$ and CH$_4$ pools directly or indirectly in the contrasting study sites. For instance, NO$_2^-$-based anaerobic methane oxidation (AOM) could affect the results without direct effects on methanogenesis since our experiment only measures net CH$_4$ accumulation. However, considering the slow CH$_4$ oxidation rates observed in other freshwater experiments (B. Zhu *et al*., 2012), it is unlikely that CH$_4$ levels can be significantly affected by AOM during our incubations. We propose the NO$_2^-$ amendment results show effects likely

based on the direct inhibition of methanogenesis and propose 3 plausible explanations. First, the introduction of NO_2^- can change redox potential and thus decrease CH_4 production. NO_x have naturally high redox potentials, methanogenesis operates preferentially at negative potentials, and soil communities have been shown to be sensitive to changes in redox conditions (Fetzer and Conrad, 1993; Jugsujinda et al., 2008; S. Hirano et al., 2013). Moreover, the magnitude of observed inhibition is consistent with the redox gradients measured in-situ. Methanogens of BVA soil would experience the greatest difference in redox because the CH_4/CO_2 balance in BVA is most reduced (Fig. 5.4), and hence, exposure to oxidized radicals would result in harsh disruption of the redox balance. Second, denitrifying microorganisms concomitantly can deplete H_2 or acetate as substrates, thus competing with methanogens. The predominance of the hydrogenotrophic or acetoclastic methanogenic pathway together with the substrate preference of the indigenous denitrifying community could lead to our observed results (Klüber and Conrad, 1998a; Conrad, 1999). Third, NO_2^- negatively affects methanogens on a physiological level. Here, derivatives of transformation processes from NO_2^- might be stronger agents than NO_2^- itself. Under natural soil conditions, NO_2^- can biotically or abiotically be transformed into NO and N_2O (Buessecker et al., 2019), and elevated NO concentrations affects a variety of cellular processes, often leading to cytotoxicity (Saraiva et al., 2004). Similarly, N_2O at ~0.1 mM levels has been found to be an inhibitor of methanogenesis in environmental samples (Balderston and Payne, 1976). N_2O has been shown to bind and inactivate vitamin B_{12} (Drummond and Matthews, 1994a; Drummond and Matthews, 1994b), a key metabolite for methanogens because its cobalt(I) center serves at methyl acceptor during methanol to methane transformation

(Matthews, 2001). Resistance of some methanogenic groups to N_2O exposure by vitamin B_{12} synthesis or the presence of complementing phyla generating vitamin B_{12} (e.g. *Thaumarchaeota*, Doxey *et al.*, 2014) could result in the differential suppression of CH_4 production across sites as observed in our incubations.
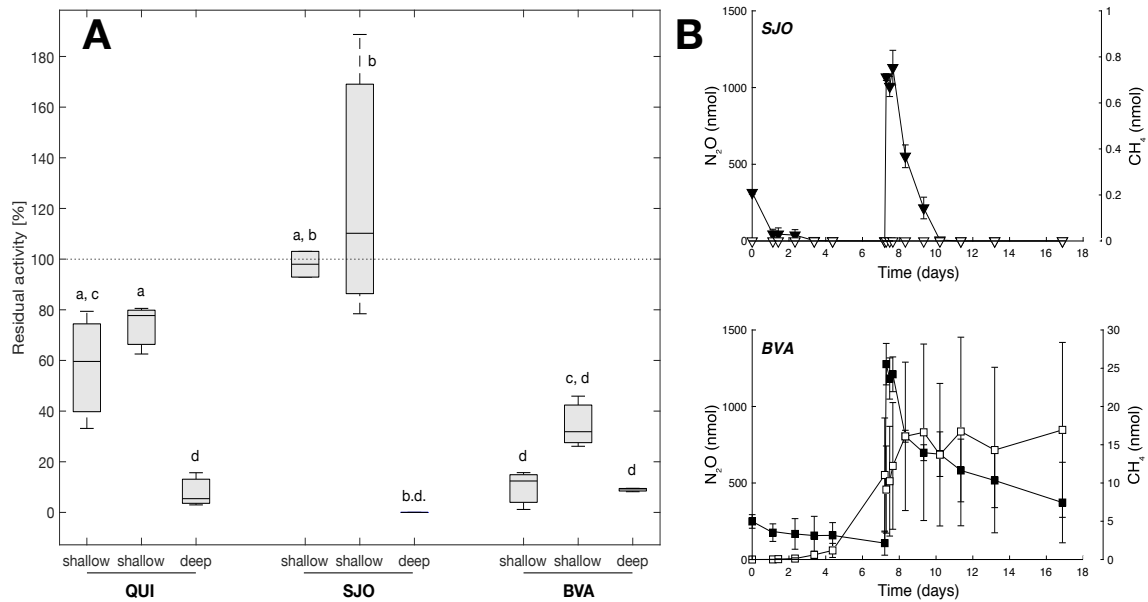

Figure 5.7. Effect of NO_2^- amendment on methanogenic activity of peat soil incubated under anoxic conditions and effect of N_2O on enrichment cultures. (A) For each site, shallow (0-15 cm) and deep (15-30 cm) soil was used as slurry for batch incubations in N_2-flushed microcosms (n = 3). Samples were each derived from three independent sampling points within the peatland, two from shallow soil and one from deeper soil. We expected vertical differences based on the position in the NO_x gradient measured *in-situ*. Residual activity denotes fractional CH_4 production relative to controls without additions. Boxplots comprise 1st and 3rd quartile and the median as centerline. Deep soil manipulation from SJO showed CH_4 levels beyond detectability. Levels not connected by the same letter are significantly different (Student's t, p = 0.05). **(B)** N_2O (full symbols) and CH_4 (open symbols) abundances in enrichment cultures from SJO and BVA. Error bars denote one standard deviation.

To probe the scenario in which NO_2^- transforms into N_2O to then affect methanogenesis (ii), we chose two sites that showed the most contrasting sensitivity to NO_2^- additions (SJO and BVA). From these soils, we derived methanogenic enrichment

cultures in order to reduce microbial complexity and exposed them to N_2O by headspace injections. Enrichments obtained after 7 (SJO) and 4 (BVA) dilution-to-extinction transfers sustained methanogenic growth and still contained a low number of bacteria (per PCR tests, data not shown). Under H_2/CO_2 overpressure (no organic substrates added) and without added N_2O, SJO and BVA enrichments showed linear CH_4 production by 0.6 and 4.7 nmol day^{-1}, respectively. Enrichments receiving N_2O injections showed N_2O reduction concomitant to CH_4 production after a few days of incubation (Fig. 5.7B). CH_4 accumulation halted when cultures were spiked with 28 µM N_2O (dissolved concentration) and resumed when N_2O fell below a threshold of ~10 µM in BVA and to < 0.004 µM in SJO (after 17 days). N_2O only controls and H_2/CO_2 only controls showed no change of N_2O in non-inoculated media (data not shown). Surprisingly, fast N_2O consumption was observed in the SJO enrichment despite known hindrance that pH < 5 poses for N_2O reductases (B. Liu *et al.*, 2010; B. Liu *et al.*, 2014). CH_4 production was measured at significantly lower levels than BVA. In fact, methanogenesis barely recovered in SJO to 0.13 nmol CH_4 accumulated after 83 days. Thus, N_2O – a stable nitrogen oxide species under peat soil conditions (contrary to NO_2^-) – that can only be removed enzymatically, inhibits methanogenesis if present above a distinct threshold. We determined thresholds of 0.004-10 µM pointing at a wide range in individual N_2O affinity among methanogenic communities. The equilibrated N_2O soil gas concentrations we measured *in-situ* (Fig. 5.1) correspond to 0.05-0.1 µM N_2O dissolved in soil pore water. Thus, steady-state N_2O could have retarding effects on CH_4 accumulation at SJO peatland but is insufficient to affect methanogenesis at BVA. This may contribute to the general emission pattern of higher CH_4 emissions from BVA peat

and low CH$_4$ emissions from SJO peat (Finn *et al*., in prep.). The NO$_2^-$ or N$_2$O effects on CH$_4$ accumulation in soil incubations or culture enrichments suggest that complex links between the nitrogen and carbon cycle occur in Amazon peatlands. These may likely comprise interactions of nitrifying microbes and methanogens, which may account for the general spatial variation in CH$_4$ production observed in peatlands. Nevertheless, further work is required to elucidate such interactions and potential implications.

Conclusion

Taken together, the PMFB harbors peatlands with diverse edaphic chemistries, which is especially reflected in pH, DOC, NO$_3^-$ pore water concentrations and C/N ratios of shallow soils. Based on the physicochemical conditions in the waterlogged peats (redox, trace metal availability, substrates) the tropical soils provide feasible conditions for microbial methanogenesis, predominantly via the hydrogenotrophic pathway. The overall microbial communities show strong patterns of vertical stratification in the top 1m. Bathyarchaeota are highly abundant throughout the profiles, suggesting they may play a role in organic carbon degradation especially in deeper soil layers. Thaumarchaeota and Nitrospira have similar ecological niches as producers of NO$_x$ species. Thaumarchaeota are more abundant in the low-pH sites SJO and QUI, whereas Nitrospira appear more dominant in the more neutral-pH soil BVA. Our data revealed high potential of novel and diverse methanogens affiliated with the Methanomicrobiales order. We presented evidence that soil NO$_x$ species impact methanogen abundances and activities. Our lab incubations showed significant effects of NO$_2^-$ and N$_2$O on the soil methanogenic activity. This may have broad implications on how pulses of nitrogen

126

oxides, that are controlled by nitrifying/denitrifying groups and abiotic factors, could

explain spatial and seasonal variation observed in CH_4 emission data from tropical peat.

CHAPTER 6

CONCLUSIONS

The research presented in previous chapters suggests an important role of coupled abiotic-biotic N_2O cycling in both ancient marine and modern terrestrial systems. The truncated core of the denitrification reaction chain, that is, the reduction of NO_2^- to N_2O, is present in all instances studied (Fig. 6.1). However, (i) the degree of how much non-enzymatic catalysis contributes to cycling rates, (ii) the source of the reactant NO_2^-, and (iii) the fate of product N_2 is different. I will briefly summarize how these three aspects (i-iii) compare between the early Earth and the modern Amazon basin in order to grasp how this processes transcended through planetary environments.

It is a challenge to discern between abiotic and biotic reactions, especially in modern Earth sediments and soils that are dominated by microbial activity. We determined that γ irradiation is the most advantageous treatment for peat soil to arrest microbial activity and, concomitantly, to cause the least effect on soil iron and dissolved organic matter composition (Chapter 3). Similar to the widespread use of techniques to estimate a general denitrification capacity for soils (Yoshinari *et al.*, 1977), we hope to have established a more systematic assessment of abiotic N_2O fluxes from soil. This will help achieve a more complete picture of the true extent of (i). A first step was made with our work presented in Chapter 4. While abiotic N_2O production contributed to total N_2O production by 4-56%, we uncovered the potential of two peatlands to denitrify added NO_2^- completely (given high NO production rates). If we scale these findings up, roughly 20% of tropical peatlands could be capable of complete abiotic denitrification without intervention of denitrifying microbes. On the consumption side, we observed diverse

N_2O-reducing microbial groups and high N_2O reducing potential of all peat soils tested based on *nosZ* gene quantities (Chapter 4). Rapid consumption was also apparent in acidic soil (pH < 4) under artificial conditions (Chapter 5) and *in-situ* (Chapter 4). In contrast, ferruginous seawater containing Fe^{2+}-bearing minerals sustained fully abiotic formation of N_2O because we created sterile conditions. A complete abiotic N_2O cycle was indeed conceivable, but was later on likely co-opted by microbes. The degree to which N_2O was produced abiotically therefore shifted in time, and life accelerated existing reaction pathways rather than inventing them from scratch. N_2O reduction was also in the early oceans mainly biotically mediated (Fig. 1.1). A striking difference to tropical peatlands was the scarcity of organic substrates in the Archean. This had tremendous influence on N_2O respiration rates assuming heterotrophic lifestyles. Rates of N_2O consumption were likely fluctuating as *Bacillus*-type N_2O reducers were dependent on 2 sources of organic compounds. First, autotrophic microbes could have fixed inorganic carbon into biomass of which organic substrate for N_2O reduction was then derived. Second, organic hazes, which comprised photochemically fixed carbon from a methane-rich atmopshere, could have delivered substrate for anaerobic heterotrophs to the early oceans. Both sources remain speculative, but they hint to how essential the consumption component is for the cycle to become apparent in the first place. If microbial consumption is too aggressive, such as in the *Las Vueltas* peatland (Chapter 4), N_2O cycling becomes hidden, similar to the cryptic sulfur cycle in oxygen minimum zones (Canfield *et al*., 2010). Thus, the substrate source for microbial N_2O reduction is critical to the overall N_2O production/consumption balance.

The source of NO_2^- (ii) was fundamentally different on the anoxic Earth, because the aerobic nitrification branch of the modern nitrogen cycle had not yet evolved. We performed back-of-the-envelope calculations in Chapter 2 focusing on the question if abiotic nitrogen fixation rates possibly limited mineral-catalyzed N_2O production in the oceans. Indeed, even moderate N_2O fluxes based on average NO_2^- concetrations in surface waters (20-35 µM) were impossible to reach, despite optimal mineral surface availability. Limitations of NO_2^- are perhaps less severe in tropical peatlands (Fig. 6.1). Ammonium derived from organic matter mineralization is abundant predominantly in deeper peat soil layers (up to ~3 mg L^{-1}, Chapter 5). We identified Thaumarchaeota as candidate group to carry out ammonia oxidation in acidic peats (Chapter 5). The pH-dependent ammonium-ammonia equilibrium gives archaea an advantage because of higher ammonia affinities in comparison to their bacterial counterparts (D. G. Lewis *et al*., 2014). Bacteria of the class Nitrospira were more prevalent NO_x producers in more alkaline peat (Chapter 5). Moreover, this group presumably drives the NO_3^-/NO_2^- ratio in these soils because they are capable of NO_2^- oxidation to NO_3^- under sufficient O_2 levels. NO_3^- is a much stronger source for NO_2^- in peat soils than in early oceans, where photo-reduction (albeit at lower rates) could have occurred (Ranjan *et al*., 2019). In the tropics, NO_3^- is either derived from wet deposition or from denitrifier activity (Chapter 5). Given the stronger source pathways from ammonium and NO_3^-, NO_2^- turnover is higher in tropical peat soils and can sustain mixed abiotic-biotic N_2O production rates orders of magnitude higher than those in early oceans.

The fate of the product of N_2O reduction, N_2 (iii), appears enigmatic in both systems. Based on the current literature, little is known about the flow of N_2 following

the reduction reaction. It is reasonable to assume direct conversion into biomass could be an efficient way to relieve nitrogen limitation, especially in oligotrophic peats or seawater. We confirmed sufficient availability of Mo in three peatlands of the Pastaza-Marañón basin in Chapter 5. Because nitrogen fixation is a trait found in a multitude of microbial taxa, we are unable to assign this activity to an organism based on the experimental setup of our study. Tropical conditions are suggestively optimal for an efficient nitrogenase catalysis (Houlton *et al*., 2008); more so than in early oceans (Glass *et al*., 2009). To assess nitrogen fixation after N_2O reduction in peat soil, isotopic labeling could be deployed and tracer signal could be searched for in cell biomass.
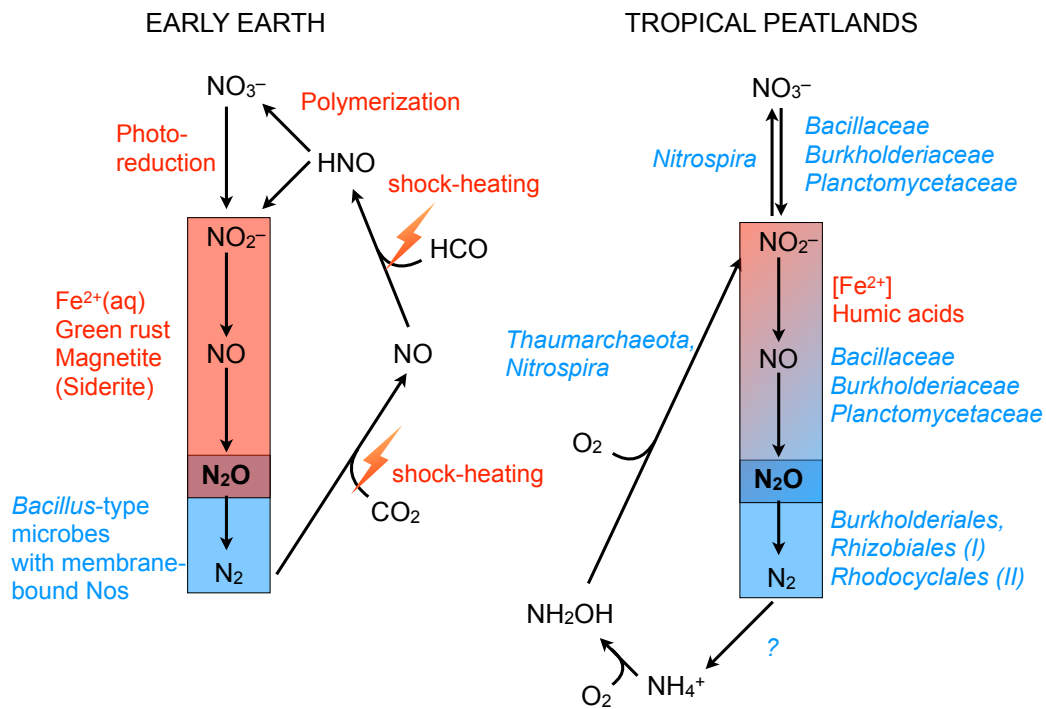
EARLY EARTH   TROPICAL PEATLANDS

NO_3^- — Polymerization
Photo-reduction — HNO — shock-heating
NO_2^- — HCO
$Fe^{2+}(aq)$ / Green rust / Magnetite / (Siderite)
NO — NO
N_2O — shock-heating / CO_2
Bacillus-type microbes with membrane-bound Nos
N_2

NO_3^-
Nitrospira — *Bacillaceae* / *Burkholderiaceae* / *Planctomycetaceae*
NO_2^- — [Fe^{2+}] / Humic acids
Thaumarchaeota, Nitrospira
NO — *Bacillaceae* / *Burkholderiaceae* / *Planctomycetaceae*
O_2
N_2O — *Burkholderiales, Rhizobiales (I)* / *Rhodocyclales (II)*
N_2
NH_2OH
O_2 / NH_4^+ / ?

Figure 6.1. Coupled abiotic-biotic N_2O cycling placed into the chemical framework of the early Earth and tropical peatlands of the Amazon. Red color indicates abiotic processes and blue color biotic ones.

131

To build on the findings presented in this thesis, another angle future research could be directed towards is the reaction mechanism of mineral-catalyzed NO_2^- reduction to N_2O. Specifically, what role nitrosyl plays in the intermediary cycling of NO and the retention of NO at the mineral surface would be of high interest (Chapter 2). Respectively, the fate of mineral-associated NO could be further investigated. NO provides great prospects of a suitable electron acceptor for early benthic life. In Chapter 2, we proposed NO could be shuttled to the ocean floor including the assumption that NO remains stable under changing temperature-pressure conditions on its way along the water column. Changing the setting to tropical peatlands, the driver of abiotic N_2O formation, organic functional groups of peat organic matter, should be properly characterized. The body of studies on N_2O release from NO_2^- interactions with soil organics is deficient, despite the importance of abiotic N_2O production from organic-rich soils we revealed in Chapter 3 and 4. The identification of responsible functional groups would contribute to more accurate estimates of potential N_2O emissions based on distinct soil composition. Moreover, the biological adaptation to soil N_2O fluxes bears many questions to follow up on. How are Nos enzymes adapted to function under low soil pH? This question is justified given the observed N_2O consumption at pH levels deemed inhibiting histidine ligation of Cu enzymes. For what purpose do clade II N_2O reducers consume N_2O? We found clade II abundances do not increase with abiotic N_2O flux potential (Chapter 4), which would be expected if N_2O were to be used as energy source. Detoxification could be an alternative purpose for Nos genes in clade II genomes because N_2O can be harmful to some species, leading us to another question. What are the physiological effects of N_2O on microbes? Besides the known tampering in vitamin B_{12}

metabolism, we have little insight into what N_2O does to the microbial cell; if effects are of physiological nature or redox effects play a role (Chapter 5). Pure culture tests and transcriptome analysis could be a fruitful avenue towards a better understanding of the motivation of N_2O consumption, and thus, its evolution.

We conclude that the geochemical conditions on the early Earth could have allowed abiotic N_2O formation. Existing abiotic denitrification pathways were likely co-opted by early organisms leading to the modern enzymatically driven nitrogen cycle. Provided suitable catalysts for the spontaneous chemical reduction of nitrogen oxides, such as found in organic-rich soils of the Amazon basin, abiotic N_2O formation still occurs today to significant extent. To evaluate the molecular differences between abiotic and biotic N_2O formation, or the nature of biological processes in general, the movement of electrons during reaction would have to be addressed. In Chapter 1, I singled out the oriented collision and accelerated electron transfer as key properties distinguishing biotic from abiotic reactions. The catalysts in the two systems studied (iron minerals and humic acids) succeed in providing a directed orientation to reactants and speed up the transfer of electrons. Density functional theory could be suited to quantify abiotic-biotic differences in the allocation of electrons during the transition state (Kohn and Sham, 1965; A. J. Cohen *et al*., 2008). Testing such calculations on their environmental relevance, it would be necessary to derive activation energies of mixed and abiotic (under sterile conditions) reactions from environmental samples more frequently. This work shows how overestimation of the contribution of biological catalysis may result in a biased understanding of a system. It underlines the importance to disentangle abiotic and biotic reactions, especially if disparities are subtle and their observable boundaries vanish.

REFERENCES

Abràmoff M. D., Magalhães P. J. and Ram S. J. (2004) *Image processing with ImageJ*, Laurin Publishing.

Afkhami A., Madrakian T. and Maleki A. (2006) Indirect kinetic spectrophotometric determination of hydroxylamine based on its reaction with iodate. *Analytical Sciences* **22**, 329–331.

Airapetian V. S. and Usmanov A. V. (2016) Reconstructing the solar wind from its early history to current epoch. *The Astrophysical Journal Letters* **817**, L24.

Airapetian V. S., Glocer A., Gronoff G., Hébrard E. and Danchi W. (2016) Prebiotic chemistry and atmospheric warming of early Earth by an active young Sun. *Nature Geoscience* **9**, 452–455.

Anantharaman K., Hausmann B., Jungbluth S. P., Kantor R. S., Lavy A., Warren L. A., Rappé M. S., Pester M., Loy A., Thomas B. C. and Banfield J. F. (2018) Expanded diversity of microbial groups that shape the dissimilatory sulfur cycle. *The ISME Journal* **12**, 1715–1728.

Anbar A. D. and Holland A. D. (1992) The photochemistry of manganese and the origin of banded iron formations. *Geochimica et Cosmochimica Acta* **56**, 2595–2603.

Anderson G. M. (2005) *Thermodynamics of Natural Systems*. second edition, Cambridge University Press.

Arrhenius S. (1889a) Über die Dissociationswärme und den Einfluss der Temperatur auf den Dissociationsgrad der Elektrolyte. *Zeitschrift für Physikalische Chemie* **4U**, 96–116.

Arrhenius S. (1889b) Über die Reaktionsgeschwindigkeit bei der Inversion von Rohrzucker durch Säuren. *Zeitschrift für Physikalische Chemie* **4U**, 226–248.

Artz R., Chapman S. and Campbell C. (2006) Substrate utilisation profiles of microbial communities in peat are depth dependent and correlate with whole soil FTIR profiles. *Soil Biology and Biochemistry* **38**, 2958–2962.

Babbin A. R., Bianchi D., Jayakumar A. and Ward B. B. (2015) Rapid nitrous oxide cycling in the suboxic ocean. *Science* **348**, 1127–1129.

Bacon M. P., Brewer P. G., Spencer D. W., Murray J. W. and Goddard J. (1980) Lead-210, polonium-210, manganese and iron in the Cariaco Trench. *Deep Sea Research* **27**, 119–135.

Bai R., Wang J.-T., Deng Y., He J.-Z., Feng K. and Zhang L.-M. (2017) Microbial Community and Functional Structure Significantly Varied among Distinct Types of

Paddy Soils But Responded Differently along Gradients of Soil Depth Layers. *Frontiers in Microbiology* **8**, 71–16.

Bai Y., Wang J., Zhan Z., Guan L., Jin L., Zheng G. and Huang Z. (2018) The variation of microbial communities in a depth profile of peat in the Gahai Lake wetland natural conservation area. *Geomicrobiology Journal* **35**, 484–490.

Balderston W. L. and Payne W. J. (1976) Inhibition of methanogenesis in salt marsh sediments and whole-cell suspensions of methanogenic bacteria by nitrogen oxides. *Applied and Environmental Microbiology* **32**, 264–269.

Barron A. R., Wurzburger N., Bellenger J. P., Wright S. J., Kraepiel A. M. L. and Hedin L. O. (2008) Molybdenum limitation of asymbiotic nitrogen fixation in tropical forest soils. *Nature Geoscience* **2**, 42–45.

Barta J., Tahovska K., Santruckova H. and Oulehle F. (2017) Microbial communities with distinct denitrification potential in spruce and beech soils differing in nitrate leaching. *Scientific Reports* **7**, 1–15.

Battaglia G. and Joos F. (2018) Marine N_2O emissions from nitrification and denitrification constrained by modern observations and projected in multimillennial global warming simulations. *Global Biogeochemical Cycles* **32**, 92–121.

Beneduzi A., Costa P. B., Parma M., Melo I. S., Bodanese-Zanettini M. H. and Passaglia L. M. P. (2010) *Paenibacillus riograndensis* sp. nov., a nitrogen-fixing species isolated from the rhizosphere of *Triticum aestivum*. *International Journal Of Systematic And Evolutionary Microbiology* **60**, 128–133.

Berns A. E., Philipp H., Narres H. D., Burauel P., Vereecken H. and Tappe W. (2008) Effect of gamma-sterilization and autoclaving on soil organic matter structure as studied by solid state NMR, UV and fluorescence spectroscopy. *Journal of Soil Science* **59**, 540–550.

Blankinship J. C., Becerra C. A., Schaeffer S. M. and Schimel J. P. (2014) Separating cellular metabolism from exoenzyme activity in soil organic matter decomposition. *Soil Biology and Biochemistry* **71**, 68–75.

Bocher F., Géhin A., Ruby C., Ghanbaja J., Abdelmoula M. and Génin J.-M. R. (2004) Coprecipitation of Fe(II–III) hydroxycarbonate green rust stabilised by phosphate adsorption. *Solid State Sciences* **6**, 117–124.

Bondoso J., Albuquerque L., Lobo-da-Cunha A., da Costa M. S., Harder J. and Lage O. M. (2014) *Rhodopirellula lusitana* sp. nov. and *Rhodopirellula rubra* sp. nov., isolated from the surface of macroalgae. *Systematic and Applied Microbiology* **37**, 157–164.

Bouwman A. F., Beusen A. H. W., Griffioen J., Van Groenigen J. W., Hefting M. M.,

Oenema O., Van Puijenbroek P. J. T. M., Seitzinger S., Slomp C. P. and Stehfest E. (2013) Global trends and uncertainties in terrestrial denitrification and N_2O emissions. *Philosophical Transactions of the Royal Society B: Biological Sciences* **368**, 20130112.

Bowler M. W., Montgomery M. G., Leslie A. G. W. and Walker J. E. (2006) How azide inhibits ATP hydrolysis by the F-ATPases. *Proceedings of the National Academy of Sciences* **103**, 8646–8649.

Brandes J. A., Boctor N. Z., Cody G. D., Cooper B. A., Hazen R. M. and Yoder H. S. (1998) Abiotic nitrogen reduction on the early Earth. *Nature* **395**, 365–367.

Bratsch S. G. (2009) Standard electrode potentials and temperature coefficients in water at 298.15 K. *Journal of Physical and Chemical Reference Data* **18**, 1–21.

Brinson M. M. and Malvárez A. I. (2002) Temperate freshwater wetlands: types, status, and threats. *Environmental Conservation* **29**, 115–133.

Buchfink B., Xie C. and Huson D. H. (2015) Fast and sensitive protein alignment using DIAMOND. *Nature Methods* **12**, 59–60.

Buessecker S., Tylor K., Nye J., Holbert K. E., Urquiza-Muñoz J. D., Glass J. B., Hartnett H. E. and Cadillo-Quiroz H. (2019) Effects of sterilization techniques on chemodenitrification and N_2O production in tropical peat soil microcosms. *Biogeosciences* **16**, 4601–4612.

Buick R. (2007) Did the Proterozoic "Canfield Ocean" cause a laughing gas greenhouse? *Geobiology* **5**, 97–100.

Bunzl K., Schmidt W. and Sansoni B. (1976) Kinetics of ion exchange in soil organic matter. IV. Adsorption and desorption of Pb^{2+}, Cu^{2+}, Cd^{2+}, Zn^{2+} and Ca^{2+} by peat. *Journal of Soil Science* **27**, 32–41.

Burns L. C., Stevens R. J. and Laughlin R. J. (1995) Determination of the simultaneous production and consumption of soil nitrite using ^{15}N. *Soil Biology and Biochemistry* **27**, 839–844.

Burns L. C., Stevens R. J. and Laughlin R. J. (1996) Production of nitrite in soil by simultaneous nitrification and denitrification. *Soil Biology and Biochemistry* **28**, 609–616.

Burns R. C. (1969) The nitrogenase system from *Azotobacter* activation energy and divalent cation requirement. *Biochimica et Biophysica Acta (BBA) - Enzymology* **171**, 253–259.

Byrne J. M., Klueglein N., Pearce C., Rosso K. M., Appel E. and Kappler A. (2015) Redox cycling of Fe(II) and Fe(III) in magnetite by Fe-metabolizing bacteria. *Science*

347, 1473–1476.

Cadillo-Quiroz H., Yashiro E., Yavitt J. B. and Zinder S. H. (2008) Characterization of the archaeal community in a minerotrophic fen and terminal restriction fragment length polymorphism-directed isolation of a novel hydrogenotrophic methanogen. *Applied and Environmental Microbiology* **74**, 2059–2068.

Canfield D. E., Rosing M. T. and Bjerrum C. (2006) Early anaerobic metabolisms. *Philosophical Transactions of the Royal Society B: Biological Sciences* **361**, 1819–1836.

Canfield D. E., Stewart F. J., Thamdrup B., De Brabandere L., Dalsgaard T., Delong E. F., Revsbech N. P. and Ulloa O. (2010) A cryptic sulfur cycle in oxygen-minimum–zone waters off the Chilean coast. *Science* **330**, 1375–1378.

Cape J. N., Kirika A., Rowland A. P., Wilson D. R., Jickells T. D. and Cornell S. (2001) Organic nitrogen in precipitation: Real problem or sampling artefact? *The Scientific World Journal* **1**, 230–237.

Caporaso J. G., Kuczynski J., Stombaugh J., Bittinger K., Bushman F. D., Costello E. K., Fierer N., Peña A. G., Goodrich J. K., Gordon J. I., Huttley G. A., Kelley S. T., Knights D., Koenig J. E., Ley R. E., Lozupone C. A., McDonald D., Muegge B. D., Pirrung M., Reeder J., Sevinsky J. R., Turnbaugh P. J., Walters W. A., Widmann J., Yatsunenko T., Zaneveld J. and Knight R. (2010) QIIME allows analysis of high-throughput community sequencing data. *Nature Methods* **7**, 335–336.

Catling D. C., Zahnle K. J. and McKay C. P. (2001) Biogenic methane, hydrogen escape, and the irreversible oxidation of early Earth. *Science* **293**, 839–843.

Chameides W. L. (1986) Photochemistry of the Atmospheric Aqueous Phase. In *Chemistry of Multiphase Atmospheric Systems* Springer, Berlin, Heidelberg. pp. 369–413.

Chen J. and Strous M. (2013) Denitrification and aerobic respiration, hybrid electron transport chains and co-evolution. *Biochimica et Biophysica Acta (BBA) - Bioenergetics* **1827**, 136–144.

Chen J., Hanke A., Tegetmeyer H. E., Kattelmann I., Sharma R., Hamann E., Hargesheimer T., Kraft B., Lenk S., Geelhoed J. S., Hettich R. L. and Strous M. (2017) Impacts of chemical gradients on microbial community structure. *The ISME Journal* **11**, 920–931.

Chin K.-J., Liesack W. and Janssen P. H. (2001) *Opitutus terrae* gen. nov., sp. nov., to accommodate novel strains of the division "*Verrucomicrobia*" isolated from rice paddy soil. *International Journal of Systematic Bacteriology* **51**, 1965–1968.

Ciais P., Sabine C., Bala G., Bopp L., Brovkin V., Canadell J., Chhabra A., DeFries R.,

Galloway J., Heimann M., Jones C., Le Quéré C., Myneni R. B., Piao S. and Thornton P. (2013) Carbon and other biogeochemical cycles. In *Climate Change 2013: The Physical Science Basis. Contribution of working group I to the fifth assessment report of the intergovernmental panel on climate change*.

Cleemput O. V. and Samater A. H. (1996) Nitrite in soils: accumulation and role in the formation of gaseous N compounds. *Fertilizer Research* **45**, 81–89.

Cohen A. D., Raymond R., C S. M., Alvarado A. and Malavassi L. (1986) Características geológicas de los depósitos de turba en Costa Rica (estudio preliminar). *Revista Geológica de América Central*, 47–67.

Cohen A. J., Mori-Sánchez P. and Yang W. (2008) Insights into current limitations of density functional theory. *Science* **321**, 792–794.

Conrad R. (1999) Contribution of hydrogen to methane production and control of hydrogen concentrations in methanogenic soils and sediments. *FEMS Microbiology Ecology* **28**, 193–202.

Conrad R., Klose M., Claus P. and Enrich-Prast A. (2010) Methanogenic pathway, ^{13}C isotope fractionation, and archaeal community composition in the sediment of two clear-water lakes of Amazonia. *Limnology and Oceanography* **55**, 689–702.

Conthe M., Wittorf L., Kuenen J. G., Kleerebezem R., van Loosdrecht M. C. M. and Hallin S. (2018) Life on N_2O: Deciphering the ecophysiology of N_2O respiring bacterial communities in a continuous culture. *The ISME Journal* **12**, 1142–1153.

Cory R. M. and McKnight D. M. (2005) Fluorescence spectroscopy reveals ubiquitous presence of oxidized and reduced quinones in dissolved organic matter. *Environmental Science & Technology* **39**, 8142–8149.

Criquet J., Rodriguez E. M., Allard S., Wellauer S., Salhi E., Joll C. A. and Gunten von U. (2015) Reaction of bromine and chlorine with phenolic compounds and natural organic matter extracts – Electrophilic aromatic substitution and oxidation. *Water Research* **85**, 476–486.

Daebeler A., Bodelier P. L., Yan Z., Hefting M. M., Jia Z. and Laanbroek H. J. (2014) Interactions between Thaumarchaea, *Nitrospira* and methanotrophs modulate autotrophic nitrification in volcanic grassland soil. *The ISME Journal* **8**, 2397–2410.

Daims H., Lebedeva E. V., Pjevac P., Han P., Herbold C., Albertsen M., Jehmlich N., Palatinszky M., Vierheilig J., Bulaev A., Kirkegaard R. H., Bergen von M., Rattei T., Bendinger B., Nielsen P. H. and Wagner M. (2015) Complete nitrification by *Nitrospira* bacteria. *Nature* **528**, 504–509.

Davidson E. A., Chorover J. and Dail D. B. (2003) A mechanism of abiotic immobilization of nitrate in forest ecosystems: The ferrous wheel hypothesis. *Global*

Change Biology **9**, 228–236.

Davidson E. A., de Araújo A. C., Artaxo P., Balch J. K., Brown I. F., Bustamante M. M.
C., Coe M. T., DeFries R. S., Keller M., Longo M., Munger J. W., Schroeder W.,
Soares-Filho B. S., Souza C. M. and Wofsy S. C. (2012) The Amazon basin in
transition. *Nature* **481**, 321–328.

Dietrich L. E., Tice M. M. and Newman D. K. (2006) The co-evolution of life and Earth.
Current Biology **16**, 395–400.

Domeignoz-Horta L. A., Putz M., Spor A., Bru D., Breuil M. C., Hallin S. and Philippot
L. (2016) Non-denitrifying nitrous oxide-reducing bacteria - An effective N_2O sink in
soil. *Soil Biology and Biochemistry* **103**, 376–379.

Downs R. T. (2006) The RRUFF project : an integrated study of the chemistry,
crystallography, Raman and infrared spectroscopy of minerals. *Program and
Abstracts of the 19th General Meeting of the International Mineralogical Association
in Kobe, Japan, 2006*.

Doxey A. C., Kurtz D. A., Lynch M. D., Sauder L. A. and Neufeld J. D. (2014) Aquatic
metagenomes implicate *Thaumarchaeota* in global cobalamin production. *The ISME
Journal* **9**, 1–11.

Draper F. C., Roucoux K. H., Lawson I. T., Mitchard E. T. A., Coronado E. N. H.,
Lähteenoja O., Montenegro L. T., Sandoval E. V., Zaráte R. and Baker T. R. (2014)
The distribution and amount of carbon in the largest peatland complex in Amazonia.
Environmental Research Letters **9**, 1–12.

Drewer J., Zhao J., Leduning M. M., Levy P. E., Sentian J., Gubry-Rangin C. and Skiba
U. M. (2020) Linking nitrous oxide and nitric oxide fluxes to microbial communities
in tropical forest soils and oil palm plantations in Malaysia in laboratory incubations.
Frontiers in Forests and Global Change **3**, 1–14.

Drexel T. R., Haitzer M., Ryan J. N., Aiken G. R. and Nagy K. L. (2002) Mercury(II)
sorption to two Florida everglades peats: Evidence for strong and weak binding and
competition by dissolved organic matter released from the peat. *Environmental
Science & Technology* **36**, 4058–4064.

Drummond J. T. and Matthews R. G. (1994a) Nitrous oxide degradation by cobalamin-
dependent methionine synthase: Characterization of the reactants and products in the
inactivation reaction. *Biochemistry* **33**, 3732–3741.

Drummond J. T. and Matthews R. G. (1994b) Nitrous oxide inactivation of cobalamin-
dependent methionine synthase from *Escherichia coli*: Characterization of the
damage to the enzyme and prosthetic group. *Biochemistry* **33**, 3742–3750.

Ducluzeau A.-L., van Lis R., Duval S., Schoepp-Cothenet B., Russell M. J. and Nitschke

W. (2009) Was nitric oxide the first deep electron sink? *Trends in Biochemical Sciences* **34**, 9–15.

Duggleby R. G. (1995) [3] Analysis of enzyme progress curves by nonlinear regression. In *Methods in Enzymology* Methods in Enzymology. Academic Press. pp. 61–90.

Eddy S. R. (2011) Accelerated profile HMM searches. *PLOS Computational Biology* **7**, e1002195.

Edgar R. (2010) Search and clustering orders of magnitude faster than BLAST. *Bioinformatics* **26**, 2460–2461.

Edgar R. C. (2016) UNOISE2: improved error-correction for Illumina 16S and ITS amplicon sequencing. *bioRxiv* **13**, 081257.

Eichorst S. A., Kuske C. R. and Schmidt T. M. (2011) Influence of plant polymers on the distribution and cultivation of bacteria in the phylum *Acidobacteria*. *Applied and Environmental Microbiology* **77**, 586–596.

Elberling B., Askaer L., Jørgensen C. J., Joensen H. P., Kühl M., Glud R. N. and Lauritsen F. R. (2011) Linking Soil O_2, CO_2, and CH_4 concentrations in a Wetland Soil: Implications for CO_2 and CH_4 Fluxes. *Environmental Science & Technology* **45**, 3393–3399.

Ermler U., Grabarse W., Shima S., Goubeaud M. and Thauer R. K. (1997) Crystal structure of methyl-coenzyme M reductase: The key enzyme of biological methane formation. *Science* **278**, 1457–1462.

Espenberg M., Truu M., Mander Ü., Kasak K., Nõlvak H., Ligi T., Oopkaup K., Maddison M. and Truu J. (2018) Differences in microbial community structure and nitrogen cycling in natural and drained tropical peatland soils. *Scientific Reports* **8**, 1–12.

Ettwig K. F., Butler M. K., Le Paslier D., Pelletier E., Mangenot S., Kuypers M. M. M., Schreiber F., Dutilh B. E., Zedelius J., de Beer D., Gloerich J., Wessels H. J. C. T., van Alen T., Luesken F., Wu M. L., van de Pas-Schoonen K. T., Camp den H. J. M. O., Janssen-Megens E. M., Francoijs K.-J., Stunnenberg H., Weissenbach J., Jetten M. S. M. and Strous M. (2010) Nitrite-driven anaerobic methane oxidation by oxygenic bacteria. *Nature* **464**, 543–548.

Evans P. N., Parks D. H., Chadwick G. L., Robbins S. J., Orphan V. J., Golding S. D. and Tyson G. W. (2015) Methane metabolism in the archaeal phylum Bathyarchaeota revealed by genome-centric metagenomics. *Science* **350**, 434–438.

Fang Y., Koba K., Makabe A., Takahashi C., Zhu W., Hayashi T., Hokari A. A., Urakawa R., Bai E., Houlton B. Z., Xi D., Zhang S., Matsushita K., Tu Y., Liu D., Zhu F., Wang Z., Zhou G., Chen D., Makita T., Toda H., Liu X., Chen Q., Zhang D.,

Li Y. and Yoh M. (2015) Microbial denitrification dominates nitrate losses from forest ecosystems. *Proceedings of the National Academy of Sciences* **112**, 1470–1474.

Fellman J. B., Hood E. and Spencer R. G. M. (2010) Fluorescence spectroscopy opens new windows into dissolved organic matter dynamics in freshwater ecosystems: A review. *Limnology and Oceanography* **55**, 2452–2462.

Fetzer S. and Conrad R. (1993) Effect of redox potential on methanogenesis by *Methanosarcina barkeri*. *Archives of Microbiology* **160**, 108–113.

Finn D. R., Ziv-El M., van Haren J., Park J. G., Del Aguila Pasquel J., Muñoz J. D. U. and Cadillo-Quiroz H. Methanogens and methanotrophs show nutrient-dependent community assemblage patterns across tropical peatlands of the Pastaza-Marañón basin, Peruvian Amazonia. *Frontiers in Microbiology*.

Fish J. A., Chai B., Wang Q., Sun Y., Brown C. T., Tiedje J. M. and Cole J. R. (2013) FunGene: the functional gene pipeline and repository. *Frontiers in Microbiology* **4**, 1–14.

Foglar L., Briški F., Sipos L. and Vuković M. (2005) High nitrate removal from synthetic wastewater with the mixed bacterial culture. *Bioresource Technology* **96**, 879–888.

Gandois L., Teisserenc R., Cobb A. R., Chieng H. I., Lim L. B. L., Kamariah A. S., Hoyt A. and Harvey C. F. (2014) Origin, composition, and transformation of dissolved organic matter in tropical peatlands. *Geochimica et Cosmochimica Acta* **137**, 35–47.

Gaucher E. A., Miyamoto M. M. and Benner S. A. (2001) Function–structure analysis of proteins using covarion-based evolutionary approaches: Elongation factors. *Proceedings of the National Academy of Sciences* **98**, 548–552.

Glass J. B., Simon F. W. and Anbar A. D. (2009) Coevolution of metal availability and nitrogen assimilation in cyanobacteria and algae. *Geobiology* **7**, 100–123.

Godfrey L. V. and Falkowski P. G. (2009) The cycling and redox state of nitrogen in the Archaean ocean. *Nature Geoscience* **2**, 725–729.

Goffredi S. K., Jang G. E., Woodside W. T. and Ill W. U. (2011) Bromeliad catchments as habitats for methanogenesis in tropical rainforest canopies. *Frontiers in Microbiology* **2**, 1–14.

Gordon A. D., Smirnov A., Shumlas S. L., Singireddy S., DeCesare M., Schoonen M. A. A. and Strongin D. R. (2013) Reduction of nitrite and nitrate on nano-dimensioned FeS. *Origins of Life and Evolution of Biospheres* **43**, 305–322.

Gore A. (1983) 4B: Mires – swamp, bog, fen and moor, general studies. In *Methanogens and methanotrophs show nutrient-dependent community assemblage patterns across*

tropical peatlands of the Pastaza-Marañón basin, Peruvian Amazonia

Gough D. O. (1981) Solar interior structure and luminosity variations. In *Physics of Solar Variations* Springer, Dordrecht. pp. 21–34.

Grabb K. C., Buchwald C., Hansel C. M. and Wankel S. D. (2017) A dual nitrite isotopic investigation of chemodenitrification by mineral-associated Fe(II) and its production of nitrous oxide. *Geochimica et Cosmochimica Acta* **196**, 388–402.

Graf D. R. H., Jones C. M. and Hallin S. (2014) Intergenomic Comparisons Highlight Modularity of the Denitrification Pathway and Underpin the Importance of Community Structure for N_2O Emissions. *PLoS One* **9**, e114118.

Graf D. R. H., Zhao M., Jones C. M. and Hallin S. (2016) Soil type overrides plant effect on genetic and enzymatic N_2O production potential in arable soils. *Soil Biology and Biochemistry* **100**, 125–128.

Gruber N. and Galloway J. N. (2008) An Earth-system perspective of the global nitrogen cycle. *Nature* **451**, 293–296.

Gu B., Bian Y., Miller C. L., Dong W., Jiang X. and Liang L. (2011) Mercury reduction and complexation by natural organic matter in anoxic environments. *Proceedings of the National Academy of Sciences* **108**, 1–5.

Gumbricht T., Cuesta R. M. R., Verchot L., Herold M., Wittmann F., Householder E., Herold N. and Murdiyarso D. (2017) An expert system model for mapping tropical wetlands and peatlands reveals South America as the largest contributor. *Global Change Biology* **23**, 3581–3599.

Halevy I. and Bachan A. (2017) The geologic history of seawater pH. *Science* **355**, 1069–1071.

Halevy I., Alesker M., Schuster E. M., Popovitz-Biro R. and Feldman Y. (2017) A key role for green rust in the Precambrian oceans and the genesis of iron formations. *Nature Geoscience* **10**, 135–139.

Hall Sharon J and Matson P. A. (1999) Nitrogen oxide emissions after nitrogen additions in tropical forests. *Nature* **400**, 152–155.

Hall Sharon J and Matson P. A. (2003) Nutrient status of tropical rain forests influences soil N dynamics after N additions. *Ecological Monographs* **73**, 107–129.

Hall Steven J and Silver W. L. (2013) Iron oxidation stimulates organic matter decomposition in humid tropical forest soils. *Global Change Biology* **19**, 2804–2813.

Hallin S., Philippot L., Löffler F. E., Sanford R. A. and Jones C. M. (2018) Genomics and ecology of novel N_2O-reducing microorganisms. *Trends in Microbiology* **26**, 43–

55.

Hamilton S. K. and Ostrom N. E. (2007) Measurement of the stable isotope ratio of dissolved N_2 in ^{15}N tracer experiments. *Limnology and Oceanography: Methods* **5**, 233–240.

Hansen H. and Koch C. B. (1998) Reduction of nitrate to ammonium by sulphate green rust: activation energy and reaction mechanism. *Clay Minerals* **33**, 87–101.

Hansen H., Borggaard O. K. and Sorensen J. (1994) Evaluation of the free energy of formation of Fe(II)-Fe(III) hydroxide-sulphate (green rust) and its reduction of nitrite. *Geochimica et Cosmochimica Acta* **58**, 2599–2608.

Haroon M. F., Hu S., Shi Y., Imelfort M., Keller J., Hugenholtz P., Yuan Z. and Tyson G. W. (2013) Anaerobic oxidation of methane coupled to nitrate reduction in a novel archaeal lineage. *Nature* **500**, 1–6.

Hatano R., Toma Y., Hamada Y., Arai H., Susilawati H. L. and Inubushi K. (2016) Methane and nitrous oxide emissions from tropical peat soil. In *Tropical Peatland Ecosystems* Springer, Tokyo. pp. 339–351.

Heil J., Liu S., Vereecken H. and Brüggemann N. (2015) Abiotic nitrous oxide production from hydroxylamine in soils and their dependence on soil properties. *Soil Biology and Biochemistry* **84**, 107–115.

Heitmann T., Goldhammer T., Beer J. and Blodau C. (2007) Electron transfer of dissolved organic matter and its potential significance for anaerobic respiration in a northern bog. *Global Change Biology* **13**, 1771–1785.

Henry S., Bru D., Stres B., Hallet S. and Philippot L. (2006) Quantitative detection of the *nosZ* gene, encoding nitrous oxide reductase, and comparison of the abundances of 16S rRNA, *narG, nirK, and nosZ* genes in soils. *Applied and Environmental Microbiology* **72**, 5181–5189.

Herbold C. W., Pelikan C., Kuzyk O., Hausmann B., Angel R., Berry D. and Loy A. (2015) A flexible and economical barcoding approach for highly multiplexed amplicon sequencing of diverse target genes. *Frontiers in Microbiology* **6**, 8966.

Hirano S., Matsumoto N., Morita M., Sasaki K. and Ohmura N. (2013) Electrochemical control of redox potential affects methanogenesis of the hydrogenotrophic methanogen *Methanothermobacter thermautotrophicus*. *Letters in Applied Microbiology* **56**, 315–321.

Hirano T., Jauhiainen J., Inoue T. and Takahashi H. (2009) Controls on the Carbon Balance of Tropical Peatlands. *Ecosystems* **12**, 873–887.

Holmes M. E., Chanton J. P., Tfaily M. M. and Ogram A. (2015) CO_2 and CH_4 isotope

compositions and production pathways in a tropical peatland. *Global Biogeochemical Cycles* **29**, 1–18.

Holtan-Hartwig L., Dörsch P. and Bakken L. R. (2002) Low temperature control of soil denitrifying communities: kinetics of N$_2$O production and reduction. *Soil Biology and Biochemistry* **34**, 1797–1806.

Homyak P. M., Kamiyama M., Sickman J. O. and Schimel J. P. (2017) Acidity and organic matter promote abiotic nitric oxide production in drying soils. *Global Change Biology* **23**, 1735–1747.

Houlton B. Z., Sigman D. M. and Hedin L. O. (2006) Isotopic evidence for large gaseous nitrogen losses from tropical rainforests. *Proceedings of the National Academy of Sciences* **103**, 8745–8750.

Houlton B. Z., Wang Y.-P., Vitousek P. M. and Field C. B. (2008) A unifying framework for dinitrogen fixation in the terrestrial biosphere. *Nature* **454**, 327–330.

Householder J. E., Janovec J. P., Tobler M. W., Page S. and Lähteenoja O. (2012) Peatlands of the Madre de Dios River of Peru: Distribution, Geomorphology, and Habitat Diversity. *Wetlands* **32**, 359–368.

Höfferle Š., Nicol G. W., Pal L., Hacin J., Prosser J. I. and Mandić-Mulec I. (2010) Ammonium supply rate influences archaeal and bacterial ammonia oxidizers in a wetland soil vertical profile. *FEMS Microbiology Ecology* **74**, 302–315.

Hu B. L., Shen L. D., Lian X., Zhu Q., Liu S., Huang Q., He Z. F., Geng S., Cheng D. Q., Lou L. P., Xu X. Y., Zheng P. and He Y. F. (2014) Evidence for nitrite-dependent anaerobic methane oxidation as a previously overlooked microbial methane sink in wetlands. *Proceedings of the National Academy of Sciences* **111**, 4495–4500.

Hu R. (2013) Atmospheric photochemistry, surface features, and potential biosignature gases of terrestrial exoplanets. Massachusetts Institute of Technology.

Hu R. and Diaz H. D. (2019) Stability of nitrogen in planetary atmospheres in contact with liquid water. *The Astrophysical Journal* **886**, 1–8.

Hu R., Seager S. and Bains W. (2012) Photochemistry in terrestrial exoplanet atmospheres. I. Photochemistry model and benchmark cases. *The Astrophysical Journal* **761**, 1–29.

Hu R., Seager S. and Bains W. (2013) Photochemistry in terrestrial exoplanet atmospheres. II. H$_2$S and SO$_2$ photochemistry in anoxic atmospheres. *The Astrophysical Journal* **769**, 1–6.

Huang J., Golombek A., Prinn R., Weiss R., Fraser P., Simmonds P., Dlugokencky E. J., Hall B., Elkins J., Steele P., Langenfelds R., Krummel P., Dutton G. and Porter L.

(2008) Estimation of regional emissions of nitrous oxide from 1997 to 2005 using multinetwork measurements, a chemical transport model, and an inverse method. *Journal of Geophysical Research* **113**, 197–19.

Huson D. H., Albrecht B., Bağcı C., Bessarab I., Górska A., Jolic D. and Williams R. B. H. (2018) MEGAN-LR: new algorithms allow accurate binning and easy interactive exploration of metagenomic long reads and contigs. *Biology Direct* **13**, 1–17.

Huson D. H., Beier S., Flade I., Górska A., El-Hadidi M., Mitra S., Ruscheweyh H.-J. and Tappu R. (2016) MEGAN Community Edition - Interactive Exploration and Analysis of Large-Scale Microbiome Sequencing Data. *PLOS Computational Biology* **12**, e1004957.

Hutchins C. M., Teasdale P. R., Lee J. and Simpson S. L. (2007) The effect of manipulating sediment pH on the porewater chemistry of copper- and zinc-spiked sediments. *Chemosphere* **69**, 1089–1099.

Ishii S., Ohno H., Tsuboi M., Otsuka S. and Senoo K. (2011) Identification and isolation of active N_2O reducers in rice paddy soil. *The ISME Journal* **5**, 1936–1945.

Jackson C. R., Liew K. C. and Yule C. M. (2008) Structural and functional changes with depth in microbial communities in a tropical malaysian peat swamp forest. *Microbial Ecology* **57**, 402–412.

Jauhiainen J., Kerojoki O., Silvennoinen H., Limin S. and Vasander H. (2014) Heterotrophic respiration in drained tropical peat is greatly affected by temperature – a passive ecosystem cooling experiment. *Environmental Research Letters* **9**, 1–18.

Jauhiainen J., Takahashi H., Heikkinen J. E. P., Martikainen P. J. and Vasander H. (2005) Carbon fluxes from a tropical peat swamp forest floor. *Global Change Biology* **11**, 1788–1797.

Jenkinson D. S. and Powlson D. S. (1976) The effects of biocidal treatments on metabolism in soil—I. Fumigation with chloroform. *Soil Biology and Biochemistry* **8**, 167–177.

Jetten M. (1992) Methanogenesis from acetate: a comparison of the acetate metabolism in *Methanothrix soehngenii* and *Methanosarcina* spp. *FEMS Microbiology Letters* **88**, 181–197.

Ji Q., Babbin A. R., Jayakumar A., Oleynik S. and Ward B. B. (2015) Nitrous oxide production by nitrification and denitrification in the Eastern Tropical South Pacific oxygen minimum zone. *Geophysical Research Letters* **42**, 10,755–10,764.

Johnson J. W., Oelkers E. H. and Helgeson H. C. (1992) SUPCRT92: A software package for calculating the standard molal thermodynamic properties of minerals, gases, aqueous species, and reactions from 1 to 5000 bar and 0 to 1000°C. *Computers*

& Geosciences **18**, 899–947.

Jones C. M., Graf D. R., Bru D., Philippot L. and Hallin S. (2013) The unaccounted yet abundant nitrous oxide-reducing microbial community: a potential nitrous oxide sink. *The ISME Journal* **7**, 417–426.

Jones C. M., Spor A., Brennan F. P., Breuil M.-C., Bru D., Lemanceau P., Griffiths B., Hallin S. and Philippot L. (2014) Recently identified microbial guild mediates soil N_2O sink capacity. *Nature Climate Change* **4**, 801–805.

Jones C., Crowe S. A., Sturm A., Leslie K. L., MacLean L. C. W., Katsev S., Henny C., Fowle D. A. and Canfield D. E. (2011) Biogeochemistry of manganese in ferruginous Lake Matano, Indonesia. *Biogeosciences* **8**, 2977–2991.

Jones L. C., Peters B., Pacheco J. S. L., Casciotti K. L. and Fendorf S. (2015) Stable isotopes and iron oxide mineral products as markers of chemodenitrification. *Environmental Science & Technology* **49**, 3444–3452.

Joosten H. and Clark D. (2002) Wise use of mires and peatlands. *International Mire Conservation Group and International Peat Society*.

Joye S. B., Boetius A., Orcutt B. N., Montoya J. P., Schulz H. N., Erickson M. J. and Lugo S. K. (2004) The anaerobic oxidation of methane and sulfate reduction in sediments from Gulf of Mexico cold seeps. *Chemical Geology* **205**, 219–238.

Jugsujinda A., DeLaune R. D. and Lindau C. W. (2008) Influence of nitrate on methane production and oxidation in flooded soil. *Communications in Soil Science and Plant Analysis* **26**, 2449–2459.

Jun L. A. B., Gilmour C. M. and Bollen W. B. (1970) Non-biological reduction of nitrite in soil. *Nature* **225**, 664–664.

Junk W. J., Piedade M. T. F., Schöngart J., Cohn-Haft M., Adeney J. M. and Wittmann F. (2011) A classification of major naturally-occurring Amazonian lowland wetlands. *Wetlands* **31**, 623–640.

Kaiser J., Röckmann T., Brenninkmeijer C. A. M. and Crutzen P. J. (2003) Wavelength dependence of isotope fractionation in N_2O photolysis. *Atmospheric Chemistry and Physics* **3**, 303–313.

Kampschreur M. J., Kleerebezem R., de Vet W. W. J. M. and van Loosdrecht M. C. M. (2011) Reduced iron induced nitric oxide and nitrous oxide emission. *Water Research* **45**, 5945–5952.

Kandeler E. and Gerber H. (1988) Short-term assay of soil urease activity using colorimetric determination of ammonium. *Biology and Fertility of Soils* **6**, 68–72.

Kanokratana P., Uengwetwanit T., Rattanachomsri U., Bunterngsook B., Nimchua T., Tangphatsornruang S., Plengvidhya V., Champreda V. and Eurwilaichitr L. (2010) Insights into the phylogeny and metabolic potential of a primary tropical peat swamp forest microbial community by metagenomic analysis. *Microbial Ecology* **61**, 518–528.

Kappelmeyer U., Kuschk P. and Stottmeister U. (2003) Model experiments on the influence of artificial humic compounds on chemodenitrification. *Water, Air, and Soil Pollution* **147**, 317–330.

Kashyap A. K., Pandey K. D. and Gupta R. K. (1991) Nitrogenase activity of the antarctic cyanobacterium *Nostoc commune*: Influence of temperature. *Folia Microbiologica* **36**, 557–560.

Kasting J. F. (2014) Atmospheric composition of Hadean–early Archean Earth: The importance of CO. *Geological Society of America Special Papers*, 19–28.

Kasting J. F. (1990) Bolide impacts and the oxidation state of carbon in the Earth's early atmosphere. *Origins of Life and Evolution of Biospheres* **20**, 199–231.

Kerndorff H. and Schnitzer M. (1980) Sorption of metals on humic acid. *Geochimica et Cosmochimica Acta* **44**, 1701–1708.

Khramenkov S. V., Kozlov M. N., Kevbrina M. V., Dorofeev A. G., Kazakova E. A., Grachev V. A., Kuznetsov B. B., Polyakov D. Y. and Nikolaev Y. A. (2013) A novel bacterium carrying out anaerobic ammonium oxidation in a reactor for biological treatment of the filtrate of wastewater fermented sludge. *Microbiology* **82**, 628–636.

Kim J. K., Park K. J., Cho K. S., Nam S.-W., Park T.-J. and Bajpai R. (2005) Aerobic nitrification–denitrification by heterotrophic *Bacillus* strains. *Bioresource Technology* **96**, 1897–1906.

Kirschke S., Bousquet P., Ciais P., Saunois M., Canadell J. G., Dlugokencky E. J., Bergamaschi P., Bergmann D., Blake D. R., Bruhwiler L., Cameron-Smith P., Castaldi S., Chevallier F., Feng L., Fraser A., Heimann M., Hodson E. L., Houweling S., Josse B., Fraser P. J., Krummel P. B., Lamarque J.-F., Langenfelds R. L., Le Quéré C., Naik V., O'Doherty S., Palmer P. I., Pison I., Plummer D., Poulter B., Prinn R. G., Rigby M., Ringeval B., Santini M., Schmidt M., Shindell D. T., Simpson I. J., Spahni R., Steele L. P., Strode S. A., Sudo K., Szopa S., van der Werf G. R., Voulgarakis A., van Weele M., Weiss R. F., Williams J. E. and Zeng G. (2013) Three decades of global methane sources and sinks. *Nature Geoscience* **6**, 813–823.

Klüber H. D. and Conrad R. (1998a) Effects of nitrate, nitrite, NO and N_2O on methanogenesis and other redox processes in anoxic rice field soil. *FEMS Microbiology Ecology* **25**, 301–318.

Klüber H. D. and Conrad R. (1998b) Inhibitory effects of nitrate, nitrite, NO and N_2O on methanogenesis by *Methanosarcina barkeri* and *Methanobacterium bryantii*. *FEMS Microbiology Ecology* **25**, 331–339.

Knorr K.-H. and Blodau C. (2009) Impact of experimental drought and rewetting on redox transformations and methanogenesis in mesocosms of a northern fen soil. *Soil Biology and Biochemistry* **41**, 1–12.

Kohn W. and Sham L. J. (1965) Self-consistent equations including exchange and correlation effects. *Physical Review* **140**, A1133–A1138.

Krissansen-Totton J., Olson S. and Catling D. C. (2018) Disequilibrium biosignatures over Earth history and implications for detecting exoplanet life. *Science Advances* **4**, eaao5747.

Kumar S., Stecher G. and Tamura K. (2016) MEGA7: molecular evolutionary genetics analysis version 7.0 for bigger datasets. *Molecular Biology and Evolution* **33**, 1870–1874.

Laneuville M., Kameya M. and Cleaves H. J. II (2018) Earth without life: A systems model of a global abiotic nitrogen cycle. *Astrobiology* **18**, 897–914.

Lawson I. T., Jones T. D., Kelly T. J., Coronado E. N. H. and Roucoux K. H. (2014) The Geochemistry of Amazonian Peats. *Wetlands* **34**, 905–915.

Lazar C. S., Baker B. J., Seitz K., Hyde A. S., Dick G. J., Hinrichs K.-U. and Teske A. P. (2016) Genomic evidence for distinct carbon substrate preferences and ecological niches of Bathyarchaeota in estuarine sediments. *Environmental Microbiology* **18**, 1200–1211.

Lähteenoja O., Reátegui Y. R., Räsänen M., Torres D. D. C., Oinonen M. and Page S. (2011) The large Amazonian peatland carbon sink in the subsiding Pastaza-Marañón foreland basin, Peru. *Global Change Biology* **18**, 164–178.

Lähteenoja O., Ruokolainen K., Schulman L. and Alvarez J. (2009) Amazonian floodplains harbour minerotrophic and ombrotrophic peatlands. *Catena* **79**, 140–145.

Lewis B. L. and Landing W. M. (1991) The biogeochemistry of manganese and iron in the Black Sea. *Deep Sea Research* **38**, 773–803.

Lewis D. G., Habbena W. M. and Stahl D. A. (2014) Thermodynamic characterization of proton-ionizable functional groups on the cell surfaces of ammonia-oxidizing bacteria and archaea. *Geobiology* **12**, 157–171.

Li Y.-H. and Gregory S. (1974) Diffusion of ions in sea water and in deep-sea sediments. *Geochimica et Cosmochimica Acta* **38**, 703–714.

Liengaard L., Figueiredo V., Markfoged R., Revsbech N. P., Nielsen L. P., Prast A. E. and Kühl M. (2014) Hot moments of N_2O transformation and emission in tropical soils from the Pantanal and the Amazon (Brazil). *Soil Biology and Biochemistry* **75**, 26–36.

Liu B., Frostegård Å., Bakken L. R. and Bailey M. (2014) Impaired reduction of N_2O to N_2 in acid soils is due to a posttranscriptional interference with the expression of *nosZ*. *mBio* **5**, e01383–14.

Liu B., Mørkved P. T., Frostegård Å. and Bakken L. R. (2010) Denitrification gene pools, transcription and kinetics of NO, N_2O and N_2 production as affected by soil pH. *FEMS Microbiology Ecology* **72**, 407–417.

Liu D., Ding W., Jia Z. and Cai Z. (2012) The impact of dissolved organic carbon on the spatial variability of methanogenic archaea communities in natural wetland ecosystems across China. *Applied Microbiology and Biotechnology* **96**, 253–263.

Llirós M., Armisen T. G., Darchambeau F., Morana C., Margarit X. T., Inceoğlu Ö., Borrego C. M., Bouillon S., Servais P., Borges A. V., Descy J. P., Canfield D. E. and Crowe S. A. (2015) Pelagic photoferrotrophy and iron cycling in a modern ferruginous basin. *Scientific Reports* **5**, 1–8.

Lovelock J. E. (1988) *The ages of Gaia: A biography of our living Earth*, W.W. Norton & Company, Inc., New York.

Lueders T., Wagner B., Claus P. and Friedrich M. W. (2003) Stable isotope probing of rRNA and DNA reveals a dynamic methylotroph community and trophic interactions with fungi and protozoa in oxic rice field soil. *Environmental Microbiology* **6**, 60–72.

Luther G. W. (2010) The Role of One- and Two-Electron Transfer Reactions in Forming Thermodynamically Unstable Intermediates as Barriers in Multi-Electron Redox Reactions. *Aquatic Geochemistry* **16**, 395–420.

Luther G. W., Findlay A. J., MacDonald D. J., Owings S. M., Hanson T. E., Beinart R. A. and Girguis P. R. (2011) Thermodynamics and kinetics of sulfide oxidation by oxygen: A look at inorganically controlled reactions and biologically mediated processes in the environment. *Frontiers in Microbiology* **2**, 1–9.

Lycus P., Bøthun K. L., Bergaust L., Shapleigh J. P., Bakken L. R. and Frostegård Å. (2017) Phenotypic and genotypic richness of denitrifiers revealed by a novel isolation strategy. *The ISME Journal* **11**, 2219–2232.

Lycus P., Soriano-Laguna M. J., Kjos M., Richardson D. J., Gates A. J., Milligan D. A., Frostegård Å., Bergaust L. and Bakken L. R. (2018) A bet-hedging strategy for denitrifying bacteria curtails their release of N_2O. *Proceedings of the National Academy of Sciences* **115**, 11820–11825.

MacQueen J. (1967) Some methods for classification and analysis of multivariate observations. In *Proceedings of the Fifth Berkeley Symposium on Mathematical Statistics and Probability* pp. 281–297.

Magyari E. (2010) Exact analytical solutions of diffusion reaction in spherical porous catalyst. *Chemical Engineering Journal* **158**, 266–270.

Mancinelli R. L. and McKay C. P. (1988) The evolution of nitrogen cycling. *Origins of Life and Evolution of Biospheres* **18**, 311–325.

Mandić-Mulec I., Stefanic P. and van Elsas J. D. (2015) Ecology of *Bacillaceae*. *Microbiology Spectrum* **3**, 1–24.

Manzoni S., Trofymow J. A., Jackson R. B. and Porporato A. (2010) Stoichiometric controls on carbon, nitrogen, and phosphorus dynamics in decomposing litter. *Ecological Monograph* **80**, 89–106.

Marcus R. A. and Sutin N. (1985) Electron transfers in chemistry and biology. *Biochimica et Biophysica Acta (BBA) - Reviews on Bioenergetics* **811**, 265–322.

Martineau C., Mauffrey F. and Villemur R. (2015) Comparative analysis of denitrifying activities of *Hyphomicrobium nitrativorans*, *Hyphomicrobium denitrificans*, and *Hyphomicrobium zavarzinii*. *Applied and Environmental Microbiology* **81**, 5003–5014.

Massie S. T. and Hunten D. M. (1981) Stratospheric eddy diffusion coefficients from tracer data. *Journal of Geophysical Research: Atmospheres* **86**, 9859–9868.

Matthews R. G. (2001) Cobalamin-dependent methyltransferases. *Accounts of Chemical Research* **34**, 681–689.

McCalley C. K. and Sparks J. P. (2009) Abiotic gas formation drives nitrogen loss from a desert ecosystem. *Science* **326**, 837–840.

McDevitt C. A., Ogunniyi A. D., Valkov E., Lawrence M. C., Kobe B., McEwan A. G. and Paton J. C. (2011) A molecular mechanism for bacterial susceptibility to zinc. *PLoS Pathogens* **7**, 1–9.

McDonnell A. M. P. and Buesseler K. O. (2010) Variability in the average sinking velocity of marine particles. *Limnology and Oceanography* **55**, 2085–2096.

McIlvin M. R. and Altabet M. A. (2005) Chemical conversion of nitrate and nitrite to nitrous oxide for nitrogen and oxygen isotopic analysis in freshwater and seawater. *Analytical Chemistry* **77**, 5589–5595.

McKenney D. J., Johnson G. P. and Findlay W. I. (1984) Effect of temperature on consecutive denitrification reactions in brookston clay and fox sandy loam. *Applied*

and Environmental Microbiology **47**, 919–926.

McKenney D. J., Lazar C. and Findlay W. J. (1990) Kinetics of the nitrite to nitric oxide reaction in peat. *Soil Science Society of America Journal* **54**, 106–112.

McKnight D. M., Boyer E. W., Westerhoff P. K., Doran P. T., Kulbe T. and Andersen D. T. (2001) Spectrofluorometric characterization of dissolved organic matter for indication of precursor organic material and aromaticity. *Limnology and Oceanography* **46**, 38–48.

Min H. and Zinder S. H. (1989) Kinetics of acetate utilization by two thermophilic acetotrophic methanogens: *Methanosarcina* sp. strain CALS-1 and *Methanothrix* sp. strain CALS-1. *Applied and Environmental Microbiology* **55**, 488–491.

Miranda K. M., Espey M. G. and Wink D. A. (2001) A rapid, simple spectrophotometric method for simultaneous detection of nitrate and nitrite. *Nitric Oxide* **5**, 62–71.

Miroshnichenko M. L., Rainey F. A., Hippe H., Chernyh N. A. and Bonch-Osmolovskaya E. A. (1998) *Desulfurella kamchatkensis* sp. nov. and *Desulfurella propionica* sp. nov., new sulfur-respiring thermophilic bacteria from Kamchatka thermal environments. *International Journal of Systematic Bacteriology* **48**, 475–479.

Moers M. E. C., Baas M., Boon J. J. and De Leeuw J. W. (1990) Molecular characterization of total organic matter and carbohydrates in peat samples from a cypress swamp by pyrolysis-mass spectrometry and wet-chemical methods. *Biogeochemistry* **11**, 251–277.

Mohagheghi A., Grohmann K., Himmel M., Leighton L. and Updegraff D. M. (1986) Isolation and characterization of *Acidothermus cellulolyticus* gen. nov., sp. nov, a new genus of thermophilic, acidophilic, cellulolytic bacteria. *International Journal of Systematic Bacteriology* **36**, 435–443.

Moraghan J. T. and Buresh R. J. (1977) Chemical reduction of nitrite and nitrous oxide by ferrous iron. *Soil Science Society of America Journal* **41**, 47–50.

Morrissey E. M., Berrier D. J., Neubauer S. C. and Franklin R. B. (2013) Using microbial communities and extracellular enzymes to link soil organic matter characteristics to greenhouse gas production in a tidal freshwater wetland. *Biogeochemistry* **117**, 473–490.

Nakamura T., Oda T., Fukasawa Y. and Tomii K. (2017) Template-based quaternary structure prediction of proteins using enhanced profile–profile alignments. *Proteins: Structure, Function, and Bioinformatics* **86**, 274–282.

National Institute of Standards and Technology, U.S. Department of Commerce (1998) *NIST–JANAF Thermochemical Tables*. **25**.

Navarro-Gonzalez R., Molina M. J. and Molina L. T. (1998) Nitrogen fixation by volcanic lightning in the early Earth. *Geophysical Research Letters* **25**, 3123–3126.

Nelson D. W. and Bremner J. M. (1969) Factors affecting chemical transformations of nitrite in soils. *Soil Biology and Biochemistry* **1**, 229–239.

Noll M., Matthies D., Frenzel P., Derakshani M. and Liesack W. (2005) Succession of bacterial community structure and diversity in a paddy soil oxygen gradient. *Environmental Microbiology* **7**, 382–395.

Ondov B. D., Bergman N. H. and Phillippy A. M. (2011) Interactive metagenomic visualization in a Web browser. *BMC Bioinformatics* **12**, 1–10.

Onley J. R., Ahsan S., Sanford R. A., Löffler F. E. and Drake H. L. (2018) Denitrification by *Anaeromyxobacter dehalogenans*, a common soil bacterium lacking the nitrite reductase genes *nirs* and *nirk*. *Applied and Environmental Microbiology* **84**, A556.

Orellana L. H., Rodriguez-R L. M., Higgins S., Chee-Sanford J. C., Sanford R. A., Ritalahti K. M., Löffler F. E., Konstantinidis K. T. and Bailey M. (2014) Detecting nitrous oxide reductase (*nosZ*) genes in soil metagenomes: Method development and implications for the nitrogen cycle. *mBio* **5**, e01193–14.

Ormeci B., Sanin S. L. and Peirce J. J. (1999) Laboratory study of NO flux from agricultural soil: Effects of soil moisture, pH, and temperature. *Journal of Geophysical Research: Atmospheres* **104**, 1621–1629.

Ostrander C. M., Nielsen S. G., Owens J. D., Kendall B., Gordon G. W., Romaniello S. J. and Anbar A. D. (2019) Fully oxygenated water columns over continental shelves before the Great Oxidation Event. *Nature Geoscience* **12**, 186–191.

Ostrom N. E., Gandhi H., Trubl G. and Murray A. E. (2016) Chemodenitrification in the cryoecosystem of Lake Vida, Victoria Valley, Antarctica. *Geobiology* **14**, 575–587.

Otte J. M., Blackwell N., Ruser R., Kappler A., Kleindienst S. and Schmidt C. (2019) N_2O formation by nitrite-induced (chemo)denitrification in coastal marine sediment. *Scientific Reports* **9**, 5693–13.

Ottley C. J., Davison W. and Edmunds W. M. (1997) Chemical catalysis of nitrate reduction by iron (II). *Geochimica et Cosmochimica Acta* **61**, 1819–1828.

Page S., Rieley J. O., Shotyk O. W. and Weiss D. (1999) Interdependence of peat and vegetation in a tropical peat swamp forest. *Philosophical Transactions of the Royal Society B: Biological Sciences* **354**, 1885–1897.

Palmer K. and Horn M. A. (2012) Actinobacterial nitrate reducers and proteobacterial denitrifiers are abundant in N_2O-metabolizing palsa peat. *Applied and Environmental Microbiology* **78**, 5584–5596.

Palmer K. and Horn M. A. (2015) Denitrification activity of a remarkably diverse fen denitrifier community in finnish lapland is N-oxide limited. *PLoS One* **10**, e0123123.

Palmer K., Biasi C. and Horn M. A. (2012) Contrasting denitrifier communities relate to contrasting N_2O emission patterns from acidic peat soils in arctic tundra. *The ISME Journal* **6**, 1058–1077.

Park D., Kim H., Yoon S. and Kivisaar M. (2017) Nitrous oxide reduction by an obligate aerobic bacterium, *Gemmatimonas aurantiaca* strain T-27. *Applied and Environmental Microbiology* **83**, 43.

Park J. Y. and Lee Y. N. (1988) Solubility and decomposition kinetics of nitrous acid in aqueous solution. *The Journal of Physical Chemistry* **92**, 6294–6302.

Park S., Pérez T., Boering K. A., Trumbore S. E., Gil J., Marquina S. and Tyler S. C. (2011) Can N_2O stable isotopes and isotopomers be useful tools to characterize sources and microbial pathways of N_2O production and consumption in tropical soils? *Global Biogeochemical Cycles* **25**, 1–16.

Parton W., Silver W. L., Burke I. C., Grassens L., Harmon M. E., Currie W. S., King J. Y., Adair E. C., Brandt L. A., Hart S. C. and Fasth B. (2007) Global-scale similarities in nitrogen release patterns during long-term decomposition. *Science* **315**, 361–364.

Pearce C. I., Qafoku O., Liu J., Arenholz E., Heald S. M., Kukkadapu R. K., Gorski C. A., Henderson C. M. B. and Rosso K. M. (2012) Synthesis and properties of titanomagnetite ($Fe_{3-x}Ti_xO_4$) nanoparticles: A tunable solid-state Fe(II/III) redox system. *Journal of Colloid and Interface Science* **387**, 24–38.

Penton C. R., St Louis D., Pham A., Cole J. R., Wu L., Luo Y., Schuur E. A. G. and Tiedje J. M. (2015) Denitrifying and diazotrophic community responses to artificial warming in permafrost and tallgrass prairie soils. *Frontiers in Microbiology* **6**, 439.

Pepper S. E., Borkowski M., Richmann M. K. and Reed D. T. (2010) Determination of ferrous and ferric iron in aqueous biological solutions. *Analytica Chimica Acta* **663**, 172–177.

Pett-Ridge J., Silver W. L. and Firestone M. K. (2006) Redox fluctuations frame microbial community impacts on N-cycling rates in a humid tropical forest soil. *Biogeochemistry* **81**, 95–110.

Pérez T., Garcia-Montiel D., Trumbore S., Tyler S., de Camargo P., Moreira M., Piccolo M. and Cerri C. (2006) Nitrous oxide nitrification and denitrification ^{15}N enrichment factors from Amazon forest soils. *Ecological Applications* **16**, 2153–2167.

Pérez T., Trumbore S. E., Tyler S. C., Matson P. A., Monasterio I. O., Rahn T. and Griffith D. W. T. (2001) Identifying the agricultural imprint on the global N_2O

budget using stable isotopes. *Journal of Geophysical Research: Atmospheres* **106**, 9869–9878.

Philippot L., Andersson S. G. E., Battin T. J., Prosser J. I., Schimel J. P., Whitman W. B. and Hallin S. (2010) The ecological coherence of high bacterial taxonomic ranks. *Nature Methods* **8**, 523–529.

Pihlatie M., Syväsalo E., Simojoki A., Esala M. and Regina K. (2004) Contribution of nitrification and denitrification to N_2O production in peat, clay and loamy sand soils under different soil moisture conditions. *Nutrient Cycling in Agroecosystems* **70**, 135–141.

Pomowski A., Zumft W. G., Kroneck P. M. H. and Einsle O. (2011) N_2O binding at a [4Cu:2S] copper–sulphur cluster in nitrous oxide reductase. *Nature* **477**, 234–237.

Porter L. K. (1969) Gaseous products produced by anaerobic reaction of sodium nitrite with oxime compounds and oximes synthesized from organic matter. *Soil Science Society of America Journal* **33**, 696–702.

Poulton S. W. and Canfield D. E. (2011) Ferruginous conditions: A dominant feature of the ocean through Earth's history. *Elements* **7**, 107–112.

Pracht J., Boenigk J., Isenbeck-Schröter M., Keppler F. and Schöler H. F. (2001) Abiotic Fe(III) induced mineralization of phenolic substances. *Chemosphere* **44**, 613–619.

Price M. N., Dehal P. S. and Arkin A. P. (2009) FastTree: computing large minimum evolution trees with profiles instead of a distance matrix. *Molecular Biology and Evolution* **26**, 1641–1650.

Puglisi E., Zaccone C., Cappa F., Cocconcelli P. S., Shotyk W., Trevisan M. and Miano T. M. (2014) Changes in bacterial and archaeal community assemblages along an ombrotrophic peat bog profile. *Biology and Fertility of Soils* **50**, 815–826.

Raczyńska E. D., Krygowski T. M., Zachara J. E., Ośmiałowski B. and Gawinecki R. (2005) Tautomeric equilibria, H-bonding and π-electron delocalization in o-nitrosophenol. A B3LYP/6-311 + G(2df,2p) study. *Journal of Physical Organic Chemistry* **18**, 892–897.

Ranjan S., Todd Z. R., Rimmer P. B., Sasselov D. D. and Babbin A. R. (2019) Nitrogen oxide concentrations in natural waters on early Earth. *Geochemistry, Geophysics, Geosystems* **20**, 2021–2039.

Rasmussen T., Brittain T., Ben C Berks, Watmough N. J. and Thomson A. J. (2005) Formation of a cytochrome c–nitrous oxide reductase complex is obligatory for N_2O reduction by *Paracoccus pantotrophus*. *Dalton Transactions*, 3501–3506.

Ravishankara A. R., Daniel J. S. and Portmann R. W. (2009) Nitrous oxide (N_2O): The

dominant ozone-depleting substance emitted in the 21st century. *Science* **326**, 123–125.

Raymond J., Siefert J. L., Staples C. R. and Blankenship R. E. (2004) The natural history of nitrogen fixation. *Molecular Biology and Evolution* **21**, 541–554.

Räsänen M. E., Salo J. S. and Kalliola R. J. (1987) Fluvial perturbance in the western amazon basin: Regulation by long-term sub-andean tectonics. *Science* **238**, 1398–1401.

Robens C. (2017) Testing the quantumness of atom trajectories. Rheinische Friedrich-Wilhelms-Universität Bonn.

Roberson A. L., Roadt J., Halevy I. and Kasting J. F. (2011) Greenhouse warming by nitrous oxide and methane in the Proterozoic Eon. *Geobiology* **9**, 313–320.

Rock J. D., Mahnane M. R., Anjum M. F., Shaw J. G., Read R. C. and Moir J. W. B. (2005) The pathogen Neisseria meningitidisrequires oxygen, but supplements growth by denitrification. Nitrite, nitric oxide and oxygen control respiratory flux at genetic and metabolic levels. *Molecular Microbiology* **58**, 800–809.

Roco C. A., Bergaust L. L., Bakken L. R., Yavitt J. B. and Shapleigh J. P. (2017) Modularity of nitrogen-oxide reducing soil bacteria: linking phenotype to genotype. *Environmental Microbiology* **19**, 2507–2519.

Rodrigo M. A., Miracle M. R. and Vicente E. (2001) The meromictic lake La Cruz (Central Spain). Patterns of stratification. *Aquatic Sciences* **63**, 406–416.

Rogers R. D. (1977) Abiological methylation of mercury in soil. *Journal of Environmental Quality* **6**, 463–467.

Rosenberg E., DeLong E. F., Lory S., Stackebrandt E. and Thompson F. eds. (2014) *The Prokaryotes*, Springer-Verlag, Heidelberg, New York, Dordrecht, London, 4th Edition.

Sakabe A., Itoh M., Hirano T. and Kusin K. (2018) Ecosystem-scale methane flux in tropical peat swamp forest in Indonesia. *Global Change Biology* **24**, 5123–5136.

Samarkin V. A., Madigan M. T., Bowles M. W., Casciotti K. L., Priscu J. C., McKay C. P. and Joye S. B. (2010) Abiotic nitrous oxide emission from the hypersaline Don Juan Pond in Antarctica. *Nature Geoscience* **3**, 341–344.

Sander S. P., Friedl R. R., Barker J. R., Golden D. M., Kurylo M. J., Wine P. H., Abbatt J., Burkholder J. B., Kolb C. E., Moortgat G. K., Huie R. E. and Orkin V. L. (2009) *Chemical kinetics and photochemical data for use in Atmospheric Studies, Evaluation Number 16*, Pasadena, CA : Jet Propulsion Laboratory, National Aeronautics and Space Administration, 2009.

Sanford R. A., Wagner D. D., Wu Q., Chee-Sanford J. C., Thomas S. H., Cruz-García C., Rodríguez G., Massol-Deyá A., Krishnani K. K., Ritalahti K. M., Nissen S., Konstantinidis K. T. and Löffler F. E. (2012) Unexpected nondenitrifier nitrous oxide reductase gene diversity and abundance in soils. *Proceedings of the National Academy of Sciences* **109**, 19709–19714.

Saraiva L. M., Vicente J. B. and Teixeira M. (2004) The role of the flavodiiron proteins in microbial nitric oxide detoxification. In *Advances in Micobial Physiology* (ed. R. K. Poole). pp. 78–120.

Saraste M. and Castresana J. (1994) Cytochrome oxidase evolved by tinkering with denitrification enzymes. *FEBS Letters* **341**, 1–4.

Schindlbacher A., Boltenstern S. Z. and Bahl K. B. (2004) Effects of soil moisture and temperature on NO, NO_2, and N_2O emissions from European forest soils. *Journal of Geophysical Research: Atmospheres* **109**, 1–12.

Schwintzer C. R. (1979) Nitrogen fixation by Myrica gale root nodules Massachusetts wetland. *Oecologia* **43**, 283–294.

Seitzinger S., Harrison J. A., Böhlke J. K., Bouwman A. F., Lowrance R., Peterson B., Tobias C. and Van Drecht G. (2006) Denitrification across landscapes and waterscapes: a synthesis. *Ecological Applications* **16**, 2064–2090.

Senga Y., Hiroki M., Nakamura Y., Watarai Y., Watanabe Y. and Nohara S. (2010) Vertical profiles of DIN, DOC, and microbial activities in the wetland soil of Kushiro Mire, northeastern Japan. *Limnology* **12**, 17–23.

Senga Y., Hiroki M., Terui S. and Nohara S. (2015) Variation in microbial function through soil depth profiles in the Kushiro Wetland, northeastern Hokkaido, Japan. *Ecological Research* **30**, 1–10.

Serge I Gorelsky, Somdatta Ghosh A. and Solomon E. I. (2005) Mechanism of N_2O reduction by the μ4-S tetranuclear CuZ cluster of nitrous oxide reductase. *Journal of the American Chemical Society* **128**, 278–290.

Shirokova L. S., Bredoire R., Rols J.-L. and Pokrovsky O. S. (2016) Moss and peat leachate degradability by heterotrophic bacteria: the fate of organic carbon and trace metals. *Geomicrobiology Journal* **34**, 641–655.

Shock E. and Canovas P. (2010) The potential for abiotic organic synthesis and biosynthesis at seafloor hydrothermal systems. *Geofluids* **10**, 161–192.

Shock E. L., Holland M., Meyer-Dombard D., Amend J. P., Osburn G. R. and Fischer T. P. (2010) Quantifying inorganic sources of geochemical energy in hydrothermal ecosystems, Yellowstone National Park, USA. *Geochimica et Cosmochimica Acta* **74**, 4005–4043.

Smirnov A., Hausner D., Laffers R., Strongin D. R. and Schoonen M. A. (2008) Abiotic ammonium formation in the presence of Ni-Fe metals and alloys and its implications for the Hadean nitrogen cycle. *Geochemical Transactions* **9**, 5–20.

Sorensen J. and Thorling L. (1991) Stimulation by lepidocrocite (γ-FeOOH) of Fe(II)-dependent nitrite reduction. *Geochimica et Cosmochimica Acta* **55**, 1289–1294.

Stanton C. L., Reinhard C. T., Kasting J. F., Ostrom N. E., Haslun J. A., Lyons T. W. and Glass J. B. (2018) Nitrous oxide from chemodenitrification: A possible missing link in the Proterozoic greenhouse and the evolution of aerobic respiration. *Geobiology* **16**, 597–609.

Staubwasser M., Schoenberg R., Blanckenburg F. V., Krüger S. and Pohl C. (2013) Isotope fractionation between dissolved and suspended particulate Fe in the oxic and anoxic water column of the Baltic Sea. *Biogeosciences* **10**, 233–245.

Stedman G. (1959) Mechanism of the azide–nitrite reaction – Part II. *Journal of the Chemical Society*, 2949–2954.

Stedmon C. A., Markager S. and Bro R. (2003) Tracing dissolved organic matter in aquatic environments using a new approach to fluorescence spectroscopy. *Marine Chemistry* **82**, 239–254.

Steinberg L. M. and Regan J. M. (2009) *mcrA*-targeted real-time quantitative PCR method to examine methanogen communities. *Applied and Environmental Microbiology* **75**, 4435–4442.

Steinberg L. M. and Regan J. M. (2008) Phylogenetic comparison of the methanogenic communities from an acidic, oligotrophic fen and an anaerobic digester treating municipal wastewater sludge. *Applied and Environmental Microbiology* **74**, 6663–6671.

Stiefel P., Schmidt-Emrich S., Maniura-Weber K. and Ren Q. (2015) Critical aspects of using bacterial cell viability assays with the fluorophores SYTO9 and propidium iodide. *BMC Microbiology* **15**, 1–9.

Stocker B. D., Roth R., Joos F., Spahni R., Steinacher M., Zaehle S., Bouwman L., Xu-Ri and Prentice I. C. (2013) Multiple greenhouse-gas feedbacks from the land biosphere under future climate change scenarios. *Nature Climate Change* **3**, 666–672.

Stone M. M., Kan J. and Plante A. F. (2015) Parent material and vegetation influence bacterial community structure and nitrogen functional genes along deep tropical soil profiles at the Luquillo Critical Zone Observatory. *Soil Biology and Biochemistry* **80**, 273–282.

Stookey L. L. (1970) Ferrozine – a new spectrophotometric reagent for iron. *Analytical Chemistry* **42**, 779–781.

Stumm W. and Morgan J. J. eds. (2012) *Aquatic Chemistry*. 3rd ed., John Wiley & Sons.

Suenaga T., Hori T., Riya S., Hosomi M., Smets B. F. and Terada A. (2019) Enrichment, isolation, and characterization of high-affinity N_2O-reducing bacteria in a gas-permeable membrane reactor. *Environmental Science & Technology* **53**, 12101–12112.

Suenaga T., Riya S., Hosomi M. and Terada A. (2018) Biokinetic characterization and activities of N_2O-reducing bacteria in response to various oxygen levels. *Frontiers in Microbiology* **9**, 147–10.

Suharti and de Vries S. (2005) Membrane-bound denitrification in the gram-positive bacterium *Bacillus azotoformans*. *Biochemical Society Transactions* **33**, 130–133.

Sullivan M. J., Gates A. J., Appia-Ayme C., Rowley G. and Richardson D. J. (2013) Copper control of bacterial nitrous oxide emission and its impact on vitamin B_{12}-dependent metabolism. *Proceedings of the National Academy of Sciences* **110**, 19926–19931.

Summers D. P. and Chang S. (1993) Prebiotic ammonia from reduction of nitrite by iron (II) on the early Earth. *Nature* **365**, 630–633.

Summers D. P. and Khare B. (2007) Nitrogen fixation on early Mars and other terrestrial planets: experimental demonstration of abiotic fixation reactions to nitrite and nitrate. *Astrobiology* **7**, 333–341.

Sun Z.-X., Su F.-W., Forsling W. and Samskog P.-O. (1998) Surface Characteristics of Magnetite in Aqueous Suspension. *Journal of Colloid and Interface Science* **197**, 151–159.

Swanner E. D., Mloszewska A. M., Cirpka O. A., Schoenberg R., Konhauser K. O. and Kappler A. (2015) Modulation of oxygen production in Archaean oceans by episodes of Fe(II) toxicity. *Nature Geoscience* **8**, 126–130.

Taketani R. G., Yoshiura C. A., Dias A. C. F., Andreote F. D. and Tsai S. M. (2010) Diversity and identification of methanogenic archaea and sulphate-reducing bacteria in sediments from a pristine tropical mangrove. *Antonie van Leeuwenhoek* **97**, 401–411.

Takeuchi M., Yoshioka H., Seo Y., Tanabe S., Tamaki H., Kamagata Y., Takahashi H. A., Igari S., Mayumi D. and Sakata S. (2011) A distinct freshwater-adapted subgroup of ANME-1 dominates active archaeal communities in terrestrial subsurfaces in Japan. *Environmental Microbiology* **13**, 3206–3218.

Tamaki H., Wright C. L., Li X., Lin Q., Hwang C., Wang S., Thimmapuram J., Kamagata Y. and Liu W.-T. (2011) Analysis of 16S rRNA amplicon sequencing options on the Roche/454 next-generation titanium sequencing platform. *PLoS One* **6**, e25263.

Tang A. C. I., Stoy P. C., Hirata R., Musin K. K., Aeries E. B., Wenceslaus J. and Melling L. (2018) Eddy Covariance Measurements of Methane Flux at a Tropical Peat Forest in Sarawak, Malaysian Borneo. *Geophysical Research Letters* **45**, 4390–4399.

Tang Y., Yu G., Zhang X., Wang Q., Ge J. and Liu S. (2018) Changes in nitrogen-cycling microbial communities with depth in temperate and subtropical forest soils. *Applied Soil Ecology* **124**, 218–228.

Tarduno J. A., Blackman E. G. and Mamajek E. E. (2014) Detecting the oldest geodynamo and attendant shielding from the solar wind: Implications for habitability. *Physics of the Earth and Planetary Interiors* **233**, 68–87.

Teh Y. A., Murphy W. A., Berrio J.-C., Boom A. and Page S. E. (2017) Seasonal variability in methane and nitrous oxide fluxes from tropical peatlands in the western Amazon basin. *Biogeosciences* **14**, 3669–3683.

Thorn K. A. and Mikita M. A. (2000) Nitrite fixation by humic substances nitrogen-15 nuclear magnetic resonance evidence for potential intermediates in chemodenitrification. *Soil Science Society of America Journal* **64**, 568–582.

Thorn K. A., Younger S. J. and Cox L. G. (2010) Order of functionality loss during photodegradation of aquatic humic substances. *Journal of Environmental Quality* **39**, 1416–1428.

Tolman W. B. (2010) Binding and activation of N_2O at transition-metal centers: Recent mechanistic insights. *Angewandte Chemie International Edition* **49**, 1018–1024.

Trevors J. T. (1996) Sterilization and inhibition of microbial activity in soil. *Journal of Microbiological Methods* **26**, 53–59.

Troshina O., Oshurkova V., Suzina N., Novikov A., Shcherbakova V., Vinokurova N., Machulin A., Kopitsyn D. and Ariskina E. (2015) *Sphaerochaeta associata* sp. nov., a spherical spirochaete isolated from cultures of *Methanosarcina mazei* JL01. *International Journal Of Systematic And Evolutionary Microbiology* **65**, 4315–4322.

Tsai M.-L., Hadt R. G., Vanelderen P., Sels B. F., Schoonheydt R. A. and Solomon E. I. (2014) $[Cu_2O]^{2+}$ Active site formation in Cu–ZSM-5: Geometric and electronic structure requirements for N_2O activation. *Journal of the American Chemical Society* **136**, 3522–3529.

Tuominen L., Kairesalo T. and Hartikainen H. (1994) Comparison of methods for inhibiting bacterial activity in sediment. *Applied and Environmental Microbiology* **60**, 3454–3457.

Van Cleemput O. and Baert L. (1984) Nitrite: a key compound in N loss processes under acid conditions? *Plant and Soil* **76**, 233–241.

Van Cleemput O., Patrick W. H. and McIlhenny R. C. (1976) Nitrite decomposition in flooded soil under different pH and redox potential conditions. *Soil Science Society of America Journal* **40**, 55–60.

van Kessel M. A. H. J., Speth D. R., Albertsen M., Nielsen P. H., Camp den H. J. M. O., Kartal B., Jetten M. S. M. and Lücker S. (2015) Complete nitrification by a single microorganism. *Nature* **528**, 555–559.

Vaz-Moreira I., Figueira V., Lopes A. R., De Brandt E., Vandamme P., Nunes O. C. and Manaia C. M. (2011) *Candidimonas nitroreducens* gen. nov., sp. nov. and *Candidimonas humi* sp. nov., isolated from sewage sludge compost. *International Journal Of Systematic And Evolutionary Microbiology* **61**, 2238–2246.

Venterea R. T. and Rolston D. E. (2000) Nitric and nitrous oxide emissions following fertilizer application to agricultural soil: Biotic and abiotic mechanisms and kinetics. *Journal of Geophysical Research: Atmospheres* **105**, 15117–15129.

Veverica T. J., Kane E. S., Marcarelli A. M. and Green S. A. (2016) Ionic liquid extraction unveils previously occluded humic-bound iron in peat soil pore water. *Soil Science Society of America Journal* **80**, 771–782.

Viebrock A. and Zumft W. G. (1988) Molecular cloning, heterologous expression, and primary structure of the structural gene for the copper enzyme nitrous oxide reductase from denitrifying *Pseudomonas stutzeri*. *Journal of Bacteriology* **170**, 4658–4668.

Viollier E., Michard G., Jézéquel D., Pèpe M. and Sarazin G. (1997) Geochemical study of a crater lake: Lake Pavin, Puy de Dôme, France. Constraints afforded by the particulate matter distribution in the element cycling within the lake. *Chemical Geology* **142**, 225–241.

Wang J. H., Baltzis B. C. and Lewandowski G. A. (1995) Fundamental denitrification kinetic studies with Pseudomonas denitrificans. *Biotechnology and Bioengineering* **47**, 26–41.

Wang Q., Quensen J. F., Fish J. A., Lee T. K., Sun Y., Tiedje J. M. and Cole J. R. (2013) Ecological patterns of nifh genes in four terrestrial climatic zones explored with targeted metagenomics using Framebot, a new informatics tool. *mBio* **4**, e00592–13.

Wang S., Zhuang Q., Lähteenoja O., Draper F. C. and Cadillo-Quiroz H. (2018) Potential shift from a carbon sink to a source in Amazonian peatlands under a changing climate. *Proceedings of the National Academy of Sciences* **115**, 12407–12412.

Wang X., Helgason B., Westbrook C. and Bedard-Haughn A. (2016) Effect of mineral sediments on carbon mineralization, organic matter composition and microbial community dynamics in a mountain peatland. *Soil Biology and Biochemistry* **103**, 16–27.

Wanninkhof R. (2014) Relationship between wind speed and gas exchange over the ocean revisited. *Limnology and Oceanography: Methods* **12**, 351–362.

Watanabe T., Wang G., Taki K., Ohashi Y., Kimura M. and Asakawa S. (2010) Vertical changes in bacterial and archaeal communities with soil depth in Japanese paddy fields. *Soil Science and Plant Nutrition* **56**, 705–715.

Weber E. B., Lehtovirta-Morley L. E., Prosser J. I. and Gubry-Rangin C. (2015) Ammonia oxidation is not required for growth of Group 1.1c soil Thaumarchaeota. **91**, 1–7.

Weiss R. F. and Price B. A. (1980) Nitrous oxide solubility in water and seawater. *Marine Chemistry* **8**, 347–359.

Whiticar M. J. (1999) Carbon and hydrogen isotope systematics of bacterial formation and oxidation of methane. *Chemical Geology* **161**, 291–314.

Williams A. G. B. and Scherer M. M. (2001) Kinetics of Cr(VI) reduction by carbonate green rust. *Environmental Science & Technology* **35**, 3488–3494.

Wilson H. F. and Xenopoulos M. A. (2009) Effects of agricultural land use on the composition of fluvial dissolved organic matter. *Nature Geoscience* **2**, 37–41.

Winton R. S., Flanagan N. and Richardson C. J. (2017) Neotropical peatland methane emissions along a vegetation and biogeochemical gradient. *PLoS One* **12**, e0187019.

Wolf D. C., Dao T. H., Scott H. D. and Lavy T. L. (1989) Influence of sterilization methods on selected soil microbiological, physical, and chemical properties. *Journal of Environmental Quality* **18**, 39–44.

Wolf E. T. and Toon O. B. (2010) Fractal organic hazes provided an ultraviolet shield for early Earth. *Science* **328**, 1266–1268.

Wong G. X., Hirata R., Hirano T., Kiew F., Aeries E. B., Musin K. K., Waili J. W., Lo K. S. and Melling L. (2020) How do land use practices affect methane emissions from tropical peat ecosystems? *Agricultural and Forest Meteorology* **282-283**, 107869.

Wong G. X., Hirata R., Hirano T., Kiew F., Aeries E. B., Musin K. K., Waili J. W., Lo K. S. and Melling L. (2018) Micrometeorological measurement of methane flux above a tropical peat swamp forest. *Agricultural and Forest Meteorology* **256-257**, 353–361.

Wong M. L., Charnay B. D., Gao P., Yung Y. L. and Russell M. J. (2017) Nitrogen oxides in early Earth's atmosphere as electron acceptors for life's emergence. *Astrobiology* **17**, 975–983.

Wullstein L. H. and Gilmour C. M. (1966) Non-enzymatic formation of nitrogen gas. *Nature* **210**, 1150–1151.

Xia K., Skyllberg U. L., Bleam W. F., Bloom P. R., Nater E. A. and Helmke P. A. (1998) X-ray absorption spectroscopic evidence for the complexation of Hg(II) by reduced sulfur in soil humic Substances. *Environmental Science & Technology* **33**, 257–261.

Yang S., Liebner S., Winkel M., Alawi M., Horn F., Dörfer C., Ollivier J., He J.-S., Jin H., Kühn P., Schloter M., Scholten T. and Wagner D. (2017) In-depth analysis of core methanogenic communities from high elevation permafrost-affected wetlands. *Soil Biology and Biochemistry* **111**, 66–77.

Yao H., Gao Y., Nicol G. W., Campbell C. D., Prosser J. I., Zhang L., Han W. and Singh B. K. (2011) Links between ammonia oxidizer community structure, abundance, and nitrification potential in acidic soils. *Applied and Environmental Microbiology* **77**, 4618–4625.

Yoon J. H. (2003) *Paenibacillus kribbensis* sp. nov. and *Paenibacillus terrae* sp. nov., bioflocculants for efficient harvesting of algal cells. *International Journal Of Systematic And Evolutionary Microbiology* **53**, 295–301.

Yoon S., Nissen S., Park D., Sanford R. A., Löffler F. E. and Kostka J. E. (2016) Nitrous oxide reduction kinetics distinguish bacteria harboring clade I nosz from those harboring clade II NosZ. *Applied and Environmental Microbiology* **82**, 3793–3800.

Yoshinari T., Hynes R. and Knowles R. (1977) Acetylene inhibition of nitrous oxide reduction and measurement of denitrification and nitrogen fixation in soil. *Soil Biology and Biochemistry* **9**, 177–183.

Yvon-Durocher G., Caffrey J. M., Cescatti A., Dossena M., del Giorgio P., Gasol J. M., Montoya J. M., Pumpanen J., Staehr P. A., Trimmer M., Woodward G. and Allen A. P. (2012) Reconciling the temperature dependence of respiration across timescales and ecosystem types. *Nature* **487**, 472–476.

Yvon-Durocher G., Jones J. I., Trimmer M., Woodward G. and Montoya J. M. (2010) Warming alters the metabolic balance of ecosystems. *Philosophical Transactions of the Royal Society B: Biological Sciences* **365**, 2117–2126.

Zahran H. H. (1999) *Rhizobium*-legume symbiosis and nitrogen fixation under severe conditions and in an arid climate. *Microbiology and Molecular Biology Reviews* **63**, 968–989.

Zaichikova M. V., Berestovskaya Y. Y., Akimov V. N., Kizilova A. K. and Vasilieva L. V. (2010) *Xanthobacter xylophilus* sp. nov., a member of the xylotrophic mycobacterial community of low-mineral oligotrophic waters. *Microbiology* **79**, 83–88.

Zegeye A., Bonneville S., Benning L. G., Sturm A., Fowle D. A., Jones C., Canfield D. E., Ruby C., MacLean L. C., Nomosatryo S., Crowe S. A. and Poulton S. W. (2012) Green rust formation controls nutrient availability in a ferruginous water column.

Geology **40**, 599–602.

Zelles L., Palojärvi A., Kandeler E., Lützow Von M., Winter K. and Bai Q. Y. (1997) Changes in soil microbial properties and phospholipid fatty acid fractions after chloroform fumigation. *Soil Biology and Biochemistry* **29**, 1325–1336.

Zhang L.-M., Hu H.-W., Shen J.-P. and He J.-Z. (2011) Ammonia-oxidizing archaea have more important role than ammonia-oxidizing bacteria in ammonia oxidation of strongly acidic soils. *The ISME Journal* **6**, 1032–1045.

Zheng W., Liang L. and Gu B. (2011) Mercury reduction and oxidation by reduced natural organic matter in anoxic environments. *Environmental Science & Technology* **46**, 292–299.

Zhu B., van Dijk G., Fritz C., Smolders A. J. P., Pol A., Jetten M. S. M. and Ettwig K. F. (2012) Anaerobic oxidization of methane in a minerotrophic peatland: Enrichment of nitrite-dependent methane-oxidizing bacteria. *Applied and Environmental Microbiology* **78**, 8657–8665.

Zhu X., Silva L. C. R., Doane T. A. and Horwath W. R. (2013) Iron: The forgotten driver of nitrous oxide production in agricultural soil. *PLoS One* **8**, e60146.

Zhu-Barker X., Cavazos A. R., Ostrom N. E., Horwath W. R. and Glass J. B. (2015) The importance of abiotic reactions for nitrous oxide production. *Biogeochemistry* **126**, 251–267.

Zhuang Q., Lu Y. and Chen M. (2012) An inventory of global N_2O emissions from the soils of natural terrestrial ecosystems. *Atmospheric Environment* **47**, 66–75.

APPENDIX A

CHAPTER 1 SUPPLEMENTARY TABLE

Table A.1. Activation energies of biotic, mixed, or abiotic nitrogen reduction reactions.

Process	Mechanism	Activation energy (kJ mol^{-1})	Reference
Nitrate (NaNO$_3$) reduction to ammonium by sulfate green rust	abiotic	83.9	(Hansen and Koch, 1998)
Nitrate [Ba(NO$_3$)$_2$] reduction to ammonium by sulfate green rust	abiotic	90.5	(Hansen and Koch, 1998)
Nitrate reduction by Fe^{2+} to ammonium	abiotic	70	(Ottley *et al.*, 1997)
Nitrate reduction	biotic	50.1	(Foglar *et al.*, 2005)
Nitrate reduction	biotic	35.9	(J. H. Wang *et al.*, 1995)
Nitrite reduction to NO	biotic	30.1	(J. H. Wang *et al.*, 1995)
NO production	abiotic	67	(Venterea and Rolston, 2000)
	mixed	85.3	(Schindlbacher *et al.*, 2004)
	mixed	100.4	(Schindlbacher *et al.*, 2004)
	mixed	158.2	(Schindlbacher *et al.*, 2004)
	mixed	125.3	(Schindlbacher *et al.*, 2004)
	mixed	147.9	(Schindlbacher *et al.*, 2004)
	mixed	172.3	(Schindlbacher *et al.*, 2004)
	mixed	179.3	(Schindlbacher *et al.*, 2004)
	mixed	198.6	(Schindlbacher *et al.*, 2004)
	mixed	41.2	(Schindlbacher *et al.*, 2004)
	mixed	81.3	(Schindlbacher *et al.*, 2004)
	mixed	41.2	(Schindlbacher *et al.*, 2004)
	mixed	93.3	(Schindlbacher *et al.*, 2004)
	mixed	76.7	(Schindlbacher *et al.*, 2004)
	mixed	63.2	(Schindlbacher *et al.*, 2004)
	mixed	70	(McKenney *et al.*, 1984)
	mixed	79	(McKenney *et al.*, 1984)
	mixed	39.9	(McKenney *et al.*, 1984)
	mixed	42.8	(McKenney *et al.*, 1984)

Table A.1 continued.

Process	Mechanism	Activation energy (kJ mol^{-1})	Reference
NO production	abiotic	52.4	(McKenney et al., 1984)
	mixed	40.3	(Ormeci et al., 1999)
	mixed	42.6	(Ormeci et al., 1999)
	mixed	51.7	(Ormeci et al., 1999)
N$_2$O production	mixed	57.6	(Schindlbacher et al., 2004)
	mixed	133.2	(Schindlbacher et al., 2004)
	mixed	102.2	(Schindlbacher et al., 2004)
	abiotic	18.4	(Samarkin et al., 2010)
	mixed	84	(McKenney et al., 1984)
N$_2$O consumption	abiotic	250	(Tolman, 2010)
	mixed	28	(Holtan-Hartwig et al., 2002)
	mixed	49	(Holtan-Hartwig et al., 2002)
	mixed	57	(Holtan-Hartwig et al., 2002)
	mixed	59	(Holtan-Hartwig et al., 2002)
	mixed	60	(Holtan-Hartwig et al., 2002)
	biotic	54.4	(Serge I Gorelsky et al., 2005)
	biotic	10.46	(Tsai et al., 2014)
Nitrogen fixation	biotic	44.4	(Schwintzer, 1979)
	biotic	61.1	(R. C. Burns, 1969)
	biotic	59	(Kashyap et al., 1991)
	biotic	33	(Kashyap et al., 1991)
	abiotic	945.4	(National Institute of Standards and Technology, U.S. Department of Commerce, 1998)

APPENDIX B

SUPPLEMENTARY TABLES AND FIGURES FOR CHAPTER 2
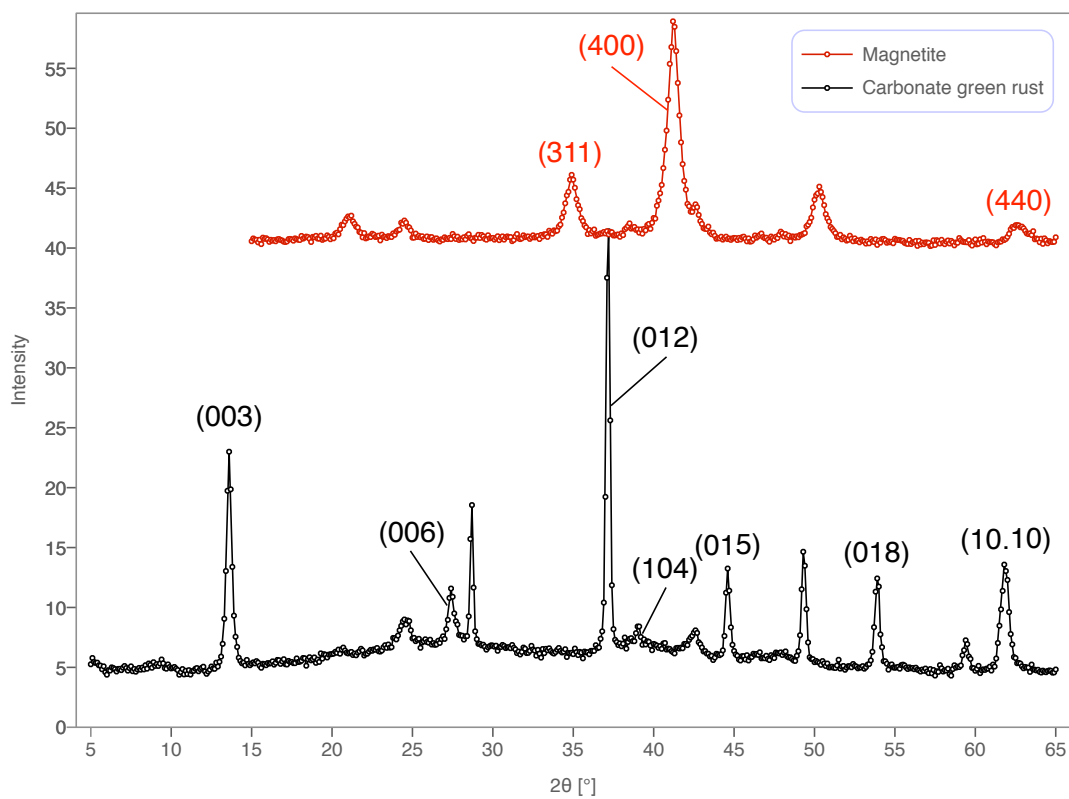
Fig. B.1. XRD patterns obtained for magnetite and green rust. Patterns resemble XRD data previously obtained for magnetite (Byrne *et al*., 2015) and GR (Bocher *et al*., 2004).
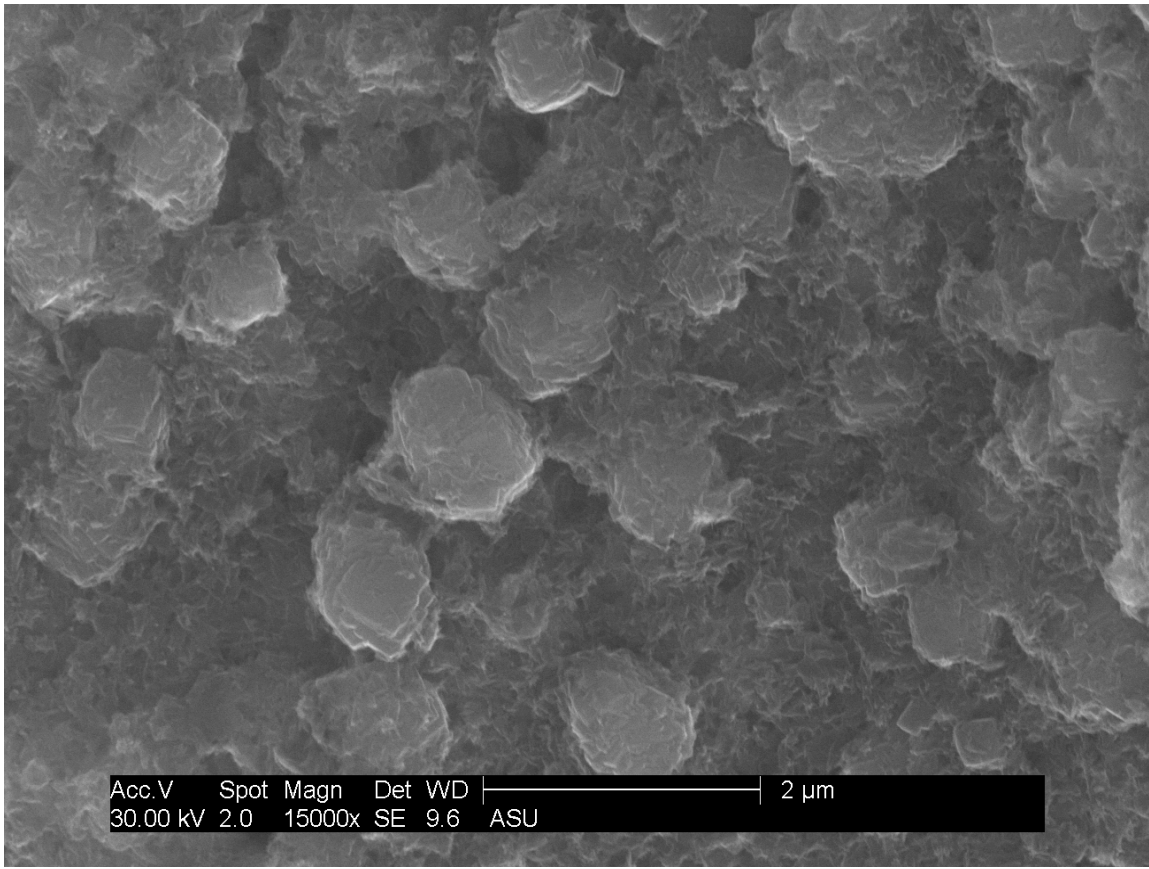
Fig. B.2. SEM image of a wet carbonate green rust sample. Precipitates are made of layered hexagonal sheets of approximately 1 μm in diameter.

Fig. B.3. Photograph of carbonate green rust prior to harvest of precipitates (see *Methods*).
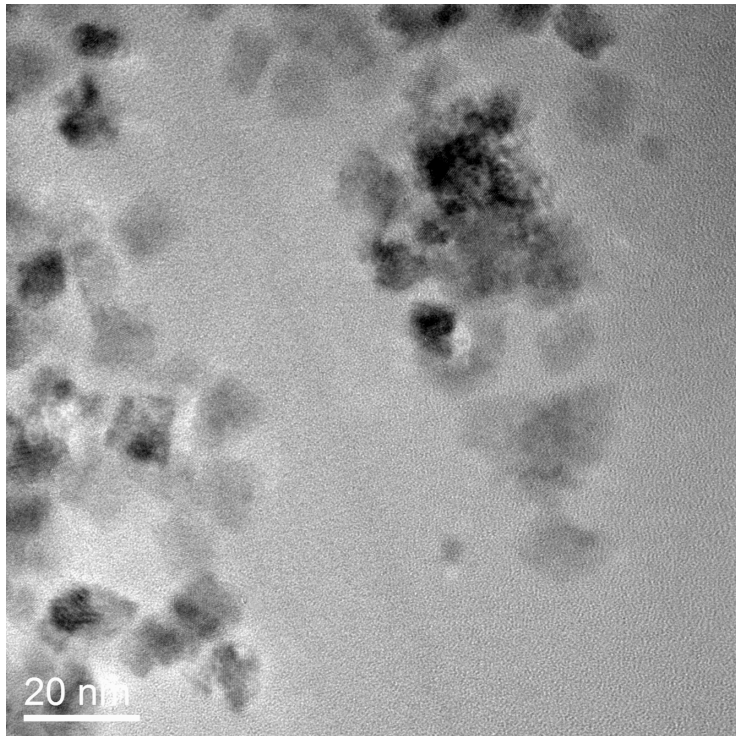
Fig. B.4. TEM image of magnetite. The particles are roughly spherical and approximately 15 μm in size.
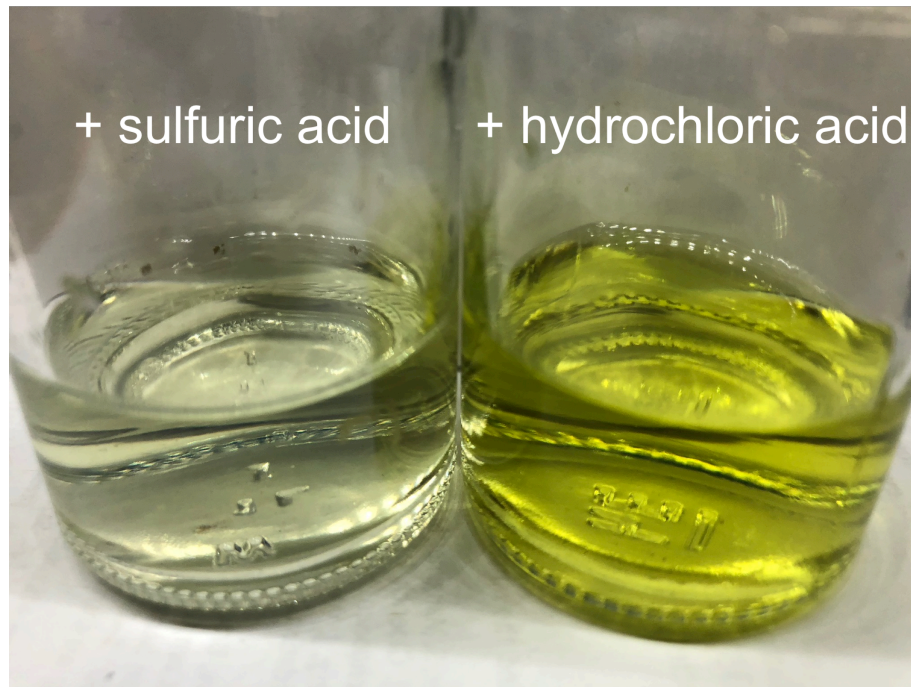
Fig. B.5. Photograph of acid-digested particle suspension 20 hours after acid addition. No particles were visible anymore, excluding any surface effects from our measurements (Table B.2).
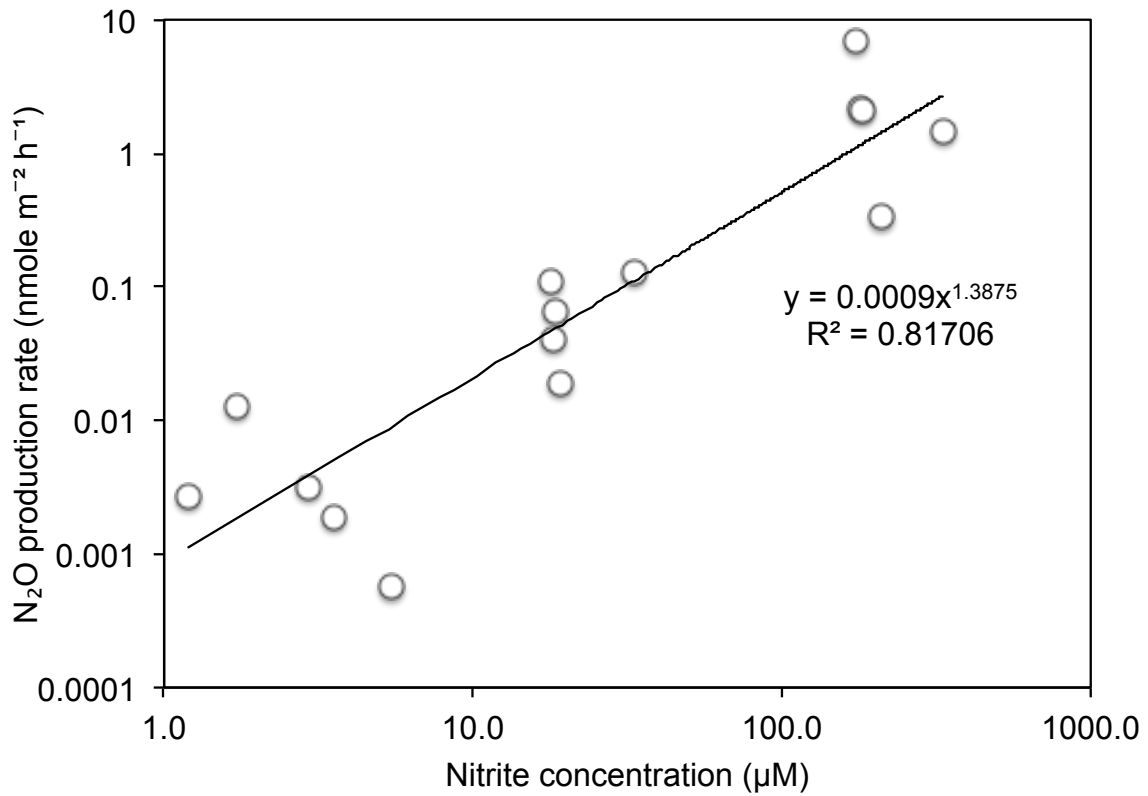
Fig. B.6. N$_2$O production rates (normalized to mineral surface area) as a function of nitrite concentration for 15 green rust incubation runs. The apparent reaction order of ~1.4 is consistent with previously reported values from soil (Venterea and Rolston, 2000).
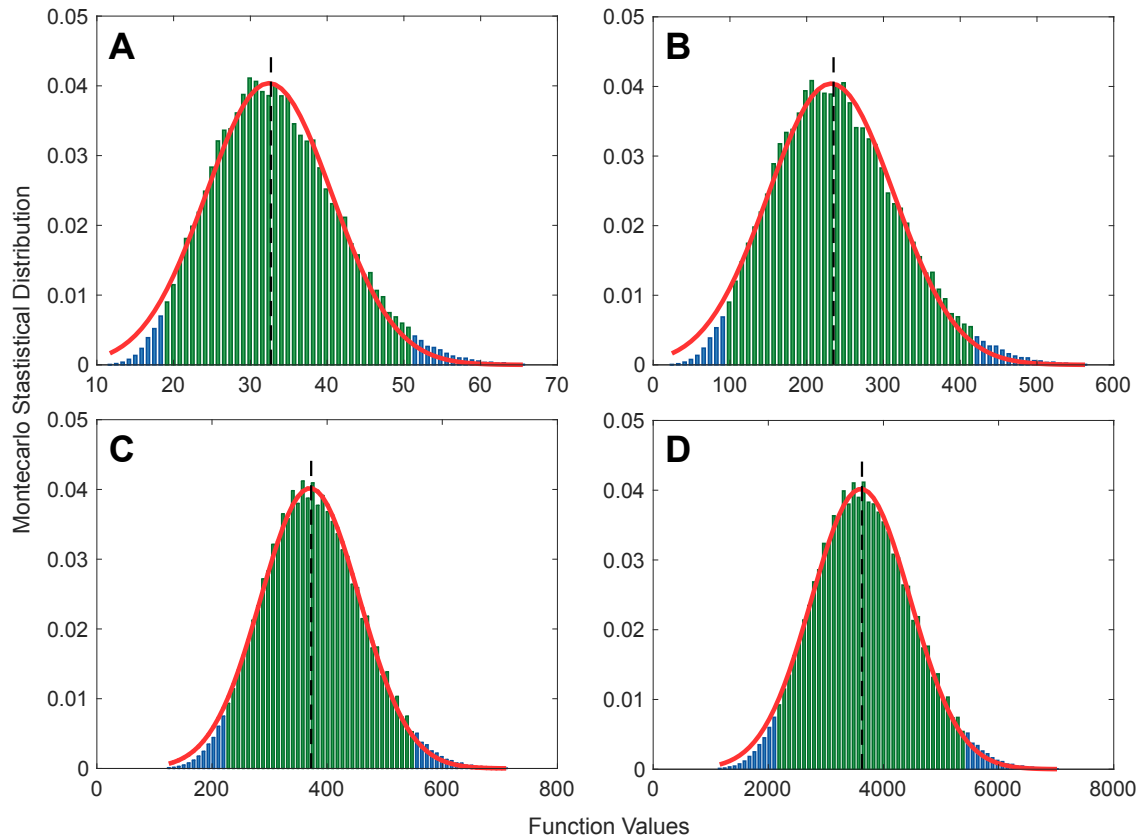
Fig. B.7. N_2O fluxes (center of distribution, dashed line) under variation of N_2O production rates from green rust r(GR). 95% confidence interval marked in green. (A) With [GR] half that found in Kabuno Bay at low NO_2^- levels. (B) With [GR] five times that found in Kabuno Bay at low NO_2^- levels. (C) With [GR] half that found in Kabuno Bay at moderate NO_2^- levels. (D) With [GR] five times that found in Kabuno Bay at moderate NO_2^- levels.
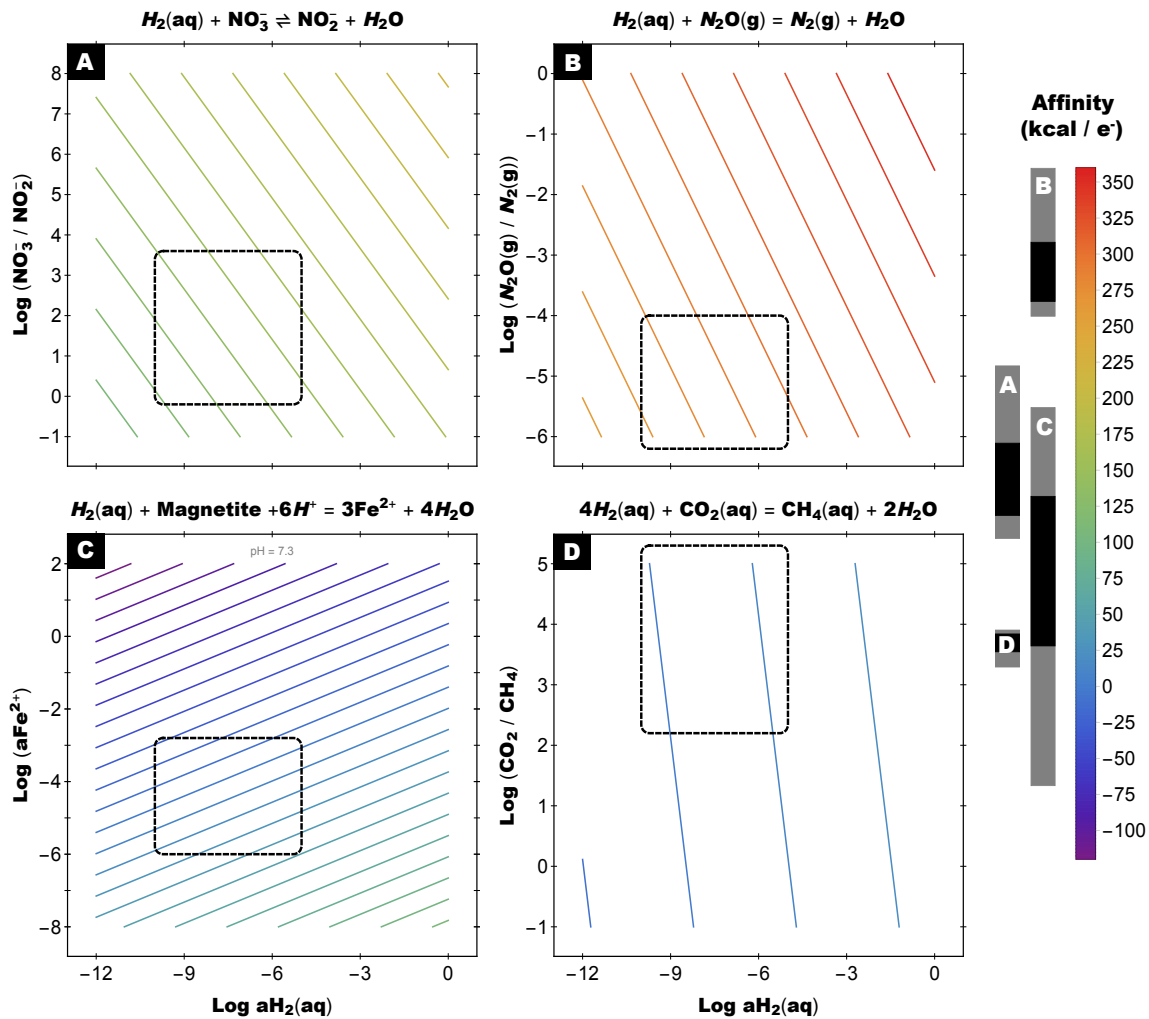
Fig. B.8. Affinity landscapes for (A) Reduction of nitrate by molecular hydrogen (H_2), (B) Reduction of N_2O gas by H_2, (C) Magnetite reduction by H_2 at pH 7.3, and (D) CO_2 reduction by H_2 (methanogenesis). The colored curves in each plot represent lines of constant affinity, set 10 kcal apart. Black boxes represent regions of likely species activities (see text); i.e., each of these regions is aligned on the scale bar to the right for easier comparison between reactions.

Table B.1. BET surface area of dried, anoxically prepared minerals.

Carbonate green rust	Surface area ($m^2\ g^{-1}$)	Mean	_SD_
Sample 1	60.2088	57.1107	5.6369
Sample 2	60.5191		
Sample 3	50.6042		

Magnetite	Surface area ($m^2\ g^{-1}$)	Mean	_SD_
Sample 1	56.9048	56.2855	0.8758
Sample 2	55.6662		

Table B.2. NO control incubations. Amount of NO produced in nmoles per reaction vial. Controls with acid treatment are marked as "(+) acid" and controls without acid treatment are marked with "(–) acid". Incubations without nitrite substrate addition are marked with "(–) NO_2^-". Initial amount of NO_2^- corresponds to moderate levels (Table B.3). Nitrite concentration was measured in particulate and particle-free (supernatant after centrifugation) sample liquid prior to acid addition and was < 2.5 μM throughout, except for magnetite incubations after 50 hrs. For magnetite incubations after 50 hrs, values in brackets are the measured NO quantity minus the residual NO_2^- quantity. Incubations without precipitates (artificial seawater only) are marked with "(–) mineral".

H_2SO_4 addition (hrs after NO_2^- injection)		after 50 hrs	after 220 hrs
Magnetite	(+) acid	286.6 (221)	195
	(–) NO_2^-	1.3	n.d.
Green rust	(+) acid	24	34.3
	(–) NO_2^-	1.5	n.d.
(–) mineral		28.8	n.d.

HCl addition (hrs after NO_2^- injection)		after 50 hrs	after 220 hrs
Magnetite	(+) acid	227 (164.4)	164
	(–) NO_2^-	n.d.	1.1
Green rust	(+) acid	24.5	34
	(–) NO_2^-	n.d.	0.9
(–) mineral		207.5	n.d.
Magnetite	(–) acid	4.5	11.9
Green rust	(–) acid	1	2.1

Table B.3. Experimental data collected from anoxic artificial seawater incubations and mineral suspensions. Area and concentration units per volume of artificial seawater (dissolved ions) or per volume of headspace gas (nitrogen gases). Product yield was determined by [N_2O-N or NO-N]/[NO_2^--N]. NO_2^--N was the mean of replicates measured right after injection of stock solution. N_2O-N was the mean of measured values, which plateaued on the N_2O production curve (constant [N_2O]). NO-N was the mean of replicate values at the last measurement (after outgassing, when solution was clear). Top: n=3; bottom: n=2.

Mineral		initial [NO_2^-] (μM)	Specific surface area (m² mL⁻¹)	N_2O production rate* (nM day⁻¹)	N_2O yield (% N)	NO yield (% N)	pH†	Fe²⁺(aq) in supernatant§ (μM)	NH_4^+ formation‡
Magnetite	*low*	1.6±0.3	1.86	72.7±30.8	11.4±1.7		7.01	< 0.5, 28.1±0.8	–
	moderate	32.0±0.4	1.86	482.1±6.6	7.8±0.2	87.2±8.3	6.97	0.7±0.5, 25.6±0.7	–
	high	314.6±2.8	1.86	7800.5±1070.9	12.1±2.2		7.00	4.1±1.6, 31.9±3.7	–
Green rust	*low*	0.9±0.1	1.89	121.1±10.3	80.9±17.9		7.75	21.5±8.1, 40.5±4.0	–
	moderate	34.4±0.1	1.89	5894.4±1647.2	62.8±2.7	7.1±0.4	8.07	23.0±1.6, 36.2±3.7	+
	high	271.2±5.3	1.89	65065.8±5144	35.2±11.3		7.96	46.8±15.9, 48.9±2.7	–
Fe(aq)	*high*	322.8±5.3	-	6.7±0.7	0.02±0.003		7.01	500.2±1.2	+
Green rust	*low*	5.5±0.5	0.366±0.003	17.9±5.6ᵃ	1.9±0.9		7.07	23.4±1.4	–
	low	2.9±0.6	0.082±0.0005	6.2±4.8ᵃ	2.8±0.6		6.92	57.6±0.6	–
	low	1.7±0.05	0.016±0.0003	4.7±0.9ᵃ	4.3±0.2		6.91	73.6±0.9	–
	low	3.5±0.2	0.005±0.0003	0.3±0.2ᵃ	0.7±0.2		6.99	31.1	–
	moderate	18.2±0.5	0.368±0.002	361.5±18.6ᵇ	29.2±4.4		7.14	23.4±0.1	+
	moderate	18.0±1.6	0.079±0.002	207.4±46.8ᵇ	46.4±14.2		6.93	42.7	–
	moderate	18.7±0.6	0.016±0.0003	24.9±10.2ᵇ	5.3±0.2		6.94	66.7±1.9	+
	moderate	19.2±0.1	0.005±0.0005	2.6±1.6ᵇ	3.4±0.3		6.95	33.1±1.5	+
	high	180.0±12.1	0.367±0.0008	19553.5±6955.2ᶜ	39.2±0.3		7.03	3.1	–
	high	172.5±6.3	0.081±0.0003	13631.4±2298.7ᶜ	101.2±2.2		6.94	< 0.5	+
	high	183.8±5.4	0.017±0.0003	865.6±66.6ᶜ	66.7±8.1		6.98	< 0.5	+
	high	208.4±2.1	0.006±0.0003	49.2±8.7ᶜ	1.2±0.2		7.06	< 0.5	+

Surface area-rate linear correlation (r^2) is ᵃ0.95, ᵇ0.86, ᶜ0.76.

* Rate values determined by slope of the linear part on the N_2O production curves.

† Replicates were mixed equally for pH measurements conducted at the end of incubations.

§ Top: first value measured immediately after suspending Fe minerals, second value measured 73 hours after NO_2^- injection; Bottom: value measured 199 hours after NO_2^- injection.

‡ NH_4^+ was measured when all NO_2^- was consumed. Concentrations were negligible throughout and too low for accurate quantification. We therefore only assessed qualitatively if NH_4^+ formation was observed (+) or not (–). A (+) sign was assigned when raw reads of light absorption were above those for the lowest standard (3 μM).

Table B.4. N_2O fluxes with uncertainties and seawater N_2O steady-state concentrations. We used Monte Carlo simulations to estimate uncertainties in the final flux values caused by variation in abiotic N_2O production rates from GR (Fig. A.7). The error propagated for 95% CI always fell within one order of magnitude of the mean. For comparison, the modern marine average N_2O flux is 56.6 nmol m^{-2} h^{-1} (Battaglia and Joos, 2018) and steady-state N_2O levels in modern oxygen minimum zones mostly reside between 10-50 nM throughout water depth profiles (Babbin *et al*., 2015). The Fe mineral particle density observed in Kabuno Bay (KB) served as reference (see text).

initial $[NO_2^-]$ (μM)	$[GR]$ (μM Fe^{2+})	particulate GR surface area (m^2 L^{-1})	Reference ocean depth (m)	$\Phi_{sed} + \Phi_{par}$ (nmol m^{-2} h^{-1})[*]	Steady-state $[N_2O]$[†] (nM)
1-5 μM (low)	50% KB	0.0499	40-140	32.68 [19.07 - 50.63]	0.04
1-5 μM (low)	500% KB	0.499	40-140	234.99 [98.09 - 413.92]	0.3
20-35 μM (moderate)	50% KB	0.0499	40-140	372.3 [219.8 - 550.6]	0.5
20-35 μM (moderate)	500% KB	0.499	40-140	3627.0 [2103.7 - 5411.5]	4.7

[*] 95% confidence interval (CI) given in brackets.

[†] at shallow water depth affected by wind turbulent mixing.

APPENDIX C

SUPPLEMENTARY TABLES AND FIGURES FOR CHAPTER 4
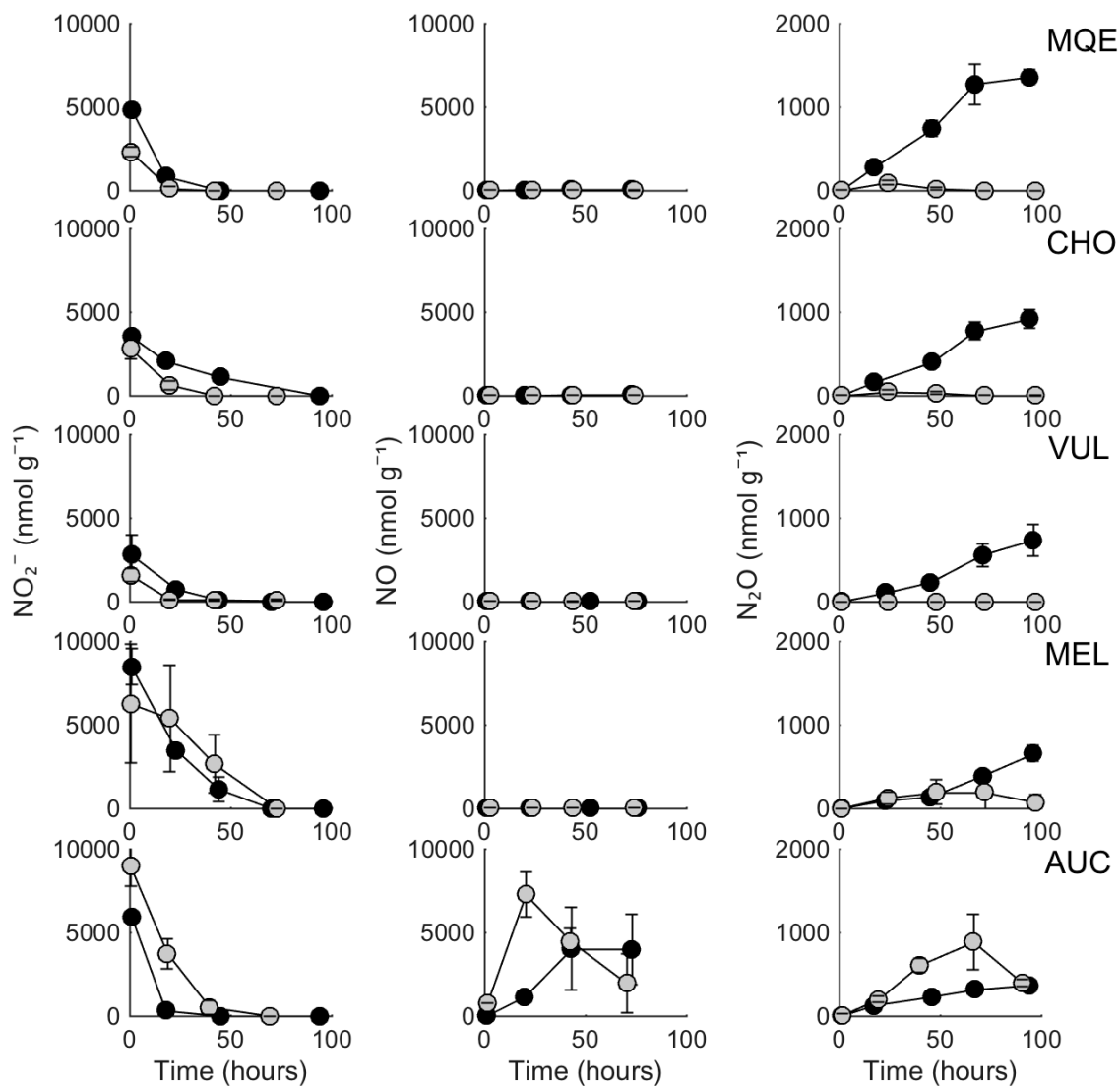
Fig. C.1. Nitrite, NO and N_2O concentrations as a function of time in chemodenitrification assays. Gamma-irradiated and untreated batch incubations are marked in black and gray, resepectively. Sites (rows) are ordered after their characterization as high-N_2O (MQE, CHO, VUL, MEL) or high-NO (AUC, FCA, QUI, SRQ, SJO, SCB) site. See Table 4.1 for three-letter code of the peatlands. Samples were collected from liquid and headspace after initial amendment with 100 μM NO_2^-. Units were normalized to soil dry weight. Error bars denote *SD*.
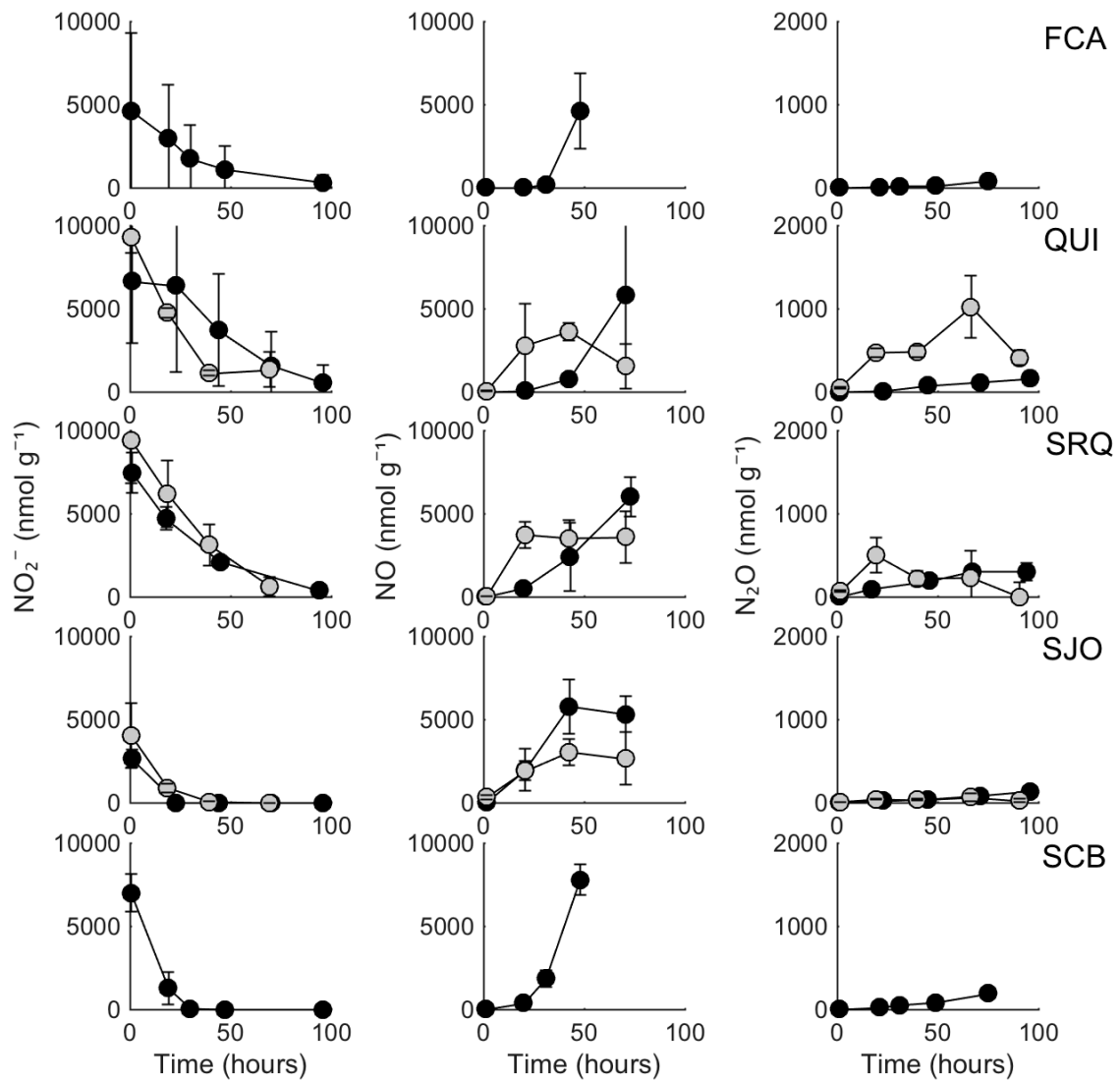
Fig. C.1 continued.
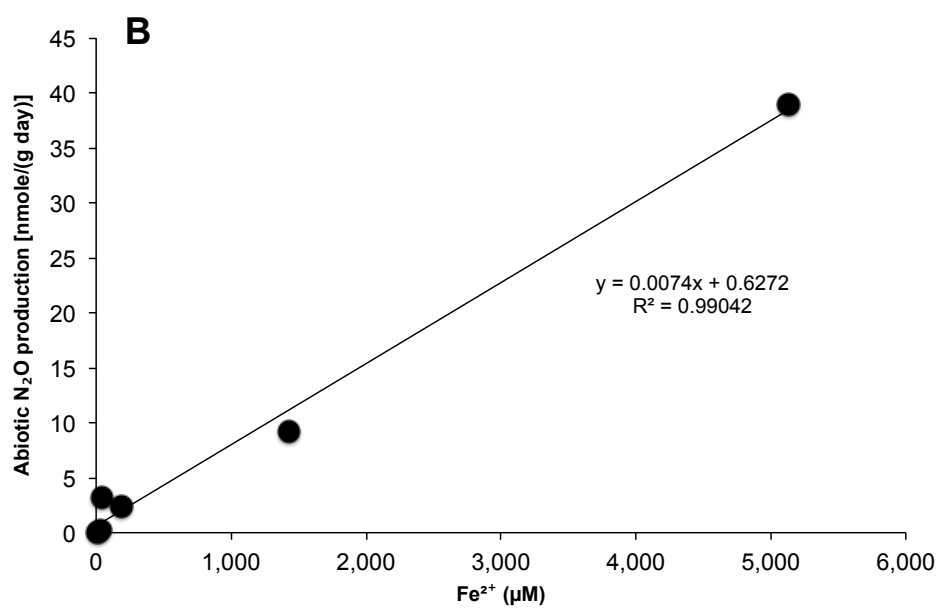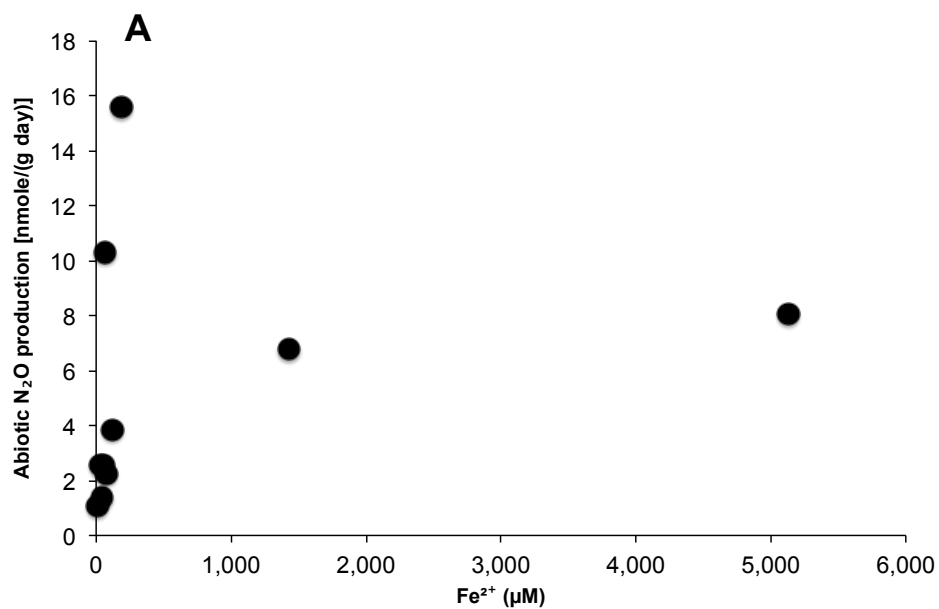
Fig. C.2. N₂O production as a function of Fe^{2+} concentration in laboratory incubations (A) and *in-situ* incubations (B). Regression line formula and R^2 are given in (B).
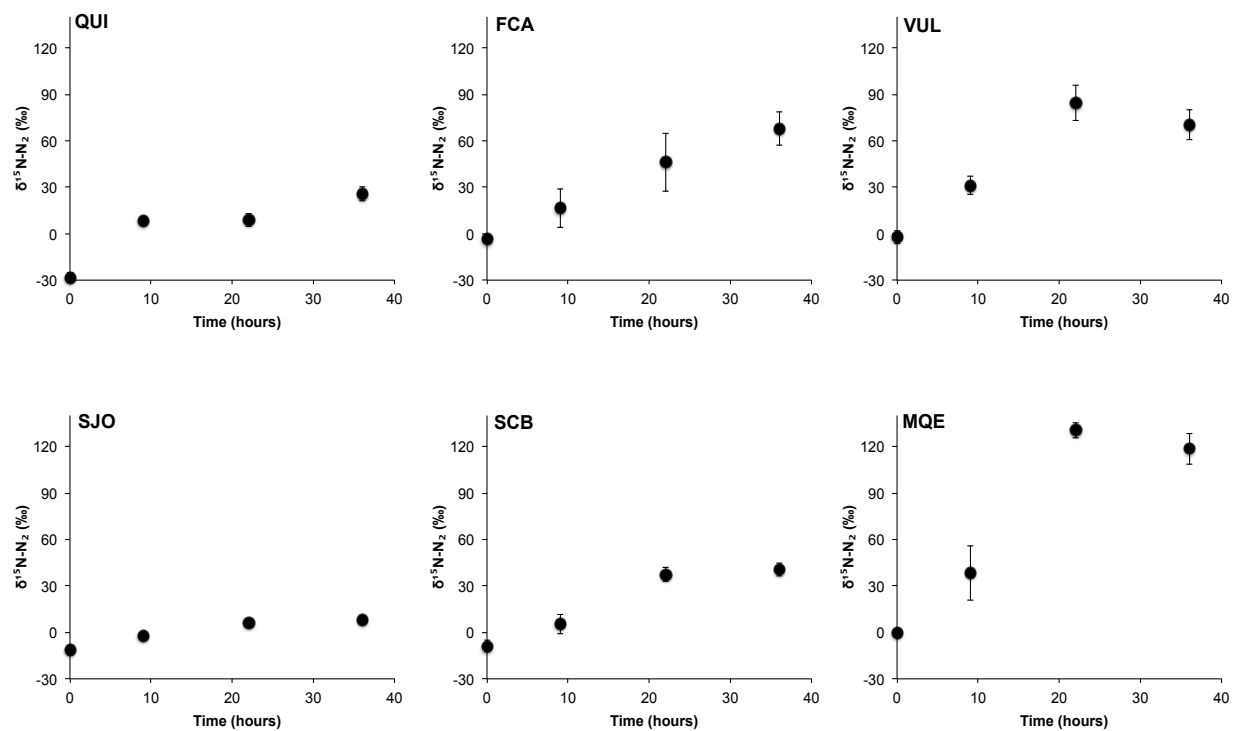
Fig. C.3. Isotopic composition of N_2 as a function of time in incubations enriched with $(^{15}N)_2O$ at t = 0 hours. Air-N_2 was used as standard for isotope composition. See Table 4.1 for three-letter code of the peatlands. Error bars denote *SD*.
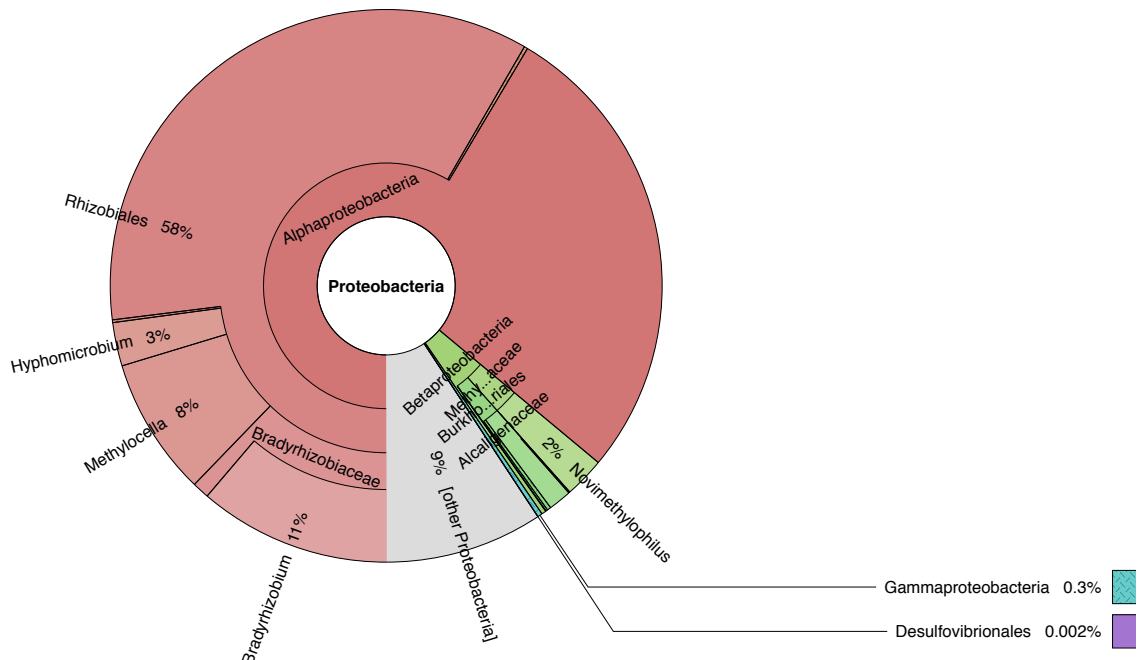
MQE
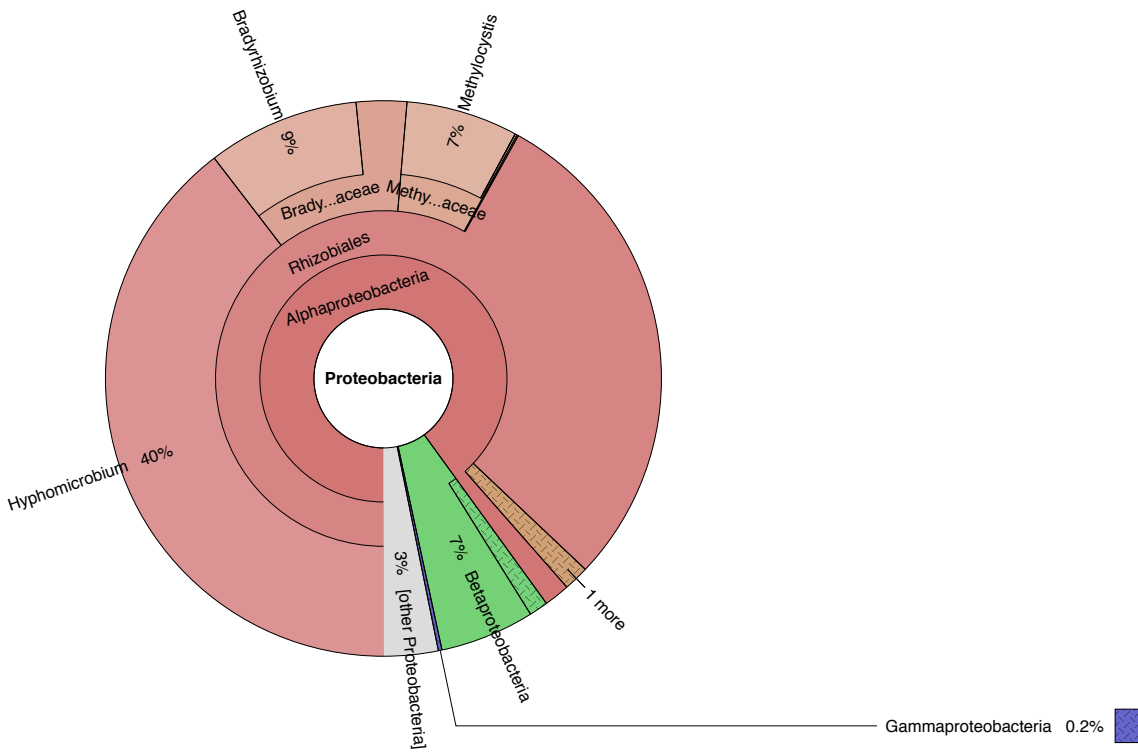
CHO

Fig. C.4. Krona plots of *nosZ* I phylogeny based on amplicon sequencing.
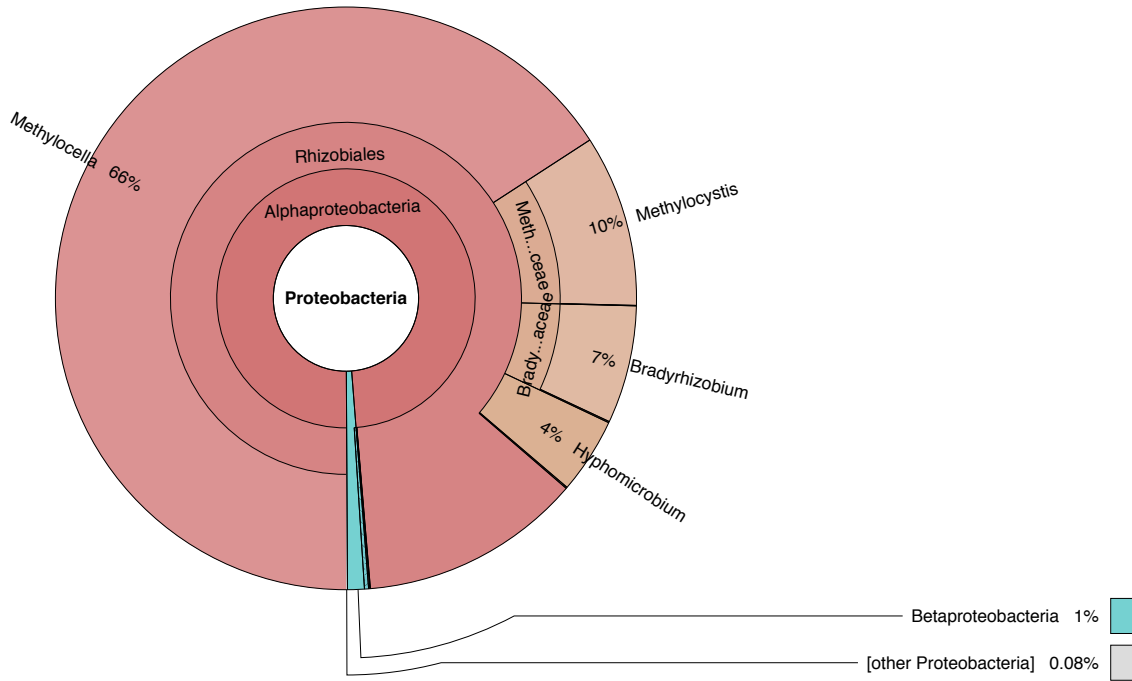
VUL
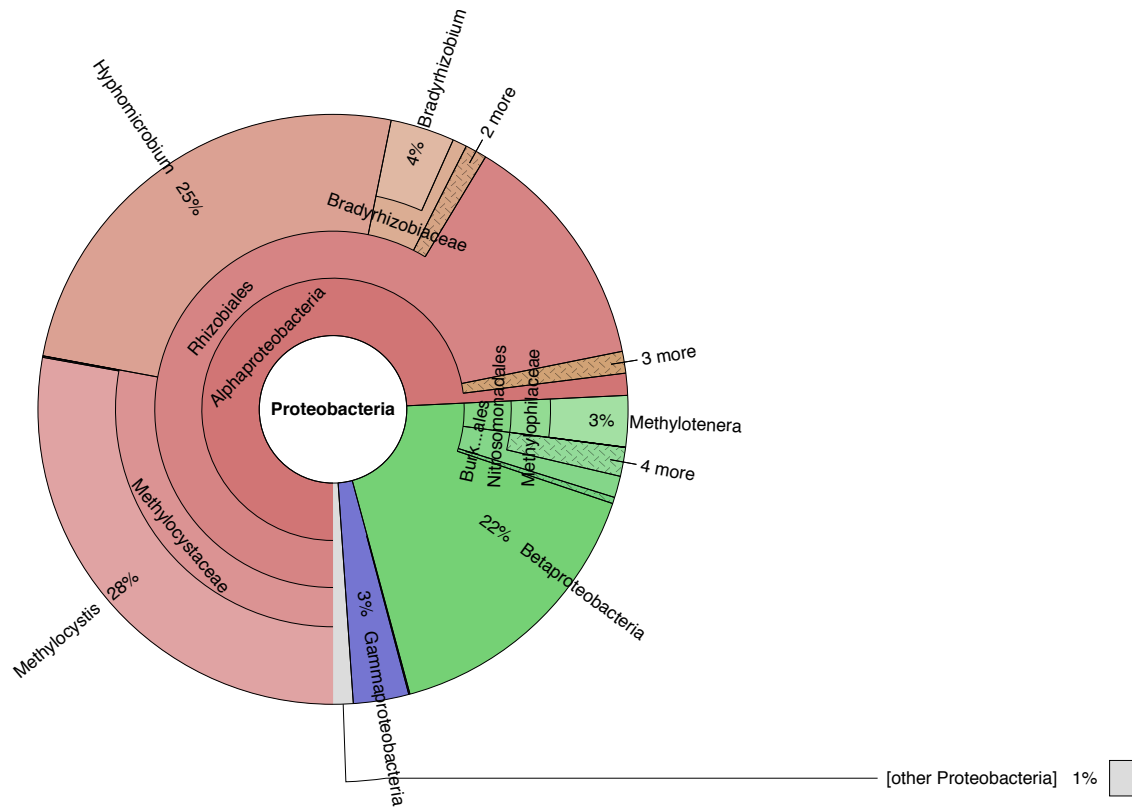
MEL

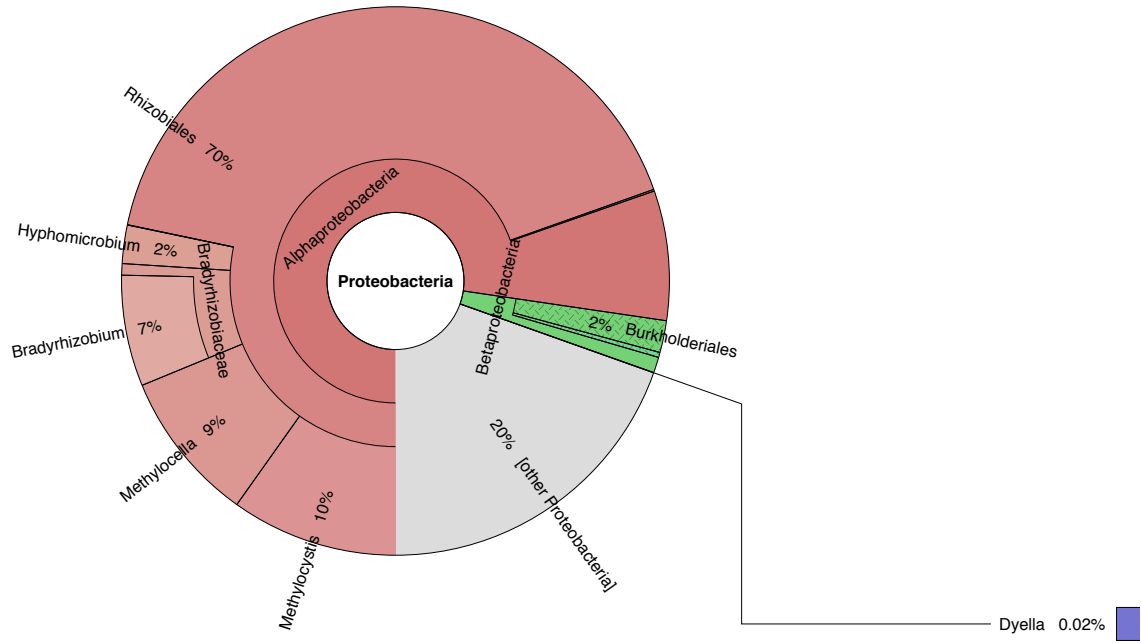Fig. C.4 continued. Krona plots of *nosZ* I phylogeny based on amplicon sequencing.
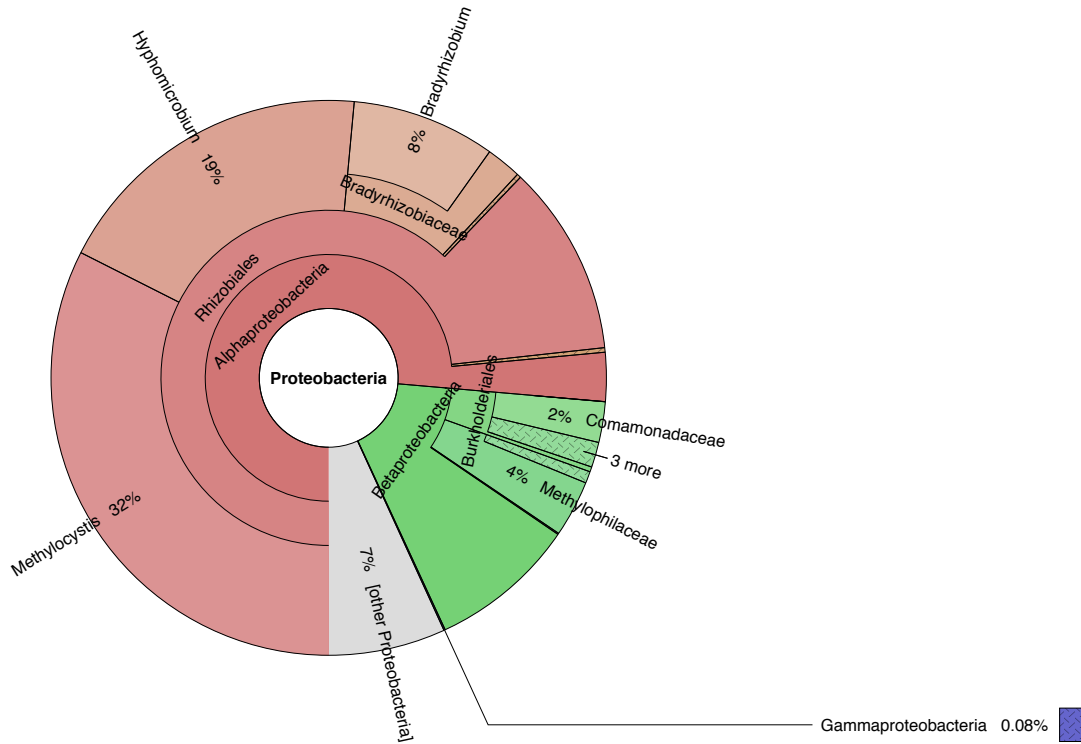
186

AUC

FCA

Fig. C.4 continued. Krona plots of *nosZ* I phylogeny based on amplicon sequencing.
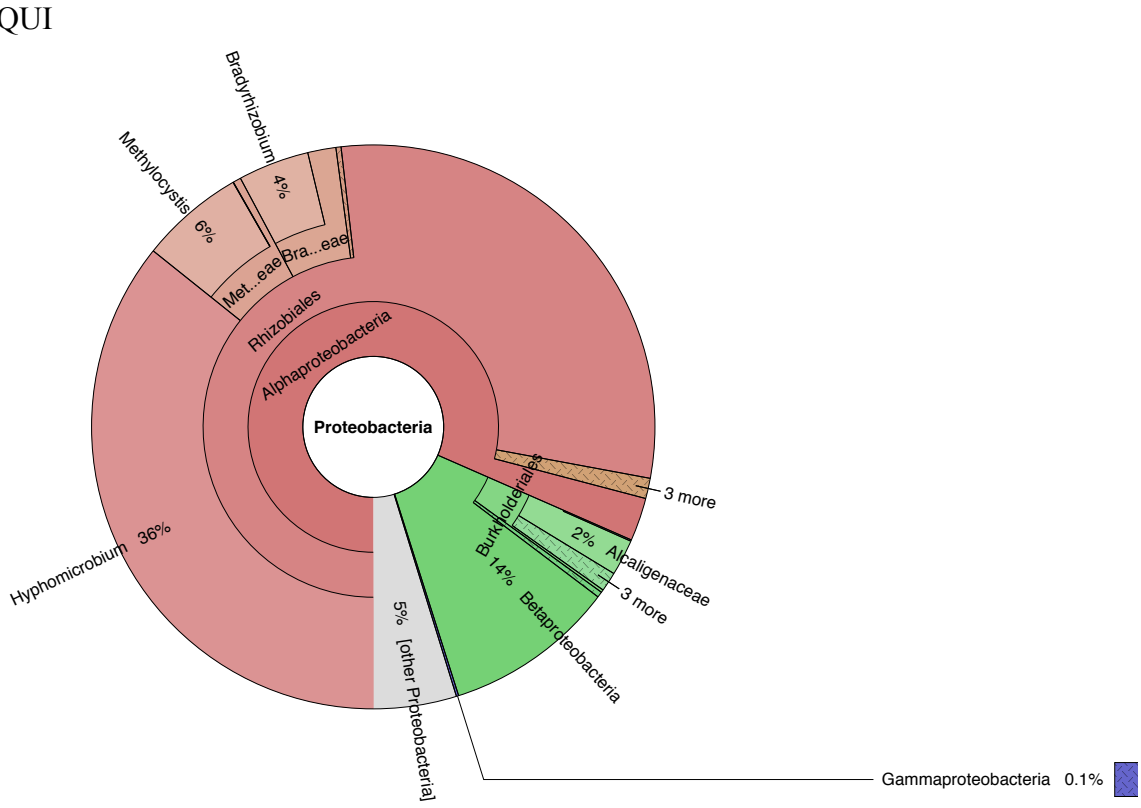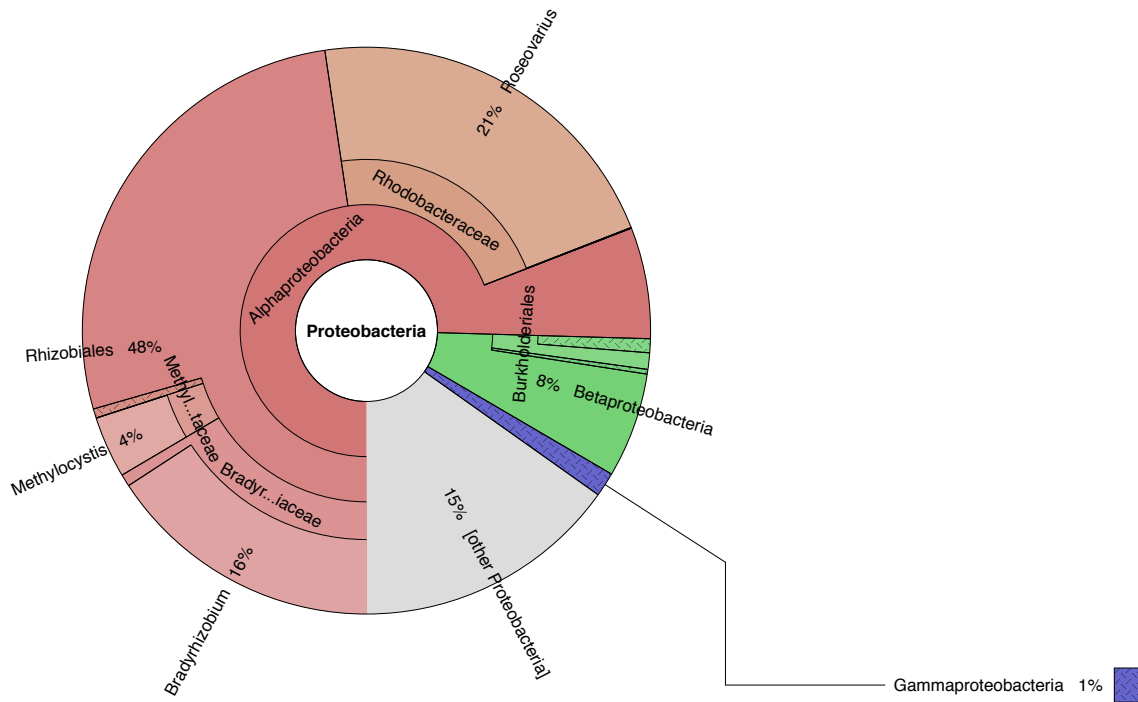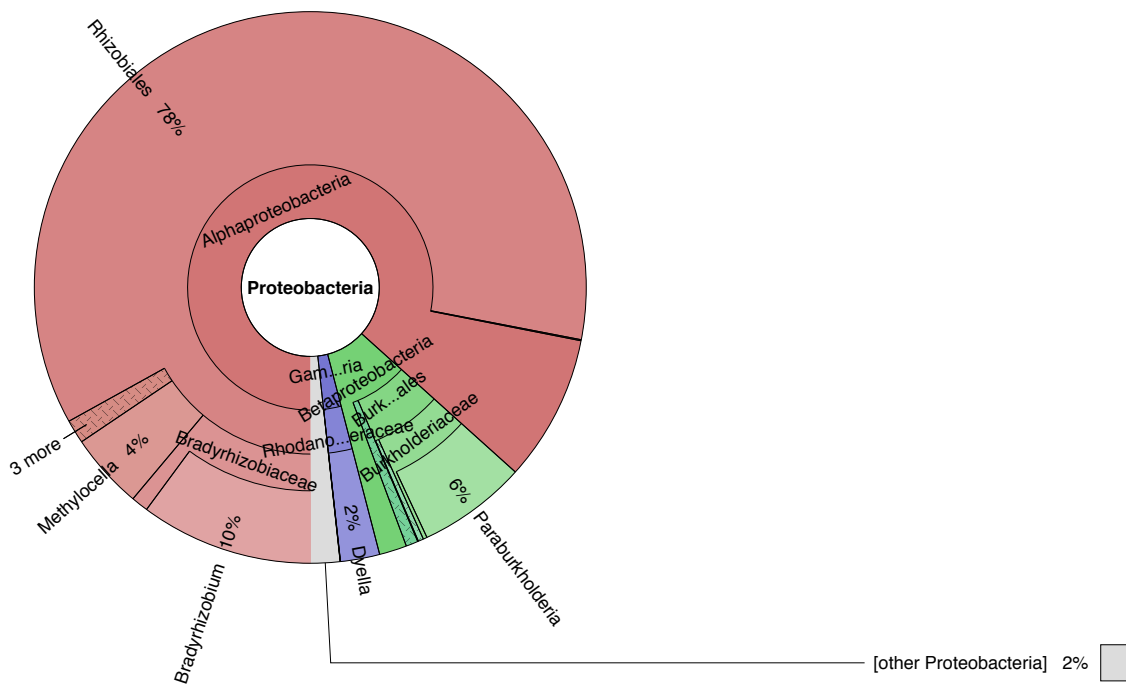
187

QUI

SRQ

Fig. C.4 continued. Krona plots of *nosZ* I phylogeny based on amplicon sequencing.

SJO

Gammaproteobacteria 1%

[other Proteobacteria] 2%

SCB

Fig. C.4 continued. Krona plots of *nosZ* I phylogeny based on amplicon sequencing.

189

APPENDIX D

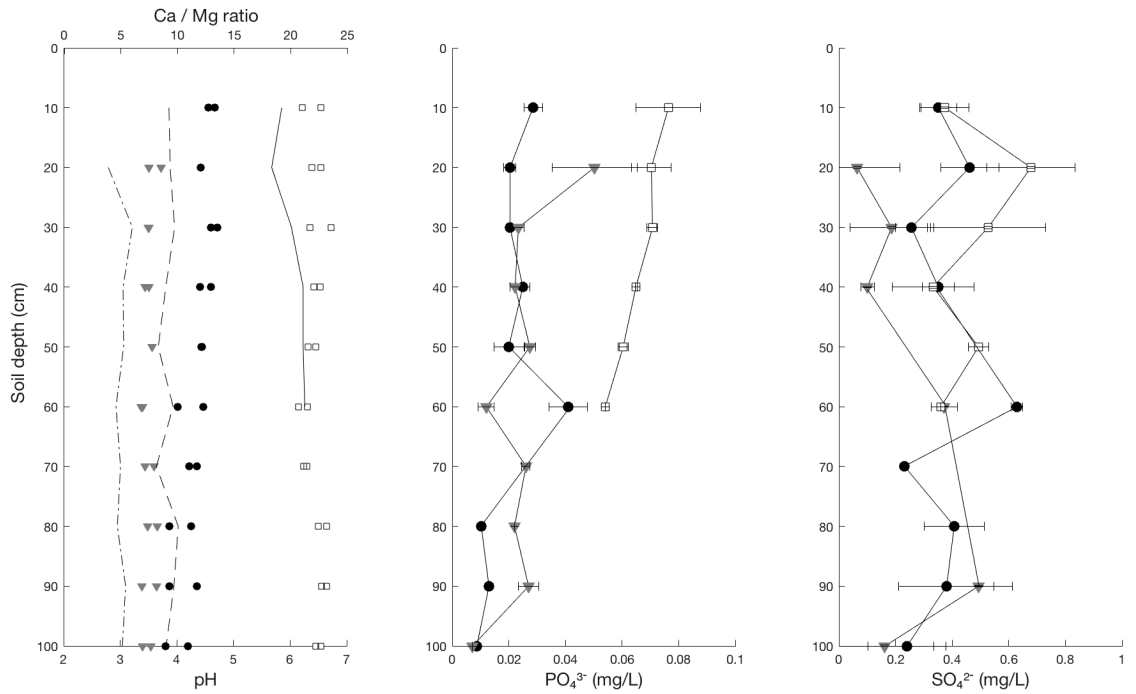SUPPLEMENTARY TABLES AND FIGURES FOR CHAPTER 5

Figure D.1. Left panel: Ca/Mg ratio in lines for QUI (dashed), BVA (solid), and SJO (point-dashed). pH in symbols for QUI (circles), SJO (triangles), and BVA (squares). Each point is derived from one replicate soil core. Middle panel: PO_4^{3-} concentration with data points representing the mean of values from replicate soil cores. Right panel: SO_4^{2-} concentration with data points representing the mean of values from replicate soil cores. Error bars denote one *SD* and symbols are consistent with left panel.
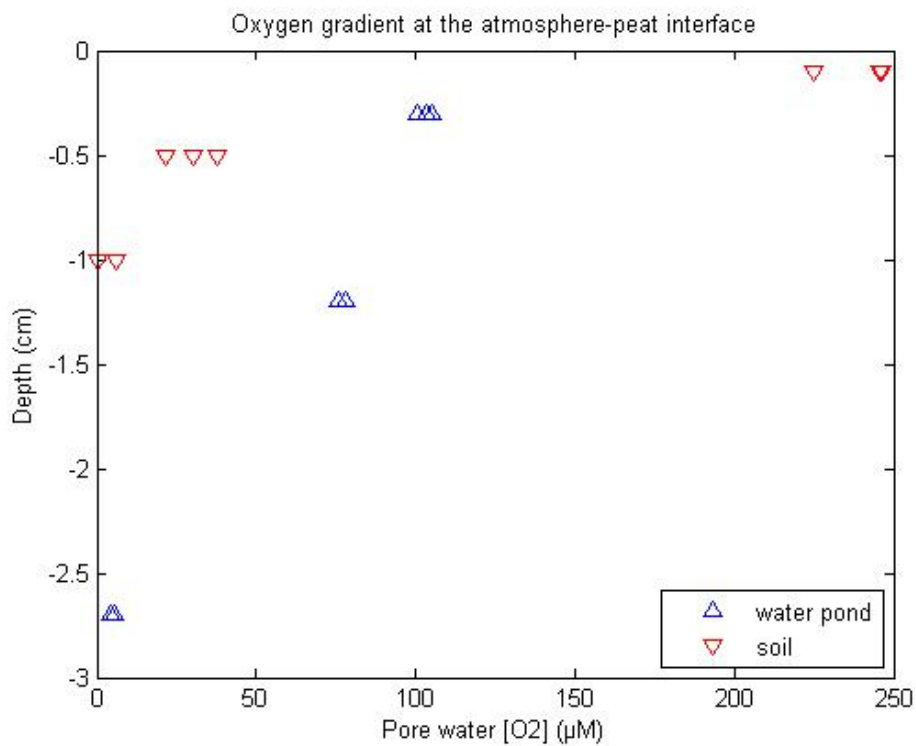
Figure D.2. Dissolved oxygen concentration in water of saturated soil. Measurements were done using a microelectrode, which was either inserted directly into soft peat (red symbols) or into a shallow (~3 cm) water pond (blue symbols). Measurements were conducted in QUI peatland.
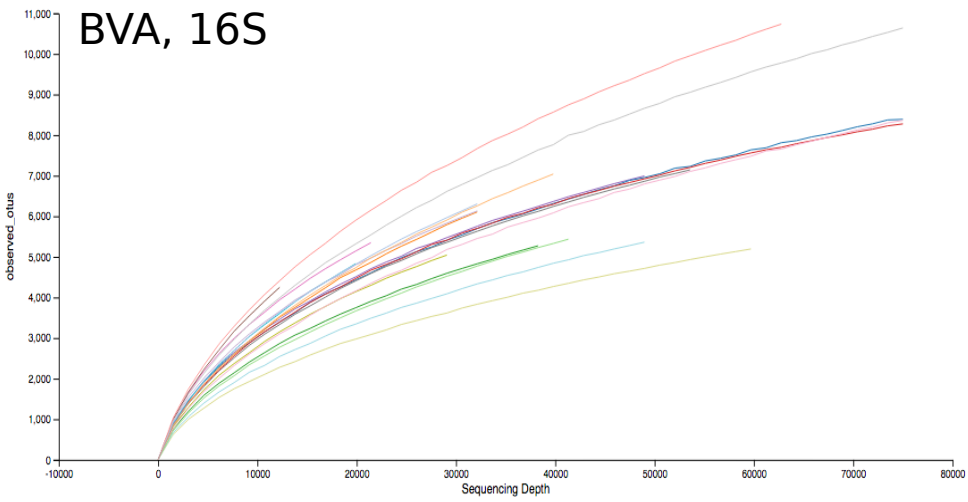
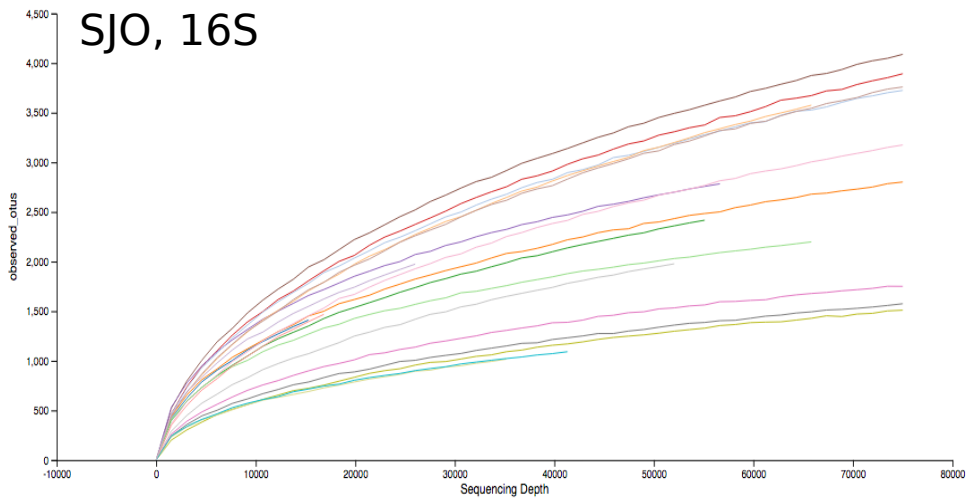Figure D.3. Alpha-rarefaction curves for 16S rRNA sequences.

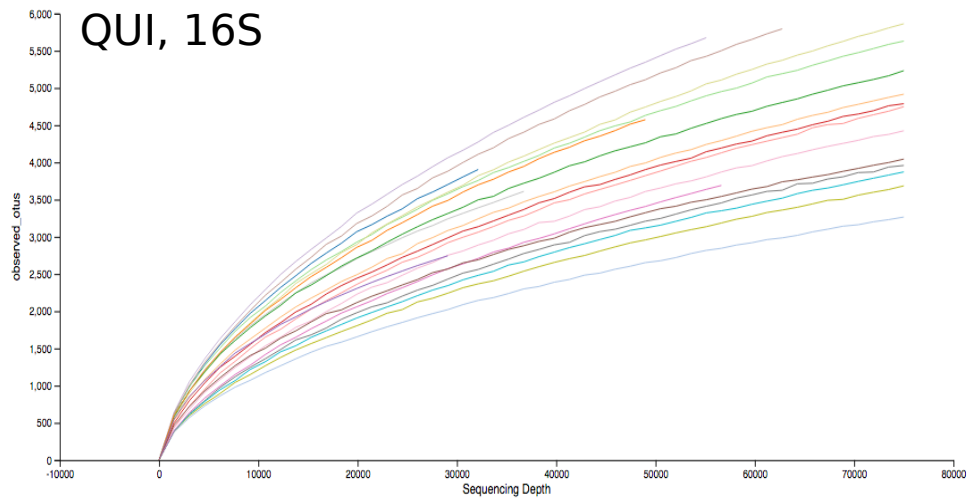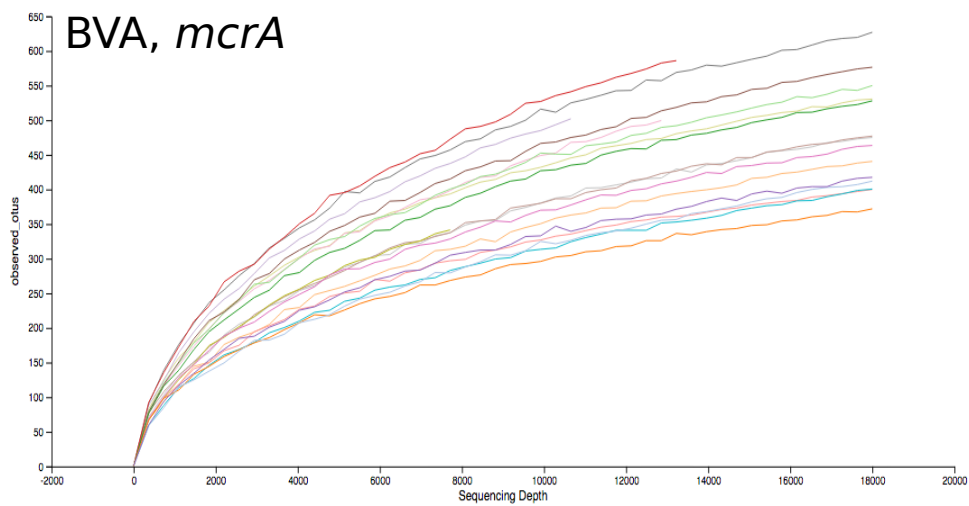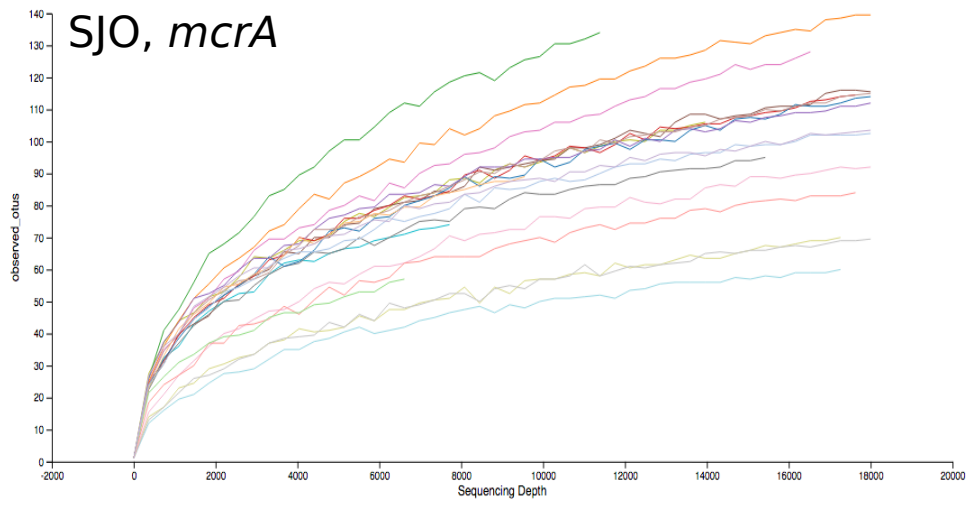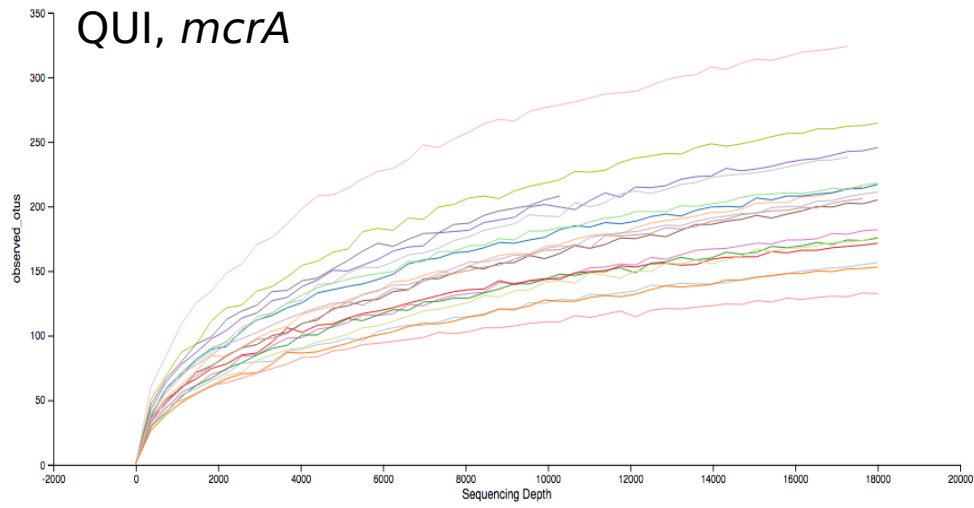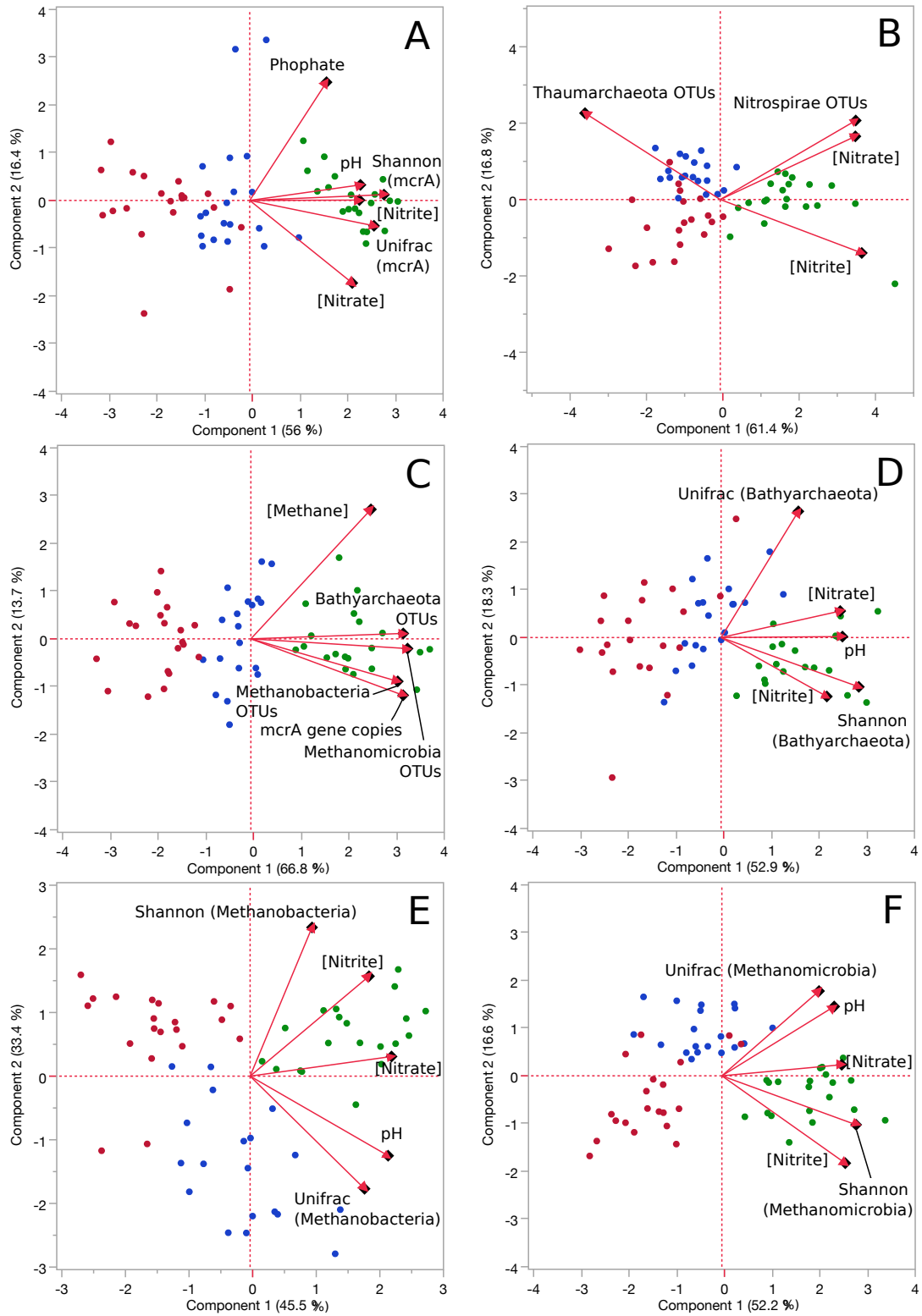Figure D.3 continued. Alpha-rarefaction curves for *mcrA* sequences.

Figure D.4. Principal component (PC) plots. QUI (blue), SJO (red) and BVA (green). Figure 5.3 is identical to panels C and D.
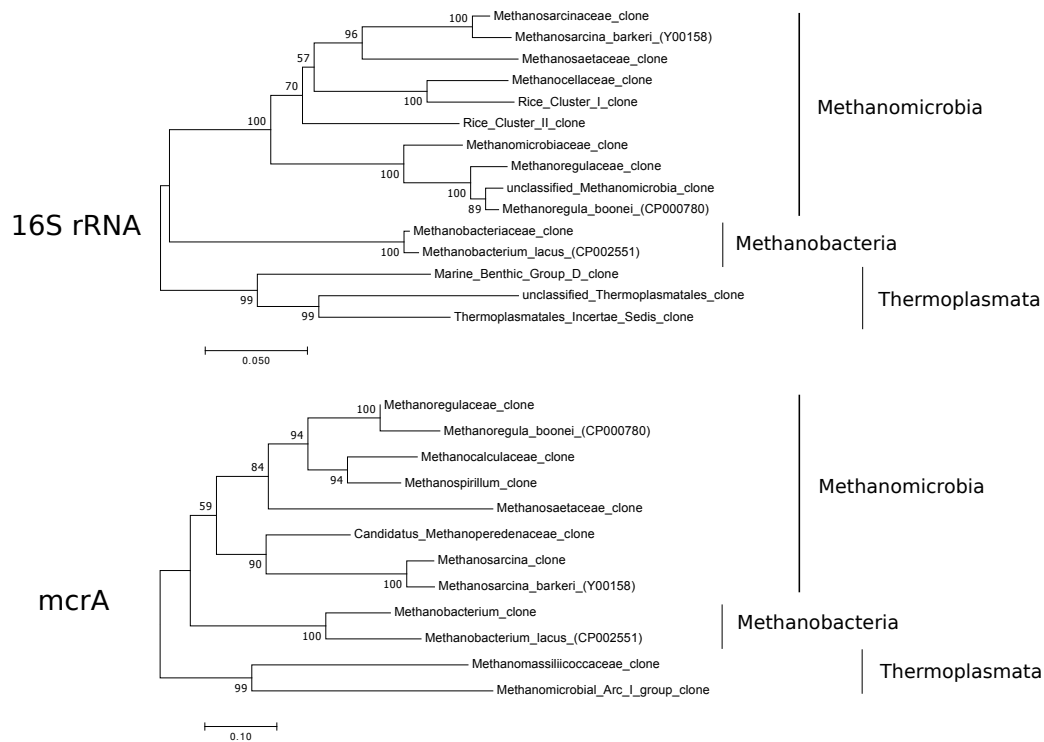
Figure D.5. 16S rRNA and *mcrA* phylogenetic trees based on the neighbor-joining method and 100 iterations. The trees reflect congruency of classified sequences from 16S and *mcrA* amplicon sequencing.

Table D.1. OTU abundances and microbial family traits.

Taxon	Core	Mean relative abundance along depth (%)	N metabolic reaction	Potential syntrophy with methanogen	Reference
Acido-bacteriaceae	QUI-1	5.0	N respiration not a dominant feature of this family.		(Rosenberg *et al.*, 2014)
	QUI-2	3.5			
	SJO-1	8.3			
	SJO-2	6.0			
	BVA-1	0.7			
	BVA-2	0.7			
Solibacteraceae	QUI-1	1.3	N respiration not a dominant feature of this family.		(Eichorst *et al.*, 2011)
	QUI-2	0.8			
	SJO-1	2.3			
	SJO-2	1.3			
	BVA-1	0.3			
	BVA-2	0.2			
Acido-thermaceae	QUI-1	1.3	Denitrification (*Acidothermus*) not verified in culture.		(Barta *et al.*, 2017) (Mohagheghi *et al.*, 1986)
	QUI-2	0.5			
	SJO-1	1.6			
	SJO-2	1.4			
	BVA-1	0.1			
	BVA-2	0.1			
Bacillaceae	QUI-1	8.4	Denitrification, DNRA and sole N₂O reduction (*Bacillus* and *Geobacillus*). Nitrate reduction verified in culture.		(Mandić-Mulec *et al.*, 2015)
	QUI-2	2.1			
	SJO-1	0.0			
	SJO-2	0.0			
	BVA-1	0.2			
	BVA-2	0.2			
Paeni-bacillaceae	QUI-1	2.7	Nitrate reduction and N fixation (*Paenibacillus*). Nitrate reduction verified in culture.		(J. H. Yoon, 2003) (Beneduzi *et al.*, 2010)
	QUI-2	0.1			
	SJO-1	0.0			
	SJO-2	0.0			
	BVA-1	0.9			
	BVA-2	0.6			

Table D.1 continued

Taxon	Core	Mean relative abundance along depth (%)	N metabolic reaction	Potential syntrophy with methanogen	Reference
Nitrospiraceae	QUI-1	0.5	Nitrite oxidation (*Nitrospira*), Fe^{2+} oxidation (*Lepto-spririllum*). Nitrite oxidation verified in culture.		(Rosenberg *et al*., 2014)
	QUI-2	0.5			
	SJO-1	0.7			
	SJO-2	0.9			
	BVA-1	3.7			
	BVA-2	3.3			
Plancto-mycetaceae			Anammox (Cand. Anammoxi-microbium), Nitrate reduction (*Planctomyces, Rhodopirellula*). Nitrate reduction verified in culture.		(Khramenkov *et al*., 2013)
	QUI-1	3.0			
	QUI-2	1.6			(Bondoso *et al*., 2014)
	SJO-1	1.9			
	SJO-2	1.9			
	BVA-1	2.2			
	BVA-2	2.1			
Bradyrhi-zobiaceae			Nitrite oxidation (*Nitrobacter*), N fixation (*Brady-rhizobium*). N mineralization and nitrate production activity verified in culture.		(Zahran, 1999) (Rosenberg *et al*., 2014)
	QUI-1	0.1			
	QUI-2	0.1			
	SJO-1	0.2			
	SJO-2	0.1			
	BVA-1	0.2			
	BVA-2	0.1			
Hypho-microbiaceae			Denitrification (*Hypho-microbium*). Nitrate reduction verified in culture.		(Martineau *et al*., 2015)
	QUI-1	0.5			
	QUI-2	0.3			
	SJO-1	0.1			
	SJO-2	0.6			
	BVA-1	0.9			
	BVA-2	0.7			
Xantho-bacteraceae			N fixation.		(Rosenberg *et al*., 2014)
	QUI-1	2.3			
	QUI-2	1.7			
	SJO-1	4.1			
	SJO-2	5.4			
	BVA-1	2.0			
	BVA-2	1.9			

Table D.1 continued

Taxon	Core	Mean relative abundance along depth (%)	N metabolic reaction	Potential syntrophy with methanogen	Reference
Rhodo-spirillaceae	QUI-1	0.5	N fixation (*Azospirillum*), Nitrate reduction (*Azospirillum, Magneto-spirillum*), N$_2$O reduction (*Azospririllum*). Nitrate reduction verified in culture.		(Rosenberg *et al.*, 2014)
	QUI-2	0.4			
	SJO-1	0.6			
	SJO-2	0.5			
	BVA-1	0.2			
	BVA-2	0.2			
Alcaligenaceae	QUI-1	0.2	Nitrate reduction (*Candidimonas*), Nitrite reduction (*Alcaligenes*). Nitrate reduction verified in culture.		(Rosenberg *et al.*, 2014) (Vaz-Moreira *et al.*, 2011)
	QUI-2	0.2			
	SJO-1	0.5			
	SJO-2	0.4			
	BVA-1	0.0			
	BVA-2	0.0			
Burk-holderiaceae	QUI-1	0.3	Denitrification. Nitrate reduction verified in culture.		(Rosenberg *et al.*, 2014)
	QUI-2	1.6			
	SJO-1	18.6			
	SJO-2	11.1			
	BVA-1	0.2			
	BVA-2	0.2			
Coma-monadaceae	QUI-1	0.0	Nitrate reduction (*Comamonas, Brachymonas, Diaphorobacter*). Nitrate reduction verified in culture.		(Rosenberg *et al.*, 2014)
	QUI-2	0.0			
	SJO-1	0.4			
	SJO-2	0.0			
	BVA-1	1.1			
	BVA-2	1.2			
Neisseriaceae	QUI-1	0.0	Nitrite and NO reduction (*Neisseria*). Nitrite reduction verified in culture.		(Rock *et al.*, 2005)
	QUI-2	0.0			
	SJO-1	1.9			
	SJO-2	0.0			
	BVA-1	0.2			
	BVA-2	0.3			

Taxon	Core	Mean relative abundance along depth (%)	N metabolic reaction	Potential syntrophy with methanogen	Reference
Nitroso-monadaceae			Ammonia oxidation. Verified in culture.		(Rosenberg *et al.*, 2014)
	QUI-1	0.1			
	QUI-2	0.0			
	SJO-1	0.0			
	SJO-2	0.0			
	BVA-1	0.8			
	BVA-2	0.7			
Desulfu-rellaceae				H_2 con-sumption and syntrophic association with methanogen? Competition possible.	(Miroshnichenko *et al.*, 1998)
	QUI-1	0.5			
	QUI-2	0.4			
	SJO-1	0.9			
	SJO-2	0.5			
	BVA-1	0.8			
	BVA-2	0.7			
Syntrophaceae	QUI-1	1.0		Propionate oxidation and syntrophy with methano-gens. Syntrophy studied in cultures.	(Lueders *et al.*, 2003)
	QUI-2	1.2			
	SJO-1	0.6			
	SJO-2	0.8			
	BVA-1	2.1			
	BVA-2	1.7			
Syntropho-bacteraceae				Fermenter or syntrophic association with H_2/formate-utilizing partners. Syntrophy studied in cultures.	(Rosenberg *et al.*, 2014)
	QUI-1	0.8			
	QUI-2	0.6			
	SJO-1	1.1			
	SJO-2	0.8			
	BVA-1	0.4			
	BVA-2	0.3			
Pseudo-monadaceae			Denitrification (*Pseudomonas*). Nitrate and nitrite reduction verified in culture.		(Rosenberg *et al.*, 2014)
	QUI-1	2.2			
	QUI-2	1.9			
	SJO-1	0.0			
	SJO-2	0.0			
	BVA-1	1.0			
	BVA-2	1.3			

Table D.1 continued

Taxon	Core	Mean relative abundance along depth (%)	N metabolic reaction	Potential syntrophy with methanogen	Reference
Spirochaetaceae	QUI-1	0.8		Fermenter with known syntrophic association with methano-gens (*Sphaero-chaeta*). Syntrophy studied in cultures.	(Troshina *et al.*, 2015)
	QUI-2	0.7			
	SJO-1	0.5			
	SJO-2	0.6			
	BVA-1	1.0			
	BVA-2	1.0			
Opitutaceae	QUI-1	0.1	N fixation (*Diplosphaera*) and nitrate reduction (*Opitutus*). Nitrate reduction verified in culture.	Propionate production (*Opitutus*). Syntrophy not assessed in culture.	(Chin *et al.*, 2001)
	QUI-2	0.1			
	SJO-1	0.1			
	SJO-2	0.1			
	BVA-1	0.0			
	BVA-2	0.1			

APPENDIX E

DECLARATIONS OF CONSENT FROM CO-AUTHORS

Chapter 2

An abiotic N$_2$O cycle on the anoxic early Earth.

Co-authors H. Imanaka, T. Ely, R. Hu, S.J. Romaniello, and H. Cadillo-Quiroz have

provided consent for inclusion of this paper in the dissertation.

Chapter 3

Effects of sterilization techniques on chemodenitrification and N$_2$O production in tropical

peat soil microcosms. (published in *Biogeosciences* 16, 4601–4612)

Co-authors Kaitlyn Tylor, Joshua Nye, Keith E. Holbert, Jose D. Urquiza Muñoz,

Jennifer B. Glass, Hilairy E. Hartnett, and Hinsby Cadillo-Quiroz have provided consent

for inclusion of this paper in the dissertation.

Chapter 5

Microbial communities and the putative interactions of methanogens with nitrogen oxides

in diverse peatlands of the Amazon basin.

Co-authors Z. Zamora, A.F. Sarno, D. R. Finn, A.M. Hoyt, J. van Haren, J.D. Urquiza

Muñoz, and H. Cadillo-Quiroz have provided consent for inclusion of this paper in the

dissertation.